Stent pour implantation percutanée d'une valve cardiaque

Coralie Marchand

Year 2009 N° d'ordre : 09MULH.....

STENT FOR PERCUTANEOUS HEART VALVE IMPLANTATION

by

Coralie Marchand

Supervisors : Pr B.Durand, Dr F.Heim

Thesis

presented to the

University of Mulhouse

in partial fulfillment of the requirements for the degree of

Doctor in Mechanics

Submitted : May 22th, 2009

Examination Committee :

Pr. Subhash K. BATRA	NC State University, USA	reviewer
Pr Régis RIEU	Université Aix Marseille 2	reviewer
Pr Nabil CHAKFE	Faculté de Médecine, Strasbourg	examiner
Pr Bernard DURAND	Université de Mulhouse	PhD Advisor
Dr Frédéric HEIM	Université de Mulhouse	PhD co-Advisor

conducted at

UNIVERSITE DE HAUTE ALSACE, E.D. 494
Laboratoire de Physique et Mécanique Textiles, UMR CNRS 7189

TABLE OF CONTENTS

Résumé :

Cette étude à pour but de développer un concept de stent atraumatique pour le remplacement percutanée de la valve aortique. Le stent est obtenu à partir de brins de Nitinol tressés, ce qui lui permet, de part sa géométrie et sa structure, d'être compressible, auto-expansible, et atraumatique. Le principe de fabrication des prototypes et les contraintes qui lui est associé sont présentées. Les performances de ces prototypes, en terme d'ancrage, de régurgitation statique et de régurgitation dynamique sont ensuite évaluées par des essais in vitro, pour lesquel le banc de test en flux pulsé a été optimisé afin de prendre en considération la compliance de la racine aortique. Les résultats obtenus permettent de mettre en évidence les différents paramètres de fabrication stent, tant au niveau dimensionnel (hauteur du cylindre, angle du cône...) qu'au niveau structurel (rigidité), qui ont une influence significative sur le comportement de l'endoprothèse.

Mots clés :
valve cardiaque, valve aortique, stent, prothèse, endoprothèse, implantation percutanée

Abstract :

The goal of this work is to develop an atraumatic stent concept for percutaneous aortic valve replacement. Shape setted braided nitinol wires, thanks to their specific geometry and elasticity, allows stent's compressibility, self deployment and aortic root preservation.
Prototypes manufacturing technique and relatives constraints are presented. Performance of the obtained prototypes are evaluated in vitro, in terms of sealing, static and dynamic regurgitation. More specifically, the pulsatile bench testing has been optimized to take in account the compliant constraint of the aortic valve environment. The results bring to the fore which are the dimensions (head height, cone angle...) and the structures features that do influence the endoprosthesis behavior significantly.

Key words :
heart valve, aortic valve, stent, prosthesis, endoprosthesis, percutaneous implantation

INTRODUCTION

Aujourd'hui à ces débuts, le remplacement valvulaire par voie mini invasive est une technique moins traumatisante que la chirurgie à cœur ouvert, particulièrement adaptée aux patients fragiles. Cependant, les stents actuellement utilisés sont inadaptés à cette nouvelle application et dégradent leur site d'implantation.

L'objectif de ce travail est de développer un stent qui respecte aussi bien la géométrie, les tissus, et les fonctions de la racine aortique. Nous avons conçu, réalisé et testé in vitro un stent qui assure, uniquement de part les surfaces de contact générées, le maintien et le fonctionnement de l'endoprothèse valvulaire en position aortique, sans employer de force d'expansion élevée ni de crochets.

Une synthèse bibliographique est présentée dans le chapitre 1 et met en avant les contraintes liées au remplacement valvulaire par voie mini invasive et les limites des travaux menés jusque là.

Le chapitre suivant présente le concept du stent. Sa conception est détaillée ainsi que les modèles mécaniques permettant de décrire le comportement du stent et assurer son dimensionnement.

La fabrication du stent est présentée dans le chapitre 3. Le choix des paramètres de tressages des éléments du stent est détaillé ainsi que le processus de mise en forme de l'alliage Nickel-Titane utilisé.

Les prototypes ainsi obtenus sont testés in vitro suivant des conditions opératoires décrites dans le chapitre 4 et obtenues via l'optimisation du banc de test sous flux pulsé.

Les résultats obtenus son présentés dans le dernier chapitre et mettent en évidence l'influence des différents paramètres de fabrication sur le comportement de l'endoprothèse. Enfin, les performances du dispositif permettent de valider le concept du stent vis à vis des prothèses valvulaires actuelles.

Chapitre 1 BIBLIOGRAPHIE

A raison de 5,5L/min, le cœur assure la circulation du sang dans l'organisme. Oxygéné par les poumons, le sang arrive dans le ventricule gauche via la valve mitrale et est éjecté dans l'aorte à travers la valve aortique, 70 fois par minute. Cette dernière est composé de 3 feuillets valvulaires. La valve aortique s'ouvre en systole et se referme en diastole afin d'empêcher le reflux sanguin, provoqué par la résistance systémique et la compliance artérielle.
Les trois feuillets valvulaires sont reliés à la parois aortique le long de l'anneau aortique composé majoritairement de tissus fibreux. Chaque feuillet fait face à un renflement, appelé sinus de Vasalva, qui abrite les orifices coronaires. La géométrie de la racine aortique est particulière et ses dimensions sont décrites par Thubrikar et al.
Au cours du cycle cardiaque, l'écoulement du sang dans les sinus participent au mécanisme de fermeture de la valve, et les dimensions de l'environnement aortique varient selon la pression sanguine. Le stent valvulaire devra donc respecter les spécificités géométriques de la racine aortique tout en s'accommodant de ses variations dimensionnelles.

La sténose aortique par calcification est l'une des pathologies valvulaires les plus courantes qui conduit au remplacement valvulaire par implantation chirurgicale d'une prothèse. Elles sont de deux types, mécaniques et biologiques. Les prothèses mécaniques existent depuis 1952 et se déclinent selon différents design. Avec un élément obstruant le passage du sang, elle sont thrombogènes contrairement aux prothèses biologiques qui, fabriquées à partir de tissu animal, adoptent la géométrie de la valve native. L'implantation de ces deux types de prothèses valvulaires requiert une chirurgie lourde, avec arrêt cardiaque et mise en place d'une circulation extra-corporelle du sang.

Depuis une trentaine d'année, la chirurgie vasculaire par voie percutanée c'est largement développée. Cette technique permet de procéder au remplacement vasculaire par voie mini-invasive, sans ouvrir les tissus. Des cathéters sont insérés par les voies naturelles et déploient

sur les sites à traiter un ballonnet, un stent ou encore une endoprothèse afin de palier une sténose ou un anévrisme. Plusieurs matériaux peuvent être utilisés pour la réalisation des stent, suivant différentes structures, conduisant ainsi à deux modes d'expansion distincts. Ainsi constitués, les stents sont implantés afin de restaurer le passage du flux sanguin à travers les conduits vasculaires obstrués. Depuis 1990, les stents sont aussi utilisés dans le traitement des anévrismes, associés à des prothèses. Ces dernières assurent le remplacement des conduits vasculaires dilatés tandis que les stents assurent leur ancrage dans les tissus. Ces opérations par voie mini-invasive sont aujourd'hui largement utilisées. Cependant, l'implantation des stents induit des réactions inflammatoires non maitrisées, liées principalement au comportement mécanique des conduits stentés.

Le concept de ce travail réside ainsi dans le fait d'implanter une prothèse valvulaire par voie percutanée, à l'aide d'un stent qui respecterai en particulier le comportement mécanique du site d'implantation. De nombreux patients aujourd'hui exclus de la chirurgie conventionnelle pourraient ainsi se voir proposer un remplacement valvulaire par opération mini-invasive ne nécessitant pas d'arrêt cardiaque. La première implantation sur cas humain fut réalisée en 2000 par Bonhoeffer, et en 2002 par Cribier en position aortique. Plusieurs travaux de recherche sont actuellement menés pour le développement d'endoprothèses valvulaires aortiques mais seuls 2 dispositifs, Edwards et Corevalve, sont testés cliniquement. De géométries globalement cylindriques, l'ancrage de ces endoprothèses est assuré par une force d'expansion élevée du dispositif et aucun positionnement longitudinal ni angulaire n'est assuré. Bien que ces stents assurent un remplacement valvulaire efficace, ils ne respectent la racine aortique et leur implantation n'est pas aisée. Pour répondre à ces inconvénients, plus d'une dizaine de prototypes sont en cours de réalisation. Tandis que certains se focalisent sur le mode d'ancrage ou le mode d'accès de l'endoprothèse, d'autres travaillent à l'adéquation du stent à la géométrie de la racine aortique et au développement de nouvelles prothèses valvulaires. Enfin, des outils permettant la résection de la valve native calcifiée sont étudiés.

L'ensemble des techniques aujourd'hui développées montre l'enthousiasme porté au remplacement valvulaire aortique par voie percutanée. Cependant, aucun dispositif ne permet à ce jour d'être tout à la fois compressible, expansible, et non dégradant pour les tissus, l'écoulement sanguin et les fonctions vitales abritées par la racine aortique. Des travaux doivent encore être menés avant de pouvoir procéder à des remplacements valvulaires aortique percutanée en toute sécurité.

Chapitre 2 CONCEPTION ET COMPORTEMENT MECANIQUE DU STENT

Les stent conçus pour palier les rétrécissements vasculaires ne sont pas appropriés, de part leur géométrie et leur mode d'ancrage, au remplacement valvulaire. En effet, la distribution et le transfert des efforts au sein de la racine aortique est spécifique et s'effectue principalement le long de l'anneau aortique et des commissures. Le stent présenté dans ce chapitre s'attache à respecter la géométrie et les tissus de la valve aortique ainsi que son fonctionnement.

La racine aortique comporte plusieurs spécificités telles que la disposition des sinus de Valsalva face aux feuillets valvulaire, les orifices coronaires, et la valve mitrale. En tenant compte de ces contraintes, le stent a été conçu en 4 éléments géométriques s'apposant parfaitement à la paroi aortique. Le stent est composé de 3 piliers rectilignes reliant une base conique à 3 arches radialement déployées et à une tête cylindrique. Ces éléments permettent respectivement de supporter la prothèse valvulaire, assurer un ancrage diastolique sur l'anneau aortique, orienter la prothèse valvulaire face au sinus tout en assurant l'ancrage systolique, et enfin éviter le basculement de l'endoprothèse. L'ancrage et l'étanchéité du dispositif sont assurés par apposition permanente des surfaces du stent sur les tissus. Afin d'y parvenir et ce malgré la compliance de l'environnement, le stent est composé de fils de Nitinol, tressés ou non.

Le nitinol est un alliage de Nickel et de Titane, ayant la capacité d'être superélastique au-delà de sa température de transition Af, en phase austénitique, et déformable plastiquement en dessous de Af, en phase martensitique. Le grand domaine élastique de ce matériau (>=8%) permet d'obtenir un stent auto-expansible, autorisant ainsi un stent de géométries complexes. D'autre part, l'étude générale de l'interaction d'un stent avec des tissus biologiques montre que le faible « module » d'élasticité du nitinol permet de respecter la compliance des tissus, en minimisant les efforts qui leurs sont appliqués.

Afin d'assurer au stent une grande flexibilité et expansivité tout en contrôlant son taux de couverture et sa résistance à la compression, ses différents composants ont été réalisés sous forme de tresses et de brins juxtaposés mis en forme. Le comportement mécanique de chacun d'entre eux a été modélisé afin de vérifier l'adéquation de la structure choisie avec les besoins du stent.

Le rôle des arches est d'assurer un contact permanent dans les sinus, tout au long du cycle cardiaque. Le comportement mécanique des arches est déduit d'un modèle de poutre courbe en flexion encastrée en un point. La déformation des sinus par les arches est négligeable en systole et maximale en diastole. Les calculs permettent d'évaluer la compliance résiduelle des sinus en fonction du Nitinol employé et d'optimiser ainsi le comportement du stent dans les sinus.

Les piliers ont pour fonction de relier la tête à la base du stent, tout en supportant les arches et les feuillets valvulaires. Ils sont formés de deux brins rectilignes juxtaposés. Le déploiement des arches dans les sinus ainsi que la pression diastolique sur la prothèse tendent à faire fléchir les piliers. Un modèle de poutre en flexion en appuis en ses extrémités permet de déterminer le comportement mécanique des piliers. On constate ainsi que des brins de Nitinol de diamètre 0,6mm limitent la déformation des piliers à 1mm au niveau des commissures de la valve.

La base conique et la tête cylindrique du stent sont toutes deux en appuis sur les tissus est nécessitent des surfaces de contact suffisantes permettant de répartir les efforts et assurer l'étanchéité de l'endoprothèse. Ces éléments du stent doivent d'autre part, sans dégrader les tissus, résister à la compression afin que l'ancrage et le positionnement du stent soient efficaces. Le comportement des tresses a été étudié afin de vérifier de leur adéquation face aux exigences du stent. On montre tout d'abord que le taux de couverture des stents tressés est supérieur à celui des stents laser pour des taux d'expansion élevés. D'autre part, le comportement mécanique de la tresse est déduit du modèle de Kirchoff Love tout en prenant en considération l'interaction des brins en leurs extrémités : la compliance résiduelle théorique de l'aorte stentée est de 90%.

Le Nitinol associé à une structure tressée assure un comportement mécanique adéquat des différents composants du stent. La résistance à la compression est adaptée aux conditions in vivo, tout en conservant la compliance de l'environnement aortique. De plus, la superélasticité autorise la compression et le déploiement du stent suivant des formes complexes.

Chapitre 3 FABRICATION DU STENT

Les méthodes de fabrication adoptées pour la réalisation des éléments du stent sont détaillées dans ce chapitre. Les différents parties du stent sont réalisées indépendamment puis assemblées. Elles sont constituées de fils de Nitinol devant chacun reproduire une forme rectiligne, courbe, ou zig-zag selon que l'on réalise les piliers, les arches ou les tresses. Les géométries empruntées par ces fils sont définis en fonctions des contraintes de tressage, d'assemblage et de résistance du stent. Ensuite, les traitements thermiques utilisés pour fixer la forme des fils de Nitinol sont présentés en portant un intérêt particulier aux modifications des propriétés physiques et mécaniques du matériau.

L'une des contraintes de tressage consiste en l'utilisation d'un unique fil pour la réalisation de la tresse, ce qui permet de minimiser l'endommagement des tissus aux extrémités du stent ainsi qu'au points de jonction des brins. D'autre part, les tresses doivent présenter une symétrie à 120° afin être reliées aux 3 piliers et respecter la disposition feuillets valvulaires face aux sinus, tout en vérifiant qu'elles n'interfèrent pas entre elles lors de la compression du stent. Enfin, les paramètres de tressage sont directement liés à la résistance à la compression des tresses et à leur densité de maillage modifiant ainsi la distribution des efforts sur les tissus. L'ensemble de ces contraintes sont prises en considération pour choisir les paramètres de tressage ce qui permet de définir les géométries finales devant être inculquée aux fils de Nitinol tressés.

La géométrie des fils utilisés pour la réalisation des piliers se déduit des paramètres de tressage fixés précédemment afin de respecter la hauteur de l'endoprothèse et offrir un moyen d'assemblage, à l'aide de boucles aux extrémités des piliers. La géométrie des arches est quant à elle globalement définie par les dimensions natives de la racine aortique, en terme de courbure et de longueur. Afin de limiter les points de jonctions entre brins de nitinol, les trois arches constituent un même élément obtenus à partir d'un seul fil métallique.

Enfin, les paramètres des différents constituants du stent doivent prendre en compte la

compliance de l'environnement afin d'assurer un contact permanent du stent sur les tissus tout en minimisant les efforts. Les dimensions et paramètres finalement choisis pour la mise en forme des brins de Nitinol sont présentés dans ce chapitre.

Les géométries calculées sont inculquées aux fils de Nitinol par traitement thermique. Cette opération se définie par la température et la durée du traitement, le support de mise en forme, le refroidissement et l'histoire du matériau. Ces paramètres ont une influence directe sur les propriétés mécanique et physique du Nitinol traité, à savoir son domaine élastique et sa température de transition austénitique Af. Afin de maitriser ces données, les faire correspondre aux besoins d'utilisation et définir les conditions opératoires optimales, une campagne de mesure a été réalisée. La température de transition Af, le plateau de contrainte en charge et le pseudo module d'élasticité du Nitinol ont été mesurés par DSC et par des tests en traction.
On constate tout d'abord que seules des températures de traitement supérieures à 500°C permettent de faire chuter la température de transition Af de telle façon que le matériau soit superélastique dans les conditions d'utilisation. D'autre part, la mise en forme du nitinol est efficace dès lors que la température Af diminue, après avoir subie une première augmentation. Enfin, le refroidissement rapide des échantillons par trempe à l'eau permet d'obtenir des résultats reproductibles et prévisibles. Chaque traitement thermique s'accompagne d'une chute de la valeur du plateau de contrainte en charge du Nitinol tandis que l'évolution du pseudo-module d'élasticité concorde avec l'état du matériau au cours du traitement : il chute en phase martensitique puis augmente et se stabilise en phase austénitique. Ces comportements s'observent sur des durées de 10 à 50min selon l'inertie thermique des support de mise en forme utilisés. Enfin, les propriétés physiques et mécaniques issus de deux traitements thermiques successifs sont indépendantes des paramètres du premier traitement.

Compte tenu de ces résultats et des difficultés de réalisation des composants du stent, la mise en forme des brins est réalisée en deux temps. Le premier traitement thermique vise à faciliter la réalisation de la pièce en plaçant le matériaux en phase martensitique et en lui inculquant une forme temporaire. Le second traitement, à 560°C, fixe les géométries et propriétés que l'on souhaite précisément obtenir. Chaque support de mise en forme, plane ou tridimensionnelle, est étalonné afin de connaître la loi d'évolution des propriétés du Nitinol. On est ainsi capable d'assurer la reproductibilité du procédé de fabrication du stent en contrôlant les propriétés du nitinol, ce qui garantie l'élasticité du stent et le respect de la compliance des tissus.

Chapitre 4 BANC DE TEST

Les performances des prothèses valvulaires sont généralement évaluées en terme de régurgitation statique et dynamique. L'une permet de caractériser la fuite de la valve en position fermée tandis que l'autre s'intéresse au comportement dynamique de la valve sous flux pulsé. Les tests habituellement réalisés sur les prothèses valvulaires ont du être adaptés à la caractérisation d'endoprothèses dont on souhaite évaluer la capacité à se maintenir dans un environnement compliant. Les bancs de tests utilisés et les modifications apportées sont présentés dans ce chapitre.

Un moulage en silicone a tout d'abord été réalisé afin de reproduire l'anatomie particulière de la racine aortique tout en conservant les variations dimensionnelles de cette dernière au cours du cycle cardiaque. Les paramètres de ce moulage (diamètres et épaisseurs) ont été définis en tenant compte des données bibliographiques concernant l'environnement valvulaire aortique et de la loi de comportement du silicone utilisé. Les endoprothèses sont ainsi insérées dans le moulage en silicone pour leur caractérisation sous pression dans un cadre proche des conditions natives.

Le test en statique doit permettre de vérifier l'étanchéité des dispositifs valvulaires en position fermée, état correspondant à la phase diastolique. Dans le cas particulier des endoprothèses, ce test permet plus particulièrement de caractériser l'étanchéité para-valvulaire de l'implant et la qualité de l'ancrage diastolique assuré par le stent. L'évolution de la pression exercée par une colonne d'eau sur la prothèse valvulaire en position fermée nous informe sur l'évolution du débit de fuite de la valve en fonction de la pression statique.

Afin de caractériser les prothèses sous flux pulsé, nous avons utilisé un banc de test existant, développé par Heim selon la norme ISO/CD 5840 relative aux prothèses valvulaires. Le banc utilisé est basé sur le modèle de Windkessel à 3 éléments, avec un générateur de flux, une

compliance artérielle et une résistance systémique. Toutefois, l'allure du signal de pression résultant s'éloigne du signal théorique en comportant plus particulièrement de forts pics de valeurs et ne peut être expliqué par des calculs prenant en compte l'inertie du fluide et la loi d'évolution du débit. Le banc de test en flux pulsé ne peut donc pas être utilisé tel quel pour la réalisation de test sur une racine aortique souple. Des essais complémentaires menés en parallèles d'une modélisation théorique des conduites ont permis de montrer que les pics de pression observés sont issus de coup de bélier, ceux-ci étant principalement provoqués par la restriction imposée par le débitmètre. En effet, celui-ci requiert, pour une mesure précise basée sur l'effet Coriolis, une conduite de 8mm de diamètre seulement. Afin de s'en affranchir, une mesure de débit différentielle a été mise en place. Après calibrage et insertion dans le circuit d'une compliance ventriculaire, le signal de pression émis par le banc test en flux pulsé modifié correspond au signal natif. Les prothèses et endoprothèses peuvent donc être caractérisées sous flux pulsés sous conditions hémodynamiques afin que leur performances soient évaluées et comparées.

Chapitre 5 TESTS ET RESULTATS

L'objectif du travail réalisé dans ce chapitre est d'évaluer in vitro les performances de la prothèse valvulaire stentée. En particulier, on souhaite valider le concept du stent, en vérifiant si l'ancrage par obstacle du stent dans la racine aortique est efficace. Différents prototypes sont testés, afin d'étudier l'influence des paramètres dimensionnels et structurels sur le comportement de l'endoprothèse. On constate que la rigidité des éléments du stent a un impact direct sur le temps de fermeture de la valve tandis que leurs dimensions affectent le positionnement et augmentent ainsi la régurgitation. La manière dont le stent modifie les performances de la prothèse valvulaire est aussi étudiée en comparant les performances des prothèses stentée et non-stentée. Enfin, les performances de l'endoprothèse sont comparées à celles des prothèses commercialisées.

Afin de caractériser les prothèses et endoprothèses valvulaires de manière fiable, des conditions opératoires ont été définies. Le placement et le conditionnement des prothèses valvulaires ont en particulier été étudiés afin que ceux-ci n'influencent pas les mesures. En effet, le ré-arrangement de la structure du matériau textile au cours des essais modifie sensiblement le temps de fermeture et la fuite statique de la prothèse textile. D'autre part, le stent doit assurer seul le positionnement de l'endoprothèse dans la racine aortique, a contrario des prothèses implantées par voie chirurgicale. Ces constatations liées aux réglages du banc de test ont permis de définir un protocole de mesure.

Afin d'optimiser les performances du stent, plusieurs prototypes ont été testés en faisant varier les paramètres du stent, déterminant ainsi leur impact sur le comportement de l'endoprothèse.
Les paramètres dimensionnels concernent la hauteur de la tête cylindrique du stent, l'angle et la largeur de la base conique ainsi que la longueur des arches. Les paramètres de structure concernent la rigidité des arches et des piliers. Les valeurs empruntées par ces différents

paramètres ont été définies afin d'obtenir un compromis entre fonctionnalité de l'endoprothèse et dégradation minimale de l'environnement aortique.

Les résultats des essais menés ont permis de mettre en évidence le fait que les performances de l'endoprothèse sont affectés de 2 manières. Tandis que l'une correspond au mauvais positionnement du stent dans la racine aortique et se traduit principalement par une augmentation de la régurgitation statique, l'autre est relative à la modification du temps de fermeture de la valve ce qui affecte le volume de fuite dynamique.
Plus précisément, les essais ont permis de valider le fait qu'une base conique de trop grande largeur ne permet pas au stent d'assurer une étanchéité parfaite du dispositif par appui sur l'anneau aortique. D'autre part, le positionnement axial du stent est dégradé par l'emploi d'une base conique d'angle trop ouvert qui ne centre pas la base du stent sur l'anneau aortique, et par une hauteur trop faible de la tête cylindrique qui n'empêche pas le basculement du stent. Enfin, l'utilisation d'arches de faible longueur induit une forte dégradation des sinus de part une forte concentration de contraintes. Les paramètre dimensionnels du stent sont révélateurs du bon positionnement de l'endoprothèse dans la racine aortique.
D'autre part, on constate que la déformabilité des piliers supportant les feuillets valvulaires est caractéristique d'un temps de fermeture accru de la prothèse ce qui peut s'expliquer par une augmentation de l'énergie de flexion requise par les feuillets valvulaires textiles. Afin de faciliter l'implantation par voie percutanée, il est nécessaire de revoir le design du support de valve afin d'optimiser les performances valvulaire sans pour autant rigidifier les piliers. Enfin, l'utilisation d'arches flexibles minimisent la dégradation des sinus tout en assurant pleinement les fonctions de l'endoprothèse.

Les essais réalisés sur les prothèses valvulaires stentée et non stentée on permis de montrer que le stent assure l'étanchéité paravalvulaire de l'endoprothèse par un appui efficace de la base conique sur l'anneau aortique. Cependant, l'association de la valve textile au stent retarde le temps de fermeture de la prothèse, ce qui s'explique par la flexibilité des piliers citée précédemment. Les performances de l'endoprothèse peuvent donc être optimisées, bien que celles-ci soit déjà comparables à celles obtenues pour 2 prothèses actuellement commercialisées, une valve mécanique St Jude et une bioprothèse Mitroflow.

Les résultats des tests in vitro présentées dans ce chapitre valident, à travers des performances encourageantes, le concept du stent, tout en définissant les paramètre optimaux du dispositif.

CONCLUSIONS ET PERSPECTIVES

Ce travail a permis de valider le concept de stent valvulaire aortique dont le maintien est assuré sur le site d'implantation par surfaces de contact plutôt que par force d'expansion.

La bibliographie a prouvée l'intérêt porté par la communauté médicale à cette nouvelle technique d'implantation, tant du point de vue mini-invasif que du point de vue du respect de la racine aortique, de part les nombreux prototypes en développement.

La géométrie du stent proposée se conforme à celle de la racine aortique et utilise les surfaces de contact ainsi créées pour se maintenir. Le stent est composé de 4 parties fonctionnelles prenant appui sur l'anneau aortique, les sinus et l'aorte. Les modèles mécaniques associés à ces composants montrent que le stent peut, avec une structure tressée en Nitinol, respecter la compliance de la racine aortique tout en étant compressible et de hauteur constante. Les conditions de tressage du stent avec un fil unique sont détaillée dans le chapitre 3.

Afin de de caractériser l'aptitude des prototypes à se maintenir dans l'environnement aortique, un moulage en silicone a été réalisé pour reproduire les dimensions et la compliance de la racine aortique tandis que les conditions de pression hémodynamiques ont été obtenues en optimisant le banc de test en flux pulsé existant.

Les régurgitations statiques et dynamiques des prototypes sont évaluées. Les résultats sont encourageants avec des performances comparables à celles des prothèses commercialisées. Les résultats montrent en particulier l'influence des paramètres dimensionnels et structurels des constituants du stent sur l'ancrage et les performances valvulaires de l'endoprothèse.

Le travail réalisé permet de valider le concept du stent avec des performances remarquables. Cependant, plusieurs travaux essentiels restent à réaliser. Il est en effet indispensable de s'intéresser aux capacités de l'endoprothèse à être implanter par voie percutanée, ce qui requiert compressibilité, « trackability », déploiement et positionnement de l'endoprothèse. D'autre part, le comportement en fatigue du dispositif sous sollicitations répétées doit être étudié, tant du point de vue des matériaux que des fonctions valvulaires. Enfin, des implantations devront être réalisées sur animaux afin de caractériser les performances in vivo de l'endoprothèse.

INTRODUCTION

Calcific aortic stenosis ist the most common valvular disease observed in western countries. Alone in the US, it has been estimated that between 2-3 % of the elderly population have calcific aortic stenosis, while 1 to 2 % of Americans have congenital bicuspid aortic disease. Worldwide, aortic valve replacement represents today around 250000 cases and that number is expected to increase by 5 % per year over the coming years. It represents a 1 billion dollars market. To face valve diseases, mechanical replacement prostheses have been developed and implanted since the early 1950's. Appreciated for their long term durability, these prostheses require, however, anticoagulant medication, which generate side effects. Bioprostheses (porcine valves or valves made from bovine pericarde), which appeared then in the 60's, are far less thrombogenic, but also less durable and tend to degenerate under severe calcification. In spite of the existing replacement solutions, among the diseased patients about 10 % are considered high risk and approximately 15% are declined by the patient or the physicians. These critical cases are at first elderly people with multiple pathologies, most of whom require replacement of the aortic valve due to calcification or degeneration. Some of these patients are too ill or weak to withstand the stress of open heart surgery. The second critical population is the children, since many of these patients require heart valve replacement due to congenital heart disease. Some of these children are not treated until they are older because it is difficult to find a heart valve small enough for them, or because multiple highly invasive surgeries will be required to replace the valve as they grow.

The rapid developments and success in percutaneous (non invasive) vascular surgery over the last 2 decades, with the now common stent grafts implantation, make this technique today attractive even for aortic valve replacement. "Percutaneous" surgery, also called "non-invasive" surgery means that the procedure is done through the skin instead of doing open chest surgery. Less traumatic for the patient, this technique may be particularly adapted to elderly people, in a society where life's expectancy increases permanently, and for children as well. But since the success of Pr Cribier's first attempt on human and today, the stents on

which the valve prosthesis (mainly bioprosthesis) is mounted remain almost ever standard stents. Classic stents, which proved good functionality for vessel enlargement and non invasive aneurysm treatment, do, however, not have appropriate geometry for heart valve stenting. Aortic wall anchoring of a classic cylindrical shaped stent, with little hooks associated to a high expansion force becomes very traumatic for surrounding tissues especially when the load (pressure on closed valve) is axially oriented. The dissection of the native aortic valve shows that the aortic annulus (base of the valve) as well as the commissures (line along which valve leaflet is fixed to the aorta wall) support the valve and transmit most of the applied stresses to the aortic wall. This stress transfer mechanism from the valve to the aorta is generally not respected with stented valve prostheses. This may lead to premature environmental tissue degradation and stent migration. Some works have already been done on the development of better adapted stents and other mini invasive valve support means. However, most of them are in some way traumatic for the surrounding tissues.

The goal of the present work is to develop a stent designed in respect to the heart valve geometrical environment as well as in respect to the valve functions. We design, realize and test in vitro a stent positioned and maintained in an aortic environment through geometrical surface matching. The anchoring of hooks in surrounding tissue is thus avoided.

The bibliographic synthesis presented in the first chapter of this book, highlights the needs in term of percutaneous valve implantation. After a presentation of the valve diseases and the classic surgical replacement solutions, the brief presentation of the existing stents technologies allow to understand the limits of classic stenting when applied to heart valve implantation. The use of vascular cylindrical stents, classically used to enlarge stenosed vessels, for non invasive valve implantation leads to stent migration risk, as has been reported through already performed clinical trials. These limits stimulate the development of many new designs, some of which are described further in the chapter. The new research dynamic around the development of stented valves presented here, validates the relevance of our research work.

The next chapter presents the stent's concept, based on the fact that the anchoring process by classic stents is not adapted to withstand the forces applied on heart valve in vivo. The design we describe respects the aortic root environment. The stent is positioned through surface matching rather than expansion force. The design of the device is detailed, and we present some mechanical behavior models for the different elements of the stent, in order to establish some relationships between the expected behavior and the stent's dimensioning. From the

obtained behavior laws, the stent's geometrical parameters can be set for manufacturing purpose.

Manufacturing is presented in the third chapter, in which the details of the manufacturing methods adopted for the different stent's parts are discussed. A focus is made on the geometrical braiding parameters adopted for the stent's braided parts realization. The values of the parameters are set in order to get a behavior, which globally respects the compliance of the aortic root environment once the stent is implanted. The handling of the Nitinol material used to obtain the stent's parts is then detailed in the second part of the chapter. The particular behavior of Nitinol when undergoing heat treatment for shape setting of the wire used in the manufacturing process, is described with the presentation of experiments performed on Nitinol samples. The results give information about how to shape set the material in order to obtain the required geometrical as well as mechanical properties for the final stent. Finally, we describe the obtained prototypes.

In order to test the stent prototypes in vitro, an existing testing bench (that reproduces the cardiac circulation) was optimized. Chapter four presents the testing conditions. Prototypes are mounted in a mock aortic root, which mechanical properties reproduce the properties of the native root. A theoretical model is suggested to calculate the pressure conditions to be set on the bench for reliable performances measurements. Some technical modifications of the existing bench configuration to increase measurement precision are proposed and detailed.

In the last chapter we perform some testing on the prototypes, making vary some design parameters. We analyze how the stent's positioning is influenced by design criteria, to assess which geometry leads to the best performances of the device. The performances of the stented valve are measured in term of static and dynamic regurgitation, which characterize respectively the static leakage of the closed valve and the dynamic leakage upon valve closing (directly related to closing time). These performances are then compared with those obtained for other commercially available valves, and show finally the feasibility of the concept.

Chapter I BIBLIOGRAPHY

1 HEART AND BLOOD CIRCULATION

1.1 The heart

Blood circulation ensures the different organs of the body to get fed with oxygen and nutritive substances. Blood volume represents between 5 and 6 liters for an adult and cardiac blood flow at rest is 5.5 liters / min in the average. Figure I.1 is a classic shematic representation of blood circulation in human. Blood motion is realized thanks to the heart muscle, which works as double pump device. It is composed with 4 cavities : left and right heart each composed of ventricle and atrium. The heart pulsatile pump ensures blood ejection with the ventricle contraction.

Blood arrives to the right heart though the veins at pressure hardly higher than atmospheric pressure. It flows into the right ventricle and is ejected at low pressure (30mm Hg) to the lungs through the pulmonary artery. Once the pulmonary capillaries network is reached, the blood loses CO_2 and gets O_2. Blood flows then through the veins pipe network that become always larger, until it reaches the two pulmonary veins connected to the left heart. This represents the pulmonary circulation. Blood is then ejected from the left ventricle at high pressure (110-140 mmHg) into the aorta. It reaches then some further capillaries where nutritive substances and oxygen is transmitted to surrounding tissues, while CO_2 and degenerated tissues are absorbed. Blood flows then back to the right heart through the veins. This represents the systemic circulation.

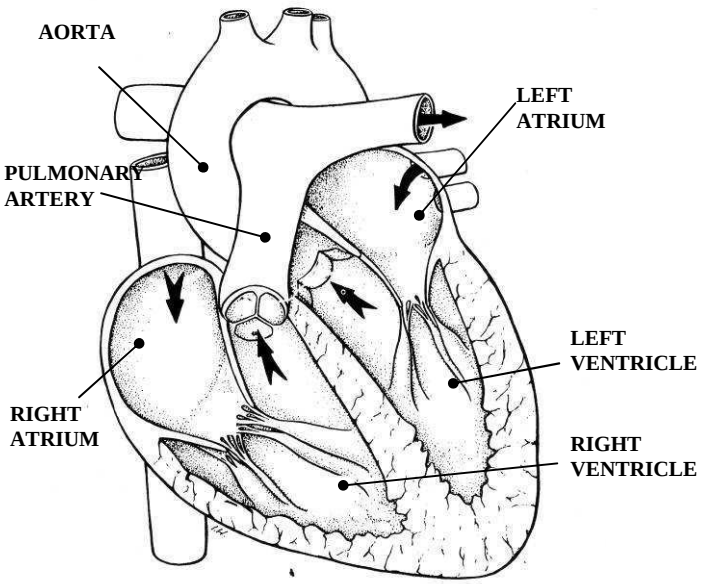

VALEURS NORMALES DE LA PRESSION DANS LES CAVITES CARDIAQUES ET LES GROSSES ARTERES (en mm de mercure)	
Oreillette droite	
pression moyenne	5
Ventricule droit	
pression systolique	30
pression télédiastolique	5
Artère pulmonaire	
pression systolique	30
pression diastolique	15
pression moyenne	20
Oreillette gauche	
pression moyenne	12
Ventricule gauche	
pression systolique	140-150
pression télédiastolique	12
Aorte	
pression systolique	150
pression diastolique	90

Fig I.1_ The heart

The flow track is around 70ml at each heart beat (systolic ejection volume), for a 70 beats/min rate. This corresponds to a cardiac flow of 5.5 l/min on average. Pressure and flow signals are time dependant over one heart beat.

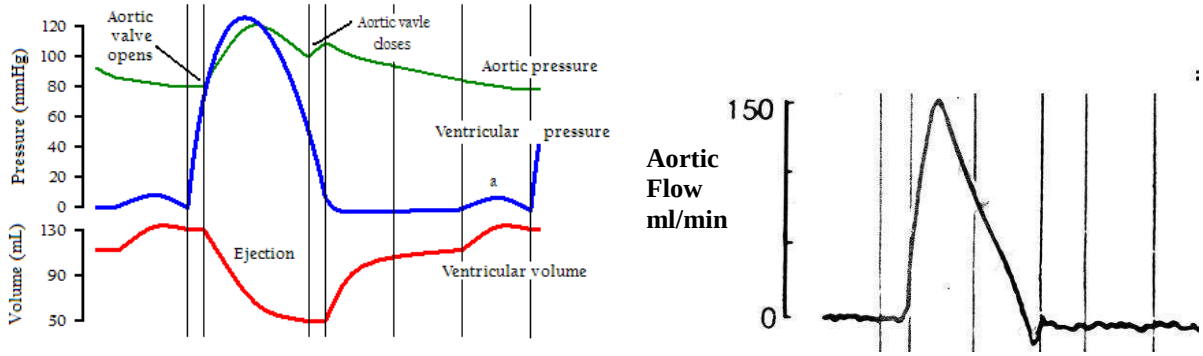

Fig I.2_ Pressure and flow signal

1.2 Cardiac valves : geometry

In order to prevent blood backflow to the heart when heart muscle relaxes (diastole), four valves regulate the flow direction: the tricuspid valve between the right atrium and right ventricle, the pulmonary valve between right ventricle and pulmonary artery, the mitral valve

between left atrium and left ventricle, the aortic valve between left ventricle and aorta. Two designs characterize these valves: with two or three leaflets.

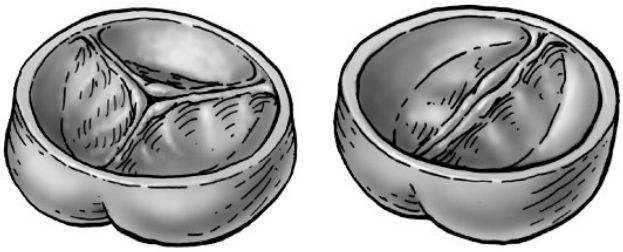

Fig I.3_ The heart valves : 2 and 3 leaflets design

When blood is ejected from ventricle (systolic phase), mitral and tricuspid valves are closed, while aortic and pulmonary valves are open. When ventricle is filled (diastolic phase), aortic and pulmonary valves are closed, while mitral and tricuspid valves are open. Aortic and pulmonary valves are called arterio-ventricular because they establish a junction between a ventricle and an artery. Tricuspid and mitral valves are called atrio-ventricular because they establish a junction between an atrium and a ventricle. Atrioventricular valves are attached to the cardiac muscle (myocard) with papillary muscles and fibrous cordae. They react as active structures simultaneously with the myocard contraction that controls their opening and closing. Arterio-ventricular valves on the contrary, also called semi-lunar valves because the leaflets they are composed with are semi-lunar shaped, are not linked to the cardiac muscle. Their opening and closing mechanism is controled with blood flow.

2 AORTIC VALVE : Anatomy

In our work, we will essentially focus on the aortic valve (3 leaflet design), which represents the most diseased valve that requires replacement. The aortic valve is composed of three leaflets and three aortic sinuses called Valsalva sinuses.

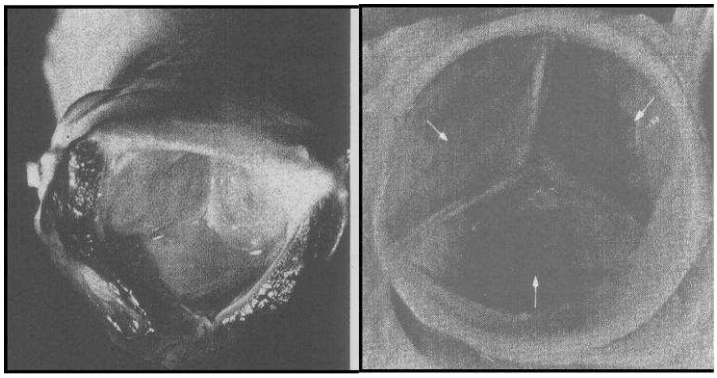

Fig I.4_ Bottom and top view of the artic valve

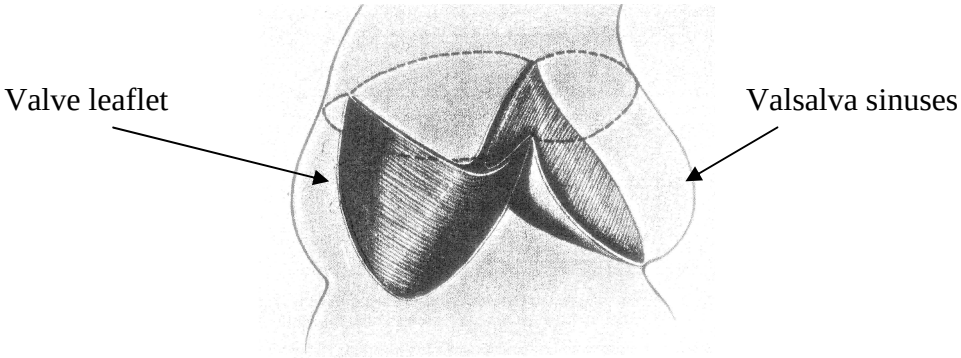

Fig I.5_ Aortic root shape

The leaflets are the mobile parts of the valve. The sinuses are cavities located behind the leaflets. They establish a junction between the aorta conduit and the left ventricle. Their geometry is close to an ellipsoid. On the ventricle side, the intersection between the sinuses and the ventricle is shaped in a scalloped way. Two sinuses include the entry of the left and right coronary arteries, and are thereof called coronary sinuses. The third sinus is the non coronary sinus.

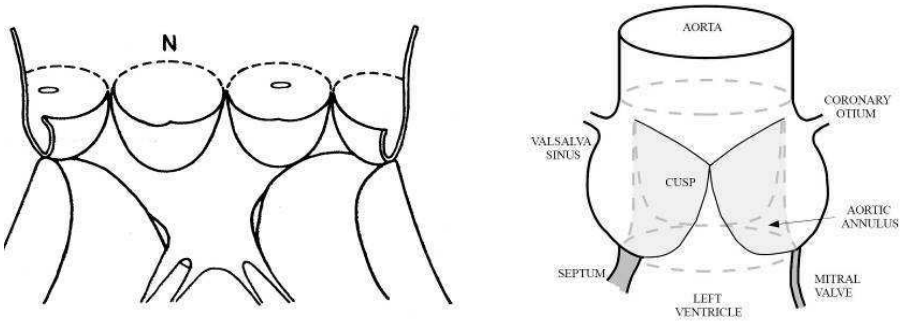

Fig I.6_ Aortic root sinuses : unrolled and native configurations

2.1 The aortic annulus

The aortic annulus is a fibrous scalloped structure that rigidifies the aortic base. However, the annulus remains soft enough to ensure proper closing of the valve. Swanson and al. [SWA. 74] showed that when pressure varies between 20 à 120mmHg, the aortic annulus diameter value increases around 10 %. This proves that the aortic root environment is a dynamic structure that undergoes dimensions variations. That flexibility needs to be taken into consideration in the development of a new heart valve stent.

2.2 Valve leaflet : anatomy

The valve leaflet, also called cusp, consists in two separate zones. The first zone, that separates the ventricle from the aorta when valve is closed, bears the diastolic pressure. The second zone participates to the valve leaflets coaptation when valve is in closed position, and ensures the flood tightness. The Nodulus of Arentius, that represents a fibrous line located in the middle of this zone, participates to that flood tightness as well. The edge of the leaflet is called free edge. The sides along which two leaflets are in junction are called the commissures. Along these commissures the aortic sinuses do merge.

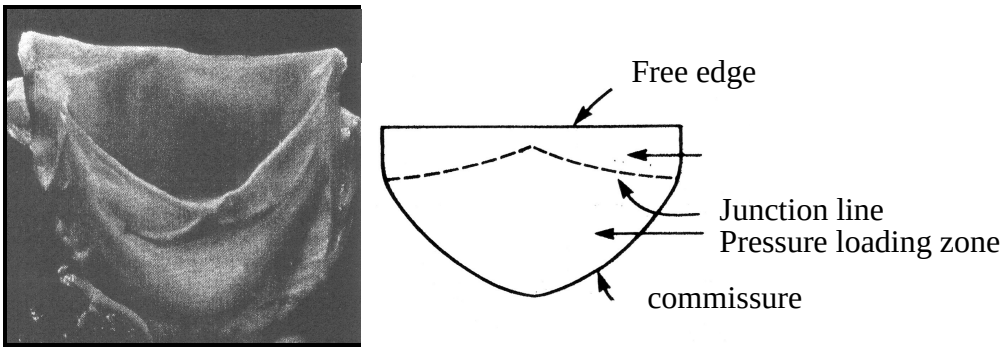

Fig I.7_ Valve leaflet: anatomy

2.3 Sinus and Leaflets : geometry

Different geometries have been suggested in literature for leaflets and sinuses. The study performed by Swanson [SWA.74] allowed visualizing the geometrical shape of valve leaflets in closed position. The author used some silicon to shape a native valve in closed position.

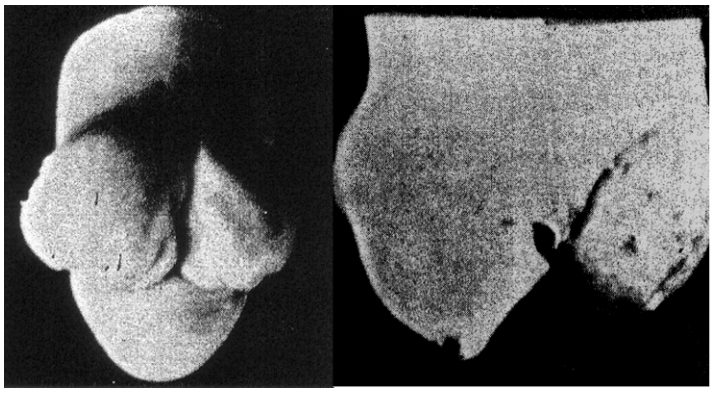

Fig I.8_ Silicon shape of native valve in closed position

Each human being is unique. The size of the sinuses as well as the size of the leaflets is never the same and varies between two people. It appears, however, that the leaflets are mainly curved in one direction when the valve is in closed position. The shape of the leaflet that undergoes diastolic pressure, is close to a cylinder. This geometry is broken at the junction with the coaptation zone. Coaptation zone can be considered as two flat zones connected with a 120° angle.

As for the sinuses, the cut of the silicon castings showed that they are circular shaped in a horizontal plan, and look more like ellipses in a vertical direction.

2.4 Valve dimensions

The healthy aortic valve is composed of 3 leaflets, while some deformed valves present only 2 or sometimes up to 4 leaflets. The design with 3 leaflets is the best adapted to the valve function. It doesn't create any blood obstruction in the aortic root. The circumference of a 3 leaflets valve in open position is around 6 R (equivalent to the addition of the 3 cusp free edges length) which is close to the value of the artery circumference $2\pi R$.

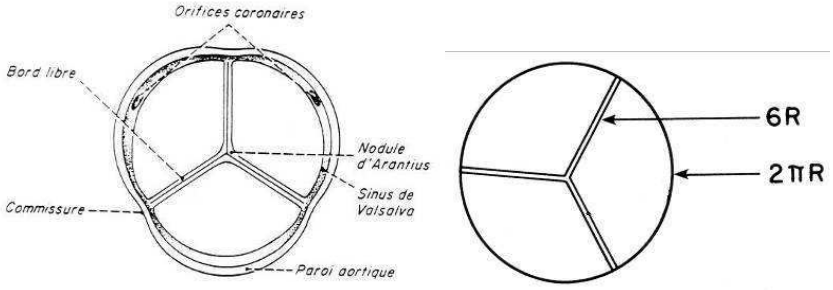

Fig I.9_ sinuses geometry

A tricuspid geometry offers a quasi circular section to the blood flow. Moreover it is the unique configuration that combines two advantages at valve closure : no free edge excessive tissue length, no free edge exaggerated traction stress. With only two leaflets, a valve would generate free edge traction. With four leaflets, too many folds would be present along the free edge in closed position. Three leaflets represents an optimum for the valve design, with reduced flexure and traction stress in the cusp free edge.

Thubrikar et Al [THU. 81], showed the relationships between the different geometrical parameters of the aortic valve among different species. The authors suggest the following model for the aortic valve :

H = closed valve height
Hs = commissures height
hs = sinus height
Cc = cusps coaptation height
Rb = basis radius
Rc = commissure radius
ds = sinus depth
α = angle between cusp and horizontal plan

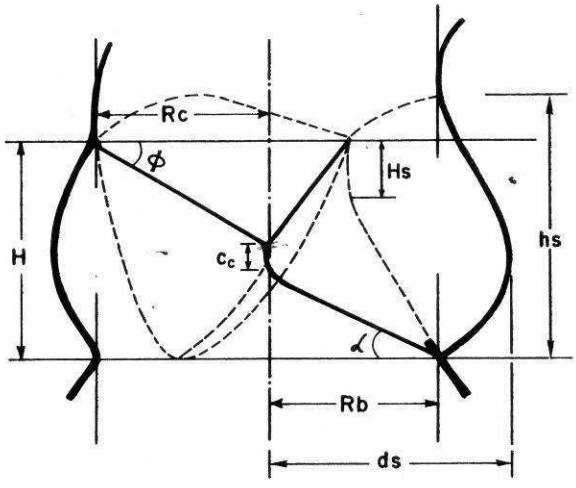

Fig I.10_ aortic valve parameters

Sauren presents a synthesis of values obtained for these parameters by different authors and for different species (human and animal) [SAU.81]. We give here a summary of these results for Rb=1.

	Rc	H	ϕ	α	Cc	Hs	Lf	Lr	ds	hs	Authors
human	1	1.42	32	22	0.34	0.71	2.48	1.4	1.46	1.76	Swanson et Clark [SWA.74]
human		1.34	33				2.42				Sands et Al [SAN.69]
Pig		1.3	28				2.2				Sands et Al [SAN.69]
veal		1.16					2.18				Sands et Al
lamb		1.08					2.13				Sands et Al [SAN.69]
Dog	0.83	1.17	34	20		0.5					Thubrikar et Al [THU.81]

Table I.11_ synthesis of valve parameters values obtained by different authors and for different species (Rb=1)

We observe that the aortic root dimensions are different between two dissections. Silver proved with his work that the 3 leaflets of a valve are rarely identical [SIL.85]. Valve dissections on patients showed that 16 % of analysed valves had three identical leaflets, 51 % had only two, and 33% had no identical leaflets. However, in spite of these differences, a valve can roughly be described with some average parameters values corresponding to a theoretical geometry with three symmetrical leaflets:

Rb=11,3 à 14 mm, H=15,7 à 19,8mm, ϕ=25 à 37° et α=15 à 27°

3 VALVE DYNAMICAL BEHAVIOR

3.1 The closing mechanism

To prevent heart muscle overloading during cardiac cycle, the valve closing mechanism must be able to occur with a minimum of energy. Blood flow generates cardiac valve movement and accelerates its closing dynamic. The Valsalva sinuses participate actively to this process. A blood vortex takes place in the sinuses during the end of the systolic phase. The energy of this vortex helps to push the valve leaflets towards the valve center, even before backflow occurs. LEONARDO da VINCI was a pioneer in noting the important role played by the fluid dynamics in the aortic valve closing mechanism, and especially with the sinus vortices.

3.2 Dynamics of the valve system

The main feature of the aortic valve, is that its closing and opening mechanism is generated by the the movement of its leaflets. However, other parts of the valve system do play a role in the working movement.

Thubrikar et al.[THU.77] studied the valvular movements with the mean of a fluoroscopic technique, using markers set along leaflets and valve commissures. The movement of the valve was identified through the movement of the markers. The authors conclude that the opening and closing geometry of the valve varies over the cardiac cycle from a circular geometry to a triangular one.

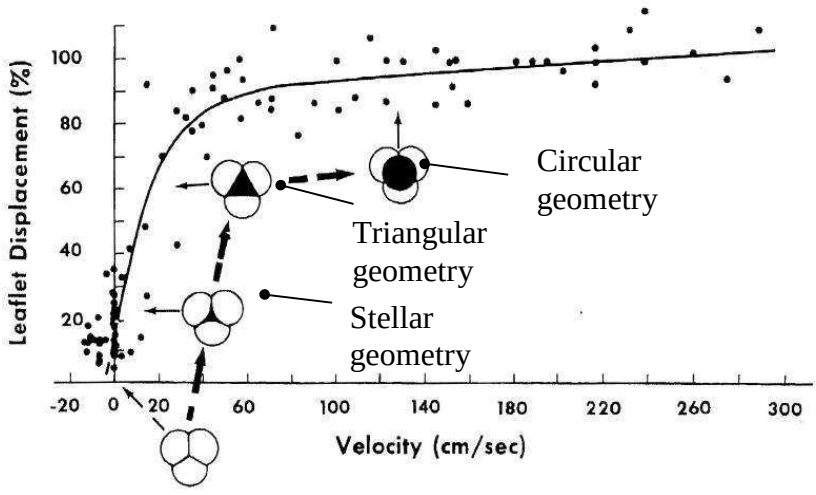

Fig I.12_ length evolution of the free edge with flow velocity

Steenhoven [STE. 81] confirmed these observations and showed that the valve environment changes its shape over the cardiac cycle. Thubrikar highlighted, with the fluoroscopic technique, the role played by the valve commissures in the closing mechanism. The commissures interact with the valve leaflets. Indeed, valve doesn't open at the moment at which blood is ejected from the ventricle as could be imagined. Leaflets are in reality connected to a tubular structure thanks to the commissures. The increase in the tubular structure diameter, leads to the leaflets separation. This occurs at begin of valve opening process, fluid is not yet in motion. The valve geometry evolves then towards a triangular and finally circular shape when valve is completely open.

This diameter enlargement at commissures level is around 10 % (Fig. I.13).

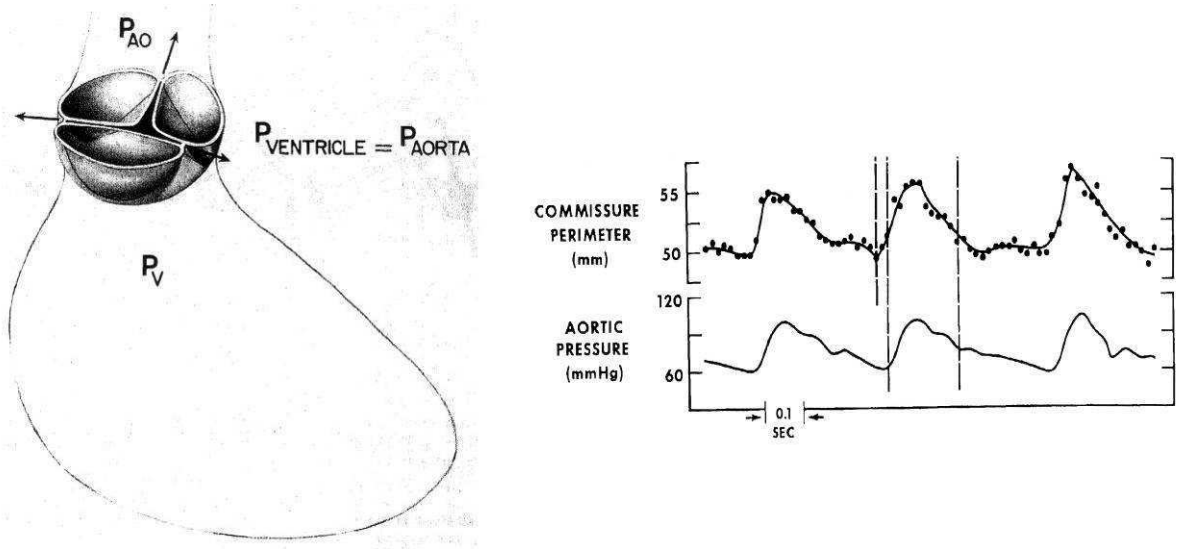

Fig I.13_ perimeter change between commissure

Thubrikar explains this expansion process in two way :

- In diastole, the leaflet tissue is extended under diastolic pressure. As soon as pressure values in the ventricle and in the aorta are the same, there's no pressure gradient left across the valve. Commissures tend to move outwards.
- In diastole, pressure value in the ventricle is low. When the value increases to reach the aortic pressure, ventricular tissue is under tension and deforms to compensate the pressure increase. The commissures, linked to the extended zone step aside.

With the same fluoroscopic technique, the authors highlighted also the elastic behavior of the aortic annulus, with perimeter extension estimated around 10%. This variation in the

dimension plays an essential role in the valve durability. It helps to limit the deformation undergone by the leaflets.

In systole, the enlargement of the aortic annulus in association with the previously described commissures movement, allows leaflets separation even before blood ejection occurs. Thanks to this mechanism, the leaflets are never in a configuration in which they would undergo a flexure stress corresponding to the one of a membrane blocked on both sides.

In diastole, the contraction of the aortic annulus gives the leaflets the possibility to come closer before blood backflow occurs. Regurgitation is hence avoided, and valve membrane stress is limited.

3.3 Conclusions

At each cardiac cycle, valvular leaflets must allow valve closing under minimal pressure, in order to avoid valve regurgitation. They must transmit diastolic pressure stresses to the supporting structure. At last, they must be able to undergo changes in shape and dimension to adapt to cardiac dynamics (aortic ring and commissures deformation). The valvular stent we develop must take these different aspects in consideration.

4 AORTIC VALVE : the prostheses

Over time, cardiac valves, and especially aortic valve, suffer from degradations. One of the main degradation process is related to calcification. Calcification consists in the abnormal deposition of calcium salts in teh valve tissue. The deposition follows the degeneration of the collagen bundles that give resistance to the leaflet's tissue. Tissue becomes hence stiffer. The patient suffers then from stenosis (partial obstruction or narrowing of the aortic conduit). Elderly people are mainly concerned with that issue.

Thrombosis is another wellkown valvular disease. It concerns people with exagerrated grease deposition in the aortic environnement. It corresponds to a physiological reaction that leads to generation of blood clots (follows platelets and fibrin deposition). These clots prevent the valve leaflets closing movement. The valve does not close completely anymore and leakage occurs, what is called aortic insufficiency.

Other valve degradations like tissue ruptures may take place and lead to valve dysfunction.

To face valve diseases, mechanical replacement prostheses have been developed and implanted since the early 1950's. Bioprostheses appeared then in the 60's.

4.1 Mechanical prostheses

The first mechanical prosthesis was implanted by Dr. Charles Hufnagel in 1952. He implanted a caged ball valve inserted in a methacrylat short pipe as artificial aortic conduit. Around 200 patients treated with the cages ball valve presented still healthy prosthesis after 30 years of implantation.

Mechanical valves exist with many designs. Most are composed of a stent and a mobile part which can be a ball or a disk. These prostheses usually have a very long durability (25 to 30 years).

The main concern with mechanical valves, is that they obstruct the blood flow. Blood stopping causes thrombus generation and important pressure gradient accross the device. The patient need to be treated with anticoagulant medecine. In order to limit the obstruction effects, the designs evolved towards better profiled valves, especially rotating disk technology. Thus, the St Jude « Bileaflet » prosthesis appeared in 1976 [ARO.89]. The material used is graphit and pyrolitic carbon. It is composed of 2 semi-circular leaflets which

open at 85°. The leaflets are maintained thanks to a pivot joint with the stent annulus. Their movement is free, and they are permanently washed with the blood flow.

We summarize in the following the constraints and problems faced with the develoment of these mechanical valves :

- Thrombosis related to stopping zones in the flow, if no sufficient washing
- Part rupture (welding zones)
- Permanent pressure gradient
- Anti-coagulant medecine required.

In the frame of the development of a new stented valve, all these criteria will have to be taken into account.

4.2 Bioprostheses

Bioprostheses represent today a standard solution to replace faulty human valves. Their main advantage is that they respect the human physiology offering central flow profile. They ensure good quality of life to the patient who doesn't need to take any anti-coagulant medecine. The durability of bioprostheses is however limited (10 to 12 years). Made up with organic material which degrades over time, they tend to become stiff and calcify easily. Their use is hence restricted to elderly people and pregnant women for whom anti-coagulant medecine is prohibited. Bioprostheses are obtained from porcine valves or bovine pericard tissue. Tissue degradation leads to reoperation in 74 % of the cases. It consists mainly in abnormal calcification processes related to collagen bundles degradation. To slow down degradation over time, tissue is treated with glutaraldhehyde. The treatment, however, modifies the mechanical properties of the valve tissue. Vesely highlighted in his work, the particular stiffness increase of treated tissue [VES.89]. A few years earlier, this had already been observed by Rousseau [ROU.83].

4.3 Mechanical versus Biological prostheses

The surgeon remains the person who decides which type of prosthesis is the best adapted to the situation. The choice is influenced by many parameters and is individual. However, long

term behavior studies are available. These studies give information about the performances of the different prostheses types.

A comparison between a mechanical valve (St Jude Bileaflet) and a bioprosthesis (Biocor) over the long term is given in a report from 1995 [MYK.95]. It presents results concerning a panel of 100 patients over a 10 years period of time. The results highlight mortality rates globally lower among patients with bioprosthesis (98% survival rate against 81%). No significant difference has been noted concerning devices's thrombogenicity. Some complications related to the use of anti-coagulant medecine were reported in the St Jude group (bleeding problems). Valvular calcification observed in the Biocor group led to reoperation in some cases.

Another study started in 1975 reports results obtained over 20 years [OXE.03]. The long term behavior of tilting disc valves and a porcine valves is compared. Survival rate after 20 years is practically the same (25% for the mechanical et 23% for the porcine). But only 3% of the patients from the bioprostheses group still have the original implant after 20 years, while 18% from the mechanical valve group is concerned. These results highlight the limits of the existing replacement solutions. Mechanical valves proved good durability but increase the bleeding risk related to anti-coagulant consumption. As to the bioprostheses, their use is limited in time, but they respect better the human physiology. Both solutions are finally not far from being equivalent.

Figure I.14 summarizes the design evolution of the valve over the years since 1952.

Fig I.14_ evolution of valve prosthesis design

5 PERCUTANEOUS VASCULAR SURGERY

5.1 The concept

"Percutaneous" surgery, also called "non-invasive" surgery means that the procedure is done through the skin instead of doing open chest surgery. The procedure consists in doing a small incision in the patient's skin at the level of the femoral artery for example. Some specific devices called catheters are then inserted through the incision in the vascular system. These catheters are hollow flexible tubes for insertion into a body vessel to distend a passageway for other medical tools. Its many uses include the diagnosis of heart disorders when inserted through a blood vessel into the heart. The strength of a percutaneous procedure is its ability to deliver any device (stent, balloon for inflation or folded heart valve) into position through the vascular system. Unlike the traditional open heart surgery, the heart does not need to be arrested during the procedure, that is conducted entirely without the use of a bypass pump. The device crimped inside the catheter is moved along with a guide-wire under fluoroscopic guidance into the correct intracardiac position. Finally the device is expanded from the collapsed state to its final diameter.

Hence a percutaneous approach in which patients are not exposed to the risks of surgery has potentially large implications for these patients. That's the reason why over the past 20 years patients and care providers have encouraged the transition from traditional open-surgical procedures, which require long hospital stays, to less invasive techniques. This demand for minimally invasive procedures has allowed novel instrumentation and implants to be designed.

5.2 History of percutaneous surgery

Non invasive surgery has been used since more than 30 years with the first human coronary balloon angioplasty performed intra-operatively in 1977 by Gruentzig, Myler and Hanna in San Francisco [GRU.77]. It consisted in the enlargement of the stenosed coronary artery thanks to balloon inflation.

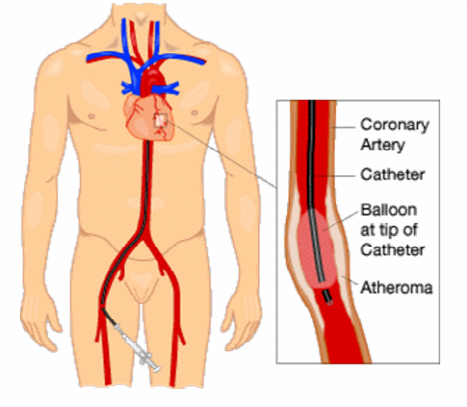

Fig I.15_Percutanous access by femoral arery and balloon inflation in implantation site

After the success of the procedure realized with wire coaxial balloon systems, further guiding catheters and steerable guidewires are developed in 1982. Since 1979 Mass and Senning (Zurich) had studied medical prostheses to support the artery wall, in order to prevent restenosis after balloon angioplasty. They had developed a metallic coil shaped endoprosthesis and performed some tests on animals.

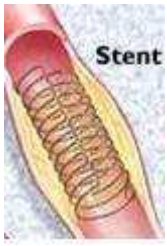

Fig I.16_ schematic representation of a stented artery

The bad results obtained led to the 1st patent by Hans Wallsten in 1982 concerning a self expandable metallic braided stent called Wallstent. The first implantation of the Wallstent in human coronary position is done par Puel J. in 1986 [ROU.87], after several years of development. Dotter et al. [DOT.83] and Cragg et al. [CRA.83] reported the first use of Nitinol material for stent purpose in 1983. At last, Palmaz pioneered balloon-expandable stainless steel mesh stents that remain in widespread clinical use today [PAL.87]. Today stents can be used alone or associated with a vascular graft (endoprosthesis).

5.3 Vascular stents

Vascular stents represent today one of the main application of percutaneous technology. They serve to hold diseased arteries (thrombosed or stenosed) open to a predetermined diameter after angioplasty and preserve a cylindrical lumen. These stents are used for a variety of

applications : peripheral and coronary arteries enlargement or lower limb, renal, carotid and neurovascular disorders improvement. The use of stents for all applications has dramatically increased since their approval by the United States Food and Drug Administration in 1994, largely as a result of therapeutic and technological advances. By far the greatest use of stents occurs in the coronary vessels. In that application the stent is often associated with balloon angioplasty before placement in the vascular environment. Balloon with stent placement is a well established and effective vascular reconstructive procedure aiming to reduce the severity of atherosclerotic stenosis. Its popularity arises due to its less invasive nature (compared to surgical alternatives) and its better clinical outcome (compared to balloon angioplasty without stenting) [SER.94], [HOH.99]. Just in the US a total of 574.000 angioplasty procedures with stenting were performed in 2003 [THO.06]. In the US the stent market has now expanded to $5 billion per year.

5.3.1 The different stent families

Stents are classified as either balloon- or self-expandable, based on their deployment mechanism. Balloon-expandable stents are crimped on a folded balloon and plastically deformed at the intended delivery site by balloon inflation. Balloon-expandable stents are mainly used in atherosclerotic coronary arteries in order to restore perfusion of downstream tissue. The material used for these stents is stainless steel.

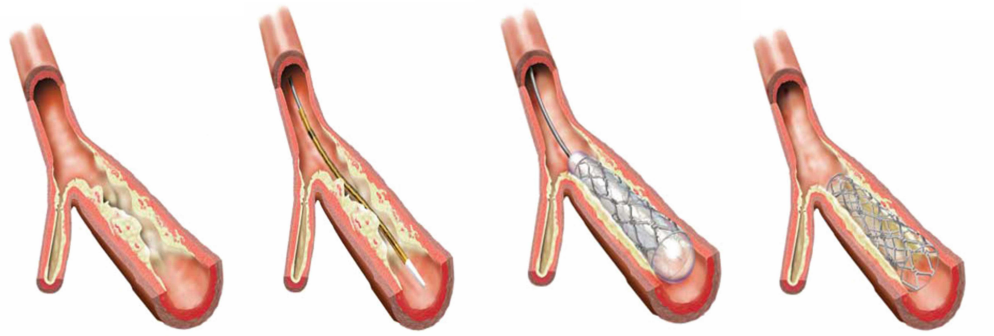

Fig I.17_ diagram of stent placement : the catheter is inserted across the lesion, the balloon is inflated, expanding the stent and compressing the plaque. The catheter and deflated balloon are removed.

In contrast, self-expandable stents are inserted into a delivery system catheter and when the target lesion is reached, the stent is released from the catheter and deployed. The market share of self-expandable stents is growing thanks to their use for peripheral arteries or extra-cardiovascular applications, where their typical features, like kink resistance and trackability, are required. The material used for these stents can be stainless steel or Nitinol.

5.3.2 Self expandable stents

When Dotter et al. experimented with Nitinol wire coils as intra-arterial scaffolds back in the early 1980s, Nitinol was known only for its unusual shape-memory effect. A coil wound to a small diameter and delivered through a catheter into the vessel would expand to a larger diameter, e.g., the diameter of the vessel lumen, upon warming with 60°C saline solution (Fig. I.18). Although the shape-memory effect looked as if it was ideally suited for the scaffolding of vessels, it took many more years for Nitinol stents to appear in the market. Dotter et al. [DOT.83] clearly were ahead of their time. The melting and processing of Nitinol, an intermetallic compound of titanium and nickel, had not been fully developed with consistent quality, nor had the properties of this material been fully understood. Presently, 20 years after Dotter et al.'s [DOT.83] experiments, Nitinol stents are self-expanding without the need for post-deployment heating. They are superelastic, i.e., crush recoverable, exert a gentle "chronic" outward force, and are generally more physiologically compatible than balloon-expandable stents. All major medical device companies as well as many smaller producers now offer Nitinol stents for (mainly peripheral) vascular and non-vascular indications. Herein, after a brief explanation of the mechanisms of shape memory and superelasticity, we describe the unique material properties of Nitinol and how they relate to the performance characteristics of Nitinol stents.

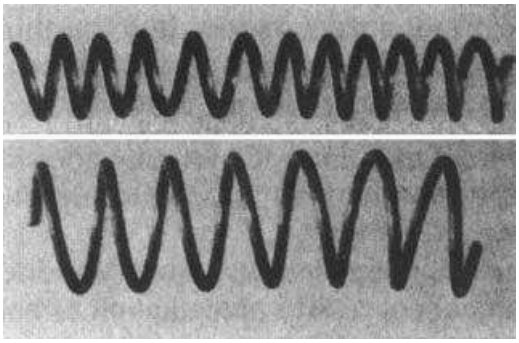

Fig I.18_ Nitinol coil stent used by Dotter et al., coiled for delivery and heat expanded [STO.04]

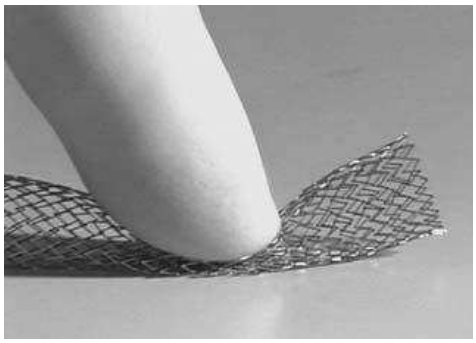

Fig I.19_ Extreme deformation of a Nitinol stent (Cordis SMART). The stent will recover after the load is removed [STO.04]

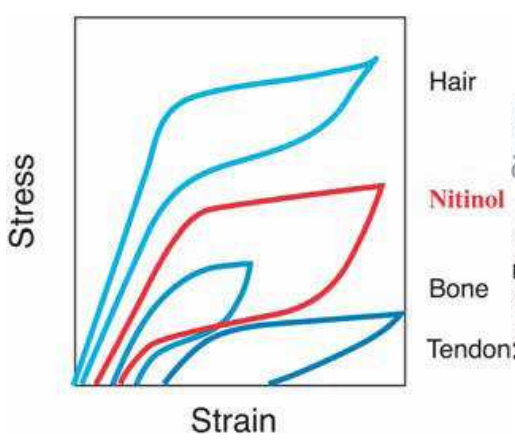

Fig I.20_ Schematic stress hysteresis and biased stiffness [STO.04]

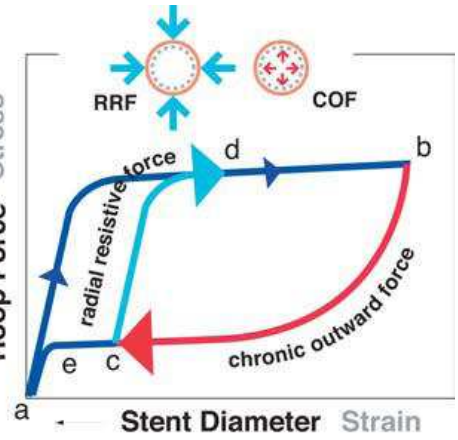

Fig I.21_ Biomechanical compatibility of Nitinol: deformation characteristics of Nitinol and living tissues [STO.04]

Conventional stent materials, such as stainless steel or cobalt-based alloys, exhibit a distinctly different elastic deformation behavior from that of the structural materials of the living body. The elastic deformation of these metals and alloys is limited to approximately 1% strain, and elongation typically increases and decreases linearly (proportionally) with the applied force. In contrast, natural materials, such as hair, tendon, and bone, can be elastically deformed, in some cases up to 10% strain in a non-linear way. When the deforming stress is released, the strain is recovered at lower stresses. As shown in Fig.I.19, the loading/unloading cycle is characterized by a pronounced hysteresis. A similar behavior is found with Nitinol alloys. As with natural materials, the loading and unloading curves show plateaus, along which large deflections (strains) can be accumulated on loading, or recovered on unloading, without significant increase, or decrease, respectively, in loads (stress). Because deformation of more than 10% strain can be elastically recovered, this behavior is called “superelasticity.” Superelastic Nitinol appears macroscopically to be simply very elastic ; however, the mechanism of deformation is quite different from conventional elasticity, or simply stretching of atomic bonds. When a stress is applied to Nitinol, and after a modest elastic deformation, the material yields to the applied stress by changing its crystal structure. This “stress-induced” phase transformation allows the material to change shape as a direct response to the applied stress. When the stresses are removed, the material reverts to the original structure and recovers its original shape. While superelasticity is the result of a stress-induced phase transformation, shape memory is the result of a thermal phase transformation. In fact, when superelastic Nitinol is cooled to below a critical temperature (the transformation temperature, which is dependent on alloy composition and processing history), it also changes its crystal structure. If no force is applied, this phase change is not accompanied by a shape change. The

material can be plastically deformed in the “low-temperature phase,” but the original shape can be restored by heating above the transformation temperature. Self-expanding Nitinol stents are manufactured with a diameter larger than that of the target vessel. Their transformation temperature is typically set to 30°C. They can be easily crimped at or below room temperature and placed in a delivery system. To prevent premature expansion during delivery into the body, the stent is constrained by a retractable sheath or by other means. At the treatment site it is released from the delivery system and expands until it hits the vessel wall and conforms to it. Now at body temperature, the stent is superelastic.

5.3.2.a Wire stent design

The evolution of Nitinol stent designs is clearly linked to the development of the material itself. Early on, Nitinol was only available in wire form. Consequently, early Nitinol stents were wire coils, similar to Dotter et al.’s [DOT.83] experimental device. Presently, coil stents made from round or flat Nitinol wire are still available. They are used mainly for non-vascular applications (e.g., Endocare’s Horizon Stent for the relief of bladder outlet obstruction), with the exception of the IntraCoil Stent (Intratherapeutics; Fig.I.22), which is indicated for the treatment of patients with superficial femoral artery and popliteal artery lesions. One advantage of simple wire coils is their retrievability in certain applications. As described previously, Nitinol loses its stiffness when cooled. The EndoCare Horizon or the D&E Memokath prostatic stents can be retrieved from the prostate by chilling the device with cold solution. The stents become soft and pliable and can be retrieved with a grasping forceps. Other early wire-based stent designs are the Cragg Stent (MinTec, Fig.I.22), a sinusoidal coil with peak-tovalley suture connections for vascular and non-vascular applications, and the knitted Ultraflex Esophageal Stent (Microvasive, BSC). Newer designs are the ZA biliary stent (Cook, Fig.I.22), a modified knitted design, and the braided Expander Stent (Medicorp). The Boston Scientific Symphony Stent is a wire formed design with struts welded to form hexagonal cells. While wire-based stents generally are very flexible, the Symphony Stent is quite rigid (Fig.I.22).

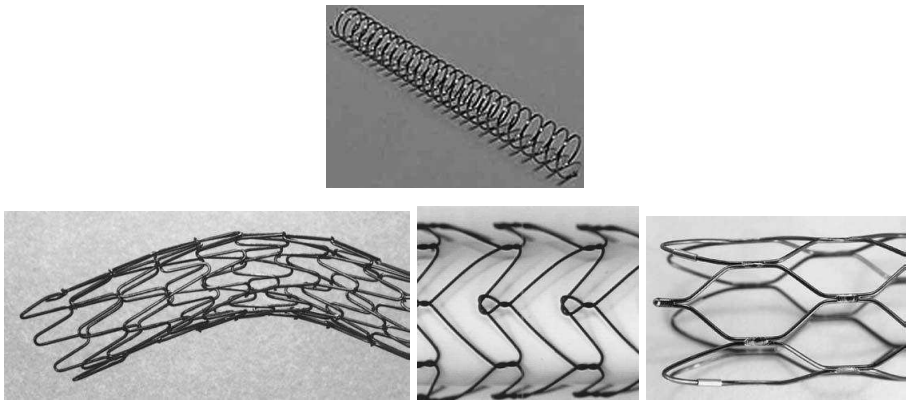

Fig I.22_ Intracoil stent (IntraTherapeutics, top), Cragg stent (MinTec, left), ZA stent (Cook, middle), Symphony stent (Boston Scientific, right) [STO.04]

5.3.2.b Sheet-based stent designs

A perceived disadvantage of braided or knitted wirebased stents is the crossing of the filaments. This increases the "wall thickness" of the stent and the delivery profile. Moreover, there are concerns about fretting corrosion or the wear of the Nitinol at the cross-over points. When Nitinol sheet became available, Angiomed (Bard) developed the first laser-cut Nitinol stent by cutting a pattern from sheet, rolling it up, and welding at specific strut locations (Fig.I.23). An interesting sheet-based Nitinol stent is the experimental "ratcheting" EndoTex stent, similar to the design suggested by Sigwart [SIG.87]. It is chemically etched from thin Nitinol sheet to produce a series of windows and a locking feature at one edge. It is rolled up to a small diameter roll and placed onto a PTCA balloon. The assembly is then placed into the vessel and the diameter of the stent is adjusted by inflating the balloon. As the balloon expands, the stent uncoils to the desired diameter to prop open the vessel. The stent is locked into place by unique tabs that slide into the stent "windows" upon balloon deflation. This design provides a wide range of diameters to custom fit for each treatment. It combines balloon expandability with the superelasticity after deployment; however, it has some of the perceived disadvantages of the knitted wire stents with non-uniform cross-section and potential fretting cross-over points. Vascular architect's Aspire stent uses a "dual-rail ladder type" frame that is also etched from Nitinol sheet and covered with ePFTFE. It is helically coiled onto a delivery system that allows deployment with a variable pitch to keep vessel side branches open.

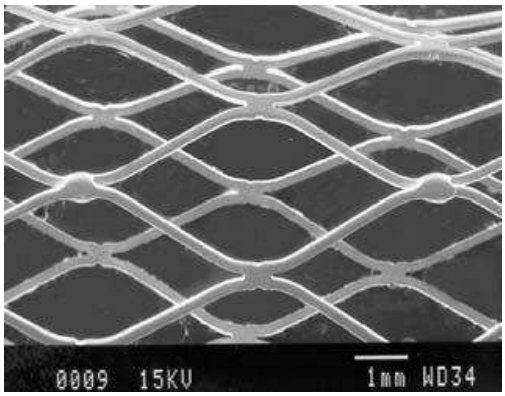

Fig I.23_ Memotherm stent (Bard Angiomed) made from sheet (note welded struts) [STO.04]

5.3.2.c Tube-based stent designs

In the mid-1990s, Nitinol seamless tubing appeared on the market in production quantities. With it came laser cutting of tubular Nitinol components. Presently, by far, most self-expanding Nitinol stents are produced by laser cutting of Nitinol tubing. Early examples are the Angiomed (Bard) Memotherm and the Scimed Radius stents. The Memotherm was a rigid, closed-cell design with a diamond shaped pattern similar to the original Palmaz balloon-expandable stent. The Radius, on the other hand, is a flexible open-cell design with sequential rings and periodic peak-to-peak non-flex bridges. Most laser-cut Nitinol stents employ variations and/or combinations of these basic design features (Fig.I.24). There are Nitinol stents in the market that are coated with silicon carbide (SiC) or diamond-like carbon (DLC). It is probably fair to state that these developments are more driven by product differentiation than actual scientific considerations.

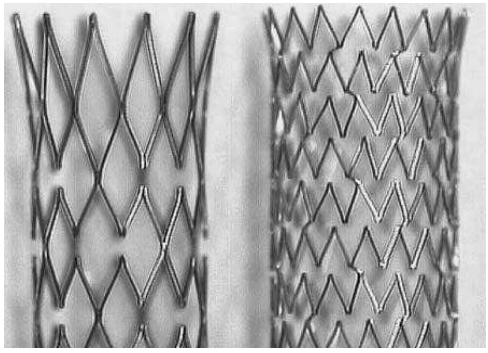

Fig I.24_ Laser-cut Nitinol tubular stents. Left : Memotherm (Bard Angiomed); Right : SMART (Cordis) [STO.04]

5.4 Vascular endoprostheses

Albert Einstein died in 1955 because of the rupture of an abdominal aortic aneurysm (AAA). One year later in 1956 MEADOX (USA) introduced the first commercially available polyester vascular graft. Since autologous graft material with the diameter of the aorta is not available, artificial vascular grafts are essential for the exclusion of AAA. Two polymers, polyester (Dacron) and polytetrafluorethylene (PTFE) haven proven their biocompatibility and long-term stability in conventional grafts since 1956 and 1975. Open surgery still needs a large abdominal incision for graft interposition. Excessive abdominal scars, which disabled an abdominal approach, inspired Parodi to choose an endoluminal access for the implantation of a graft in the AAA [PAR.95]. The success of this operation in 1990 initiated an euphoric development of endovascular devices. Increasing experience in the implantation procedure and numerous improvements of the devices has today lead to acceptable technical success rates with a reasonably low morbidity and mortality [MYE.00].

Currently, there are several thoracic endografts available for the treatment of descending thoracic aortic aneurysms (most common aneurysm type).

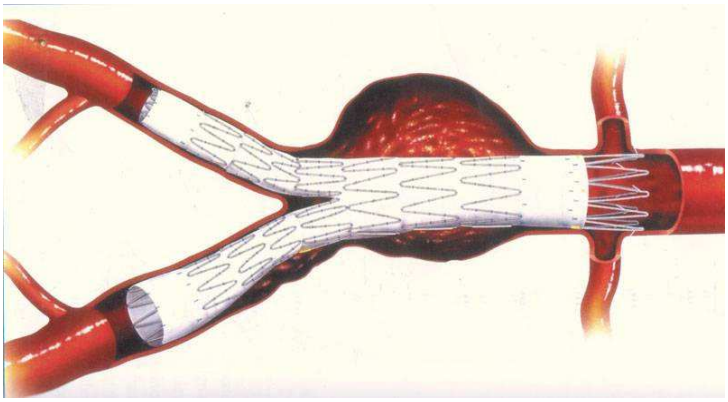

Fig I.25_ Method for treating an aortic aneurysm

They are the TAG device made by WL Gore (Flagstaff, Arizona), the TX2 device by Cook, Inc. (Bloomington, Indiana), the Talent and Valiant devices by Medtronic (Santa Rosa, California), and the Relay device by Bolton Medical (Sunrise, Florida). At this time, the only thoracic endografts approved by the FDA for use in the United States are the TAG, the TX2 and the Talent devices. The Valiant and Relay devices are also in clinical trial and currently enrolling patients.

The TAG device (Fig.I.26) is a symmetrical expanded PTFE tube with an external nitinol self-expanding stent along the entire graft surface. A circumferential PTFE sealing cuff is

located on the external surface of the endograft at the base of each flared, scalloped end. This device is currently the only device commercially available at this time.

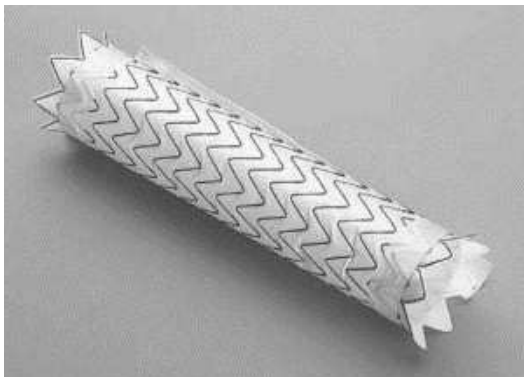

Fig I.26_ Gore TAG thoracic endoprosthesis [CHO.06]

The Medtronic Talent thoracic endograft device (Fig.I.27) was initially manufactured by World Medical Corporation and was subsequently acquired by the Medtronic Corporation. In its current state, it is a polyester graft with fabric sewn to a self-expanding nitinol wire frame. The device is modular and accommodates the use of additional main sections as well as proximal and distal extensions.

Fig I.27_ Talent Thoracic Device (Medtronic)

Once operators have advanced beyond a significant learning curve, early results have shown 95% to 100% success rate in implantation, 1% to 2% 30 days mortality rate, and 0% to 1.5% conversion rate to open repair at the time of placement or by 30 days [DAT.02], [HOW.01]. Large studies with 4 to 5 years of follow-up after placement have reported survival of 75% to 85%, need for a second procedure of 10% to 20%, and rupture rate of 0.4% to 1.0% [HER.02], [LIF.02]. The incidence of endovascular leaks at 1 year ranges from 17% to 31% and may vary among the different devices. Gore reported however 20 wire fractures were identified in 19 patients (13%) among a study concerning 139 patients. Of these wire fractures, 18 (90%) occurred in the longitudinal spine [WAN.07].

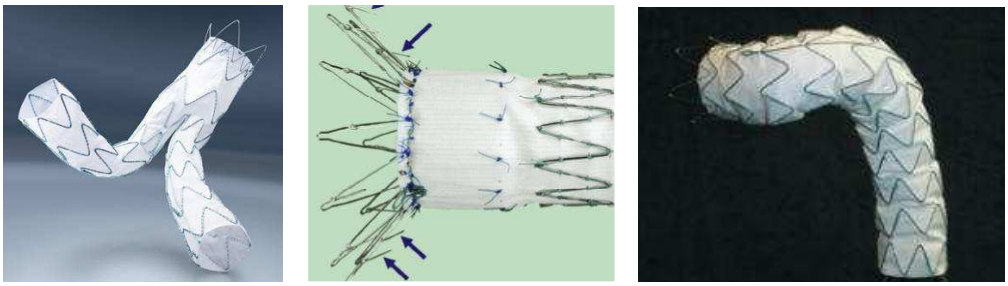

Fig I.28_ Endovascular Talent for AAAs (medtronic, left), the Zenith TX2 device distal end (Cook,middle), RELAY Thoracic stent-graft (Bolton Medical, right)

5.5 Materials and geometries

Stainless Steel, Tantalum, Niobium, CoCr alloys and Nitinol have been introduced as materials for stents in the past 15 years. However, unmet medical needs and general technological advancements have led to additional efforts to improve materials properties and to develop new materials for vascular stents, especially biodegradable materials such as magnesium and degradable polymers.

Polymer materials like poly (l-Lactid acid) PLLA seem to be generally applicable for drug eluting stents and if they finally make their way into a commercial application may offer cost advantages in stent manufacturing compared to the conventional manufacturing processes of today's stents. As an alternative to polymers, the use of degradable metallic materials such as magnesium alloys and iron, have been investigated during the past 5 years. In general, degradable materials can be used for indications which do not require a permanent mechanical enlargement of the artery. However, the main advantage of biodegradable materials is assumed to be that any long term risk associated with a foreign object implanted in the body is obviated and no long term mechanical adverse effects of conventional stents, such as stent "crushes" or strut fractures [BOS.06] to what extent the degradation process and degradation products might affect long term patency is unclear and subject to investigations.

5.6 The limits of vascular stents

Despite the constantly increasing success rate of stenting through technological progresses in the stent design and drug coatings on the stents' surface [BUR.06] the procedure can still fail because of restenosis in stents, which occurs in 30-60% of patients with complex lesions

[FAT.03]. In coronary arteries when treated with bare-metal stent designs the restenosis rates range from 20% - 40% [KAS.01].

Angioplasty was successful in reopening clogged arteries, however in many cases, immediate reclosure or arterial recoil caused failure of the angioplasty procedure. Stents provide a mechanical means of resisting recoil of the artery after balloon angioplasty, but do not prevent (and may to a certain extent even cause) another failure mode known as restenosis. Restenosis is a reclosure of the treatment site due to cell proliferation caused by local injury and a subsequent tissue response. With increasing clinical application of and experiences in stenting and increasing production quantities, requirements for stents and their manufacturing technologies have changed, too.

5.6.1 Stent artery wall interaction

5.6.1.a Biochemical response

Restenosis, which is defined as “the arterial healing response after injury incurred during transluminal coronary revascularization”, has been the principal drawback of percutaneous coronary interventions (PCI) since their introduction nearly 25 years ago.

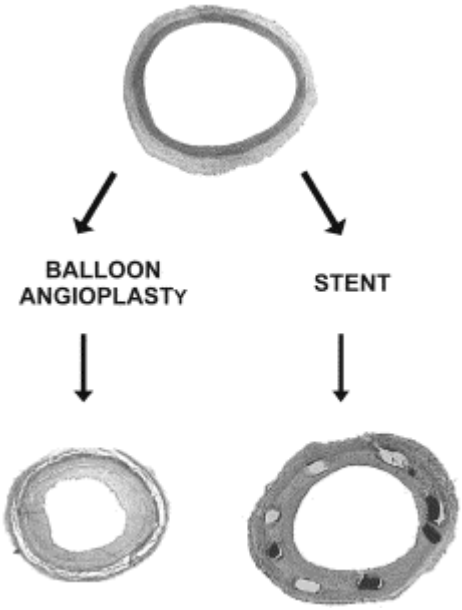

Fig.I.29_ Mechanisms of restenosis after balloon angioplasty and stenting. (Left) The mechanisms responsible for restenosis after balloon angioplasty are mainly the negative remodeling of vessel that accounts for 75% of the phenomenon and the proliferation of smooth muscle cells with neointima formation that represents the other 25%. (Right) In-stent restenosis is 100% due to smooth muscle cell proliferation; remodeling of the vessel does not occur.

An increasing body of evidence suggests that inflammation plays a pivotal role in linking early vascular injury to the detrimental consequence of neointimal growth and lumen shrinkage [WEL.02]. In this regard, the widespread use of coronary stents has altered fundamentally the vascular response to injury by causing a more intense and prolonged inflammatory state [WEL.02].

5.6.1.b Primary injury

In addition to subacute thrombosis, three additional phases of the vascular response to stenting have been described [EDE.98]. These are inflammation, proliferation, and remodeling. The late loss of lumen following thrombus deposition begins with recruitment of inflammatory cells to the stent struts and between the struts. Within a week after implantation, surface-adherent monocytes infiltrate into the neointima. Proliferation of smooth muscle cells and inflammatory cells reaches its peak after 7 days and continues for weeks after. The remodeling stage begins after approximately 3 weeks and is characterized by collagen deposition in the adventitia and media. The response is undoubtedly related to the injury to the artery wall, that includes endothelial denudation, disruption of the elastic laminae, and injury to the medial smoothmuscle cells. These acute effects are then followed by the chronic force of the stent on the artery wall. Once the initial, acute injury to the artery wall associated with stent deployment has occurred, a following in-stent restenosis mechanism takes place and can be explained by two phenomena. At first, the remaining forces on the arterial wall due to chronic stent implantation play an important role in determining how the artery heals itself. Secondly the placement of a stent in an artery affects the details of flow adjacent to the artery wall and modifies the global flow pattern. Both mechanisms require close attention.

5.6.1.c Mechanical behaviour of the artery

The placement of a stent inside an artery has profound implications on the stresses in the artery wall. Balloon expandable stents are typically deployed with balloon pressures of up to 15 atm, or more than 100 times a mean blood pressure of 100 mmHg. Given that it takes this much pressure to deform the stent out to the diameter of the artery, balloon expandable stents behave very nearly as rigid structures inside the artery. The outward force of the stent against the artery creates large, nonphysiologic stresses on the artery wall. In the case of self-

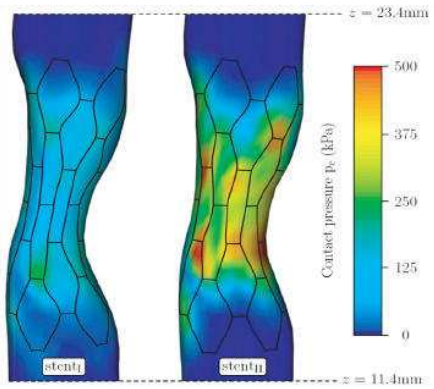

Fig I.30_ Distribution of the contact pressure after complete deflation and removal of the balloon catheter. Pressure distribution are shown for the Stent I (with strut thickness 0.1mm) and or stent II (with strut thickness 0.15mm)

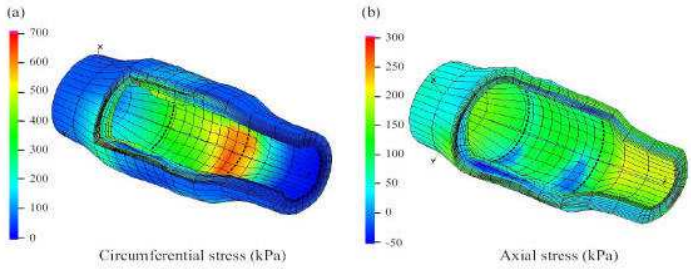

Fig.I.31_ Circumferentiel (a) and axial stress distribution (b) for a human stenotic artery at an intraluminal pressure of 13.3kPa after stent deployement. At the stent edges, indicated by dashed lines, local stress concentrations occur.

expanding stents, the additional elasticity of the stent may reduce these stresses slightly, but the fact remains that there is a chronic action/reaction contact stress between the stent and the artery wall. The analysis of stented artery wall stresses is impeded by the complexity of the artery wall, and the inherent difficulty in solving contact mechanics problems. The artery wall is a nonhomogeneous, nonisotropic, nonlinearly elastic structure that undergoes large deformations even in the absence of a stent. Stent counteracts the inward tendency of the artery contact mechanics problem complicates the analysis of stented arteries even further. A relatively simple model of stresses in a stented artery wall showed that the abrupt change in mechanical properties at the ends of the stent creates zones of intense stress concentration [MOH.00]. In another study, a finite element model of an artery wall into which a Palmaz stent or CMS (Compliance Matching Stent) had been deployed was constructed using a commercially available software package [BER.02]. The stents were given properties representative of stainless steel, while the artery wall was modeled as a thin shell with linear elastic properties. The stresses near the ends of the Palmaz stent reached 5.5 N/mm². The CMS design resulted in a much lower stress at the ends of the stent, provoking a peak stress of 1.5 N/mm².

Rogers et al. [ROG.99] constructed a computational model to estimate the stresses on the artery wall during balloon deployment, and found a fairly strong dependence on stent strut spacing. Higher stresses were predicted for higher balloon inflation pressures, larger stent strut spacings, and more compliant balloons. These behaviors were related to the ability of the balloon to conform to the backward facing step geometry, and the distance between adjacent

struts. They included in vivo evidence that endothelial cells remain in the areas adjacent to the stent struts where the balloon should not be in contact with the artery wall. This implies that direct stenting may have an advantage over angioplasty followed by stent deployment. The adaptation of the artery wall to stent-induced stress concentration was modeled in a theoretical study by Rachev et al [RAC.00]. Their model allowed the artery wall to build up additional tissue in response to increased stress until the stress returned to some threshold value close to the stress in the unstented portion of the vessel. Following adaptation, the artery wall thickness was greatest at the stent edge, and decreased monotonically away from the stent. Their results were similar to neointimal growth patterns observed in vivo [HOF.97], [HOF.96].

All the previously described works showed that the stent implantation induces a high stress increase in artery wall. The relationship between that stress concentration and the in-stent restenosis can be well established with what is currently known about how artery builds tissue up. It is known that healthy arteries exhibit stress concentrations in sites where intimal thickening is greatest [DEL.97]. It has also been shown that arteries increase their thickness near the suture lines of end-to-side anastomoses to reduce stress concentration [BAL.98]. Arteries have also been demonstrated to adapt their structure and composition to even out stress distributions following induction of hypertension [HUM.02]. The artery wall is thus an ‘‘intelligent’’ structure that adapts to reduce stress concentration. It could be that the large, non physiologic stresses created by stent deployment are too great to allow successful adaptation in every case. Restenosis may be the unfortunate result of the artery’s attempted adaptation. Supporting the potential role of stress concentration in restenosis is the fact that many of the problems with restenosis occur at the ends of the stent.

The artery wall reaction was studied in vivo by Vernhet et al.

Vernhet et al. performed an in vivo experimental study [VER.00] to evaluate changes in mechanics after endovascular stenting in small diameters arteries. Using a surgical right femoral approach, self-expanding stents (Wallstent®, Schneider, Switzerland) were placed in the infrarenal aorta of five New-Zealand white rabbits. Blood pressure changes were monitored in the aorta. Blood flow velocity was measured with a 20MHz pulsed Doppler probe and the Pulsatility Index (PI) was calculated. Aortic diameter and diameter changes were measured with a 20MHz probe in echo-tracking mode. This study demonstrated that arterial wall compliance and distensibility decreased at the stent level, and were then significantly lower than upstream and downstream. There was no significant change in PI.

Further tests were done on human.

Human atheroma differs from the minimally calcified atheroma induced by diet and intimal abrasion in New-Zeeland rabbits. Subsequent differences in wall mechanics may be expected. Vernhet et al. evaluated 15 patients 3 months or more after placement of a Carotid Wallstent® (Schneider, Bülach, Switzerland) in the extra-cranial carotid artery for the treatment of significant carotid stenosis [VER.03a]. B-mode ultrasound examination was performed with a 7.5MHz probe on the stented carotid artery and on the contralateral internal and common carotid arteries. Carotid diameter and systolic diameter changes were measured using a dedicated image processing system, while pulse blood pressure was measured. The evaluation could be completed in 8/15 patients. Compliance was significantly lower at the proximal, mid, and distal stent level, than upstream, downstream or on the contralateral internal and common carotid artery. Stenting pathological human carotid arteries induced a compliance mismatch between the native carotid artery and the stented segment. Although the underlying diseases (atherosclerosis, radiotherapy, dysplasia) may, to some extent, reduce arterial wall compliance and distensibility, the dramatic additional decrease in compliance and distensibility after stenting always resulted in a marked compliance mismatch.

Further long term testing were performed as well.

Vernhet et al. evaluated long term wall mechanics changes and related histopathologic changes induced by stent placement in small diameter arteries [VER.03b]. They found that endovascular stenting of the rabbit aorta impairs wall mechanics and that performing 30% stent over dilatation does not worsen this impairment but induces greater intra-stent intimal hyperplasia. A marked decrease in wall distensibility was observed immediately after stent deployment at the stented arterial segment and was a chronic, long-lasting phenomenon. Long-term mechanical adaptative changes of the host artery were found upstream from the stent. The increase in distensibility upstream from the stent could result from flow stagnation induced by compliance mismatch at the junction between the host artery and the extremity of the stented artery.

Therefore, endovascular stenting produces a significant decrease in arterial wall compliance and distensibility of the rabbit abdominal aorta.

5.6.1.d Flow pattern modification

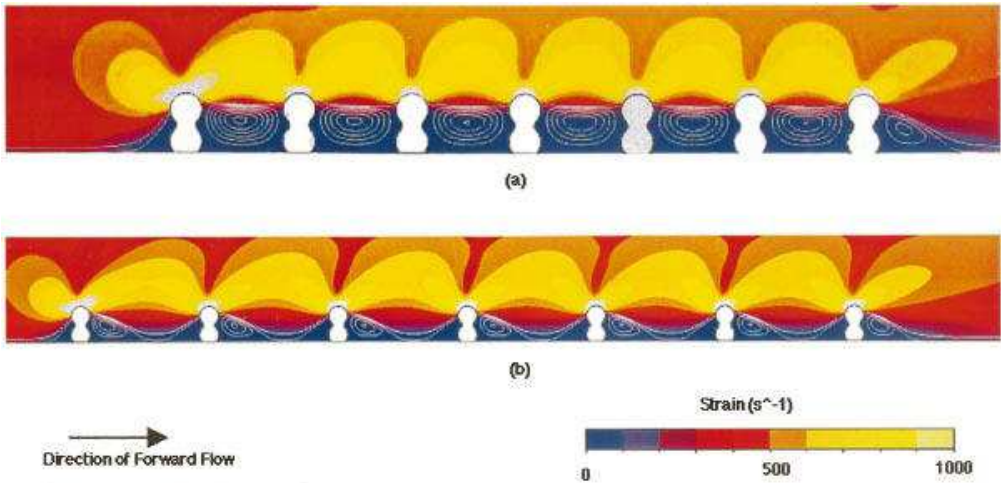

Fig I.32_ Shear rate (1/s) contours for two case with different struts spacing and thickness. Instantaneous streamlines are included as white lines in all views. The lowest shear rates were observed in between the wires and the highest shear rates were located at the tops of the wires in all cases. The zone of low shear rate extends farther at the distal end than at the proximal end.

A typical stent strut is approximately 0.15 mm in thickness, and stents are deployed into arteries at least 3 mm in diameter. Thus, the direct effects of stent strut protrusion into the lumen are confined to a region close the artery wall. The protrusion of the stent strut into the lumen of the artery corresponds to well-known flow situations from aerodynamics classified as flow over backward or forward facing steps [ROC.98]. In a backward facing step flow, the momentum of the fluid flowing over the step carries the fluid past the corner of the step, creating a region of flow separation. Under steady flow conditions, the fluid contained in this region does not mix with the fluid in the mainstream, thus there are implications on the transfer of blood-borne substances in these regions adjacent to stent struts. In a forward facing step flow situation, the step inhibits the forward movement of the fluid adjacent to the strut, creating a separation zone. The separation zones associated with forward facing steps are typically smaller than those associated with backward facing steps. The placement of a stent against the artery wall creates a series of adjacent backward and forward facing steps that may interact with one another. It is important to note that the stent struts are covered with thrombus within a few hours or days following implantation. Thus, the use of backward and forward facing steps to describe blood flow over stents is only applicable in the acute stages of implantation. There is some evidence, however, that the stent geometry is still represented in the neointimal development patterns even weeks after implantation [TOM.92]. The effects of stent strut spacing on blood flow patterns adjacent to the artery wall have been studied using computational flow dynamics techniques. These techniques have the advantage of

producing accurate information on all flow variables velocity, pressure, shear stress, etc very close to the artery wall. Experimental techniques such as laser Doppler anemometry, particle imaging velocimetry, and Doppler ultrasound all suffer from significant uncertainties when measurements are being taken within the small distances close to the wall that correspond to stent struts. The flow patterns near the struts of a Wallstent were found to depend strongly on the strut spacing [BER.00]. The Wallstent is a braided wire mesh self-expanding design. Using a commercially available CFD software package, a two-dimensional model of the wire crossover points was constructed. The bottom stent wire was assumed to be embedded by 30% of its diameter into the artery wall. Physiologic flow conditions corresponding to resting and mild exercise in the coronary arteries were applied. The flow patterns were demonstrated by plotting instantaneous streamlines and shear rate contours. Within the range of geometric parameters used to construct actual Wallstents for clinical use, the flow patterns were found to vary tremendously. With smaller stent wire spacings less than six wire diameters, the stagnation regions from adjacent struts merged together for the entire cardiac cycle, creating one single stagnation region (Fig.I.32). For wire spacings larger than six wire diameters, the stagnation regions were split for at least some portion of the cardiac cycle, with the flow reattaching in between.

All these described flow patterns do have some effects on vascular endothelial cells. Different studies demonstrate quite clearly that the flow stagnation patterns produced by stent strut protrusion into the flow stream have an effect on endothelial cell behavior [DEP.92], [TRU.95].

Perhaps the most important aspect of endothelial cell behavior with regard to stents is their ability to regrow over the denuded artery wall, stent, and neointima. In an in vitro experiment with a stainless steel strut embedded flush into a gel surface, Sprague et al. [SPR.97] demonstrated a clear dependence of endothelial cell migration on wall shear stress. They found that the stainless steel surface was 59% covered with endothelial cells after 7 days under static conditions, compared to 87% coverage with a shear stress of 15 dyn/cm² at the same time point. Walsh et al. [WAL.00] have reported results of endothelial cell regrowth patterns in simulated stented flow chambers in which the stent struts protruded into the flow stream. While no growth of the cells over the stent struts was observed over the experimental period of 7 days, lateral migration of endothelial cells was observed to occur at growth rates of approximately 15 mm/h. The initial growth of the cells appeared to be along the stent strut in the flow stagnation zone, with preferential alignment with the stent strut. Once the cells became confluent, the direction of preferential alignment was with the direction of flow.

Simon et al. [SIM.00] noted that the largest areas devoid of endothelial cells were located downstream of trapezoidal surface obstacles intended to simulate stent struts. They also noted that the tops of the obstacles exhibited no overgrowth of endothelial cells when the obstacles were more than 175 mm in height.

The compliance mismatch that occurs at the proximal and distal ends of the stent also affect overall blood flow patterns. The abrupt changes in mechanical properties at the ends of the stent create sites of propagating pressure wave reflection [FOR.01]. These pressure wave reflections, in addition to the abrupt changes in cross-sectional area, lead to large-scale flow disturbances.

These observations led to the design of a stent that provides a smoother transition in compliance at the ends of the stent Fig.I.30. Prototypes of this stent, termed the compliance matching stent (CMS), were machined and deployed in the same in vitro flow visualization system as used in Berry et al. [BER.97].

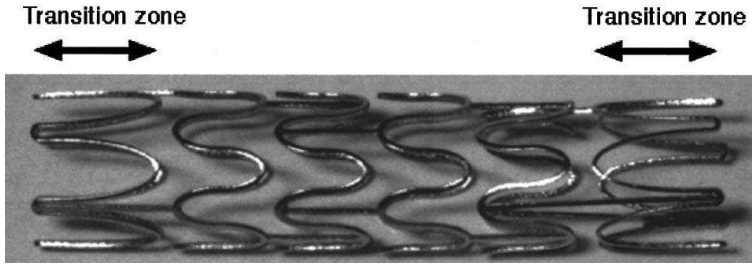

Fig I.33_ Compliance Matching Stent (CMS) profile showing rigid and transition zones

The development of large scale vortices was virtually eliminated. The production of flow disturbances by stents may also occur if the stent is deployed near a branch point and partially protrudes into the lumen due to inaccurate positioning. Stanek and al. [STA.96] showed that Wallstents placed across the ostium of the external carotid artery created additional flow disturbance and resistance.

5.6.2 Stent fatigue

With a few exceptions, stents in current clinical use are manufactured using various metals and metal alloys. Once implanted, stent undergoes cyclic loading related to the pulsatile heart flow and the compliant deformations of the artery wall. This fatigue loading may lead to material damage.

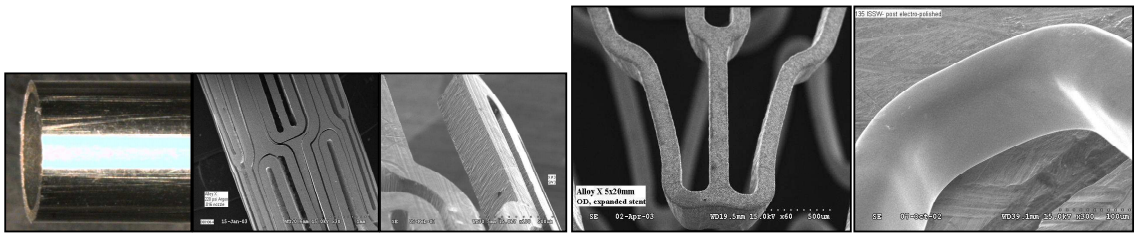

A **B** **C** **D** **E**

Fig I.34_ Manufacturing process for the Guidant ABSOLUTE self expanding stent. Starting from a NiTi hypotube (A), the stent is laser-cut (B) and voids removed (C). The stent is then bead-blasted to remove macroscopic debris (D) and subsequently electro-polished to achieve its final high quality surface finish (E).

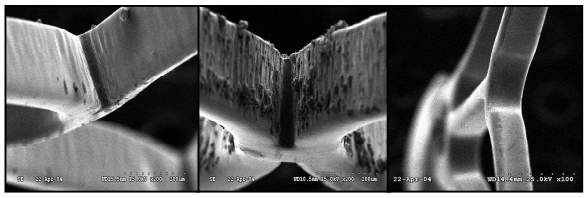

A **B** **C**

Fig I.35_ Two commercially available stents (A & B) and the ABSOLUTE stent (C) are shown under electron microscopy. The micrographs reveal dramatic differences in stent surface finish, indicative of the manufacturing process for each stent.

The stent pattern is cut from a NiTi hypotube using a precision motion controlled laser beam. The surface immediately adja-cent to the laser path, having been molten by the laser and resolidified, is now embrittled, containing substantial amount of debris created by the lasing process (Figure I.34C). This narrow surface zone is commonly termed the “heat-affected zone”. Subsequent to laser cutting, the stents must be bead-blasted to remove large debris created by the laser and then electropolished to a high degree. A representative image of the final surface finish attained in the ABSOLUTE stent can be seen in Figure I.34E.

A close examination of various commercial stents reveals dramatically different surfaces, indicative of which process was or was not employed during manufacturing. Electron micrographs of two stents available on the market (termed Stent A and B) are shown in Figure I.35. The ABSOLUTE surface finish is shown in Figure I.35C. Aside from the obvious visual differences, these surface finish variations can manifest themselves as dramatic differences in stent fatigue life. In the absence of extensive electro-polishing, micro-cracks and defects can remain on the surface, serving as initiation sites for crack propagation.

5.6.2.a In vivo cases

Indeed cyclical stress applied to any metallic structure and, more specifically, to a NiTi stent, may cause a progressive propagation of surface micro-cracks. In this process, the healthy portion of the cross-section (so called “resistant section”) gradually decreases in cross-sectional surface area, reaching a point where it is no longer able to keep the structure together and catastrophic fracture failure finally happens. Figure I.36 illustrates the process of crack propagation on a cylindrical metallic component.

Fig I.36_ Electron micrograph of a thin slide at the bottom of a V strut connection in a commercially available product, revealing a heat affected zone (light grey area) inclusive of numerous surface micro-tracks.

This phenomenon led to stent breakages observed in vivo. However only few cases of stent breakage have been reported in the literature given the large numbers implanted in different parts of the body. In the iliac artery, Sacks [SAC.96] reported a fractured Palmaz stent in a patient into whose common and external iliac arteries three Palmaz stents had been implanted in the course of a bypass operation. The explanation offered by the author is that the stent was fractured during deployment as a result of a combination of its rigidity, heavy local calcification, and because it was overlapping with another stent. Babalik [BAB.03] reported a case of a fractured stent in the popliteal artery in a patient with a limp secondary to major stenosis of the upper popliteal artery. The fracture was explained as being due to damage to the stent resulting from flexion of the knee and external compression. Similarly, Kroger [KRO.04] reported on three fractured stents in the popliteal artery, treated by by-pass surgery. Duda [DUD.02] observed six stent fractures in 33 patients (18.2%) in a study (the SIROCCO trial) designed to compare the permeability of Sirolimus coated and uncoated stents implanted to correct obstruction of the superficial femoral artery. According to the author, these

fractures were due to the length of the arterial segments treated and to the partial overlap which results in the generation of movement induced "hinge points".

Subsequent to these observations a larger study of Nitinol stent fracture in the superficial stent artery (SFA) was conducted by Allie et al. [ALL.04]. The authors investigated stent fracture in 110 patients out of 380 in whom a nitinol stent had been implanted between January 2000 and July 2003. Angiography was used with fluoroscopic analysis of the fractured stent, using the Cardiovascular Institute of the South classification system :

- Type I : Fracture of a single filament.
- Type II : Fracture of several filaments at different places.
- Type III : Fracture of several filaments leading to complete transverse fracture without fragment displacement.
- Type IV : Complete transverse fracture with fragment displacement.

Of 110 patients, 72 (65.4%) had a fractured stent with a mean lesion length of 17.5 cm (6-34 cm), a mean number of stents of 2.3 (1-5), and an average interval until the angiography examination of 11 months (2-34). There seems to be a link between the size of the fracture and its clinical and hemodynamic impact (Table I.37).

Type of stent lesion	N= 72	Stenosis > 50% or obstruction	Clinical impact
Type I	27 (37.5%)	17 (62.9%)	7 (26%)
Type II	32 (44.4%)	26 (81.2%)	15 (47%)
Type III	11 (15.2%)	11 (100%)	9 (82%)
Type IV	2 (2.7%)	1	2 (100%)*

Table I.37_ Type of the stent lesions reported by Allie [ALL.04]

6 HEART VALVE PERCUTANEOUS IMPLANTATION

6.1 What are the needs ?

Calcific aortic stenosis ist the most common valvular disease observed in western countries. Alone in the US, it has been estimated that between 2 -3 % of the elderly population have calcific aortic stenosis, while 1 to 2 % of Americans have congenital bicuspid aortic disease [DAV.06]. Worldwide, aortic valve replacement represents today around 250000 cases and that number is expected to increase by 5 % per year over the coming years. From a survival rate point of view, surgical valve therapy has an enviable track record. In the UK Heart Valve Registry for example, the mortality rate for aortic valve replacement in octogenarians is still only around 6.5 % at 1 month and 10 % at 1 year. These statistics, that are nearly the same in all the western countries, remain globally low and show that heart valve surgery is a sustainable technology. Among the diseased patients, however, 10 % are considered high risk and approximately 15% are declined by the patient or the physicians [MED.05]. These critical cases are at first elderly people with multiple pathologies, most of whom require replacement of the aortic valve due to calcification or degeneration. Some of these patients are too ill or weak to withstand the stress of open heart surgery. The second critical population is the children, since many of these patients require heart valve replacement due to congenital heart disease. Some of these children are not treated until they are older because it is difficult to find a heart valve small enough for them, or because multiple highly invasive surgeries will be required to replace the valve as they grow. More generally, those patients with severe ventricular dysfunction, low gradient / low output states, cardiogenic shock and/or significant morbidities such as diabetes chronic kidney disease or extra cardiac arteriopathy are at the greatest risk for standard surgery. Unfortunately, the spectrum of potentially successful treatment options for inoperable valvular diseases is today limited.

6.2 History

Because of the limited therapeutic options in patients deemed at high surgical risk, there has been interest in the development of a less invasive method to restore valve function already in the 1980’s. Balloon aortic valvuloplasty (BAV) was developed in the 1980s with the hope of enlarging the valve orifice percutaneously. Aortic valvuloplasty, consisting in the enlargement

of the stenosed valve thanks to balloon inflation, may offer temporary improvement in symptoms and some survival benefit in select non surgical patients with aortic stenosis, but it does not improve long term outcome. The mainstay Balloon Aortic Valvuloplasty (BAV) is a non-durable treatment with most patients requiring repeat BAV within eighteen months. Life expectancy after BAV therapy is less than 2-3 years. This situation must lead scientists, surgeons and cardiologists to consider as unacceptable that critical patients, left on side from standard relief possibilities, are not proposed any durable alternative. Non invasive surgery may become the treatment of choice for these critical people, Moreover, the number of patients inoperable with surgery, will grow with life's expectancy increase. The need for PVT (Percutaneous Valve Technology) will consequently develop. At last, another justification for PVT development is that valve surgery is resource-intensive and therefore limited or not available in many parts of the world.

The history of PVT begins with the first pulmonic balloon valvuloplasty proceeded by Kan in 1982 on pulmonary valve [KAN.82], [CRI.86]. The technique was first tested on with success. The test on aortic valve was run in 1987. This technique improved the valve area only minimally, although there was modest acute hemodynamic and symptom improvement. Serious complications occurred in ≥5% to 10%, and restenosis with clinical deterioration occurred within 6 to 12 months in most patients. Furthermore, BAV did not provide any survival benefit over medical therapy. Currently, BAV is only recommended (American College of Cardiology/American Heart Association) as a bridge to surgery or as a palliative measure in those too ill to undergo surgical AVR. The development of percutaneous surgery is directly related to the development of stents. With technological advancements in the field, an alternative to surgical AVR (Aortic Valve Replacement), PAVR (Percutaneous AVR) has emerged.

This concept was first demonstrated by Andersen et al [AND.92] in 1992, who delivered a porcine bioprosthesis attached to a wire-based stent at various aortic sites with satisfactory hemodynamic results. Early pig studies demonstrated important haemodynamic improvements with the use of a bioprosthetic valve implanted within a wire based stent at assorted aortic sites via catheter technique [AND.92]. This led finally to other large animal studies and finally to human subjects.

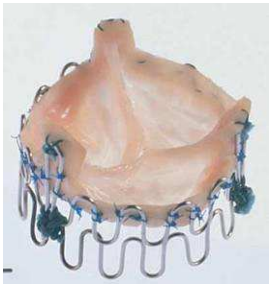

Fig I.38_ Andersen valved stent

The first in man implantation was done by Bonhoeffer et al. in pulmonary position. The team performed PHV replacement in children with congenital heart disease in a stenotic right ventricle to pulmonary artery conduit and reported in the year 2000 [BON.00a], [BON.00b].

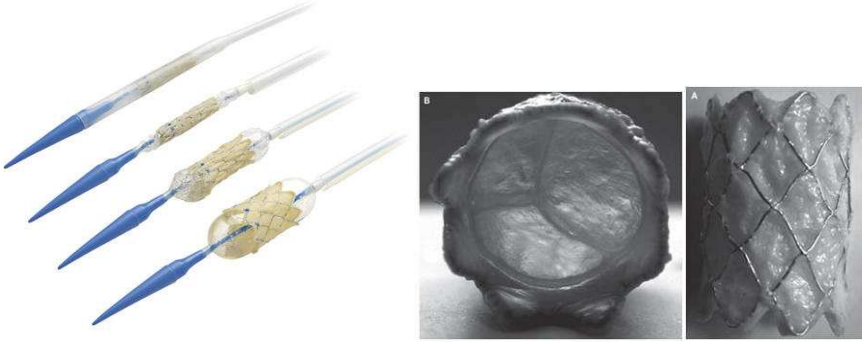

Fig I.39_ Bonhoeffer valved stent. Left: expansion of valved stent in the delivery system. Right: profile of the valved stent before compression.

Subsequent reports by Boudjemline and Bonhoeffer described percutaneous implantation of the aortic valve in animal studies and similar work by Lutter et al highlighted the problem with subcoronary position and potential risk of damage to the mitral valve in animal models [BOU.02a]. Two years after, Cribier et al [CRI.02] reported the first successful human PAVR. They performed the first PAVR in a 57 year old man with severe calcific stenosis (bicuspid valve), cardiogenic shock, and peripheral vascular vascular disease in whom valvuloplasty was performed without benefit. Various groups have now reported their early experiences with balloon and self expandable Percutaneous Heart Valves (PHVs).

The design of percutaneous implantable PHV is a promising alternative to valvuloplasty. Currently available prosthetic valves provide a valve area of >1,5 cm^2 which is a marked improvement over the maximal 1,1 cm^2 provided by valvuloplasty alone [VAH.04].

6.3 State of the technology

There are currently as many as 17 PAVR programs in active research, and among those, there are 2 PAVR prostheses in clinical trials, at least 7 more with FIM (First in Man) implant results, and others at different stages of investigation.

6.3.1 Protheses in clinical trials

Two devices are today mature enough to be used clinically, and approved by health authorities, the Edwards-Sapien (Edwards Lifesciences) and the CoreValve Revalving System (CoreValve Inc). Both stents are made of self expanding material. The valves associated with the stents are bioprostheses.

6.3.1.a The Edwards PVT

The Edwards PVT stent geometry is a cylinder, like for any other classic vascular stent. Its design is not specifically adapted to the aortic root environment (Figure I.40).

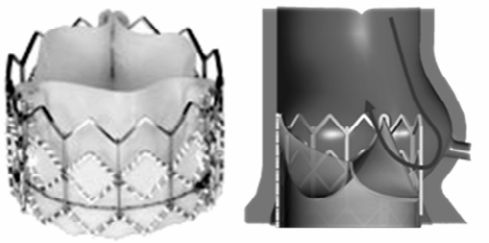

Fig I.40_ Edwards stent and blood flow disturbance in aortic sinuses

The stent is maintained in position thanks to a radial expanding force. The surgical implantation reports show that with higher stent diameter (leading to higher radial force), the device is better maintained in the aortic root. This observation suggests that the implant requires high expanding force to keep its position. An excessive force may however induce exaggerated stress in the tissues, directly related to higher calcification rate. So even if the Sapien stent is to be implanted in already highly calcified environment, high expansion force may degrade more rapidly the non calcified tissue that may be left.

The Cribier experience uses a balloon expandable technology. The balloon-expandable PHV consists of 3 pericardial leaflets, initially equine (Cribier-Edwards) and currently bovine

(Edwards-Sapien) (Edwards Life Sciences Inc, Irving, CA), mounted within a tubular, slotted, stainless steel balloon-expandable stent. Initial devices were 14 mm in length and 23 mm in expanded diameter, with a larger device available subsequently (length 16 mm, expanded diameter 26 mm). Current devices require either 22F or 24F (transfemoral) or 26F (transapical) sheath for delivery. Balloon aortic valvuloplasty is performed using standard techniques. The balloon mounted valve is then placed within the aortic annulus, and optimal positioning is aided by fluoroscopy, aortography, and transesophageal echocardiography. Because of the large delivery system, a surgical cutdown and repair of the vascular access site are still often required. In addition, as the inflatable balloon used to deliver the prosthesis tends to be propelled forward by the blood flow from the LV, flow arrest is required to accurately deploy the PHV at the annular level. This is achieved by rapid right ventricular pacing at rates of approximately 200 beat/min, using a temporary pacemaker. The entire process requires synchronization among the team members to avoid prosthesis misplacement during deployment.

Initially the experience concerned 6 patients (5 male + 1 female) aged 75 +- 12 years suffering severe aortic stenosis and multiple comorbidities who were unsuitable for surgery as determined by cardiac surgeons. 4 out of 6 suffered also from severe aortic regurgitation while mitral regurgitation was present in five patients. These patients had a mean aortic valve area of less than 0,6 cm^2, and a transvalvular pressure gradient less than 50 mmHg. The antegrade trans-septal approach was adopted, and the procedure took a mean of 134 minutes to perform. One patient who suffered from previous aortic aortic balloon valvuloplasty-induced tear died during delivery at the time of full PHV balloon inflation. Between weeks 2 and 8, 3 patients died from non cardiac complications. The last two patients were stable and showed no signs of heart failure. All patients experienced improvements in mean gradient (7.4 mmHg) and AVA (1.63 cm^2) post implantation. However, following implantation, aortic regurgitation was seen in all patients and may have been caused by imperfect apposition of the PHV stent frame against the diseased native valvular structures at the site of calcific nodules. Colour flow Doppler studies revealed mild transatrial shunting in all patients [CRI.04].

A further implantation study (2004) was reported by Cribier with 33 patients (mean age 80+-7 years) with severe aortic stenosis. Both antegrade (26 patients) and retrograde (7 patients) were used to deliver the Cribier-Edwards PHV. However, different difficulties were met at implantation time: 1_Stent migration (2 cases), 2_Intolerance to guidewire across the mitral valve (2 cases), 3_Stent-mounted catheter was too short to reach the aortic valve (one case),

4_Extensive calcification prevented retrograde crossing with the delivery system (2 cases). Finally, 26 patients were successfully implanted. Results showed 30% reduction in mean transvalvular aortic pressure gradient and 1,7 cm^2 AVA after procedure. The procedure was followed with complications for 5 patients (hypotension, heart block, urosepsis, cardiac tamponade) within 2 weeks after procedure. Further deaths due to non cardiac problems over a 24 months follow up, brought the survival rate to 30% with 11 still alive.
Further studies were conducted by Bauer et al [BAU.04] and by Webb and colleagues [WEB.06] reporting the implantation of the Cribier Edwards PHV. From this studies it can be concluded that PHV implantation in patients with severe aortic stenosis, has the potential to provide immediate improvement to patients as evidenced by AVA and pressure gradients improvement. The authors reported however, some complications associated with the PHV implantation : difficulty to pass through atherosclerotic artery, porcelain aorta, ventricular fibrillation, iliac perforation, left coronary obstruction (by displaced native aortic valve leaflet), calcified valvular nodule obstructing the left main coronary artery.

6.3.1.b The Corevalve

The second stent concept already clinically implanted is presented by CoreValve Inc. Its geometry presents the advantage of being designed as to prevent any migration risks. The stent is therefore enlarged at its upper level (Figure I.41).

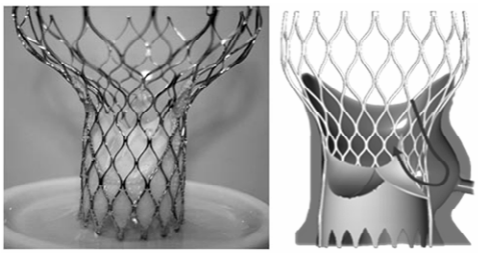

Fig I.41_ Corevalve stent and blood flow disturbance in aortic sinuses

It is also to be noted that the diameter is slightly reduced at the level of the Valsalva sinuses, in order to prevent coronary ostia flow obstruction. The geometry of this stent underwent some changes over the last two years. Figure I.42 represents the previous design versions of the today existing stent. This shows that the optimization process has already started in heart valve stent design.

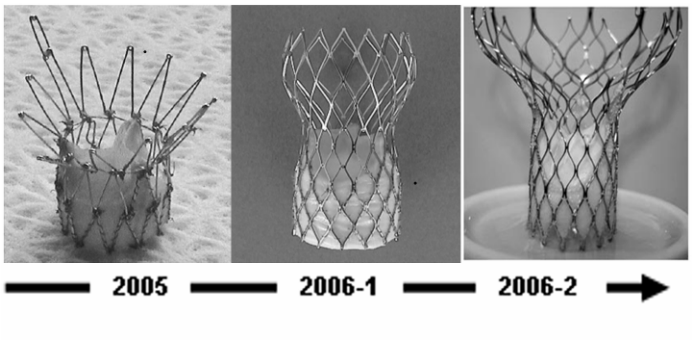

Fig I.42_ Corevalve design evolution (2005-2006)

However, as well as in the case of the cylindrical Cribier stent, the mechanism that maintains the stent in position is based again on exaggerated deformation of aortic tissue.

Grube and colleagues investigated the effects of the CoreValve, a self expanding PHV that is able to conform to the dimensions of a person's aorta and aortic valve [GRU.06]. In their study the authors implanted the CoreValve using the retrograde approach in 25 patients aged 80.3 +- 5 years who had peak transvascular aortic pressure gradient of 69.3 mmHg and a mean aortic valve area 0.72 cm^2. If 21 out of 25 patients had procedural success following complications were observed: paravalvular leakage (prosthesis not deployed deep enough within the native valve), device could not cross the heavily calcified native valve, pericardial tamponade, wire perforation of teh left ventricle, hemodynamic failure, non cardiac sepsis. Finally, none of the 18 remaining patients in whom the device was successfully implanted had an adverse event within the 30 day follow-up after leaving hospital.

6.3.1.c Conclusion

Both solutions were developed considering the recipient patients as critical, with highly calcified aortic root. The positioning of both devices is based on high radial expansion force and the geometry of the aortic root environment was not considered in their design. Indeed, the axial positioning along the aortic root as well as the placement of the valve cusps in front of the Valsalva Sinuses remains hazardous for both devices.

6.3.2 Other designs in development

Device (company)	**Valve material**	**Stent material**	**Expansion Mode**	**First in Man**	**Catheter French size**
Paniagua (ETR)					
	Pericardium	Stainless steel + Nitinol	Ballon expandable + Self-expandable	2003	Balloon=16 Self=12
Enable (ATS (3F))					
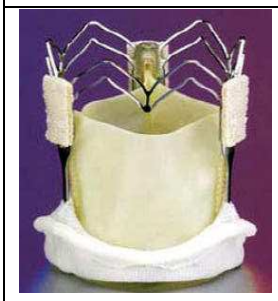	Pericardium	Nitinol	Self-expandable	2005	Not applicable
Aortx (Hansen Medical)					
 	Pericardium	Nitinol	Self-expandable	2006	24

Direct Flow (Direct Flow Medical Inc.)					
 	Pericardium	Polymer	Polymer-injected	2006	22
Lotus (Sadra Medical)					
 	Pericardium	Nitinol	Self-expandable	2007	21
JenaValve (JenaValve Techn.)					
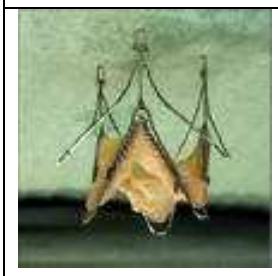	Pericardium	Nitinol	Self-expandable	2007	Not applicable
Perceval (Sorin Group)					
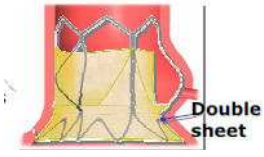	Pericardium	Nitinol	Self-expandable	2007	Not applicable

					
Heart Leaflet (Heart Leaflet Technologies)					
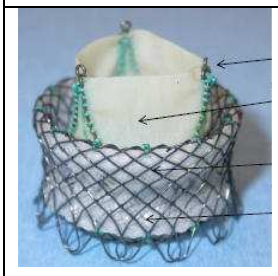	Pericardium	Nitinol	Self-expandable	n/a	16
ValveXchange (ValveXchange, inc.)					
 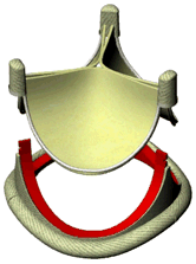	Pericardium	Nitinol	Self-expandable	n/a	Not applicable
Coremove (Zegdi) (n/a)					
	Pericardium	Nitinol	Self-expandable	n/a	39

Lutter (n/a)					
	Tissue engineered	Nitinol	Self-expandable	n/a	Not applicable
PercValve (ABS)					
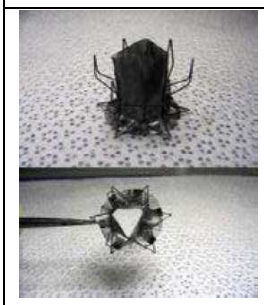	e-Nitinol	e-Nitinol	Self-expandable	n/a	10

Table I.43_ Overview of percutaneous aortic valve endoprosthesis in development

Among the devices listed above, some present specific features that deserve to focus on. If the majority of the designs ensure a stent positioning in the aortic root thanks to a radial expansion force, the Direct Flow and ValveExchange propose other alternatives. In the first case, the stent geometry is obtained by injecting polymer material in an initially empty shape that will match the aortic environment once inflated. The main advantage of that system is that the resulting forces acting on the calcified or non calcified aorta tissues, are reduced to the minimum required to keep the stent in position. Reduced stress in tissues prevent early and premature degradation of the implantation's environment. As for the ValveXchange system, the implantation procedure is close to the one adopted when doing standard valve surgery. Indeed, the system consists of a two-piece valve and the associated tools for replacing the exchangeable component. The permanent component is a surgically-implantable support frame or "docking station" that provides a structurally sound foundation for the exchangeable leaflet set. The size of the implanted support frame is adapted to the size of the aortic annulus, with no excessive stress induced on the surrounding tissues. However, the procedure requires an initial open chest surgery to implant the support frame, and thereof is not a 100% percutaneous solution. It could be imagined for people healthy enough to

withstand surgical procedure. Critical patients denied for surgery would not be candidates for the system.

The design of the Perceval valved stent is also pioneering compared with the others existing in literature. It is the only design that takes into account that stent positioning can be realized not only through expansion force. The stent is composed of two annular elements connected by anchor members. These members match the Valsalva sinus shape. Once positioned, the stent migration risk is thus limited. The main advantage of the design is that the required expansion force is reduced.

The stent is, however, positioned with the sinuses. There are 2 limits associated with that configuration. The first one is that the sinuses must bear the diastolic pressure which will induce high stress in the tissues. The transfer mechanism to the aortic annulus will not occur or be only partial. The durability of the sinus tissue will thereof be limited. Indeed, the annulus is composed of a dense fibrous network adapted to high pressure loading, which is not the case for the sinus tissues.

Another point is that once the stent is positioned, the compliance of the sinus tissue is not well respected. Under cyclic loading, aortic root and sinuses undergo dimensions changes. The geometry of anchor members makes them not very flexible as will be presented later in this work. This lack of stiffness flexibility will probably lead them to shape the sinuses once for all at implantation time, and induce permanent and constant harmful stress in the tissues. At last, the design of the anchor members may cover the coronary ostia.

6.4 Implantation techniques

There have been two approaches for BAV that have also been followed for PAVR : retrograde via the femoral artery and antegrade with transseptal puncture. At the present time, however, the retrograde approach is the predominant choice since it prevents damage the papillary muscles, chordae tendinae and subsequent mitral regurgitation recently reported with the antegrade approach [HAN.05].

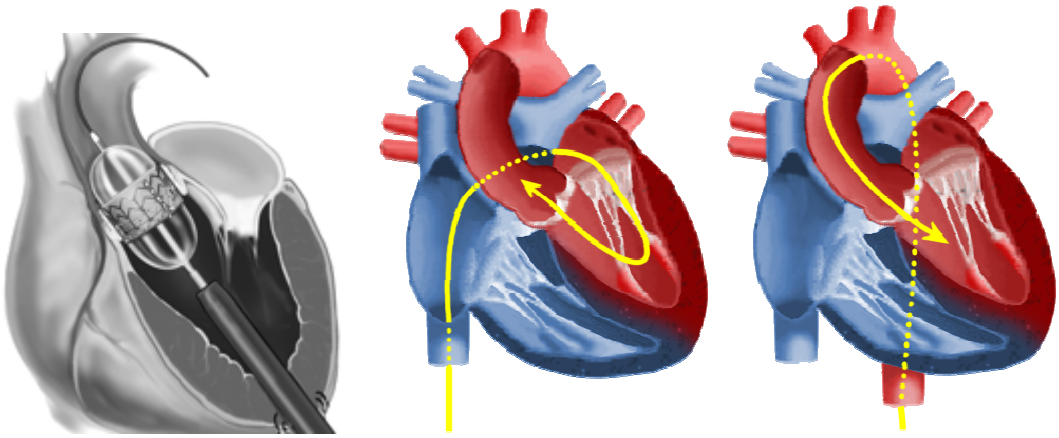

Fig I.44_ apex, antegrade and retrograde approaches for PAVR

Other proposed alternative routes include minimally invasive or thoracoscopic surgery for direct left ventricular transapical (the apex is the conical extremity of the heart ventricle) puncture or access to the descending thoracic aorta [HUB.05]. This latter technique is very hazardous, and requires strong knowledge of the local anatomy of the patient to prevent desctuction of ventricle vital zones.

6.5 Challenges

Whatever the designs adopted for PVT, the technique is still at its infancy. Some huge challenges remain before it becomes a standard valve replacement procedure. We give here a synthesis of these challenges.

The first procedural hurdle concerns vascular access. Valved stents are, by necessity, significantly larger than most existing percutaneous cardiac catheters and devices. The first-generation delivery catheters are in the order of 22–24 Fr, requiring direct femoral, iliac, or axillary arterial access via surgical exposure if a retrograde approach is used. While an antegrade transseptal approach may enable percutaneous femoral venous access with some of these devices, the large sheath size may still predispose to vascular injury.

A second design challenge for these devices is the potential for interference with other cardiac structures. Two-dimensional imaging and limited control over the device by the delivery catheter make precise three-dimensional adjustments difficult. Unlike the pulmonary valve, a prosthesis within the aortic annulus has the potential to impede coronary flow, anterior mitral leaflet mobility, and the conduction system [BOU.02b] and [CRI.06]. The current designs rely

on using the native aortic leaflets as a “stepoff” from the coronary ostia; as native leaflets are pushed aside by the stent, a space is created between the stent wall and the sinuses of Valsalva. Nonetheless, this technique can also cause the diseased leaflet to block a coronary ostium or to embolize calcium to the coronary artery [BOU.02b] and [HUB.04]. Stent architecture may also preclude future catheter access to the coronaries for possible interventions. Placement of the valve prosthesis low in the left ventricular outflow tract could impede mitral leaflet mobility, or even cause heart block by impingement on the conduction system. These pitfalls of accurate placement have spawned a next generation of devices that emphasize retrievability and repositioning during deployment.

The third challenge facing these devices is that of secure seating within the aortic annulus. First, the valve must be able to deploy accurately in the nonarrested heart. Initial approaches to this have included rapid ventricular pacing to temporarily suspend cardiac output and the use of peripheral cardiopulmonary bypass to unload the ventricle. Once the valve is placed, it must maintain a stable position within the annulus without risk of embolization. Moreover, while persistence of the native calcified aortic leaflets may provide an advantage as a “spacer” from the coronary ostia, it also predisposes to perivalvar leak. The current devices all have a perfectly round profile, which tends not to seat exactly against the irregular residual calcium. Indeed, a guiding principal of open surgical aortic valve replacement is complete decalcification to insure proper valve seating.

6.5.1 Problems with the leaflet design

Next to the previously described challenges, some problems remain with the design of the valve leaflets. Indeed, to associate a soft leaflet material with an abrasive metallic stent in a collapsed configuration may lead to interface difficulties. The development of percutaneous valve therapy builds on lessons learned from its surgical counterparts for valve replacement and repair. The chemically fixed trileaflet bovine jugular valve used in the first human percutaneous pulmonary valve replacement was studied as a surgical pulmonary valve replacement with a variety of fixation methods. Other percutaneous valves in preclinical investigation as valve replacements include equine pericardial valves and bovine pericardial valves. These chemically fixed xenograft valves, however, also share the set of problems with their surgical valve analogs. Problems include immunogenicity, lack of durability, susceptibility to infection, and the inability of these valves to grow or to self-repair. These

problems are particularly significant for percutaneous pulmonary valve replacements, since the majority of the patients are children or young adults who tend to have more rapid calcification of artificial tissue valves.

6.5.2 Device for native leaflets retrieval

The development of a new stented heart valve design must take into consideration that in a close future, some technologies may be available to remove the diseased valve before prosthesis implantation. Today, some ideas in that field are already published.

6.5.2.a The mechanical approach

In order to adapt the percutaneously implanted stent design to the aortic root environment from a geometrical point of view, it would be especially advantageous if defective heart valves could be percutaneously removed [LUT.02], [CRI.04]. Indeed, placement of a valved stent in the native position when aortic root and valve are calcified is technically very difficult. A procedure could then be carried out endovascularly, using the vascular system to guide the appropriate operation devices to the aortic annulus, and then undertake percutaneous resection of the calcified aortic valve. There are three major reasons for performing resection before implantation : the avoidance of any possible embolization, paravalvular leakage, and a small aortic valve area after sole valved stent implantation. The resection approach has been followed by Lutter at al. The team first developed an in vitro surgical procedure for minimally invasive aortic valve resection [LUT.04]. They were looking for a catheter-based system that would provide a space between the mitral valve and the ascending aorta (aortic valve ablation chamber), in which the native valve can be removed while preventing embolization of remnant particles by a filtering mechanism.

The authors report some preliminary in vitro studies in their laboratory demonstrating the possibility of ablating human calcified aortic valves with three different types of lasers (CO_2, Hol:YAG, and Erb:YAG lasers) [LUT.04]. However, the duration of the laser resection procedures proved unrealistic (>1 h), stimulating the search for new methods.
In 2005 the same authors reported some resection tests done with a high-pressure water stream scalpel, with a maximum pressure of 150 bar. The resection was performed according to 3 different protocols [QUA.05].

At first, human calcified valve leaflets (I) were resected in vitro (Fig.I.45). The cusps were fixed in a rubber band (II) and placed into an acrylic tube (III). Then, the calcified cusps were cut by the water jet scalpel : (IVa) view from beneath before resection ; (IVb) equal view during resection ; (IVc) excised calcified cusp. A polyethylene balloon was positioned just below the rubber band to close off the acrylic tube in one direction. The process was successful. The HydroJet proved comfortable to operate. On average, 0.6 securing balloons ruptured per three leaflets. Macroscopically the cut surface was clean, especially in calcified areas (IVc).

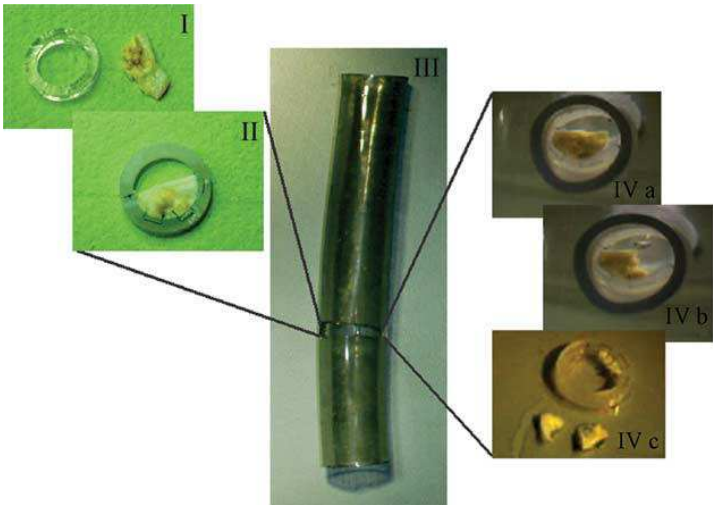

Fig I.45_ calcified valve leaflet resection by water jet scalpel

The second protocol consisted in the resection of healthy porcine aortic heart leaflets in a direct approach (the work was realized on pig hearts). The resection was performed directly on the aortic leaflets with a pressure of 60 bar. After holding them in place by forceps, leaflets were excised completely 2 mm from the aortic annulus. An inflated polyethylene balloon was positioned directly beneath the aortic valve to protect the subvalvular area. The aortic wall, the coronary ostia, the aortic annulus, the mitral valve, and the left ventricular outflow tract were macroscopically and microscopically analyzed for possible lesions (up to 40 mm distance from aortic annulus in any direction). The procedure was easily performed and leaflets were ablated completely. Tissue in the vicinity of the aortic valve revealed small lesions. The aortic annulus was moderately affected in six cases, whereas the mitral valve and the coronary ostia remained untouched. Micropathology of the affected aortic annuli demonstrated superficial lesions with a maximum lesion depth of 1400 and 1600 µm in two

cases, and an average of 460+-215 mm in the other four specimens. No dissection or penetration occured. One securing balloon ruptured.

At last endoluminal resection was performed by a surgeon on ten porcine hearts with an intact thoracic aorta (ascending, arch, and descending). The resection device was manually controlled by a flexible endoscope (outer diameter 5.0 mm, length 600 mm).

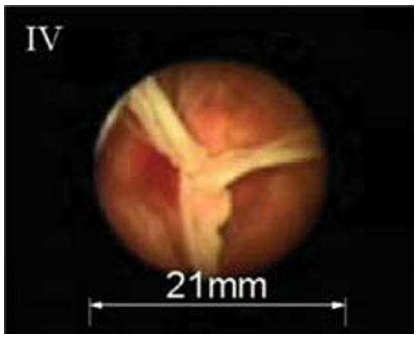

Fig I.46_ endoscopic view onto a porcine aortic valve

The ascending aorta was filled up with mains water. Preliminary studies indicated a need for combined water irrigation and suctioning of the half-closed resection chamber. The leaflets were completely excised, 2 mm from the aortic annulus. Resection tool mobility proved to be smooth and regular no increased resistance was detectable during the movement of the endoscopic tool through the aorta. Endoluminal resection of three leaflets took 12.2+/-0.8 min. Macroscopic examination revealed four superficial lesions in the aortic wall and one on the aortic annulus and the coronary ostium. The mitral valve, and the left ventricular outflow tract remained unaffected. However, the authors report that operating the grab presented difficulties with several attempts sometimes being required before leaflets were securely removed. The authors conclude that such a catheter-based system provides a space between the mitral valve and the ascending aorta, wherein the calcified valve can be removed while preventing embolization by remnant particles using an aortic valve resection chamber. The materials and equipment for such kind of procedure must however be specifically designed to improve the performance. The blood flow stopping remains also a major concern. Even if a femoro-femoral bypass is established to stop the flow in the aortic valve area, some coronary cardioplegia catheters must be blocked in the coronary ostia in order to avoid debris entering.

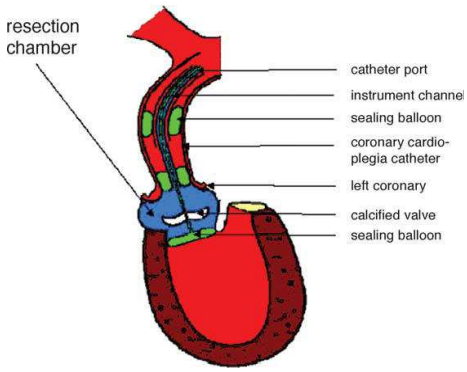

Fig I.47_ The endoscope with resection tools inside were inserted via the descending aorta to excise the aortic valve. A polyethylene balloon was placed directly beneath the aortic valve to protect the subvalvular structures.

6.5.2.b The chemical approach

Next to the above described mechanical approach to excise the calcified leaflets, a chemical approach has been considered by CORAZON. They tested successfully the dissolution of calcium on animal roots. The method has been proven to be faisable but needs some further testing before being applied to human.

6.6 Future of PVT

The promise of PAVR has already been demonstrated in select case. However, fewer than 400 total devices have been placed in humans in 2007. With the current safety and durability records of surgery, the market for PHVR (Percutaneous Heart Valve Replacement) is currently limited to those patients deemed to high risk for surgery. In one European prospective survey 30% of symptomatic patients with valvular disease were deemed to high risk for surgery [IUN.03]. Industry newsletters estimate that the number of percutaneous valve replacements performed by the year 2010 will be about 12000. However, general guidelines for testing new medical technologies begin with a feasibility study in a small number of patients to assess safety and design issues. And today the clinical trial landscape is also still under active discussion; if these percutaneous techniques are to be seen as an alternative to traditional surgical methodologies in low-risk to medium-risk patients, new techniques will need to demonstrate similar hemodynamic effects, safety, and durability to the current highly refined surgical techniques. On the other hand, it may be that the first and best applications of these percutaneous techniques may be in patients at the margins of current surgical indications.

6.7 Conclusion

From the information summarized in this chapter, we can conclude that the future of percutaneous valve repair and replacement depends on : (1) the development of collapsible and compressible valves and stents for delivery and deployment ; (2) advances in biomaterials; (3) anticalcification treatment ; (4) innovative valve to stent bonding technologies. An ideal valve for percutaneous placement should be available in a variety of sizes, biocompatible with excellent intrinsic properties and a low profile. Finally the valve should maintain its properties even after being attached into an expandable stent.

Currently there remain several barriers to widespread use of percutaneous heart valve replacement. First the unanswered question of durability and longevity of the valves remain. Second, the fundamental aspect of this technology that it be inserted in a peripheral vein or artery places certain limitations on the application of this technique in young and small patients as well as patients with either too small or too large outflow tracts. For example, based on the current device designs, the selection of patients for percutaneous pulmonic valve replacement is limited to patients older than five years with a weight greater than 20kg [FIS.04]. The development of more easily compressible and thinner materials will eventually overcome this barrier. Moreover, currently percutaneously inserted aortic valves are inserted within the centre of a predilated resident stenotic valve. In order to perform a true replacement, however, the diseased valve must be ablated and removed [LUT.04]. Finally the area that has the potential for the greatest advances in percutaneous valve technology is probably medical imaging. The surgeon’s ability to view the surgical site directly with their own eyes remains the greatest advantage. In contrast, percutaneous implantation must use medical imaging technology to substitute for direct observation like fluoroscopic visualization, live magnetic resonance imaging techniques [KUE.03] or intracardiac echocardiography. We can conclude that obstacles remain before PVR can be safely used in humans for the treatment of aortic disease.

Chapter II STENT DESIGN AND MECHANICAL BEHAVIOR

1 INTRODUCTION

Classic stents, which proved good functionality for vessel enlargement and non invasive aneurysm treatment, do however not have appropriate geometry for heart valve stenting. Aortic wall anchoring of a classic cylindrical shaped stent, with little hooks associated to a high expansion force becomes very traumatic for surrounding tissues especially when the load (pressure on closed valve) is axially oriented. The dissection of the native aortic valve [THU.81], [SUT.95], [AND.00] shows that the aortic annulus (base of the valve) as well as the commissures (line along which valve leaflet is fixed to the aorta wall) support the valve and transmit most of the applied stresses to the aortic wall. This stress transfer mechanism from the valve to the aorta is generally not respected with stented valve prosthesis but even more disturbed if stresses are transmitted to the wall only through cylindrical anchoring, what may lead to premature environmental tissue degradation [KOR.98] and stent migration. Some works have already been done on the development of better adapted stents and other mini invasive valve support means [BOU.02b], [FER.04], [STA.06]. However, most of them are in some way traumatic for the surrounding tissues. In this paper we present a stent designed in respect to the heart valve geometrical environment as well as in respect to the valve functions.
In this work, we present a stent designed in respect to the heart valve geometrical environment as well as in respect to the valve functions. The aim of the present work is to design, realize and test in vitro a stent positioned and maintained in an aortic environment through geometrical surface matching. The anchoring of hooks in surrounding tissue is thus avoided.

2 THE CONCEPT

In order to position properly the stent in its environment, the native aortic root features, as represented in Figure II.1, are to be taken into consideration.

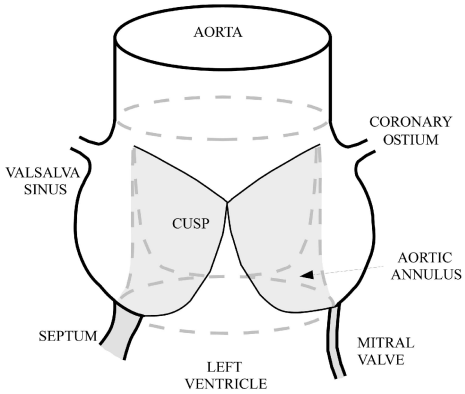

Fig.II.1_ Aortic root features

Coronary ostia and mitral valve impairments should be avoided. Moreover, Valsalva sinuses shape, involved in valve closing mechanism allowing sinus whirl to occur, should be respected. Each valve prosthesis leaflet should therefore face each sinus.

According to these features, following criteria must be considered in the development of the geometry of the stent. The ***aortic annulus*** should bear the diastolic valve pressure loading. The 3 ***Valsalva sinuses*** should help to orient the prosthesis on the aorta circumference in respect to native positioning. At last the ***aorta*** cylindrical geometry should prevent the stent from rotating and keep it oriented in flow direction.

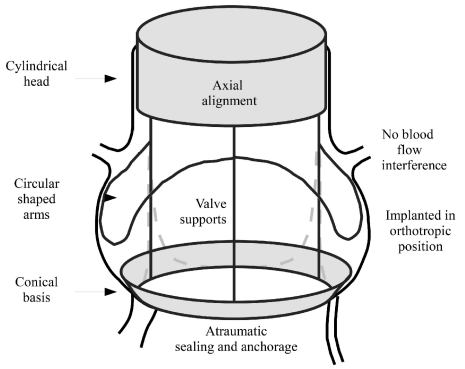

Fig.II.2_ Root-stent matching

In respect to these requirements the adopted stent geometry was defined with 4 main features as represented in Figure II.2, which shows the stent geometry matching the aortic root shape. The stent was therefore composed of 3 straight **posts** which link a **conical basis** to a **cylindrical head** and **3 circular shaped arms** radially deployed. The conical basis will be positioned on the aortic annulus and transfer the diastolic axial valve loading to it. The posts,

are positioned at regular intervals on the conical basis circumference and will hold the valve prosthesis commissures. The head, deployed and centered in the ascending aorta, will prevent the stent from tilting. The arms, one positioned in each sinus, will at last orient the prosthesis around the flow axis while creating a contact zone in the upper sinuses in opposition to the cone. Axially oriented stent movements will thus be prevented in systole.

Anchorage and sealing of the percutaneous valved stent prosthesis are thus ensured by geometrical positioning features rather than by radial expansion force or hooks anchored in biological tissue. Concerning the flow obstruction induced by the stent, even if this issue has not been studied yet in detail, some early comments can be made on some stent particulars. The specific stent arms geometry prevents coronary ostia from obstruction, and should disturb only slightly the diastolic flow in sinuses which contributes to valve closure. Moreover, with no part of the stent located under the aortic annulus, mitral valve is prevented from degradation as well.

As presented in Chapter I, different technologies as well as different materials are available for stent manufacturing. More than hundred different stent designs are commercially available or in development today. The Handbook of Coronary Stents published in 2002 by Serruys et Rensing [SER.02] lists alone 40 conorary stents. We analyze in that section the specificities and material properties of each existing stent configuration, in order to figure out which material and which manufacturing technology is the best adapted to the stented valve realization. All stents are not similar, and the choice of one stent for a specific application, is made in regard to the components properties, the operating conditions and the implantation site. In this chapter we justify the material selection, as well as the dimensions adopted for the prototype manufacturing.

3 THE MATERIAL

Although stainless steel represents historically the most used biocompatible material for stents manufacturing, other materials are today available, which specificities are particularly adapted for non-invasive surgery. These new materials make it possible to realize low profile stents and implantation devices, to create non tubular stents, to control the expansion force acting on biological tissues, to load drugs on the stent, to develop biodegradable stents.

Nitinol material appears to be very useful in the field of non-invasive technologies, as presented in chapter I. Its physical and mechanical properties are especially adapted to catheter implantation technique. The material is characterized with super-elasticity and shape memory effect [DUE.00]. Super-elasticity is the material capability to recover without plastic deformation, after undergoing up to 8 % deformation. This property provides the stent with high expansion rates (ratio between nominal and minimum diameter). Shape memory effect is related to the structural behavior of the material. Crystal network of Nitinol material changes with both temperature and mechanical stress. The material may be in two distinct states. Under a specific temperature defined as transition temperature, A_f, the alloy is in a martensitic phase. Its mechanical properties are poor and the material is easy to deform plastically. Above A_f, Nitinol is in an austenitic phase. Material recovers from the original shaping before heating. When adjusting, at manufacturing level, the A_f value to body temperature, it is possible to provide the stent with specific properties. At ambient temperature, the stent is easy to deform for insertion in the catheter. On implantation site, at body temperature, the stent tends to deploy to its nominal dimension (corresponds to the shape before deformation) and behaves elastically. Expansion occurs until the stent gets in contact with the biological tissues and stops as soon as a balance position is established between the two materials.

We detail in the following the specific reasons why we adopted Nitinol material rather than any other material for our application.

3.1 Self expanding structure

Stainless steel stents are, in general, manufactured at low diameter from laser cutting of a tube. Inserted in a catheter device, they are brought to the implantation site through the venous or arterial network for lumen reconstruction. Expansion is obtained through plastic deformation of the material with balloon inflation. The final obtained dimension is permanent and depends largely on the balloon pressure. Although this expansion process is reliable, it is not adapted to the geometry of the valve stent we develop. Basically, the geometry we give to the stent is not standard because not only cylindrical. It is composed of a conical basis, associated with three arms deployed radially and fixed on posts which support the valve. These shapes could be obtained through inflation process only with difficulties. The method would require the inflation of several specific balloons which could degrade the aortic environment as well as the valve prosthesis [SAV.07]. Moreover, the use of a balloon would increase the volume of material to be inserted in the catheter, increasing the global stiffness of the device, which is not adapted to percutaneous procedure. The use of self expandable material seems hence to be more adapted in our case.

Nitinol stents are self-expandable. This feature is related to the shape memory effect for laser cut stents, and to the hyper-elasticity for braided stents. With self-expandable stents the dimensions of the implanted artery are not dictated by the stent but are the result of the equilibrium between the stent and its environment. With the control of the transition temperature, as well as the forming process, the deployment on implantation site can be controlled as well. Arms can freely deploy in the Valsalva sinuses, and the anatomic specificities of the aortic root environment can be respected.

3.2 Interaction with tissues

The stent's rigidity is an essential parameter to characterize the ability of a stent, first to adapt to the diameter of the implanted zone, and second to follow the dimensions variations of the environment under blood pressure. These performances describe the ability of a stent to interact with the implantation environment. Stents characterized with high rigidity, may not adapt to dimensions variations but allow reconstructing the lumen. On the contrary, stents characterized with low rigidity conform to the geometry of the implantation zone. According to the expected behavior of the stent, rigidity must be adjusted. Rigidity depends both on the material and on the structure of the stent realized. Stainless steel stents are highly rigid. Elastic modulus is around 220 GPa and deformation range is 1 %. This material doesn't make it possible for the stent to adapt to dimensions variations. In our case, it is essential to keep a permanent contact between the stent and the surfaces of the aortic root to prevent any risk of migration. The expansion force should, thereof, be very high, and tissues would be deeply stressed. Although anchoring through high expansion force is of common use, the process is not adapted in a configuration in which tissue stress is expected to be limited. In general, the stents disturb stress distribution in the tissues. Basically, if aortic root compliance, and especially the compliance of the sinuses, is not respected, tissue degradation slowly occurs [THU.86], [FOK.04]. The authors report that the curvature radius of the sinuses evolves over the cardiac cycle for a native valve. Thanks to those dimensions variations, the longevity of the tissues, which adapt to stress level, is increased. Post mortem analyses highlighted the relationship between low curvature radius and tissue stiffening. With a less flexible aortic root, the valve leaflets would undergo higher elongation and decrease in collagen concentration, which would accelerate tissue degradation. At last, the gap between stent and tissue compliance, increases flow disturbances, and promotes the creation of stagnation points where thrombosis may occur [YAZ.04], [BER.02]. Basically, it is essential to keep the aortic root compliance, in order to limit the tissue traumatism induced by the stent. Elastic properties of Nitinol help reaching the goal. The stress level induced with nitinol is always lower than it would be with stainless steel. At deformation rates below 2%, the pseudo-elastic modulus of nitinol is around 25-50 GPa, ten times lower than for stainless steel. Nitinol stents are much more compliant, and conform better to implantation site. In order to better understand the advantage of using a compliant stent, we present in the following a graphic model of the stented root behavior.

3.2.1 Stent-wall interaction : graphic approach

The elasticity of a nitinol stent allows keeping a permanent contact between the stent and its implantation environment. The graphics below represents the interaction between stent and implantation site during and after implantation. Stent and implantation diameter is on 'x' axis, while radial expansion or compression force is on 'y' axis. Materials behavior is assumed to be linear in that approach, which is not the case in reality. Three behaviors are shown : (1) the conduit alone, (2) the stent alone, (3) the stented conduit.

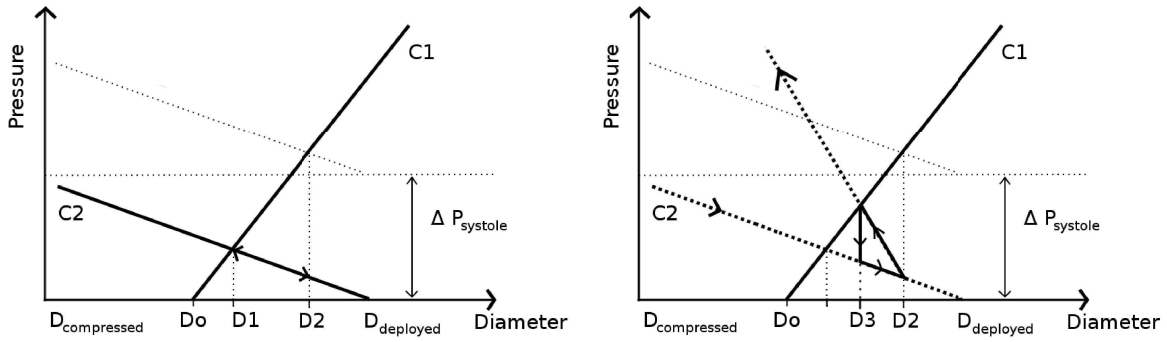

Fig.II.3_ graphic approach of the stented conduit behavior, with and without Nitinol biased behavior

3.2.1.a Behavior of the conduit without stent

The behavior of the native conduit is modeled with curve C1. It is characterized with a D_0 diameter in diastole (rest configuration) and a C compliance (supposed to remain constant). The pressure increase over the cardiac cycle, leads to conduit expansion, which is related to the tissue compliance. Compliance can be defined as the ratio between diameter D variation and pressure P variation.

$$C = \frac{\Delta D}{\Delta P}$$

Under maximal systolic pressure, the diameter of the conduit increases to reach D_{max}.

3.2.1.b Behavior of the stent

The behavior of the stent is modeled with curve C2. Initially compressed at $D_{compressed}$ when inserted in the catheter, stent deploys to reach rest diameter $D_{deployed}$.

3.2.1.c Behavior of the stented conduit

When deployed in the implantation conduit, stent gets in contact with the conduit wall at D_0, but expansion continues until the diameter D_1 is reached, corresponding to the equilibrium between the compressed stent and the extended conduit. When blood pressure increases over the cardiac cycle, conduit further expands and stent follows the expansion and contact is maintained. Indeed, if nitinol deformation rate remains below 1-2%, material behaves elastically and stented conduit diameter varies between D_1 and D_2 over cardiac cycle. It is essential in our application to respect this configuration, to avoid Nitinol hysteresis which appears for larger deformation rates. Basically, if deformation rate exceeds 1-2%, nitinol doesn't behave linearly (Figure II.4). The radial effort applied by the stent on the tissues would be higher in compression than in extension. The diameter of the stented conduit would vary between D_3 and D_2 with $D_3>D_1$. The compliance of the stented conduit would be reduced.

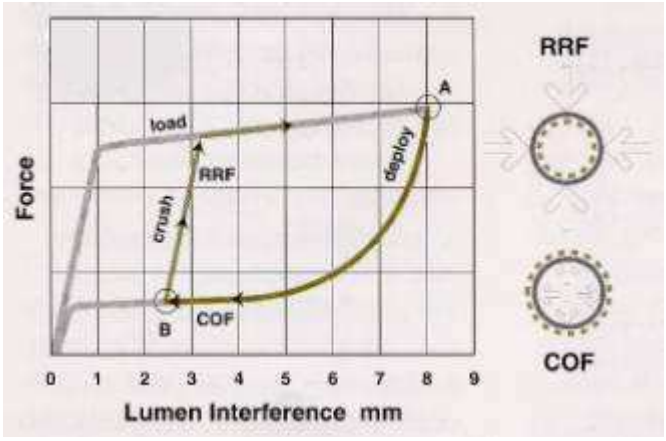

Fig.II.4_ Nitinol hysteresis

3.2.2 Stented valve and Nitinol

The compliance of the implantation site can be respected with a nitinol stent. The stented site can undergo diameter variations over the cardiac cycle even if the native compliance of the aortic root cannot be fully respected. The use of nitinol allows keeping permanent contact between the stent and the biological wall, without excessive stiffening of the wall. The positioning and anchoring of the stented valve in the aortic root is directly dependent on this permanent contact especially at the level of the arm-sinus interface. These compliance properties of the stent must be kept to validate the stent's concept.

3.2.3 Conclusion

The geometry of the stent we develop doesn't make it possible to use balloon inflation as expansion technique. The use of self-expandable material is, on the contrary, appropriate. Moreover, the stent requires permanent contact to be maintained between the aortic root and the different stent's elements. This condition prevents stent tilting and translating, while keeping the aortic root's compliance. Nitinol material is adapted to these requirements. The way how nitinol will be used in terms of stents structure, is detailed in the following section.

4 THE STENT'S STRUCTURE

Stents can be manufactured in two main ways : braided from metallic wires or laser cut from tubes. Depending on the way adopted, the stent’s properties on implantation site are different. To find which process is the best adapted to our application, several parameters are to be considered:

- the stent’s flexibility, i.e. its ability to conform to the site of implantation
- the expansion rate, i.e. the ratio between maximal and minimal diameter in deployed and compressed state
- the cover rate, i.e. the ratio between stent’s geometrical surface and effective surface covered by the metal
- the radial expansion force
- the length

Different stent structures must be compared according to these parameters, in order to select the appropriate one. When considering a coronary stent, its function is to keep open a stenosed lumen. Dimensions variation is not the focus in the application. On the contrary, goal is to prevent stent from collapsing. Laser cut tube is hence the ideal solution in that case. As to the valve stent, it must adapt to the dimensions variations of the aortic root, for efficient valve functioning. The braiding of nitinol wires is the right solution in this case. However, the stent is composed of 4 separate elements, which play a specific role each : cylindrical head, conical basis, arms and posts. The mechanical behavior of each part must hence be set separately. All the elements are first manufactured separately, and assembled together. While arms and posts are realized by shape setting of nitinol wires, head and cone are obtained from braiding.

4.1 The arms

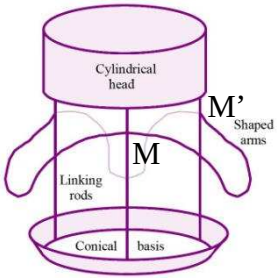

Fig.II.5_ design of the arms

The role of the arms is to push in the upper part of the sinus, and keep the contact over the whole cardiac cycle. The force applied by the arms in the sinuses must help keeping the contact between the cone and the aortic ring. The diameter and length of the wire used to realize the arms are selected according to geometrical criteria as well as mechanical ones.

4.1.1 Geometrical criteria

In order to limit the pressure forces applied by the arms in the sinuses, the contact surface area should be as large as possible : *arms cover at least half of the sinus perimeter.* The arms should conform to the sinus shape to spread the deformation along the sinus tissue : *arms curvature must respect sinus curvature*. Coronary obstruction risk should be limited : *two wires positioned in a parallel way are used to free the coronary conduits*. The vortex, which occurs in the sinuses at valve closure should be disturbed as little as possible to prevent delay in valve closing : *length of the arms is limited*. Figure II.5 shows the design which respects these criteria.

Arms are realized in practice through superposition of several wires and shape set to get the sinuses curvature. The available diameter range for the nitinol wires being limited, the rigidity of the arm can thus be more finely adjusted.

4.1.2 Mechanical criteria

One arm is connected to two posts at one end (M and M' in figure II.5), while the other end is free to flex. Flexing freedom in the sinus is thus ensured. Working with flexing arms presents the advantage of promoting interaction between arms and sinuses. A mechanical approach of this interaction, helps highlighting this advantage. Basically, a strength of material study shows that free flexing arms induce low stress in the sinus tissue.

4.1.3 The Model

In the model adopted, only the radial dimensions variations of the sinuses are considered. The sinus depth variation is considered around 20 % over the cardiac cycle. In reality, the sinuses

undergo also a slight but negligible height variation. It is essential to take the radial deformation into account, in order to validate that the anchoring of the stent is guaranteed even when sinus dimensions change over the cardiac cycle.

With that model, following assumptions are made : (1) each arm is modeled as a curved beam with constant curvature radius R, embedded at one end (point M in Figure II.5), (2) flexure occurs under distributed load q (N/m) acting on the whole length of the arm (represents the pressure load between arm and sinus). We study the behavior of the beam over the cardiac cycle in systole and in diastole.

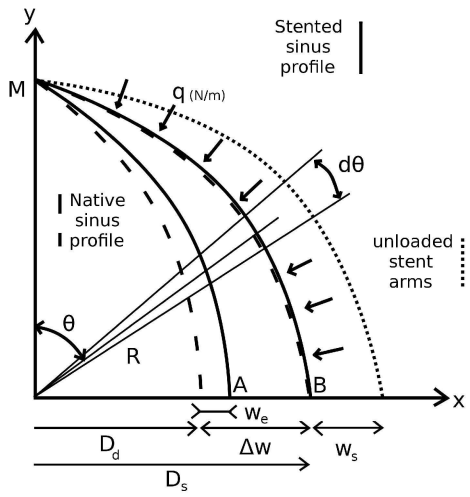

Fig.II.6_ flexed beam model

4.1.3.a In systole

The systolic pressure leads to sinus expansion, which depth becomes maximum (D_s). Sinus tissue undergoes 2 forces : (1) the force applied by the arm on the sinus, (2) the force that corresponds to systolic pression.

Force applied by the arm on the sinus

The arm is only slight deformed in that configuration (free end of the arm in position B in figure II.6). The force applied by the arm on the sinus must be high enough to prevent any axial displacement of the whole stent, which undergoes systolic flow at the cone basis level. The bottom of the stent obstructs indeed slightly the systolic flow (depends on the obstruction's rate). Systolic flow tends to push the stent axially upwards. The force of the arms must compensate this effect.

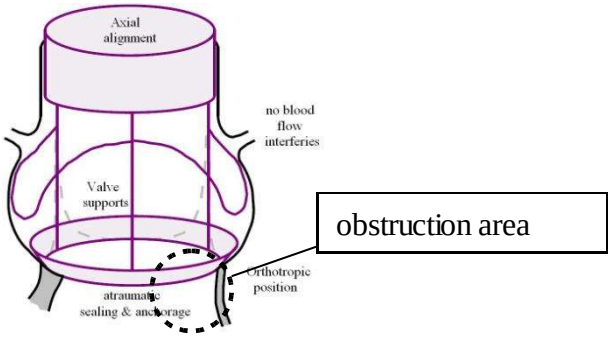

Fig.II.7_ Flow obstruction

The effort due to flow can be written as:

$$F_{flow} = p_{dyn}\frac{\pi D_v^2}{4}\alpha = \left(\frac{1}{2}\rho V^2\right)\frac{\pi D_v^2}{4}\alpha \qquad (1.2)$$

P_{dyn} = dynamic pressure applied on the conical basis

D_V = valve diameter

α = obstruction rate

Each arm must compensate for 1/3 of this effort

$$F_{arm/sinus} = \frac{1}{3}p_{dyn}\frac{\pi D_v^2}{4}\alpha \qquad (2.2)$$

With a valve diameter value D_V=21 mm an obstruction rate α=20%, and a maximal velocity of 1,35m/s, the calculated effort is 0.021N. With this effort value, the necessary distributed load value q can be calculated. $F_{arm/sinus}$ (vertically oriented) and q are related with following equation.

$$F_{arm/sinus} = \int_0^{\theta_{max}} q\,R\,d\,\theta\sin\theta = qR\left(1-\cos\theta_{max}\right) \qquad (3.2)$$

θ = angle between the arm's ends ($\theta_{max}=\pi/2$)

R = curvature radius of the arm

With R=12 mm we get q= 1.75 N/m

The radial (x axis in figure II.6) displacement of the beam's end (w_s) between rest position (not represented) and systolic position (point B) can then be calculated to precisely analyze the interaction between arm and sinus.

The strength of material's theory applied to a curved beam, allows establishing a relationship between the distributed load 'q' and the radial displacement 'w' of any point on the beam positioned with θ :

$$w = \frac{q R^4 \left(1 - \cos^2 \theta\right)}{2 EI} \qquad (4.2)$$

In which :

E = elastic modulus (MPa)

I = areal moment of inertia (mm^4)

w = radial displacement (mm)

The value of w is maximal ($w=w_s$) when $\theta=\pi/2$

The beam deformation depends on the wire diameter used to realize the arms (with the I value) and is not calculated immediately. Later, in this section we will select the wire diameter according to the expected beam deformation, which is conditioned by the expected compliance for the stent-sinus assembly. But the force due to systolic pressure influences the final compliance as well and needs first to be assessed.

Force applied by the pressure on the sinus

The systolic pressure P_s applied on the sinus surface area, generates a tensile stress in the sinus tissue defined from the theory of elasticity with :

$$\sigma = \frac{P_s R}{2 e} \qquad (5.2)$$

In which Sinus is considered as a spheric wall

Ps = systolic pressure (Pa)

R = sinus curvature radius (mm)

e = sinus wall thickness (mm)

This stress is applied in axial direction on each section area (S) of the sinus and leads to a resulting axial component F_p (in the direction of y) defined with :

$$F_p = \sigma L_s e \qquad (6.2)$$

In which

σ = stress (P_a)

L_s = sinus perimeter (mm)

e = sinus wall thickness (mm)

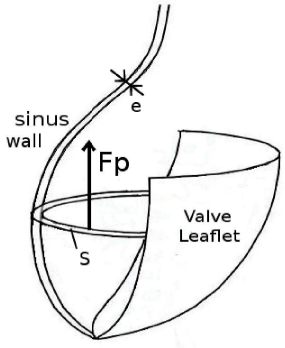

Fig.II.8_ Pressure Force in sinus

With L_s=20mm, R=12mm and P_s=120mmHg, we get F_p=1,89 N. This value is much greater than the 0,021 N obtained before for $F_{arm/sinus}$. We conclude that in systole, the arm induces only low additional stress in the tissue.

Finally, the global extension effort $F_{systole}$ applied on sinus tissue in systole, corresponds to the addition of both efforts expressed above :

$$F_{systole} = F_p + F_{arm/sinus} \qquad (7.2)$$

But force due to pressure is predominant.

4.1.3.b In diastole

Over the cardiac cycle, the pressure variation between diastole and systole induces an increase in the sinus depth of around 20% for a non stented root. If D_D represents the sinus diameter in diastole, it can be written as a function of D_S (diameter in systole) with :

$$D_s = 1{,}20\, D_D \qquad (8.2)$$

Once the arm of the stent pushes in the sinus, the sinus diameter comes back in diastole to a value D higher than D_D. D corresponds to a position of equilibrium (arm+sinus), in which arm is more flexed than it was in systole. As to the sinus, it is more expanded than it would be without stent. Following relationship between D, D_S, D_D can be written :

$$D_D < D < D_s \qquad (9.2)$$

The stent reduces the compliance of the sinus. In order to assess, how the diameter of the wire used to realize the arms influences the loss of compliance, we establish in the following section the relationship between the compliance of the stented sinus and the wire diameter. From the forces acting on the arm when equilibrium position D is reached, it is possible to calculate the radial deformation $w_e=(D-D_D)/2$ (characterized with point A in Figure II.6) of the sinus. This deformation is an additional one, which would not exist if no stent. It generates an additional pressure p_{stent} acting on the sinus besides the diastolic pressure.

- For the sinus we can write (assuming linear deformation) :

Non-stented sinus

$$P_{syst} - P_{diast} = K\left(w_{syst} - w_{diast}\right) = K\,\Delta w \qquad (10.2)$$

with K= rigidity coefficient for the sinus

P_{syst} = 120 mmHg

P_{diast} = 80 mmHg

Δw represents the sinus radial deformation between systole and diastole. Its value is 20% of the sinus radius.

Stented sinus at equilibrium

$$P_{syst} - \left(P_{diast} + P_{stent} \right) = K \left(\Delta w - w_e \right) \qquad (11.2)$$

- For the arm, we can write

$$w_s + \Delta w - w_e = \frac{qR^4}{EI} \frac{\left(1 - \cos^2\theta\right)}{2} \qquad (12.2)$$

The distributed low q can be expressed as a function of p_{stent} with : $q = p_{stent} L$ in which L represents the width of the contact zone. In practice, net structure may be wrapped around the doubled arm to spread the effort, without obstruction of the coronary ostia.

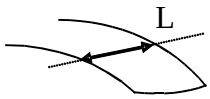

Fig.II.9_ arms width

Combining both previous equations leads to :

$$P_{stent} = \frac{\left(P_{syst} - P_{diast} \right) + K w_s}{1 + K \frac{L R^4}{EI} \frac{\left(1 - \cos^2\theta\right)}{2}} \qquad (13.2)$$

and

$$w_e = w_s + \Delta w - \frac{P_{stent} L R^4}{EI} \frac{\left(1 - \cos^2\theta\right)}{2} \qquad (14.2)$$

At manufacturing state, 2 parameters can be varied in this equation to minimize P_{stent} :

(1) the angle θ,

(2) the rigidity of arms described with I

To set θ close to 90° is interesting, while the value for I should be rather low. The wire diameter can be set, considering that the number of wires assembled to realize one arm can be n=3, for instance (makes it easier to control arms stiffness). The influence of the wire diameter on the value w_e =D-D_D can then be figured out, which gives information on the compliance modifications. The lower the value for w_e, the more compliant is the (stent+sinus) assembling. The higher the value for w_e, the less compliant is the (stent+sinus) assembling. This compliance loss ΔC can be expressed as a fraction of the original compliance of a non stented sinus.

$$\Delta C = \frac{\Delta w - w_e}{\Delta w} \qquad (15.2)$$

4.1.3.c Numerical approach

$P_{systole}$ = 120 mmHg, $P_{diastole}$ = 80mmHg, Dv = 21mm, R = 12mm, Ls = 20mm, e = 0,5mm, $E_{nitinol}$ = 25 Gpa, L = 10mm, nombre de brins n = 3, α = 20%

We plot ΔC as a function of the wire diameter.

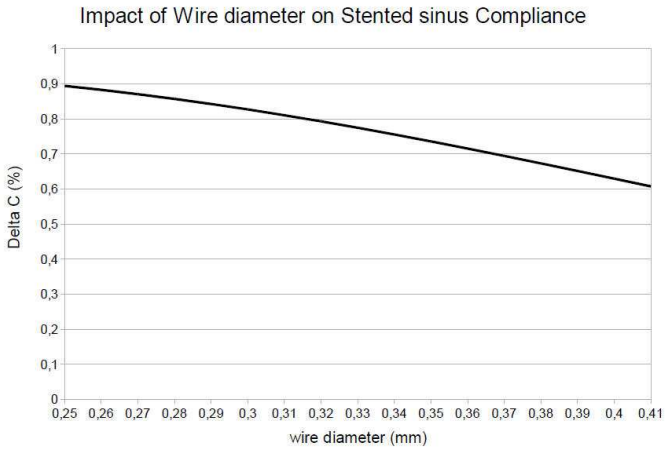

Fig.II.10_ compliance = f (wire diameter)

One may observe that the loss of compliance induced by the sinus arm, can remain low if the rigidity of the arm remains low (with d=0,26 mm 88% of the initial compliance remains). However, lower rigidity values require larger deflection of the arm at implantation time for a same effort applied in the sinus. Initial position of the arms, at rest state, need then to be higher (Fig II.11 : position 2 instead of position 1)

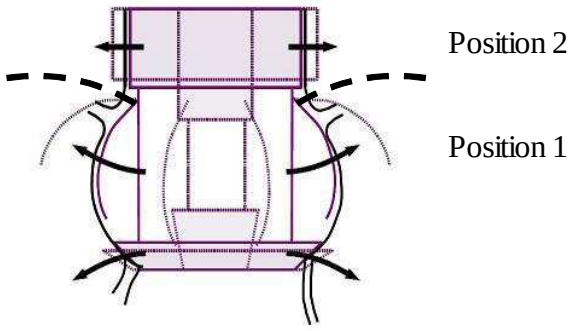

Fig.II.11_ influence of arm's rigidity on initial deployment position

This configuration requires from the arms to undergo larger deformation when inserted in the catheter. Material is more solicited and deployment may be more difficult for higher arms. For in vitro testing, a 0.406 mm diameter was selected in a first approach, which corresponds to a 40% compliance loss. This is later considered as the reference size, while further tests will be performed with lower wire diameter values.

4.1.3.d Conclusion

The assumptions made in this model limit slightly the interpretation which can be given to the compliance numerical values obtained. Sinus expansion is indeed not linear, due to the visco-elastic behavior of the material. However, the anchoring concept based on sole surface matching is validated. Tissues keep their compliance, and stent related efforts are limited. With a minimum rigidity of the arms, tissue degradation can be limited. Moreover, stent's posts deformation is limited as well. Actually, arms are linked to the posts and when they flex, they tend to flex the posts. In the following section we focus on the posts behavior.

4.2 The posts

The function of the posts is to link the cylindrical head to the conical basis, as well as to hold the valve's commissures. They have no contact with the aortic root and their size can be as reduced as possible to prevent any flow obstruction. Mechanical as well as practical criteria can be adopted for the post's development. The bending rigidity must first be high enough to provide good cohesion to the stent, and prevent any unexpected deformation.

- The overall rigidity must be high enough to make it possible for the head to center axially the whole device
- Flexure is induced in the posts by the valve leaflets in diastole
- Arms generate posts flexure at the connection point

Stents with flexible posts have already been studied in the frame of the bioprostheses development for classic surgery implantation [REI.71]. The goal was to minimize stress concentration at the commissure level of the valve, to increase valve durability. If the numerical model developed by Christie [CHR.92] validates the assumption, experimental results could not confirm the advantage of working with flexible posts rather than with rigid ones. However, the development of the stented valve requires flexibility of the device for easy non-invasive implantation. It is therefore of interest to study the influence of the posts rigidity on the global behavior of the prosthesis, in order to optimize the sizing of the different elements. The posts are realized with two wires running parallel.

4.2.1 Wire dimensioning

4.2.1.a The model

Posts are considered in that model as flexing beams free from rotating at their extremities according to figure II.12.

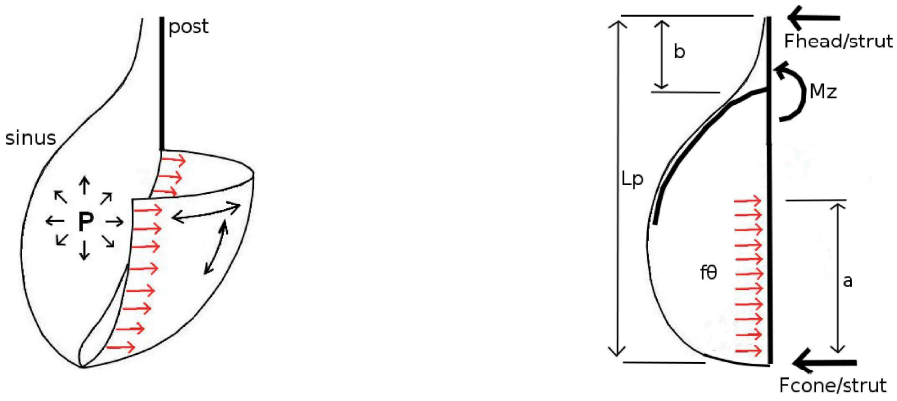

Fig.II.12_ Posts flexing model

The beam is supported at its ends by the junction to the head and the conical basis.

It undergoes following forces :

- A distributed effort f_θ (N/m) acting on a length 'a' corresponding to the height of the valve (this force represents the pressure acting on the valve leaflet)
- Torque M_Z applied by the arm on the post at the arm-post junction
- The forces acting at the supporting points ($F_{HEAD/POST}$ and $F_{CONE/POST}$)

4.2.1.b The dimensioning

The diameter of the wire used to realize the post is defined from the deformation undergone by the posts. First, posts must be rigid enough to prevent any modification in the arm positioning in the sinuses, due to too large post flexure magnitude. Indeed, the connection between arms and posts can be considered as rigid. Any movement of the posts leads to movement of the arm. Second, certain flexibility must, however, be kept for the posts to ensure good valve closing and sealing.

Global post deformation is obtained from the superposition of both deformations due to f_θ and to M_Z considered independently. Both deformations can be calculated from the strength of material theory.

- The deformation of a L_p long beam charged under distributed effort f_θ can be expressed as following :

for x between [0 ; a] $$v(x) = -\frac{f_\theta x}{24 E I L_p} \cdot \left(a^2 (2 L_p - a)^2 - 2 a (2 L_p - a) x^2 + L_p x^3 \right) \quad (16.2)$$

for x between [a ; L_p] $$v(x) = -\frac{f_\theta a^2 (L_p - x)}{24 \cdot E I L_p} \left(4 L_p x - 2 x^2 - a^2 \right) \quad (17.2)$$

Forces induced at supporting points (beam ends) are written :

$$R_{f\theta/head} = \frac{f_\theta \cdot a^2}{2 \cdot L_p} \quad \text{and} \quad R_{f\theta/cone} = \frac{a f_\theta}{L_p} \left(L_p - \frac{a}{2} \right) \quad (18.2)$$

The f_θ value can be calculated in diastole from the pressure acting on the closed valve. The valve leaflets are under circumferential tension stress σ_θ and transfer that stress to the posts. Assumption is made that the stress is considered to be applied on the post along a distance corresponding to the valve height. Following expression is obtained for f_θ :

$$\sigma_\theta = \frac{P R}{e} \quad \text{and} \quad f_\theta = P \cdot R_c \quad (19.2)$$

- The deformation of a L_p long beam charged under local M_Z torque can be expressed as following :

for $x \in [0 ; L_p - b]$; $$v(x) = \frac{M_z x}{6 E I L_p} \left(x^2 - L_p^2 + 3 b^2 \right) \quad (20.2)$$

Forces induced at supporting points (beam ends) are written:

$$R_{Mz/head} = -\frac{M_z}{L_p} \quad \text{and} \quad R_{Mz/cone} = \frac{M_z}{L_p} \quad (21.2)$$

Flexing torque M_Z can be expressed from the strength of material theory, applied to to a curve beam embedded at one end and free at the other end. M_Z can be written :

$$M_z = q R^2 (1 - \cos\theta) \quad (22.2)$$

In which :

θ = angle between the arm's ends ($\theta_{max} = \pi/2$)

R = curvature radius of the arm

q = distributed load on the arms

From these results, we can express the posts displacement at the level of the valve commissures as function of the effort and torque applied on the posts. Each post is linked to 2 valves, each valve is linked to 2 posts and each post is charged with the flexure of 2 arms. Finally, each post undergoes the force applied by one valve and one arm. The final deformation of the post and the final forces acting at the supporting points are written :

$$v(a)=\frac{P\,R\,a^3\left(L_p-a\right)}{24\,E\,I\,L_p}\left(4\,L_p-3\mathrm{a}\right)+\frac{M_z\,a}{6\,E\,I\,L_p}\left(a^2-L_p^2+3\,b^2\right) \qquad (23.4)$$

$$F_{head/post}=\frac{f_\theta\,a^2}{2\,L_p}-\frac{q\,R^2\left(1-\cos\theta\right)}{L_p} \qquad (24.4)$$

$$F_{cone/post}=\frac{f_\theta\,a}{L_p}\left(L_p-\frac{a}{2}\right)-\frac{q\,R^2\left(1-\cos\theta\right)}{L_p} \qquad (25.4)$$

The wire diameter is set to obtain a displacement value v(a) around 1mm, which corresponds to native valve commissure displacement. The calculation is done for following numerical values:

D_{valve} = 21mm ; a = 0,7 D_{valve} ; R ≈ D_{valve} /2; L_p ≈ 20mm; E ≈ 25 à 50 GPa; P = 80 mmHg; θ=π/2, q=1,75 N/m

The finally obtained diameter is d=0.6 mm, and the following corresponding values are obtained for the different forces and displacements ‘v’

commissure displacement v(a)			F head / strut			F cone / strut		
Mz	fθ	**Mz + fθ**	Mz	fθ	**Mz + fθ**	Mz	fθ	**Mz + fθ**
0.2mm	0.8mm	**1 mm**	-0.2N	0.6N	**0.4N**	0.2N	1N	**1.2N**

Table.II.13_ force and displacement obtained with our prototype configuration

Comments :

The radial displacement of the posts is only slightly influenced by the torque M_Z (v=0.2mm) induced with the arms. Forces acting at the supporting point levels must be borne by the braided head and cone. It will thereof be necessary to check if the braided elements are rigid enough to prevent any risk of collapsing.

4.2.2 Conclusion

The use of two straight wires for the post's manufacturing, make it possible to avoid any flow obstruction at posts level. The diastolic pressure applied on closed valve induces limited radial flexure in the posts, for appropriate wire diameter setting. We will study the influence of this flexure movement on the valve behavior and closing mechanism later in this work.

4.3 Braided elements

Both conical basis and cylindrical head must be characterized with enough surface area to match respectively the aorta conduit and the aortic ring. The braiding process will make it possible to generate this surface. Basically, braiding process is easier and less expensive than laser cutting to generate surface for positioning purpose. However, the mechanical behavior of braided structures needs to respect the expectations related to the stented valve. We must therefore check if braiding is compatible with our application.

Braided stents belong to the self expanding stents category. They are obtained from the interlacing of wires tilted to an angle with the axis of the device. In general, a tubular meshing is finally obtained. Braided stents are largely used in medical applications due to their flexibility, their cover rate as well as their ability to follow the implantation diameter variations. However, the radial resistance to compression is lower than for laser cut stents. Moreover, significant length variation between deployed and collapsed state limits the use of them. A geometrical approach of braiding explains this behavior. We will check, with that approach, if braiding technique is adapted to the stented valve application. Two criteria are to be taken into consideration : (1) the cover rate, (2) the radial pressure applied by the stent on the implantation environment.

4.3.1 Cover rate and length variation

Cover rate is one interesting characteristic of braided stents. It corresponds to the ratio between the surface effectively covered by the stents wires, and the surface covered by the stents geometry. In the stented valve application, this cover rate is requested to be as high as possible to spread the efforts uniformly on the tissues. In the next section we compare the cover rate of laser cut stents with the cover rate of braided stents, to justify the advantage of braided elements.

Cover rate is defined as : $\chi = \frac{s}{S}$ (26.2)

With :

S = geometrical surface area covered by the stent

s = effective surface area covered by the stent's wires

4.3.1.a Laser cut stent

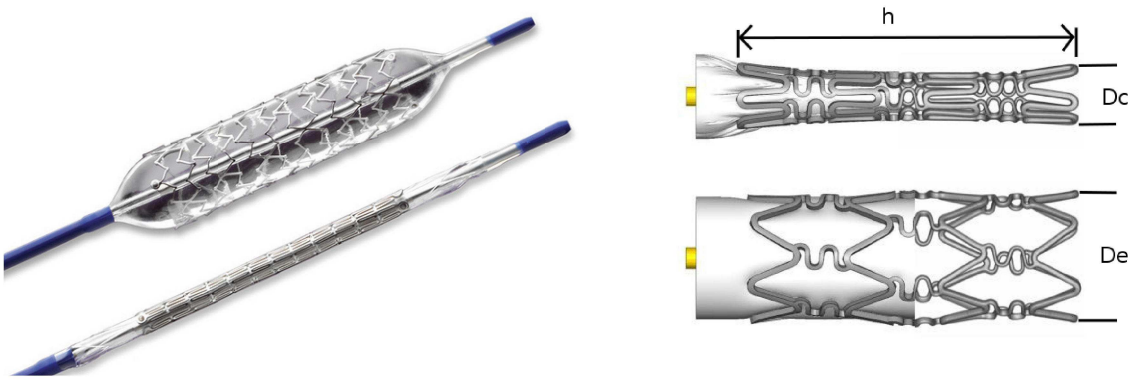

Fig.II.14_ laser cut stent in deployed and compressed configurations

The maximum cover rate is obtained in compressed state (at diameter D_C). The length variation between compressed (D_C) and expanded diameter (D_E) is in general very low for these stents and we can write:

$S = h \cdot \pi \cdot D$

$s = k \cdot S_0$ with $k \in]0, 1[$ (depends on cutting conditions)

$$\chi = \frac{s}{S} = k \frac{D_0}{D} \quad (27.2)$$

Cover rate variation can be expressed as :

$$\Delta\chi = \frac{D_E}{D_C} - 1 \quad (28.2)$$

We note that $\Delta\chi$ decrease between compressed and implantation diameters. Once implanted, cover rate varies over the cardiac cycle according to aorta diameter variations.

4.3.1.b Braided stent

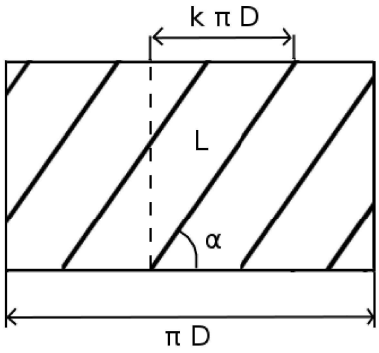

Fig.II.15_ braided geometry

We consider a stent (diameter D) obtained from the braiding of n wire parts (diameter d) tilted to an angle α with the horizontal plan (Figure II.15). The length of the wire parts is constant. Surface covered effectively by the wires is obtained from adding the surfaces covered by each wire part. We can write :

$$s = n\,d\,L = n\,d\,\frac{k\,\pi\,D}{\cos\alpha} \qquad (29.2)$$

In which :

n = number of wire parts

d = wire diameter

$$S = \pi\,D\,H = \pi\,D \cdot k\,\pi\,D\tan\alpha \qquad (30.2)$$

Cover rate can be written

$$\chi = \frac{s}{S} = \frac{nd}{\pi\,D\sin\alpha} \qquad (31.2)$$

Cover rate variation between expanded and deployed states can be written:

$$\Delta\chi = 1 - \frac{D_C \sin\alpha_C}{D_E \sin\alpha_E} \qquad (32.2)$$

In which α_C and α_E are linked with the condition that the length of each wire part is constant between deployed and expanded state.

$$\frac{D_E}{\cos\alpha_E} = \frac{D_C}{\cos\alpha_C} \qquad (33.2)$$

In order to understand the interest in working with a braided rather than laser cut stent in our application, one may compare the cover rate variations for both stents, over the cardiac cycle when diameter varies from systole to diastole. Once implanted, stent's head undergoes diameter variation which ranges from 21 à 27 mm. χ variation for the laser cut stent is around 22 %. For the braided stent this variation is function of the braiding angle α. For values

around 45° it is possible to reduce the cover rate variation to 4%. Cover rate for braided stent doesn't vary as much as it does for laser cut, in a compliant environment. The pressure distribution applied on tissues, remain thereof close to constant. However, the braided stents undergo length variations of around 30 % over the cardiac cycle. This phenomenon is to be considered when assembling the different stents parts.

4.3.2 Radial pressure

In order to minimize stress in the stent's surrounding tissues, it is essential to limit the value of the pressure applied by the stent on the implantation environment. The geometrical parameters, which characterize the structure of the braid must be set in accordance with the pressure that is to be applied on the tissues. We therefore establish, in the following section, the relationship between the mechanical behavior of the braid and its geometrical characteristics. Two configurations are considered : braided stent with both free ends and non free ends.

4.3.2.a Stent with free ends

The model adopted for this configuration is proposed by Ravi [RAV.04]. Each wire part of the braid is considered as a curved beam to which we apply the Kirchhoff–Love theory equations.

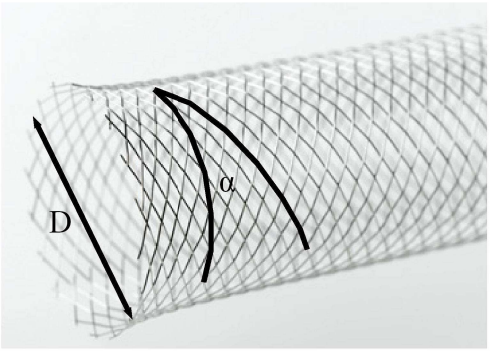

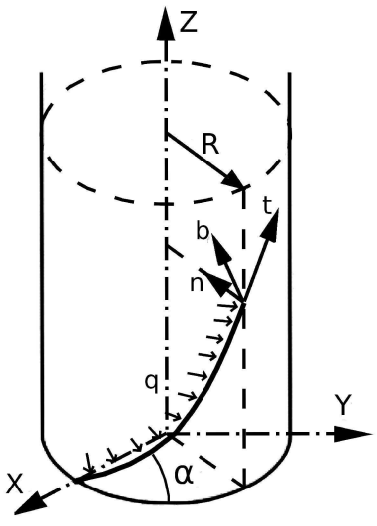

Fig.II.16_ Kirchoff-Love model

In that model, the trajectory described by the neutral axis is a circular helix. In Figure II.16 are represented the efforts applied in each section (S) of the helix.

The model works with following assumptions:

- Braid wire parts undergo :
  - Pure bending torque (around an axis perpendicular to the cylinder surface)

$$M_b = EI\left(\rho - \rho_0\right) \tag{34.2}$$

  - Pure torsion torque (around the wire neutral axis)

$$M_t = GI_0\left(\tau - \tau_0\right) \tag{35.2}$$

In which ρ and τ represent respectively the curvature and torsion at the considered point, while ρ_0 and τ_0 represent the curvature and torsion before deformation.

- The curvature ρ and torsion τ of a circular helix characterized with an angle α and a basis circle radius R are constant and can be written:

$$\rho = \frac{\cos^2\alpha}{R} \quad \text{and} \quad \tau = \frac{\cos\alpha\sin\alpha}{R} \tag{36.2}$$

- The braid is characterized with constant wire radius

$$\frac{\cos\alpha_0}{R_0} = \frac{\cos\alpha}{R} \tag{37.2}$$

The index $_0$ corresponds to the stent's state at rest

- Material respects the Hooke law

Pressure applied to the stent is modeled with a distributed force q applied on each wire part. q correspond to the pressure efforts defined per unit of height and reported to the effective length of the wire parts as well as to the number of wire parts n involved in the braid. The distributed load q can be written :

$$q = p(\pi D)\frac{1}{n}\frac{H}{L} = p\frac{\pi D\sin\alpha}{n} \tag{38.2}$$

H = stent's height

L = wire part length

p = radial pressure acting on the stent

The simplified resolution of the Kirchhoff-Love equations allows obtaining a relationship between pressure p, the braid geometrical characteristics and the stent's diameter D=2R.

$$P = \frac{n\,E\,I}{2\pi}\cdot\left(\frac{\cos\alpha_0}{R_0}\right)^4\cdot\frac{1}{\sin\alpha}\left[(1-\frac{R_0}{R})-\frac{1-\frac{\sin\alpha_0}{\sin\alpha}}{1+\nu}\right] \tag{39.2}$$

in which :

E = wire material Young modulus

I = areal moment of inertia

ν = Poisson coefficient

The friction effect between the wire parts is neglected in that approach. This result shows that the stent's resistance to compression is highly influenced by the wire section (through the I parameter) as well as by the ratio $\cos\alpha_0 / R_0$. One may note that the radial resistance is higher for low braiding angle. Figure II.17 represents the evolution of the braid diameter D as a function of the radial pressure p for different wire diameters used (α_0=45°; R_0=15mm; E=30GPa; ν=0.3).

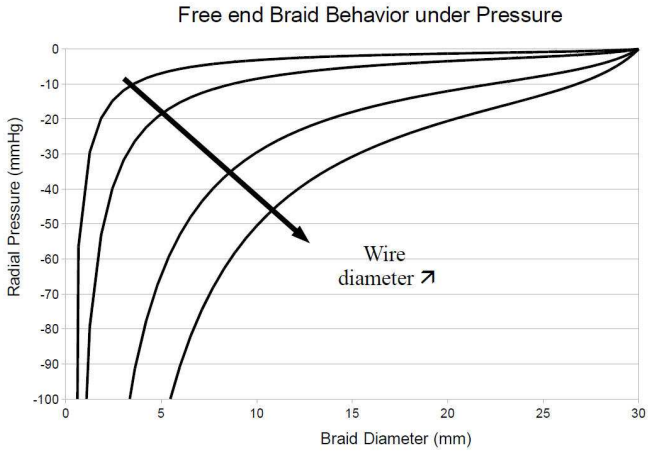

Fig.II.17_ radial pressure versus diameter (free end model)

We observe that the braided stent with free ends presents low resistance to compression. A pressure of around 10mmHg is enough to collapse the stent diameter by 50 %. This value is in the order of magnitude of what has already been observed by J.F.Dyet et al. [DYE.00] with the Wallstent. In comparison 25 to 40mmHg pressure are necessary to generate same diameter decrease with Palmaz stent (laser cut), and Symphony (welded curved wire). The low resistance of the free end configuration seems to not be adapted to our stented valve application, in which pressure values involved are much higher.

Verification of the elastic behavior assumption

In the described model the material was considered to respect the Hooks law. However, Nitinol material does respect this condition only if deformations remain below 1 to 2%, in which case a pseudo-elastic modulus can be considered. We check in that section what are the deformation rates for a stent compressed to low diameter. Each wire part undergoes pure

bending and torsion as already described before. Both solicitations generate maximum extension stress σ_{max} and shearing stress Γ_{max} at wire external surface.

$$\sigma_{max} = E\frac{d}{2}(\rho - \rho_0) \qquad \text{and} \qquad \Gamma_{max} = \frac{E(\tau - \tau_0)}{2(1+\nu)}\frac{d}{2} \quad (40.2)$$

The Von Mises resistance criterium tells us if the wire beam works in elastic conditions if we have :

$$\sigma_{equ} = \sqrt{\sigma_{max}^2 + 3\Gamma_{max}^2} < R_e \qquad R_e = \text{elastic limit of resistance} \qquad (41.2)$$

Deformation rate can hence be calculated with :

$$\varepsilon_{equ} = \sigma_{equ}/E \qquad (42.2)$$

Finally ε_{equ} can be expressed as function of the geometrical characteristics of the braid with :

$$\varepsilon_{equ} = \frac{d}{2}\frac{\cos\alpha_0}{R_0}\sqrt{(\cos\alpha - \cos\alpha_0)^2 + 3\frac{(\sin\alpha - \sin\alpha_0)^2}{2(1+\nu)}} \qquad (43.2)$$

A numerical calculation leads to 0.7 % deformation rate for the nitinol wire if the cylindrical head is compressed from 30 mm to 6 mm diameter. Nitinol material can be considered as elastic in that range of variations.

4.3.2.b Stent with non free ends

In the model presented above, the interactions between the stent's wire parts are not considered, each wire part is considered as an independent beam. With that model, the stent doesn't fit the stented valve requirements in terms of resistance to pressure. To increase the radial rigidity, it is possible to link the wire ends at each end of the stent. Moreover, this configuration presents the advantage of limiting injuries with tissues at stent's ends. The behavior of the stent under pressure is modified in this new configuration and the interaction between two neighbor wires must be taken into account. Figure II.18 represents a stent with joint wires at the ends. This configuration is easy to obtain with manual braiding.

Fig.II.18_ stent with non free ends

The mechanical behavior law for that stent can be obtained in superposing two models : (1) the Ravi free ends model; (2) a model in which each wire part is considered as a beam embedded on both ends undergoing flexure solicitation. The embedding corresponds to the junction between two wires at the stent's ends. The planar representation of Figure II.19 is the model which can be adopted for establishing the relationship between radial pressure p and diameter D.

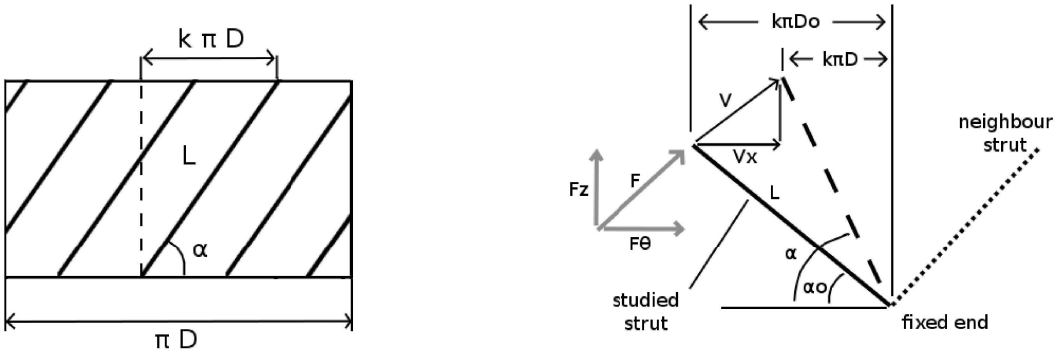

Fig.II.19_ planar model

Assumptions adopted :

- Deformation due to torsion are neglected,
- Radial pressure is represented with a local force F applied at the end of each wire part, which tends to flex the part (Figure II.19).

Beam deformation v and effort F are linked with :

$$F = \frac{3EI}{L^3} v \qquad (44.2)$$

Calculation of F=f(pressure) (Figure II.19)

F is related to F_θ with:

$$F = \frac{F_\theta}{\sin \alpha_0} \qquad (45.2)$$

F_θ, which is the circumferential component of F, can be linked to the pressure p applied on the stent defined with its length H and its diameter D.

$$F_\theta = \sigma S = \sigma (H e) = \frac{P D}{2e} H e = \frac{PDH}{2} \qquad (46.2)$$

with

S = stent's geometrical surface

H = stent's height

e = thickness (stent is modeled as a continuous membrane)

Calculation of deformation v

For a cylindrical braid composed of N meshing cells over the circumference we can write

$$v = \frac{v_x}{\sin\alpha_0} = \frac{k\,\pi\left(D - D_0\right)}{\sin\alpha_0} \qquad (47.2)$$

k is a coefficient of proportionality defined from the number of cells N with :

$$k\,\pi\,D = j \cdot b \qquad (48.2)$$

$$N\,b = \pi\,D \qquad (49.2)$$

In which b represents the width of one cell, and j the number of cells in which one wire part is involved. We finally obtain

$$k = \frac{j}{N} \qquad \text{and} \qquad v = \frac{j}{N}\frac{\pi\left(D - D_0\right)}{\sin\alpha_0} \qquad (50.2)$$

Conclusion

For one wire part we obtain :

$$P_{wire} = \frac{2}{HD}\frac{3\,E\,I}{L^3}\frac{j}{N}\pi\left(D - D_0\right) \qquad (51.2)$$

For the n=2N wire parts involved we obtain the mechanical behavior law for the whole stent:

$$P = \frac{4}{H\,D}\frac{3\,E\,I}{L^3}\,j\,\pi\left(D - D_0\right) \qquad (52.2)$$

This pressure corresponds to the flexing resistance of the wire parts at the junctions between two neighbor wires. The global resistance of the stent is obtained in adding this pressure to the pressure already obtained with the previous free ends model. In figure II.20 this global radial pressure p applied on the stent is plotted versus the diameter D variation in taking the two models into consideration (numerical values are same as the one used in the previous model). In the same figure, the behavior of the free end model is also plotted for comparison purpose. As one can observe, the resistance due to wire junction at the stent's end is predominant. The compression of the stent's diameter by 50%, requires a pressure application 6 times higher when wire ends are linked. These results are in accordance with the experimental results obtained by J.F.Dyet [DYE.00]. The authors highlight that a 30mmHg pressure is required to compress the Wallstent by 50%, as soon as the ends are clamped, while only 10 mmHg are necessary if ends are free. These results prove that, when adjusting the stent's geometrical parameters, it is possible to adapt the resistance of braided elements to valve pressure order of magnitude.

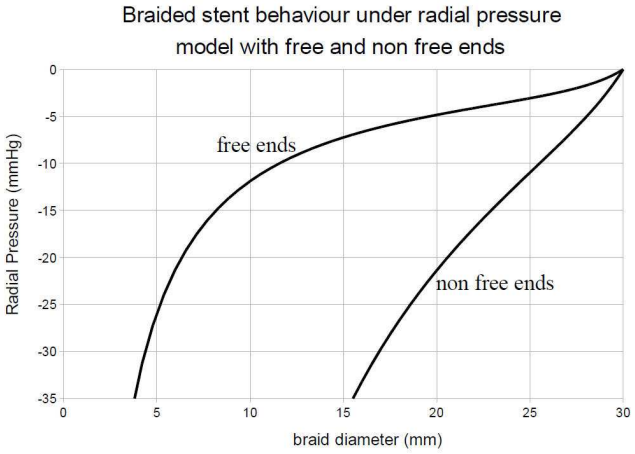

Fig.II.20_ radial pressure versus diameter (model with free and non free ends)

4.3.3 Pressure model applied to the stented valve elements

The models presented highlight that braided stents show several advantages. They first make it possible to obtain constant cover rate on tissues for more homogeneous pressure application. Second, with appropriate setting of the geometrical parameters, the compression rigidity can be adjusted to values required for heart valve stenting. The main drawback of braided stent is the length variation between deployed and collapsed state. In our application, the assembling of the individual elements will be performed in a way to keep a constant height for the whole stent (Fig II.21). We will describe the assembling in more details in the next chapter.

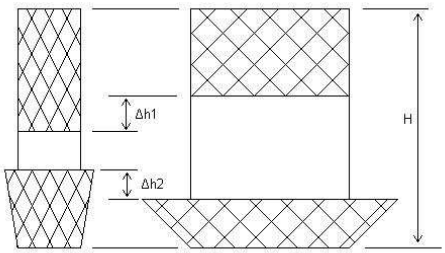

Fig.II.21_ deployed and compressed configuration

4.3.3.a Cylindrical head

From the stent behavior models described before, and from the mechanical behavior of the aorta tissue, it is possible to analyze the stented aorta behavior.

Aorta tissue

Experimental studies report in literature that the circumferential elastic modulus of aortic tissues is around 334-400kPa [FER.99]. From this value, the relationship between pressure

and diameter variation can be established.

Stress in tissue is expressed as :

$$\sigma_{aorta} = \frac{P\,D}{2\,e} \tag{53.2}$$

Corresponding deformation is written :

$$\varepsilon = \frac{\sigma}{E} = \frac{D - D_0}{D_0} \tag{54.2}$$

Finally :

$$P = 2\,e\,E\,\frac{D - D_0}{D\,D_0} \tag{55.2}$$

The behavior of the stented aorta can be analyzed with a graphical approach. Figure II.22 represents in a pressure–diameter scale, the behavior of the stent according to the model with non free ends (n=42 brins; d=0.260mm; E_{aorte} = 400kPa; e=1mm ; ΔP=50mmHg; D_0=21 mm). The behavior of the aortic tissue is also represented in the figure II.22.

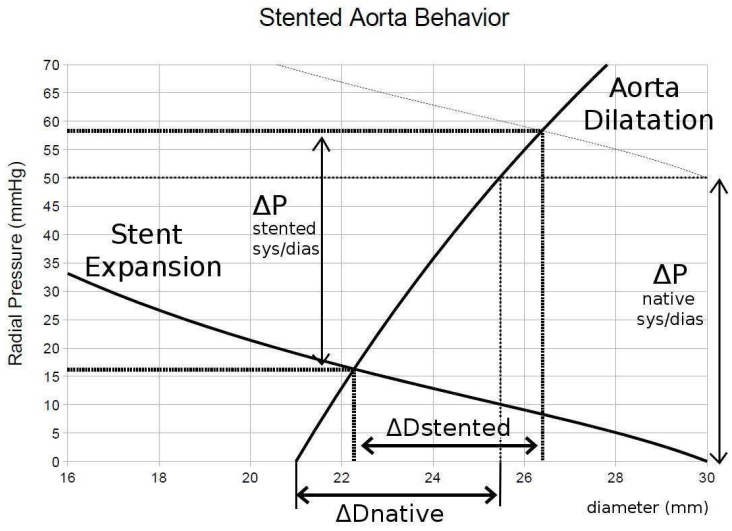

Fig.II.22_ stented aorta behavior

We observe that the stent increases only slightly the stress in the aortic tissue (pressure value variation increases from 50 to 58 mmHg). Moreover, the compliance is kept but slightly shifted (diameter oscillates between 22,3 and 26,4 mm instead of 21 and 25,5).

In that approach, the forces applied by the posts on the braid were neglected. Indeed, we proved at begin of the present chapter that these forces are low in comparison to the pressure applied.

4.3.3.b The conical basis

To study the behavior of the conical basis for dimensioning purpose, we adapted the model, initially valid for a cylindrical braid, to a conical geometry. The cone is positioned on the aortic ring and must keep the position when solicited under the diastolic pressure of around 100 mmHg.

Model adopted

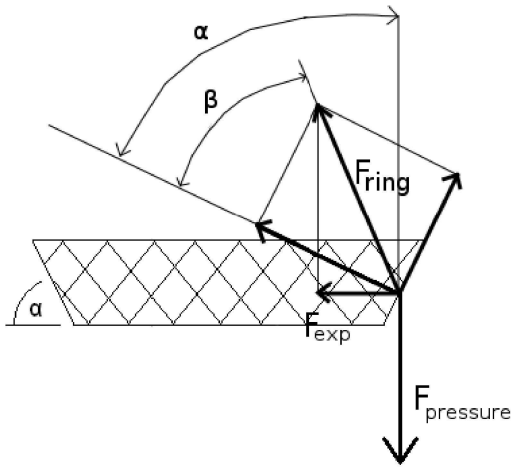

Fig.II.23_ model of the efforts applied on the ring at one particular point

Assumption : only the stent gets deformed

The conical basis undergoes 2 efforts : (1) the effort applied by the ring on the cone F_{ring}, (2) the diastolic pressure effort $F_{pressure}$. Both efforts are linked at equilibrium with :

$$\overrightarrow{F_{pressure}} + \overrightarrow{F_{ring}} = \vec{0} \qquad (56.2)$$

For the anchoring to be efficient and prevent sliding between stent and aortic ring, the stent's minimum horizontal expansion force F_{exp} must be :

$$F_{exp} = F_{pressure} \cdot \tan(\alpha - \beta) \qquad (57.2)$$

In which α = cone angle

β = adhesion angle

In reality the anchoring is not realized through sole adhesion effect. Inter-penetration between braid meshing and aortic ring tissue occurs. However, this phenomenon is not considered in that theoretical approach.

This expansion force is of lower value than the expansion force required for a cylindrical braid. (like the Edwards-Sapien stent for example) for which $\alpha=\pi/2$

$$F_{exp} = F_{pressure/valve} \ / \ \tan\beta \qquad (58.2)$$

Figure II.24 represents the expansion effort necessary for both a cylindrical and a conical braid for different cone angle values (arbitrary value of tan β = 0,3 is considered).

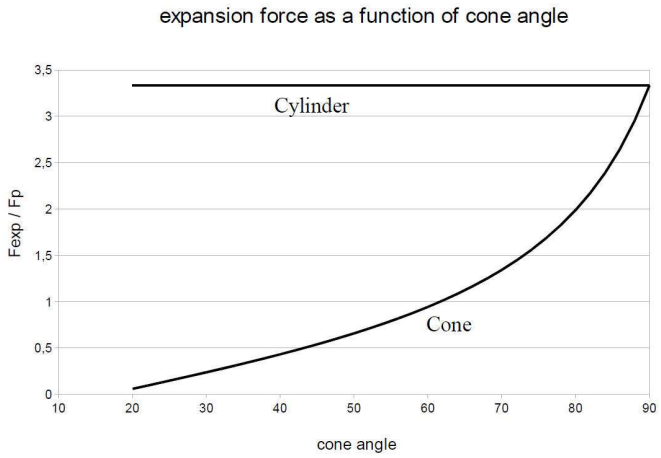

Fig.II.24_ Expansion force as a function of cone angle

In order to calculate the necessary braiding parameters for a given ring diameter and defined cone angle, we suggested to adapt the mechanical behavior model used for the cylindrical head to the cone, in modeling the wire parts as curved beams on a conical helix. However, in this configuration, the equations from the Kirchhoff-Love theory cannot be simplified. Curvature and torsion of a conical helix are indeed not constant. In that case, we adopt a model in which we approximate that the resistance to compression is mainly due to the flexure rigidity at the stent's ends, where wire parts are connected. We exclude the rigidity due to the free end model. In that approach we approximate the cone with a cylinder of equivalent diameter $D+l\cos\alpha$ (Figure II.25) and establish the relationship between applied pressure P and diameter D.

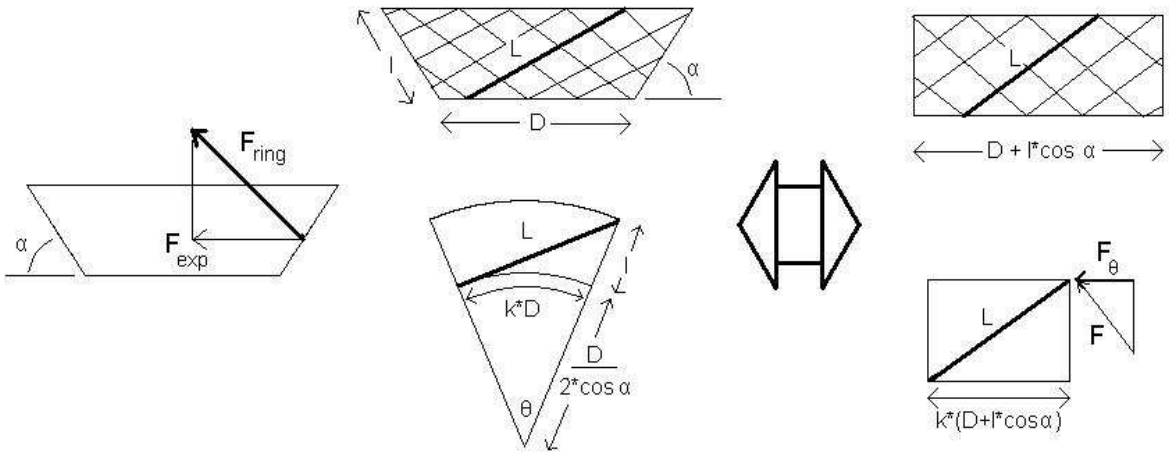

Fig.II.25_ model for the cone behavior calculation

The stent's compression from diameter D_0 to diameter D induces change in cone angle from α_0 to α. Assumption is made that the evolution is linear and can be expressed with:

$$\frac{\alpha-\frac{\pi}{2}}{D}=\frac{\alpha_0-\frac{\pi}{2}}{D_0} \tag{59.2}$$

As to the cone width l, it can be calculated, assuming that wire parts length L remains constant during compression process (Figure II.25).

$$L^2=\left(\frac{D}{2\cos\alpha}\sin\theta\right)^2+\left(\frac{D}{2\cos\alpha}+l-\frac{D}{2\cos\alpha}\cos\theta\right)^2 \tag{60.2}$$

Which leads to

$$l=\frac{D}{2\cos\alpha}(\cos\theta-1)+\sqrt{L^2-\left(\frac{D}{2\cos\alpha}\right)^2\sin^2\theta} \tag{61.2}$$

The cylinder mechanical model applied to the cylinder equivalent cone, allows finally obtaining the relation between pressure p and diameter D :

$$P_{valve}=\frac{2\cdot 4}{D_v^2}\cdot\frac{3\cdot E\cdot I}{L^3}\cdot 2N_b\cdot\pi\left(D+l\cos\alpha-D_0-l_0\cos\alpha_0\right) \tag{62.2}$$

Figure II.26 represents the plotting of the pressure versus cone diameter for this equivalent model (D_0=22mm ; l=0.3*D_0 ; α_0=40° ; N_b=2 ; $E_{Nitinol}$=25 GPa ; d_{wire}=0,26mm)

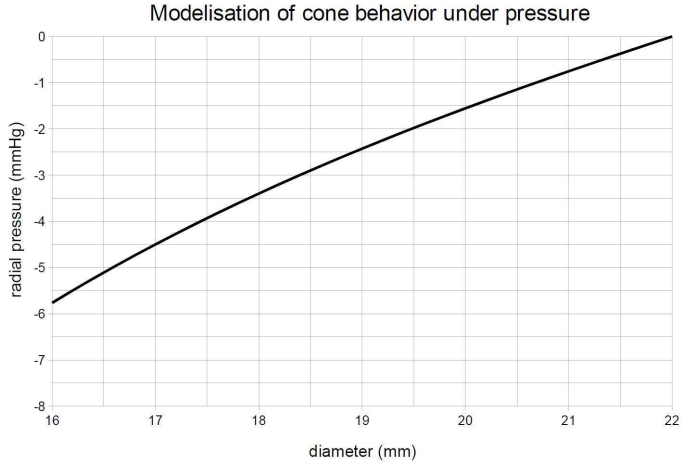

Fig.II.26_ radial pressure versus diameter (cone model)

In spite of practical results which show good efficiency of the stent conical basis through endoprosthesis anchoring under pulsatile flow, we observe that this model doesn't predict a sufficient conical basis resistance. The assumptions made in that approach, and the approximations made in the definition of the equivalent cylinder, doesn't allow to properly describe the conical braided part mechanical behavior. The geometrical braiding parameters couldn't be optimized through this model. Appropriate braiding parameters has been thus defined through experimentation.

4.3.3.c Conclusion

The braiding technique applied to the cylindrical head realization shows good results in term of mechanical behavior. The resistance to compression is adapted to the ‘in vivo’ pressure order of magnitude, while the compliance of the implantation environment is respected as well. Moreover the elastic behavior of the nitinol wires is preserved between compressed and deployed state of the braided elements.

Chapter III STENT MANUFACTURING

In this chapter we describe the manufacturing methods adopted for the different stent parts. For the braided parts, the way followed in the braided network by the Nitinol wires is defined in respect to the braiding conditions and the final assembling of the stent components. The dimensions of the parts are chosen according to these conditions and to the resistance criteria described in the previous chapter. The shape setting of the Nitinol is then presented, with a focus on the physical and mechanical properties modification undergone by the material with the thermal treatment.

1 STENT GEOMETRY AND CONSTRUCTION PARAMETERS

The Nitinol wire shape setting depends directly on the function of the considered stent part. First, the wire used for the arms is shaped from the sinus geometry. Second, the posts are obtained from straight wires. At last, the wire used for head and cone braiding is zig-zag shaped (Figure III.1).

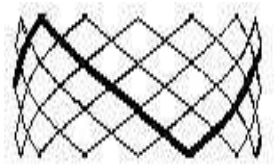

Fig III.1_Zig-zag wire path on a cylindrical braid

The different stent elements are obtained separately and then assembled. To ensure proper cohesion and working of the stented valve in the aortic environment, some manufacturing as well assembling constraints must be taken into consideration. These constraints will influence the shape definition of the different stent parts.

1.1 Constraints related to braiding

1.1.1 The braiding model

For both head and cone, the braiding process required the definition of a braiding angle (angle between crossing wires) as well as a braiding tightness of the braided mesh. The main goal was to obtain braided structures realized with only one continuous wire, to obtain looped ends. The absence of free wire ends minimizes tissue trauma, and avoids any superfluous wire junction (like welding) with associated local increased rigidity. On the other hand, the braided structure should respect the aortic root symmetry. This allows for each of the stent's posts to be located at the junction between two sinuses and ensure an equal stent behavior in each sinus. These constraints were described mathematically on the basis of figure III.2.

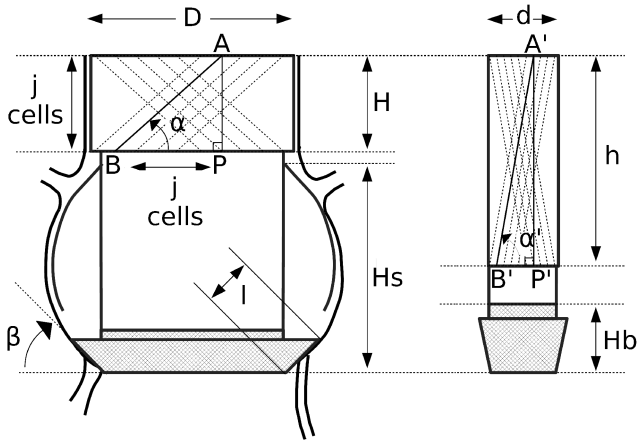

Fig III.2_stent parameters in deployed and compressed states

At first, in order for each of the stent's posts to be located at the junction between two sinuses, the braided meshing of the head must be configured with wire crossings present at every third of the circumference for both head and cone. The posts will then be sutured at these crossing points. Equation (1.3) describes this condition mathematically.

$$i = N/3 \qquad (1.3)$$

in which :

N = number of meshing cells over the head's circumference ($N \in \mathbb{N}$)

i = number of meshing cells between two sinuses ($i \in \mathbb{N}$)

Secondly, the use of a unique continuous wire for the whole braiding requires from the wire to follow a specific path in the braided structure. This path must bring the end of the braided wire back to its origin (initial point B) once the whole meshing is created, in order to obtain a continuous and symmetrical braid.

This condition could be described mathematically with equation (2.3).

$$2n\ BP = k\,\pi\,D \qquad (2.3)$$

In which :

2n = number of wire parts AB over the head's circumference ($n \in \mathbb{N}$)

BP = distance of wire part AB projected on head's circumference

k = coefficient of proportionality ($k \in \mathbb{N}$)

D = diameter of the head after braiding

At last, to ensure that a braid, defined by a binomial (n,k), have N independent meshing cells over the braid circumference, the n values of the (n,k) binomials which fulfills equation (2.3) have to be equal or superior to N. The unique solution of equation (2.3), which ensures that each wire part AB is single on the whole meshing, was obtained for n = N.

$$n = N \qquad (3.3)$$

The calculation of k can hence be obtained from the rewriting of equation (2.3), with the introduction of two more parameters :

$$2N(j\,\delta) = k(N\,\delta) \rightarrow\ j = k/2 \qquad (4.3)$$

In which :

δ = meshing cell width

j = number of meshing cells over the distance BP

The j parameter was introduced because it represents also symmetrically the number of cells over the height of the head (Figure III.2). The control of the j value is related to the control of the head height value H through equation (5.3), in which H is expressed as a function of i, j, D and α. This equation is obtained from the combination of equations (1.3), (2.3) and (3.3) while BP is expressed as a function of α.

$$H = j \cdot \frac{\pi D}{3i} \tan\alpha \qquad (5.3)$$

1.1.2 The (i,j) setting

The final (i,j) braiding parameters are chosen according to the previously described mathematical conditions. We first set the value chosen for i, as function of the number of

meshing cells required on the braid circumference (depends on the desired cover rate). We then list all the j values that provide the (n,k) binomials which respect equation (2.3). n must be an integer and admit a minimum value equal to N. Table III.3 gives an example of how the (j,k,N,n) values can be chosen for i=5 (15 cells over the circumference) in respect to the mathematical conditions.

i	N = 3*i	j	k	n = 3*i*k/j
5	15	**1**	1	n <> integer
			2	**n=N**
		2	1	n <> integer
			2	n <> integer
			3	n <> integer
			4	**n=N**
		3	1	n <> integer
			2	n<N
		4	1	n <> integer
			2	n <> integer
			3	n <> integer
			4	n <> integer
			5	n <> integer
			6	n <> integer
			7	n <> integer
			8	**n=N**
		5	1	n <> integer
			2	n<N
		6	1	n <> integer
			2	n <> integer
			3	n <> integer
			4	n<N
		7	1	n <> integer
			2	n <> integer
			3	n <> integer
			4	n <> integer
			5	n <> integer
			6	n <> integer
			7	n <> integer
			8	n <> integer
			9	n <> integer
			10	n <> integer
			11	n <> integer
			12	n <> integer
			13	n <> integer
			14	**n=N**

Table III.3_ (j,k,N,n) combinations for i=5

In that example, the only configurations that respect the specifications correspond to j=1, 2, 4, 7 ...etc….

The exact choice for j among the possible values, is then dependent on the braiding angle, braid diameter and braid height that are expected to be obtained for the stent. However, these 3 parameters are not independent. Equation (5.3) shows that braid height depends on angle. Angle is then linked to diameter. Indeed, assuming that all braided wire parts remain straight during compression process and just rotate and slip above each other, the straight distance value between points A and B in figure III.2 should be the same as the distance value between points A' and B' (Equation 6.3).

$$AB = A'B' \quad \Leftrightarrow \quad BP/\cos\alpha = B'P'/\cos\alpha' \qquad (6.3)$$

Moreover, the distances BP and B'P' (representing respectively the projection from AB and A'B' on the cylinder's circumferences in expanded and collapsed position) must represent the same proportion of the circumference in both deployed and collapsed configuration (Equation 7.3).

$$\frac{BP}{\pi D} = \frac{B'P'}{\pi d} \Leftrightarrow \qquad D/\cos\alpha = d/\cos\alpha' = D_0/\cos\alpha_0 \qquad (7.3)$$

with :

D = diameter in deployed state

d = diameter in collapsed state

D_0 = cylinder's manufacturing diameter

α = braided wire angle for cylinder in deployed position

α' = braided wire angle for cylinder in collapsed position

α_0 = braided wire angle at manufacturing state

Braids will hence be defined in further considerations with the following parameters :

- expected deployed diameter D
- manufacturing diameter and angle (D_0, α_0)
- binomial (i,j) in respect to previously described mathematical conditions
- expected height H.

1.2 Constraints related to assembling

In order to properly size and shape the different stent parts, we have to consider the assembling means. A stiff enough assembling of the parts is very relevant for stent axial alignment and to avoid stent tilting. However, some degrees of freedom have to be kept to enable compression for catheter insertion and easy deployment on implantation site. For that purpose two requirements need to be fulfilled. Relative rotation of stent parts have to be avoided to realize proper positioning and orientation in the aortic root, while relative sliding movements must be permitted to not restrain braided stent parts length variations during expansion. At last, as already described before, stent arms must be linked to the stent only on their top to allow them to flex, thus maintaining permanent contact with sinus tissues over the whole valve cycling.

The three straight linking posts were positioned on the braided stent head surface at regular intervals. Each post was fixed at one end to the upper edge of the head with one fixed suture point. Several mobile fixing stitches were then placed along the linking posts, allowing the cylindrical head to slide down along these posts (Figure III.4). By this way, the compression of the braided stent’s head isn’t impeached.

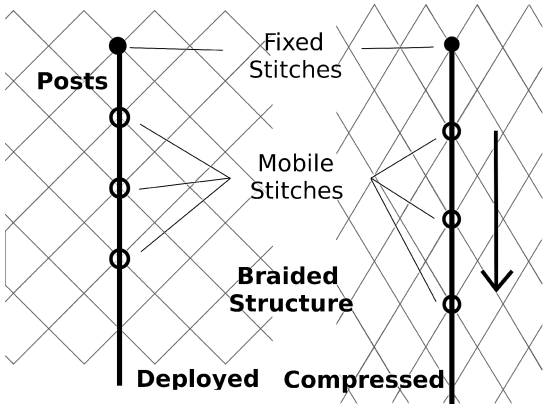

Fig III.4_Post and head assembling

The same was done on the braided stent conical annulus. Although welding Nitinol to itself could be performed using CO2 laser under Ar protective atmosphere, for example, this technique requires specific material and know-how. Fixation through suturing is a much easier way to link parts together. This securing technique is not perfect, but allows the rapid mounting and disassembling of the stent parts. In order to use the same assembling technique between the posts and the braided conical basis, the latter part is completed with a cylindrical edge at its center. Each post is fixed at its other end to the cone with one fixed suture point, located at the edge of the conical base. The added cylindrical edge allows then the addition of mobile stitches and provides for the upper part of the cone the possibility to slide upwards the stent during the compression phase. When assembled in that way, the conical basis and the head are both free to slide along linking posts upon compression.

Stent arms as well as valve prosthesis were sutured on posts by fixed stitch only, because no relative sliding movement was necessary. However these non mobile stent components must not prevent stent compression and allow relative translation of braided stent parts as seen previously. Each linking posts was therefore composed of two rods. One was used to support axially the fixed parts of the endo-prosthesis (arms and valve), while the second supported mobile stitches for braided parts's movement.

The stent is then assembled with the valve. The prosthesis used for that purpose is a textile fabric prosthesis developed by Heim and al [HEI.04]. The textile valve gives ease on manufacturing, use, and adaptability to stent geometry. The textile prosthesis is prolonged with a conical basis which is superimposed to the corresponding stent part in order to improve sealing. The valve prosthesis is first sutured on the stent conical basis, and then on one of each post's rod (at commissure's level). The corresponding rod is therefore coated with fabric in order to reduce friction between the valve and the stent. At last, the geometry of arms and posts need to be suited for assembling with the braided parts.

1.3 Geometrical specifications

1.3.1 Cylindrical head

The stented valve is guided in the aorta through the contact established between the cylindrical head of the stent and the aorta tissues. The behavior of the head in the aortic environment depends on : (1) the radial force applied by the stent on the tissue, (2) the way this force is spread on the tissue surface, (3) the height covered with the braid. These characteristics are controlled with the braiding conditions. It is therefore necessary to establish the relationship between the braiding parameters and the cylinder specifications. On that basis it is then possible to set the braiding parameters in accordance to what is expected for the cylinder.

The mathematical model adopted for a braid and presented in the previous chapter, establishes a link between the radial pressure P applied on a braided tube and the diameter variation of that tube (depends on the geometrical characteristics of that braid).

$$P_{tresse} = \frac{n \cdot E \cdot I}{2 \cdot \pi} \cdot \left(\frac{2\cos\alpha_0}{D_0} \right)^4 \cdot \frac{1}{\sin\alpha} \cdot \left[\left(1 - \frac{D_0}{D} \right) - \frac{1 - \sin\alpha_0 / \sin\alpha}{1 + \nu} \right] + \frac{2}{D \cdot L \sin\alpha} \cdot \frac{3EI}{L^3} \cdot \lambda \pi \left(D - D_0 \right) \qquad (8.3)$$

One may note that P is largely dependent on the length L of the wire parts involved in the braid height. L can be written as a function of (i, j, D_0, α_0, D, α).

$$L = AB = BP / \cos\alpha \qquad (9.3)$$

with

$$BP = \frac{j}{N} \pi D \qquad (10.3)$$

and

$$N = 3i \qquad (11.3)$$

Finally P can be written as a function of the braiding parameters (i, j, D_0, α_0) and the braid diameter D that is considered.

The values for (i, j, D_0, α_0) can then be set according to the pressure value that the stent is supposed to apply on its environment.

1.3.1.a Conditions on the pressure

A first condition is that the cylindrical head must remain in permanent contact with aorta tissues in order to ensure proper axial guiding of the stent. Its manufacturing diameter D_0 must be set according to the most adverse situation. In systole, aorta's diameter expands to reach D_{max} under blood pressure. D_{max} and D_0 must be linked with :

$$D_0 \geqslant D_{max} \qquad (12.3)$$

D_{max} is evaluated from the systolic pressure value (120mmHg) and the aorta tissue elastic modulus.

A second condition is that the pressure applied by the stent on the tissues should be reduced to a minimum value, in order to minimize tissue degradation. At systole we can write :

$$P_{max} = P_{systolic} + P_{stent/aorta} \leqslant P_{lim.} \qquad (13.3)$$

in which

P_{limit} = limit pressure applied on tissue

The finally chosen braiding parameters must also respect this inequality.

1.3.1.b Conditions related to local stress concentration

Next to the global approach of pressure loading, it is of importance to consider the local degradation of tissue due to the wire / tissue interface and the associated stress concentration. The local pressure may promote tissue inflammation and hyperplasia with high stress in the tissue [SUL.02], [GAR.00]. It requires to be controlled in order to prevent conduit stenosis.
The local stress applied at the wire / tissue interface can be calculated from the global pressure applied by the stent on the tissue global surface area. Its value depends on the stent cover rate χ.

$$\sigma_{radial} \cdot s = P \cdot S \rightarrow \sigma_{cir} = \frac{P_{stent}}{\chi_{tresse}} \cdot \frac{D}{2e} \qquad (14.3)$$

s = surface area effectively covered by the wires
S = surface area covered by the stent
P_{stent} = pressure applied by the stent on the tissues
τ = cover rate of the braided stent
D = aorta diameter
e = tissue thickness

Equation (14.3) shows that the higher the χ value, the lower the stress concentration in the aorta wall. It is interesting to assess how to set the braid parameters to maximize χ. Cover rate was already defined in the previous chapter of this book as the ratio between the surface area covered with the braid wires (s), and the braid effective surface (S) :

$$\chi_{tresse} = \frac{n \cdot d}{\pi \cdot D \cdot \sin\alpha} \qquad (15.3)$$

Combining equations (15.3) et (7.3), the cover rate can be written as a function of the braid manufacturing parameters D_0 and α_0 :

$$\chi_{tresse} = \frac{n \cdot d \cos\alpha_0}{\pi \cdot D_0 \cdot \sin\alpha \cos\alpha} \qquad (16.3)$$

One may note that the value for χ is minimized when α= 45 ° and can be written as a function of the braiding parameters (i,j,d, D_0, α_0) :

$$\chi_{tresse\ mini} = \frac{12 d \cdot i \cdot \cos\alpha_0}{\pi D_0} \qquad (17.3)$$

With d = diameter of the braided wire

It is then possible to adjust the braiding manufacturing parameters, in order to obtain a value for χ_{mini} as high as possible even in the worst configuration when α=45°. With such approach we can minimize the local stress.

The pressure that is adopted for the local stress calculation must be the one applied in the worst case. This pressure, noted P_{max}, is the highest in diastole when aorta diameter is the smallest. Stent is then in partially compressed position at $D=d_0$ diameter, d_0 being the native aorta diameter.

$$P_{max} = \frac{12 \cdot i \cdot E\,I}{\pi \sqrt{D_0^2 - d_0^2 \cos^2\alpha_0}} \cdot \left[\frac{4\cos^4\alpha_0}{D_0^3} \cdot \left(1 - \frac{D_0}{d_0} - \frac{1 - D_0 \sin\alpha_0 / \sqrt{D_0^2 - d_0^2 \cos^2\alpha_0}}{1+\nu} \right) + \frac{3^4 i^3 \cos^4\alpha_0}{\pi^2 j^3 D_0^3 d_0} \cdot \left(d_0 - D_0 \right) \right] \qquad (18.3)$$

The combination of the expressions obtained for σ_{circ}, χ_{mini} and P_{maxi} lead to the threshold value for local stress that must remain inferior to the limit adopted for the tissue.

$$\sigma_{limite} \geqslant \frac{D_0^2 E_{NiTi} I}{2 e d \cos\alpha_0 \sqrt{D_0^2 - d_0^2 \cos^2\alpha_0}} \cdot \left[\frac{4\cos^4\alpha_0}{D_0^3} \cdot \left(1 - \frac{D_0}{d_0} - \frac{1 - D_0 \sin\alpha_0 / \sqrt{D_0^2 - d_0^2 \cos^2\alpha_0}}{1+\nu} \right) + \frac{3^4 i^3 \cos^4\alpha_0}{\pi^2 j^3 D_0^3 d_0} \cdot (d_0 - D_0) \right] \quad (19.3)$$

This condition will also influence the choice for the values finally adopted for the braiding parameters.

1.3.2 Conical basis

The role of the conical basis is to ensure prosthesis anchorage in diastole, and avoid para-valvular leakage. It must therefore be characterized with enough surface area to press on the aortic ring, and resist diastolic pressure induced deformation. Moreover, the conical basis is composed of a cylindrical rim for practical purpose. The edge will help to connect the stent posts to the basis.

1.3.2.a The braiding

The conical surface as well as the cylindrical rim are braided. The braiding parameters are respectively noted (i_1,j_1, α_1, D_1) et (i_2,j_2, α_2, D_2). In order to avoid stent components assembling problems, it is preferred that conical and cylindrical surfaces be one continuous braid. The amount of meshing cells over the circumference must hence be the same, while diameter at surfaces junction must also be identical. The (i,j) parameters must respect mathematic conditions (1.3) to (3.3), and :

$$D_1 = D_2 = D \quad (20.3)$$

$$i_1 = i_2 = i \quad (21.3)$$

$$j = j_1 + j_2 \quad (22.3)$$

With :

j_1 = number of meshing cells over the cone height

j_2 = number of meshing cells over the cylindrical rim height

As to the braiding angles of the cone and rim, they remain independent.

1.3.2.b The cylindrical rim

The rim must facilitate the assembling of the conical basis to the stent posts and promote stent cohesion. Sutures at wire crossing points are used to realize the assembling of the two parts. To limit the post rotation mobility (for better cohesion), two criteria must be considered in the positioning of the suture stitches :

- Distance between fixed stitch and mobile stitches must be important
- Wire crossing angle must be low

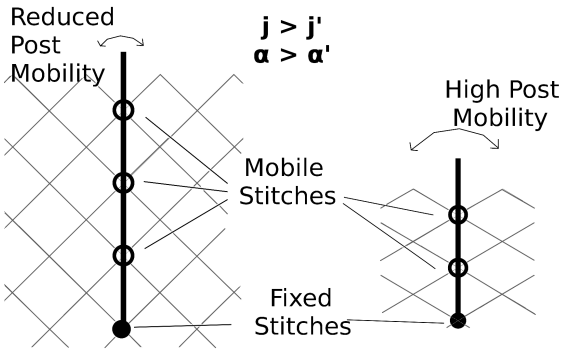

Figure II.5_stent posts assembling on the cylindrical edge

These conditions lead to minimum values for j_2 and α_2 that can be defined as follows :

$$j_2 \geqslant 3 \qquad (23.3)$$

and

$$\alpha_2 \geqslant 45° \qquad (24.3)$$

Cover rate minimization

The cylindrical rim has no specific function for the stent. It may disturb the blood flow in the sinuses, if the cover rate of the braid is too high. It is therefore of interest to reduce the cover rate as much as possible.

$$\chi_{Rc} \to 0 \qquad (25.3)$$

The χ value is minimal when $\alpha=45°$ (eq 17.3). From equation (7.3), we calculate the corresponding diameter :

$$D_{(\alpha=45°)} = \frac{D_0\sqrt{2}}{2\cos\alpha_0} \qquad (26.3)$$

Moreover, the combination of equations (7.3) and (15.3) gives χ as a function of (i, D, D_0, α_0) and the wire diameter d :

$$\chi_{Rc} = \frac{2d \cdot 3i}{\pi D} \cdot \frac{D_0}{\sqrt{D_0^2 - D^2 \cos^2 \alpha_0}} \qquad (27.3)$$

The diameter variation of the aortic ring (diameter = d_0) over the cardiac cycle can be considered as very low. It can be neglected in the calculation of the cover rate. Thus we can set the average diameter for the cone at $D_{average}=d_0$ and obtain following expression for χ :

$$\chi_{Rc} = \frac{2d \cdot 3i}{\pi d_0} \cdot \frac{D_0}{\sqrt{D_0^2 - d_0^2 \cos^2 \alpha_0}} \qquad (28.3)$$

From the combination of equations 26.3, 27.3, 28.3 we obtain the final definition for the minimal cover rate that can be obtained, and the corresponding condition between D_0 and α_0.

$$\frac{D_0}{\cos \alpha_0} = d_0 \sqrt{2} \qquad (29.3)$$

$$\chi_{Rcmini} = i\,d\,\frac{6\sqrt{2}}{\pi d_0} \quad \to 0 \qquad (30.3)$$

The braiding parameters for the cylindrical rim can be defined from these results.

1.3.2.c Conical surface

The previously described model (previous chapter) for conical braid is inadequate and cannot be adopted for the braiding parameters definition. Moreover, the added cylindrical rim may change results significantly. A qualitative approach may however be considered to ensure that the stiffness of the cone is high enough for preventing cone collapse. Indeed, the presented theoretical relationships between radial pressure and diameter evolution show that the stiffness of the braided cone depends on :

- The wire parts length
- The cone angle

To prevent any risk of collapse of the conical part under diastolic pressure, these parameters need to be controlled.

Influence of the wire length

We establish here the relationship between L and the braiding parameters, in order to analyze how to set these parameters for obtaining enough resistance of the braid. Figure III.6 is a planar representation of the cone, which shows how wires interlace.

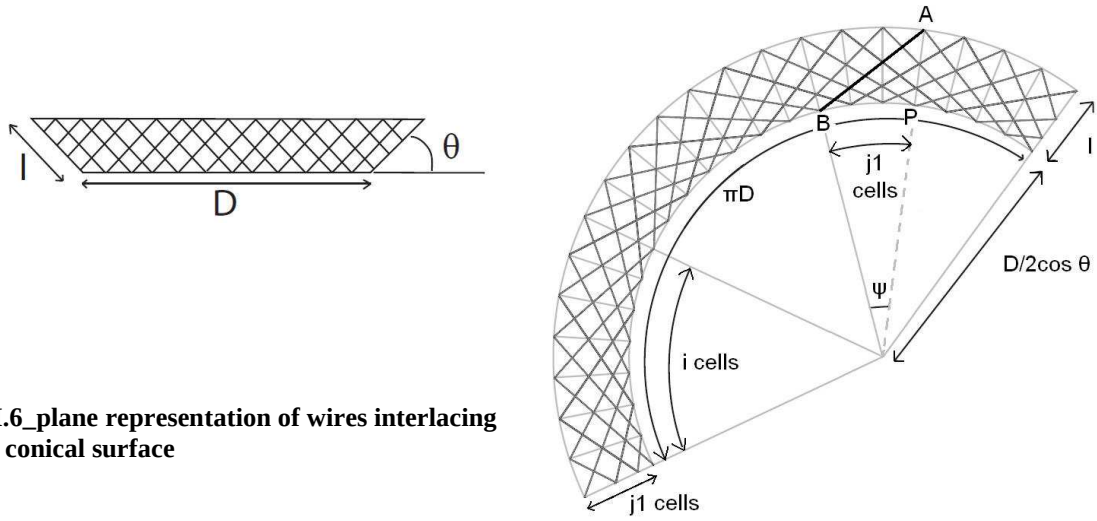

Fig III.6_plane representation of wires interlacing on the conical surface

with :

θ = conical surface angle

l = cone width

The braiding conditions lead to following geometrical definitions for the braid.

$$\widehat{BP} = \frac{D}{2\cos\theta}\cdot\psi \qquad \text{and} \qquad \widehat{BP} = \frac{j_1}{3i}\cdot\pi D \;\rightarrow\; \psi = \frac{2j_1}{3i}\cdot\pi\cos\theta \tag{31.3}$$

The length L of the wire parts AB (Figure III.6) is a constant data. It is written as a function of the braid parameters (i, j, D_0, θ_0, l_0) (see Chapter II).

$$L = AB = \sqrt{\left(\frac{D_0}{2\cos\theta_0}\sin\left(\frac{2j_1}{3i}\cdot\pi\cos\theta_0\right)\right)^2 + \left(\frac{D_0}{2\cos\theta_0} + l_0 - \frac{D_0}{2\cos\theta_0}\cos\left(\frac{2j_1}{3i}\cdot\pi\cos\theta_0\right)\right)^2} \tag{32.3}$$

D_0 can be removed and replaced with α_0 (braiding angle at manufacturing state) according to equations (20.3), (29.3), (31.3) and (32.3).

$$L = \sqrt{\begin{array}{l}\left(\dfrac{d_0\sqrt{2}}{2\cos\alpha_0\cos\theta_0}\sin\left(\dfrac{2j_1}{3i}\cdot\pi\cos\theta_0\right)\right)^2 \\ +\left(\dfrac{d_0\sqrt{2}}{2\cos\alpha_0\cos\theta_0} + l_0 - \dfrac{d_0\sqrt{2}}{2\cos\alpha_0\cos\theta_0}\cos\left(\dfrac{2j_1}{3i}\cdot\pi\cos\theta_0\right)\right)^2\end{array}} \tag{33.3}$$

The cone is more resistant if the value of L is reduced.

Equation (33.3) shows that :

- L decreases when i increases (34.3)
- L decreases when l_0 decreases (35.3)
- L decreases when j_1 decreases (36.3)
- L decreases when α_0 decreases (37.3)

We analyze here more in detail the effect of each variable on L.

◆ Variation of i

In respect to (30.3), it is not possible to increase the value for i without increasing the cover rate for the rim.

◆ Variation of α_0

Decreasing α_0 leads to an increase in the manufacturing diameter of the conical basis D_0 (Eq29.3). The collapsing resistance of the cone is increased, but the radial force on tissues increases as well, with degradation consequences.

◆ Variation of l_0 and j

Over the cardiac cycle, the cone must be large enough to withstand the aortic ring diameter changes (ΔD). Assuming the cone size (manufactured at d_0 diameter, with a θ_0 angle) doesn't vary dynamically, the condition for having permanent contact between cone and ring is :

$$l_0 \cos\theta_0 \geqslant d_0/20 \qquad (38.3)$$

[corresponds to $l_0 \cos\theta_0 \geqslant \frac{d_0}{2}\Delta D$ with ΔD =10%]

Influence of the angle

To prevent the cone from degrading the bottom part of the sinuses, two conditions must be respected : (1) the cone angle value must be important enough to press on the aortic ring rather than on the sinuses, (2) the cone width must be limited to not destroy the depth of the sinuses. Therefore we should have :

$$\theta_0 \geqslant \theta_{natif} \qquad (39.3)$$

$$\frac{d_{sinus} - d_0}{2} \geqslant l_0 \cos\theta_0 \qquad (40.3)$$

In which :

θ_{natif} = angle between the basis of the sinuses and a horizontal plan
d_{sinus} = sinus diameter
d_0 = diameter of the aortic ring

1.3.3 The posts

The role of the posts is to link the cylindrical head to the conical basis

1.3.3.a Height definition (Figure III.2)

The posts height is directly related to the height of the stent. It can be defined from 2 conditions :

1/ An important condition to be taken into consideration when setting the value of posts height H_{stent}, is that between deployed diameter D and collapsed diameter d at implantation (7mm for standard catheter), stent's head must be able to slide downwards along posts without interfering with the base of the stent. In that model, the head is supposed to be fixed to the top of the posts at its upper end, while its other end is free to slide downwards.

$$H_{stent} \geqslant h + H_b \qquad (41.3)$$

in which :

Hstent = stent height = posts height

h = cylinder height in compressed position

H_b = height of the cone's cylindrical edge in collapsed configuration.

2/ To prevent head interferences with coronary ostium at the sinotubular junction during cardiac cycle, the posts height must also respect the following geometrical condition :

$$H_{stent} \geqslant H_s + H \qquad (42.3)$$

in which :

H_s = sinus height

H = cylinder height at implanted diameter

An average value for Hs in human can be obtained from literature [SWA.74], and is around 0,87*D (D being the diameter of the aorta base). The H and h values were defined from the deformation undergone by the braided geometry between initial and compressed configuration.

H et h calculation

Assuming that all braided wire parts remain straight during compression process and just rotate and slip above each other, the straight distance value between points A and B should be the same as the distance value between points A' and B'.

$$AB = A'B' \quad \rightarrow \quad D/\cos\alpha = d/\cos\alpha' = D_0/\cos\alpha_0 \qquad (43.3)$$

and $\rightarrow$ $H = BP\tan\alpha$, $h = B'P'\tan\alpha'$ (44.3)

in which :

H = cylinder height at manufacturing diameter

h = cylinder height in compressed position

D = deployed diameter

d = collapsed diameter

D_{0h} = cylinder's manufacturing diameter

α = cylinder's deployed braided wires angle

α' = cylinder's collapsed braided wires angle

α_{0h} = cylinder's manufacturing braided wires angle

BP (resp. B'P') = length of wire part AB(resp. A'B') projected on head's circumference

Regarding to braided geometry parameters and equation (43.3), the calculation of cylinder's heights can be obtained from the rewriting of equation (44.3).

$BP = j_h\,\delta$

$\delta = \pi D/2N_h$

$i_h = N_h/3$

$$H = \frac{\pi\, j_h}{3 i_h \cos\alpha_{0h}} \cdot \sqrt{D_{0h}^2 - D^2\cos^2\alpha_{0h}}$$

and

$$h = \frac{\pi\, j_h}{3 i_h \cos\alpha_{0h}} \cdot \sqrt{D_{0h}^2 - d^2\cos^2\alpha_{0h}} \qquad (45.3)$$

in which :

δ = meshing cell width

j_h = number of meshing cells over the distance BP over the head's braid

N_h = number of meshing cells over the head's circumference

i_h = number of meshing cells between two sinuses over the head's braid

During the cardiac cycle, the stented aorta diameter oscillates between two values, minimal in diastole and maximal in systole, and will never be lower than the native diastolic aorta diameter d0. The implanted cylinder height could so be maximized in fixing $D = d_0$.

$$H_{max} = \frac{\pi j_h}{3i_h \cos\alpha_{0h}} \cdot \sqrt{D_{0h}^2 - d_0^2 \cos^2\alpha_{0h}} \qquad (46.3)$$

H_b calculation

H_b can be calculated from equations (29) et (45) applied to the rim geometry :

$$H_b = \frac{\pi j_2}{3i_b} \cdot \sqrt{2d_0^2 - d^2} \qquad (47.3)$$

In which :

j_2 = over the height of the rim

i_b = number of meshing cells over the cone circumference

d_0 = diameter of the aortic ring

d = stent diameter in compressed state

Conclusion

The combination of the previous equations equations lead to :

$$H_{stent} \geqslant \frac{\pi j_2}{3i_b} \cdot \sqrt{2d_0^2 - d^2} + \frac{\pi j_h}{3i_h \cos\alpha_{0h}} \cdot \sqrt{D_{0h}^2 - d^2 \cos^2\alpha_{0h}} \qquad (48.3)$$

$$H_{stent} \geqslant H_s + \frac{\pi j_h}{3i_h \cos\alpha_{0h}} \cdot \sqrt{D_{0h}^2 - d_0^2 \cos^2\alpha_{0h}} \qquad (49.3)$$

The height of the stent will then be defined according to the more restrictive condition between (48.3) and (49.3).

1.3.3.b Posts shape

The shape adopted for the posts must first allow the braided parts to slide along the posts. The suture points between posts and head and cone must hence be mobile for part of them. Second, their geometry must be as straight as possible to minimize flow disturbances. A straight geometry realized with Nitinol wires seems to be the best solution. One anchoring point between braided elements and posts must be fixed. The ends of the posts are thus loop-shaped for easy suturing with head and cone. Posts are composed of two wire parts running parallel. They are obtained with one continuous Nitinol wire to prevent exaggerated knotting and suture. One holds the braided elements while the other one holds the axially non mobile parts (arms and valve). The main disadvantage of the adopted assembling method, is that much material is concentrated at the conical basis level (posts loop, cone rim) and may lead to leakage problems.

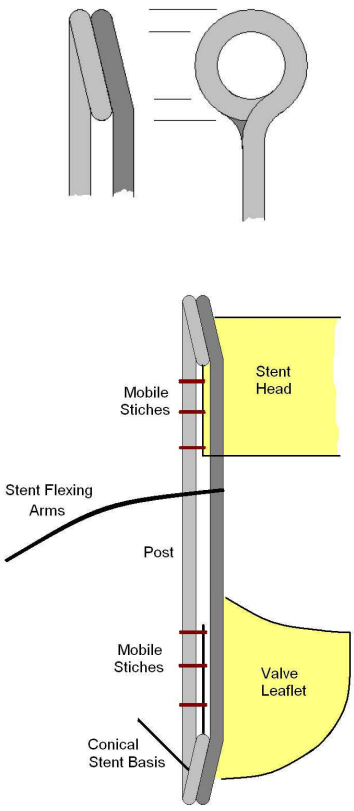

Figure III.7_schematic representation of stent posts assembling

1.3.4 The arms

The arms are an essential parts of the stent that needed close attention. Stent arms function is to ensure anchorage and sealing of the endoprosthesis in the aortic root. For that purpose, they have to remain in contact with the upper part of the sinuses, to create a force opposed to the one applied by the stent conical basis on the aortic annulus. Arms length and curvature are imposed by the native aortic root geometry. To maintain a permanent contact in upper sinuses, arms are shape set in over expanded conformation. Each stent arm is fixed to stent posts by one end only like represented in Figure III.8. In order to limit sutures on stent posts, the 3 stent arms were obtained from a continuous Nitinol wire which provided a U-shape at stent post location to facilitate sutures of the arms around stent posts.

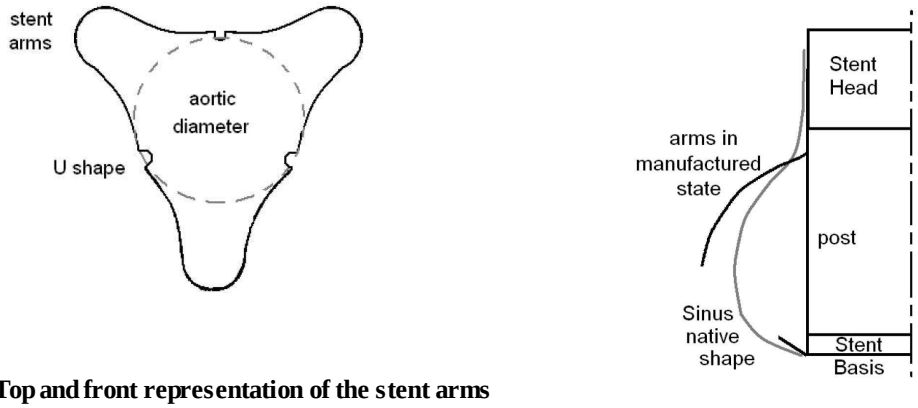

Fig III.8_Top and front representation of the stent arms

1.4 Final values adopted for the stent parameters

We adopted average values for the setting of the stent geometrical parameters, based on a 21mm diameter stented valve. These values take into consideration all the previously described conditions and the native aortic root characteristics.

1.4.1 Parameters adopted for the different stent parts

Braided Head	
i	7
D0	30mm
j	5
alpha _0	28°
dNiTi	0,260mm
EniTi	35GPa
ΔD.native	30,00%
e	1mm

Braided conical basis	
i	5
Do	21mm
jcone	2
Thêta_0	40°
l	6mm
jcylinder	5
Alpha_0	25°
dNiTi	0,260mm
EniTi	35GPa
thêta native	20-45°
ΔD anneau	5,00%

Posts	
d	0,55mm
nb wires	2
EniTi	30GPa
Hs	18,9mm
ΔP dias/sys	50mmHg

stent arms	
θ	90°
Rsinus	10.5mm
nb wires	3
dNiTi	0,406mm
EniTi	30GPa
Esinus circ	500kPa
Esinus long	670kPa

The dimension variations that appear in these tables (ΔD_{aorte}, ΔD_{anneau}, θ,….) correspond to values reported in literature. For the aorta elasticity we adopted ΔD=30% (or E=300kPa), which is the maximum value that can be found and corresponds to the worst case. Sinuses dimensions are given according to the description made by Swanson & Clark [SWA.74]. The angle at the basis of the sinuses (20°) as well as their curvature radius (between 10 and 14mm) that were adopted in our work are average values given by Beller [BEL.08] and Thubrikar [THU.81]. The behavior of the arms in the sinuses is calculated from the elastic modulus value of the sinus tissues [FER.99]. The chosen values correspond to diameter expansion of around 20% over cardiac cycle.

1.4.2 Dynamic behavior and interaction with tissues

The values adopted for the parameters as defined previously, lead to modifications in the dynamic behavior of the stented aortic root.

1.4.2.a Cylindrical head / aorta

1/ Aorta compliance is reduced by only 17 %.

2/ Pressure applied on aorta tissues increases by 4 % in systole and 18 % in diastole, which remains quite low.

3/ The circumferential stress induced in the aorta by the local wire pressure is 0.15 MPa, which is 2 times the stress induced by blood pressure variation over the cardiac cycle. This value is low in regard to the stress applied by standard stents maintained only through expansion force [MOO.02], [BED.06].

The values adopted for N (number of meshing cells over the circumference) and D_0 (diameter at manufacturing state) are in accordance with the values suggested in the Wallstent patent [WAL.91]. The document suggests the use of an empirical law, to calculate the number of wire parts over the circumference for optimal stent cohesion. The cohesion factor is described with : $C=\sqrt{D}/n$. The authors note that a value located between 0.08 and 0.16 provides good cohesion and avoid excessive stiffness. We observed the same behavior with the stented valve.

1.4.2.b Braided cone-aortic ring

The theoretical calculation for the definition of the cone (i,j) parameters, could not be directly applied in practice. In theory (i=7, j=2+3) would respect all the previously described specifications. However, the reproducibility between two stents could not be manually guaranteed because of a too fine meshing. The (i=5, j=2+5) configuration, which ensures the meshing closest to the theoretical one, gives ease to the manual braiding of the conical part and is finally adopted. It requires, however, the modification on the braiding angle that is set to 40°.

1.4.2.c Arms-sinuses

Different stiffness values were tested for the arms. Experimental testing confirms the conclusions adopted with the theoretical approach presented in Chapter II. Close to rigid arms realized with 3 wires of 0.406mm diameter, reduce drastically the compliance of the sinuses.

Further tests realized with less rigid arms (made up with one or two wires), highlighted the efficient positioning of the endo-prosthesis, with respect to the sinuses compliance.

1.4.3 Dynamic stent bevaviour and stent geometry

The previously adopted values for the stent geometrical characteristics definition are average values, which can be adopted for general in vitro testing. But variations in these characteristics may change the dynamic behavior of the device. In summary, 5 main characteristics may have an influence on the stent's performances.

- Height of the cylindrical head (H)
- Cone angle (θ)
- Cone width (l)
- Arms rigidity
- Posts rigidity

The changes in the stent's performances when varying these characteristics are studied in Chapter V.

2 MATERIAL SHAPE SETTING

We want here to define how to set the parameters for the Nitinol material shape setting process, in order to obtain the final expected shape for the stent components. The elements are obtained through a forming process associated with heat treatment, which role is to fix the structures in the desired shape. Nitinol is not easy to be shape set due to its particular behavior when heated.

2.1 Nitinol and thermal treatment

NiTi shape memory alloys can exist in two differents temperature-dependent crystal structures (phases) called martensite (lower temperature) and austenite (higher temperature or parent phase). The unique behavior of NiTi, shape memory and superelasticity, is based on the temperature dependent austenite to martensite phase transformation on an atomic scale, which is called Thermoelastic Martensitic Transformation (TMT). TMT is responsible for the functional properties of the material. These properties result from the need for the crystal lattice structure to accommodate to the minimum energy state for a given temperature. TMT can be activated, so that NiTi alloys can be transformed from austenite to martensite and vice versa, either by reducing the temperature (Thermally Induced Martensite, TIM) or by applying a mechanical stress (Stress Induced Martensite, SIM). On the other hand the martensite transforms into austenite through either increasing the temperature or removing the applied stress. This shows that mechanical loading and thermal loading have opposite effects on NiTi alloys.

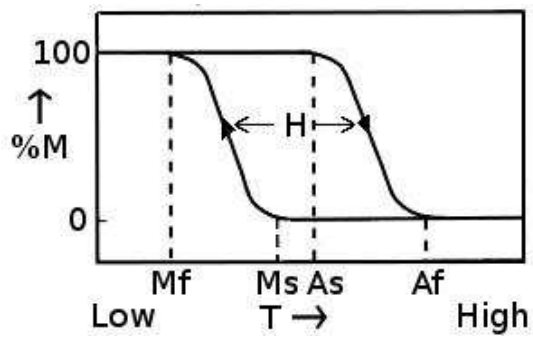

Fig III.10_Schematic thermal transformation hysteresis loop

T = temperature, %M = martensite percentage, H = hysteresis

When austenite is cooled, it begins to change onto martensite; the temperature at which this phenomenon starts is called martensite start temperature (Ms), while the temperature at which

martensite is again completely reverted is called martensite finish temperature (Mf). When martensite is heated, it begins to change into austenite; the temperature at which this phenomenon starts is called austenite start temperature (As), while the temperature at which this phenomenon is complete is called austenite finish temperature (Af).

The particular behavior of Nitinol material (superelasticity and shape memory) in comparison to more common other materials, requires to be able to control with precision the heat treatment related parameters. Only then, the reproducibility of the shape stetting can be guaranteed.

2.1.1 Forming process

2.1.1.a Theory

Our particular purpose requires the setting of a custom shape in a piece of Nitinol. Different papers describe some ways to obtain desired shapes [LIU.97], [PEL.00], [NDC]. The most common way of shape setting Nitinol is to firmly constrain into its new shape and then perform a heat treatment. The wire is clamped at one end in a tooling fixture and subsequently wrapped around pegs to create a series of shapes [MOR.03]. The end is then clamped off to hold the wire in place during heat treatment. In general, temperature as low as 400°C and time as short 1-2 minutes can set the shape but generally one uses temperature closer to 500°C. But some authors related fruitless experiences with low temperature as 300-400°C even after 180 min ageing time. Heating could be obtained with salt bath or furnace under controlled atmosphere to avoid oxidation. Rapid cooling is preferred via water quench to avoid ageing affects and sharply define the heating time. In fact, the heat treatment parameters are critical. The heat treatment causes a change to the microstructure of the nitinol and correspondingly a change to the mechanical properties and transformation temperature. High heat treatment times and temperature will increase actuation temperature of the Nitinol part. However, a specific evolution of Af could be observed about 500°C, with an initial decrease in Af, and then increase of Af. There's also a decrease in plateau stresses and in the ability of the Nitinol to resist permanent deformation.

The starting condition of the alloy will also have a strong influence of the final properties. Commonly, the nitinol may be purchased in either the straight annealed condition or in the as drawn conditions. Straight annealed means that the wire has essentially been shape into a straight length as it leaves the drawing bench. As drawn means that the wire is coiled directly

from the last drawing step. To establish the exact heat treatment temperature and time, an experimental design may be performed to specify an optimum heat treatment for a particular tool design.

2.1.1.b In practice

Nitinol wires used in our experiments are provided by Euroflex Gbmh under annealed conditions. We used body temperature response material, NiTi wire SE508, composed of Ni 55,8wt % Ti balance with a transition temperature assume to be between 5 and 18°C and loading plateau stress higher than 450MPa [EUR]. In order to control and obtain a reproducible geometry of the Nitinol wire that is to be expected, we used an aluminium shaped support for each stent part. Nitinol wires were wrapped around peaks positioned on the support according to the geometry that is to be obtained. Because it is difficult to interlace straight and elastic nitinol wires into a cylindrical / conical shape to obtain braided stent parts, they underwent 2 successive thermal treatments in flattened configuration first, to help fixing wire curvature, and then in the 3D final configuration to fix the desired shape. Specimens were heated in an air furnace with no control of Nitinol oxidation.

The problem with the Nitinol used is that its original transition temperature is very close to the handling room temperature. In our experiments, we want to keep the elastic properties of the material, i.e. in its austenitic phase, for stent compliance purpose. We therefore want to reach lower transition temperature through thermal treatment. Thus, as heat treatment affects Nitinol properties, experimentation had to be done to determinate appropriate heat treatment parameters for setting desired properties of nitinol stent parts. Moreover, if it's necessary to obtain stable and desired shape setting results, the degradation of mechanical properties through thermal treatment is a very big issue as well. Some mechanical testing will also be performed.

Finally, we studied the impact on Nitinol properties of 2 successive thermal treatments.

2.1.2 Material characterization methods

2.1.2.a The goal

The aim of this section is to analyze three main features of the material after the forming process : (1) the effective obtained geometry, (2) the transition temperature, (3) the material mechanical properties. Following parameters were varied for that purpose :

- Thermal inertia of the tooling fixture (aluminum plate)
- Heating time
- Heating temperature
- Cooling time.

2.1.2.b The process

Nitinol straight wire were wrapped around nails and clamped on an aluminum plate to impose a wire angle of 70°. Samples were treated at 450 to 560°C in an air furnace for various durations. The specimens were then cooled down to room temperature at two different cooling rate, air cooling and water quenching. Finally, the tooling fixture influence was studied through two configurations, keeping the same material desired shape setting.

The effective obtained geometry was evaluated through the angle measurement, the transition temperature was estimated with DSC technology, and the mechanical properties were obtained through tensile testing.

DSC

As already said, it's desirable to know the transformation temperature of the shape setted Nitinol parts. The transformation temperature are those temperatures at which the alloy changes from the higher temperature Austenite to the lower temperature Martensite, or vice versa. The transformation to martensitic upon austenitic phase starts at Ms temperature and finishes at Mf temperature. The reverse transformation occurs respectively at As and Af temperatures. For our application, it's particularly important to know exactly the Af value to ensure super-elastic behavior of the nitinol at in vitro testing conditions. Three ways are commonly used to determine transformation temperatures [JMM] :

- Constant load
- Active Af
- Differential Scanning Calorimetry (DSC)

In the first method, the nitinol is loaded and its deformation are monitored simultaneously with temperature as the material is cooled and heated. The active Af test is performed in bending a sample of nitinol at temperature below Ms, and then in monitoring the shape recovery while it is heated. These two methods are quite straightforward but require controlled temperature environment, especially with a start testing temperature about -50°C. For that reason, DSC was preferred to characterize the transition behavior of Nitinol, especially the austenitic finish temperature.

DSC testing is a thermal method that measures the changes in heat flow which is associated with the martensitic and austenitic phase transformations through controlled cooling / heating cycle. In heat flux DSC, the sample and reference are enclosed in a single furnace. The temperature difference is recorded and related to enthalpy change in the sample using calibration experiments.

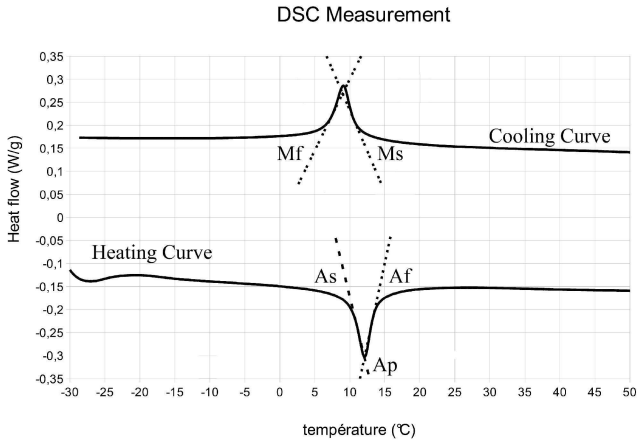

Figure III.11: A typical DSC curve for a NiTi Shape Memory Alloy

As the transformation from martensitic to austenitic phase, and vice versa, corresponds to a phase accommodation and related enthalpy modification, the alloy transformation temperature can be detected, especially when the Nitinol is fully annealed. The DSC method yields a plot such as Figure III.11. During cooling of the Nitinol material below temperature Ms in absence of stresses, the variants of the martensitic phase arrange themselves in a self accommodating manner. This transformation is exothermic and the reverse one is endothermic.

DSC measurement were carried out on a DSC 2920 TA Instrument with a heating/cooling rate of 10°C/min. Measurements were performed on specimens from Nitinol wires which have not undergone previous shape setting and thermal treatments. Specimens were prepared using segments from Nitinol wire, cut away from curved and attachments wire parts.

In this study, we focus on the effects of the heat treatment process to austenitic upon martensitic transformation. Indeed, superelasticity and mechanical properties of nitinol

depend on the temperature difference between the working temperature and the austenitic finish temperatures. Only Ap temperature is discussed. Ap is defined as the temperature of the transition peak obtained in the DSC curve while the specimen was heated up. Obtained values were plot as function of heat treatment duration. The following figure (III.12) shows a typical Ap evolution over time, for heat treatment realized at temperature above 500°C.

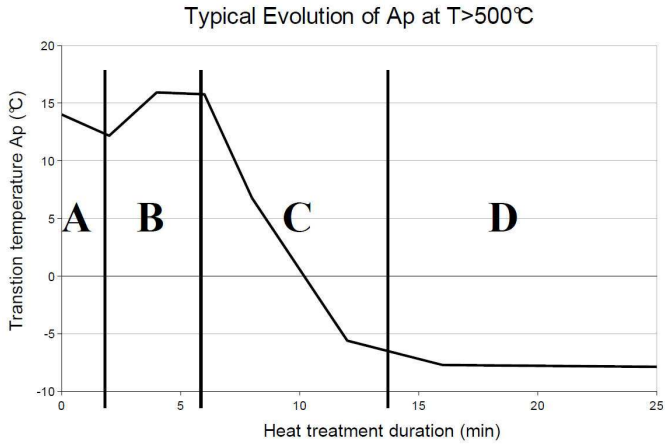

Figure III.12_ A typical Ap evolution during heat treatment at temperature above 500°C

Four typical zones can be identified on the plot :

Zone A : Ap transition temperature decreases

Zone B : Ap transition temperature increases and reaches a maximum

Zone C : transition temperature drops drastically

Zone D : temperature value becomes steady

These behaviors are explained and justified later in this document. We note t1, t2 and t3 the durations of the transitions from A to B, B to C, C to D.

Tensile testing

Mechanical properties of Nitinol material are evaluated with a tensile test using a MTS M20 Adamel Lhomargy force machine. Nitinol wire is loaded at constant strain rate and stress evolution is measured with a force sensor. Sample are 20 mm long. Low strain rate value is set ($4.2.10^{-4}$ /s) in order to keep sample temperature constant and avoid temperature influence on measurements. Figure III.13 shows the influence of strain rate value on measurement.

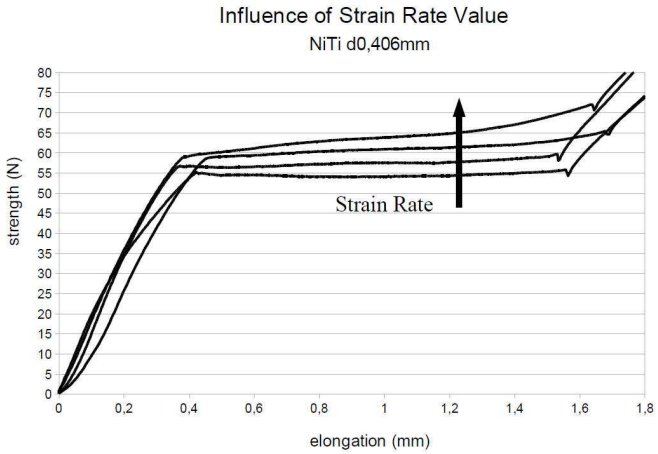

Fig III.13_influence of strain rate on mechanical properties

With low strain rates applied, the studied range for strain variations remains low. This is in accordance with the only slight deformation undergone par the nitinol material implanted in the aortic root. The hysteresis of the material is not taken into consideration. An average value for the modulus of elasticity and for the loading plateau is set for every sample. The precision obtained for the measurements remains however poor. The nitinol wire, very degrading for the clamps, first tends to slide between them. Another problem is the difficulty to evaluate the initial length of the samples. Its value is calculated from the values given by the force and displacement sensors. At last, the lab conditions do not allow controlling the temperature. Only two samples were tested each time. Hence, results cannot be statistically interpreted. They give us, however, some information about the global evolution of the material properties, as a function of the heat treatment that were performed. Figure III.14 gives the elastic properties of Nitinol wire for different diameters.

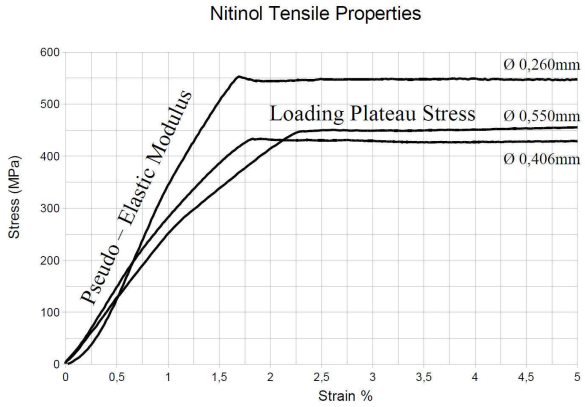

Fig III.14_ stress-strain curve of 3 nitinol wires

2.2 The Results

2.2.1 Transition temperature

2.2.1.a Plate thermal inertia

We used two tooling fixture with different mass (m_1 and m_2). It can be observed that the mass of the tooling fixture influences the evolution of the A_p value. We note that the evolution for A_p is globally the same. However, the fixture with the bigger mass induces delay in the A_p evolution (figure III.15). As to the values obtained for the elastic modulus, the shaping angle and the stress plateau, they also depend on the used fixture. The temperature of the fixtures has not been measured in the experiments, but it seems obvious that the higher the mass, the longer the time required to elevate the nitinol temperature. The inertia of the fixtures used for all the stent parts must therefore be equivalent, to ensure that the heat treatment is the same, and guarantee that the final properties of the shape set components are the same as well.

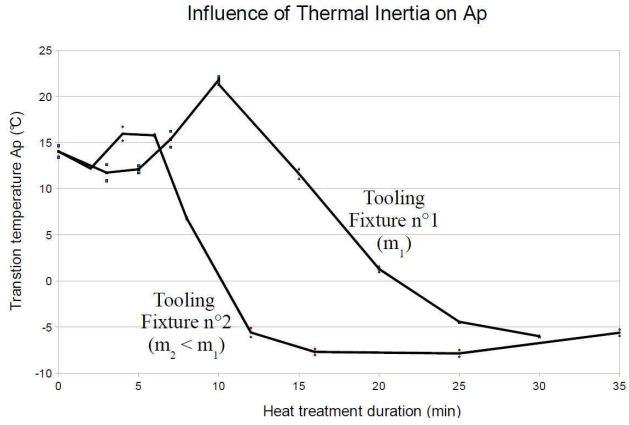

Fig III.15_ Influence of the thermal inertia on A_p (NiTi d0,406mm, 560°C)

2.2.1.b Influence of heating temperature and duration

Figure III.16 shows the evolution of A_p as a function of different heating temperatures applied. For heating duration over 10 min, the A_p value increases if temperature remains under 500°C, and decreases suddenly for temperature values above 500 °C. These results are in accordance with what can be found in other published documents [PEL.00]. The A_p increase is explained with the generation of precipitation like $Ti_{11}Ni_{14}$ / Ti_2 Ni_3 / $TiNi_3$ at heating begin. Indeed, transition temperatures for Nickel–Titanium alloys are highly dependent on the alloy composition. The NiTi matrix looses some Ni with the apparition of these precipitations. On the contrary, the generation of Titan oxides at the material surface for temperature above 500°C, reduces the amount of Titan in the matrix and induces decrease in the A_p value. The titan oxides appear in a parabolic way, which justifies the initial high decrease of A_p followed with a more steady evolution.

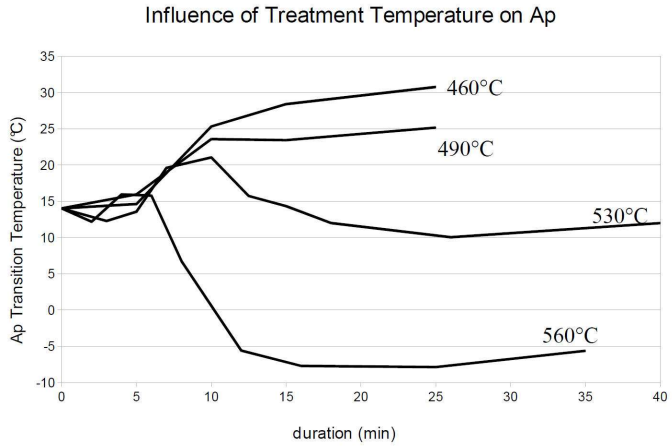

Fig III.16_ Influence of temperature on A_p

The initial A_p transition temperature for the Nitinol SE508 material is located between 5 and 18°C. The heat treatment parameters must be set to avoid an increase in A_p, in order to keep the A_f value largely under ambient temperature, which is the working temperature for the stent (need to behave elastically). Heat treatment will therefore be realized at temperature above 500°C.

We note on the first zone of the graph that A_p decreases first slightly to then increase again. Favier et al. [FAV.06] explained that initial evolution for heating temperature around 500°C, with the stress present in the material. For a non stressed sample (non formed), A_p would remain constant on that zone. On the contrary, when the sample is formed on the plate before heat treatment, a stress is induced in the structure. This stress influences A_p which is first lower and then higher than what is obtained with a non stressed sample. We did not perform any test to verify this assumption. But, in order to make our experiments as reproducible as possible, we had to try to deform the wire in a way that was always the same. The goal was to apply a stress as similar as possible to the structure whatever the component manufactured.

2.2.1.c Cooling

Water quenching is the cooling process that is most of the time recommended in literature dealing with nitinol treatment. This rapid cooling process sets the material properties immediately and allows increasing the measurements reproducibility. Low cooling of nitinol tends to prolong the thermal treatment. Final properties are hence difficult to control. Yeung et al [YEU.04] highlighted, however, that air cooling leads to A_p values 15 °C to 20 °C under values obtained with water quenching. To assess the validity of this result we realized a few tests varying the cooling process, and measured the obtained material properties. Air cooling doesn't appear to be more efficient. Moreover, the results are not constant, which proves that

A_p can either increase or decrease with air cooling. If cooling is performed once the material has reached its target temperature (560°C), air cooling will first occur over a temperature range higher than 500°C and A_p decreases. Later, the cooling occurs over a temperature range lower than 500°C and A_p increases.

2.2.2 The effective obtained geometry

The effective geometry obtained after heat treatment corresponds the one expected (an angle of 70 ° obtained with wire folding) as soon as the heating duration is long enough for A_p to decrease.

2.2.3 The mechanical properties

We focused on the measurement of 2 material characteristics : the elastic modulus (E) and the limit stress (σ_{lim}) obtained at the end of the elastic domain.

2.2.3.a Changes in the elastic modulus

Figure III.17 shows the evolution of E versus heat treatment duration, for 2 different heating temperatures. The evolution of the E value follows the evolution of the A_p value. E decreases continuously for shape setting at temperature around 530°C. A sudden increase follows an initial decrease, when heating temperature is around 560°C. This phenomenon can be explained as following : mechanical properties of the wire depend directly on the difference between transition temperature and working temperature. For A_p values close to working temperature, nitinol is in a martensitic phase and is less resistant to deformation. E value goes down. If the heating temperature is higher (560°C), A_p decreases and is lower than working temperature, nitinol is in a austenitic phase. E goes up.

We conclude that the value for E can be adjusted with appropriate setting of temperature and duration.

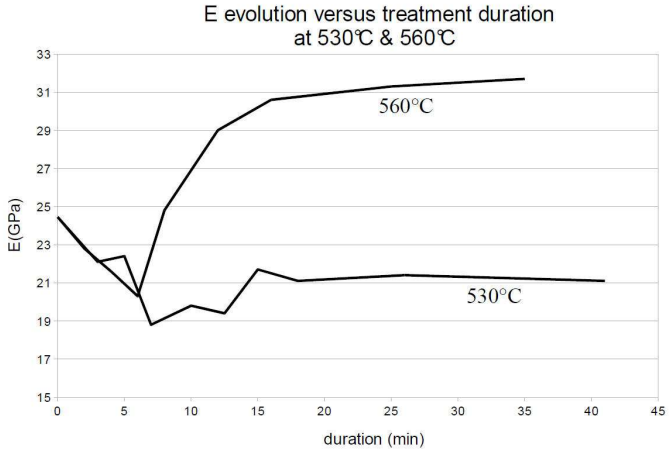

Fig III.17_ E evolution versus treatment duration at 530 and 560°C.

2.2.3.b Changes in stress limit

The limit resistance σ_{lim} (stress plateau), decreases with the heat treatment. The higher the temperature of heating, the sharper the decrease of σ_{lim}. Globally, with higher heating temperature and longer treatment duration, the elastic domain becomes more narrow for the material (Figure III.18).

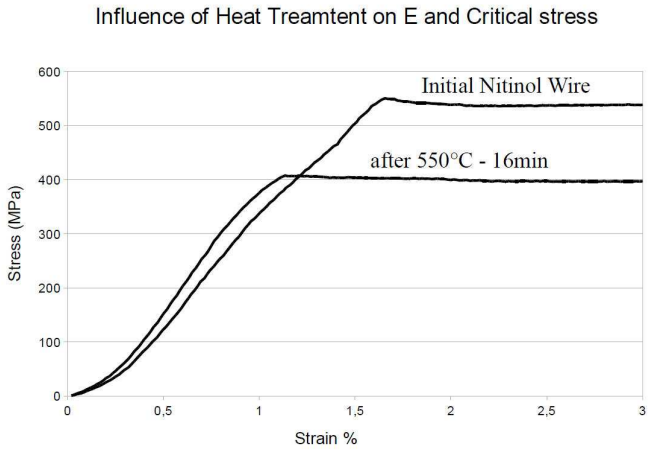

Fig III.18_ influence of treatment on E and σ_{lim}

2.2.4 Effects of 2 successive thermal treatments

In order to easily reproduce the manufacturing of the stent's braided parts, it is of interest to perform 2 successive thermal treatments. The second one is the most significant because it sets the final braid dimensions and the value for A_p. The shape setting temperature will be above 500°C, and the duration will be set so as to obtain the desired shape. The first treatment remains, on the contrary, an intermediate procedure. Nitinol wires will get the rough shape

necessary for easy braiding, but the geometry doesn't need to be perfect. As to the A_p value, it can be close to ambient temperature so for the wires to be in martensitic phase, easily deformable for braiding purpose. In respect to the previously presented material properties degradations caused by heating treatment, it is essential to characterize the effects of the first treatment on the nitinol wires. We performed 2 successive heat treatments, varying for the first one temperature and duration. Table 1 is listing the testing conditions for samples A to F :

<table>
<tr><td></td><td colspan="2">1st Heat Treatment</td><td colspan="2">2nd Heat Treatment</td></tr>
<tr><td>A</td><td>450℃</td><td>t</td><td colspan="2" rowspan="2"></td></tr>
<tr><td>B</td><td>550℃</td><td>t</td></tr>
<tr><td>C</td><td rowspan="2">450℃</td><td>8min</td><td rowspan="4">550℃</td><td rowspan="4">t</td></tr>
<tr><td>D</td><td>20min</td></tr>
<tr><td>E</td><td rowspan="2">550℃</td><td>3min30</td></tr>
<tr><td>F</td><td>8min</td></tr>
</table>

Tableau III.19_ Heat treatment testing parameters

Figure III.20 shows the transition temperature evolution for samples C to F over the 2nd thermal treatment. It can be observed that, in spite of different initial conditions, A_p temperature tends to reach the same value for all samples. Basically, whatever the sample, once the wire has reached 500°C, A_p temperature drops to a final value dictated by the second treatment. Moreover, the final A_p value reached is the same than the one obtained for sample B which did undergo no 2nd treatment. The second treatment at 550°C seems to be predominant on material history and has the bigger impact. As to the elastic modulus, plateau stress and effective final shape, the second treatment is also predominant. Figure III.21 shows, for example, that E isn't different if the material undergoes one or two thermal treatment.

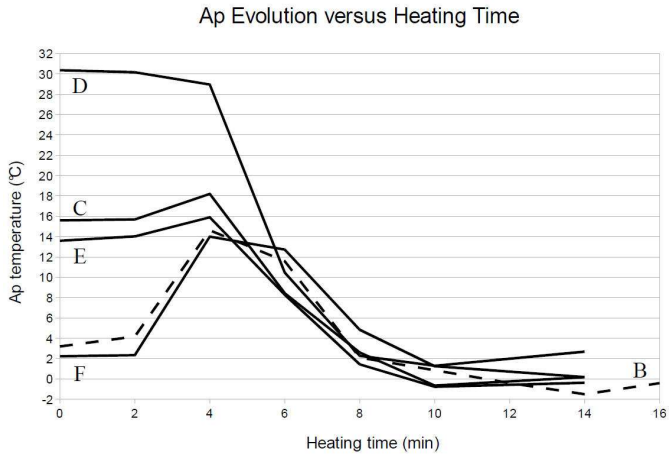

Fig III.20_ Ap evolution versus heating time for samples B to F

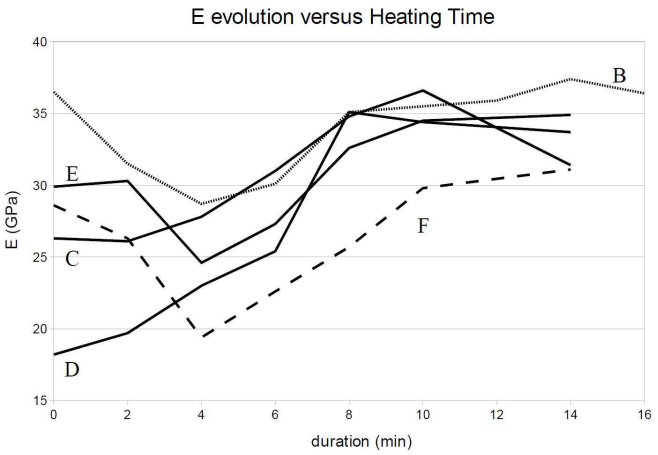

Fig III.21_ E evolution versus heating time for samples B to F

2.2.5 Colored oxides

The furnace heating process changes the color of the nitinol material. These colors depend on the heating duration and are due to interference phenomena that establish at the metal-oxide interface.

2.2.5.a Oxide growth [CHU.96]

When titanium is exposed to ambient air at room temperature, a passive oxide film is spontaneously formed on it surface, and partially composed of anatase TiO2. In air at high temperature, titanium alloy tend to react vigorously with oxygen to form crystalline oxides film, rutile TiO2. The oxidation rate follows a parabolic law, very fast in the initial period (30min), and then decreasing rapidly with time. As the oxidation progresses, titanium atoms diffuse outward while oxygens atoms diffuse inward. A multi layered scale is formed, consisting of an outer rutile layer (TiO2), a porous intermediate layer of mixture of TiO2 and Ni(Ti), and a thin inner TiNi3 layer. This leads to a local enrichments of Ni just beneath the TiO2 layer and results in an outward growth of rutile and an inward growth of Ni rich phases. The transformation temperature of the NiTi alloy decrease.

2.2.5.b Oxide colors

Titanium dioxide were commonly and abundantly used as pigments through high opacity and refractive index [MIL]. Although both anatase and rutile TiO2 are « white » pigments, they have a blue tone due to a lack of reflectance in the very blue and of the visible spectrum. Moreover, their undertone, the tint tone, is a function of particle size distribution. The relative

light scattering power of rutile TiO2 at different wavelengths varies with its particle diameter. Practically, changing the undertone of a pigment has a significant effect in tinted system, especially gray, where the effect is clearly visible. Thus changing to a blue tint tone pigment would change the tone of a gray from a red through a neutral to a blue tone. Conversely, a pigment with a large mean size scatters red light more efficiently, producing a reddish tone in gray films.

2.2.5.c Consequences

The Titanium oxides growth is linked to the evolution of the A_p temperature. Each color experimentally observed corresponds to a different state of the material, and is linked to a specific A_p value (Figure III.22). During the heat treatment it is possible to assess visually in which state the material is.

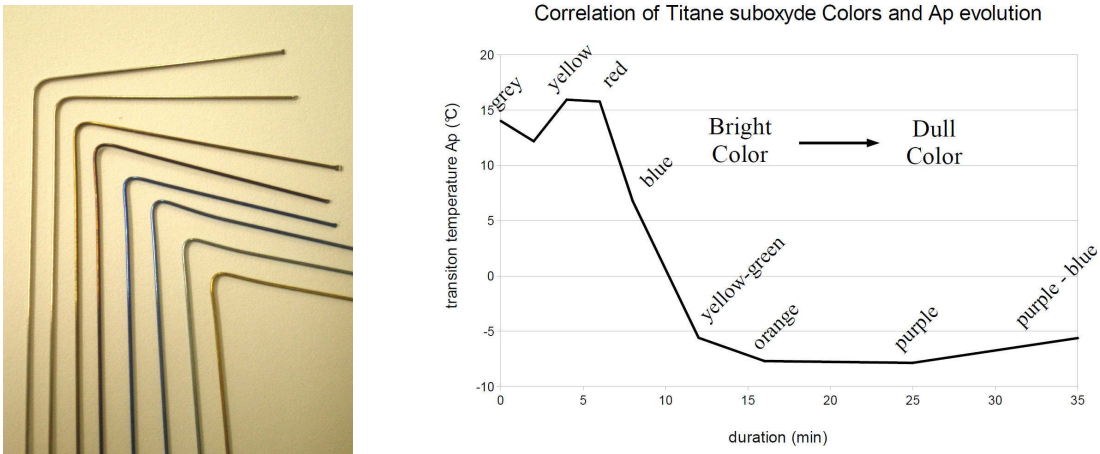

Fig III.22_ Oxyde Colors and Ap correlation

2.2.6 Parameters used

The experiments realized on nitinol highlighted the influence of operating conditions on the final material properties. These settings were then applied to the realization of the stent's parts.

2.2.6.a Manufacturing conditions

The tooling fixture

Aluminum is the material of the plates used for the nitinol wire forming process. The reduced thermal inertia of the material makes it possible to limit the heat treatment duration and to reduce the time of manufacturing.

In order to assess the « in vitro » behavior modification of the stent when varying a geometrical parameter (like the height of the cylindrical head for example), the nitinol properties must be equivalent for the 2 different designs. The thermal behavior of the wires must be the same. The tooling fixture must, therefore, be of same size to guarantee same thermal inertia and same heating conditions.

Cooling

Water quenching was adopted for cooling the nitinol wires after heat treatment. The method allows setting precisely temperature and duration of the heating process. Basically, as we already said, a longer cooling would not make it possible to control A_p with precision.

2.2.6.b Manufacturing process

Braid shape setting

The very elastic nitinol wires are difficult to manipulate and shape around expected templates. Shape setting is therefore realized in two consecutive operations.

- 1st heat treatment

The zig-zag shape of the nitinol wires is first obtained in a flat configuration (Figure III.23). We use an aluminum plate with fixed nails, around which the nitinol wire is winded. The winding geometry respects a pattern that corresponds to the expected size of the braid that is to be obtained (Figure III.24).

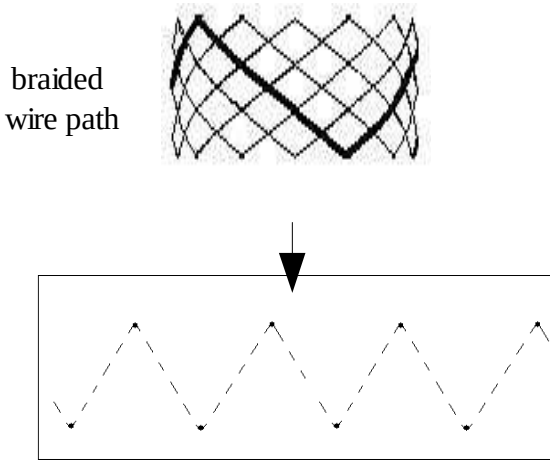

Fig III.23_ Plane representation of the braided wire path on a cylindrical braid surface

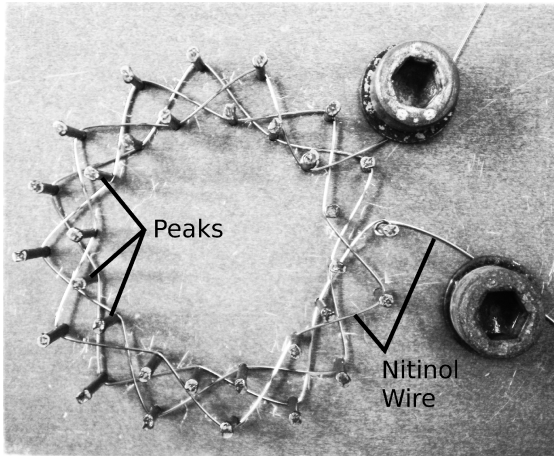

Fig III.24_ Nitinol wire shape setting on aluminum plate

To make the braiding process as easy as possible a compromise must be found as to the heat treatment conditions. Wires must be not to elastic but also not to easy to shape to avoid material rupture risks at the nail-wire interfaces. The finally adopted parameters are T=550°C for the temperature, and a heating duration just below t2 (Figure III.12). A_p is then slightly higher after treatment and elastic modulus is slightly reduced.

◆ 2nd heat treatment

Following the first heat treatment, Nitinol wire can then be easily braided and shape set at their final dimensions and geometries. To get final A_p value lower than ambient temperature, heating is performed at temperature above 500°C over a duration above t2. In order to ensure reproducibility in the manufacturing process, temperature and duration can be controlled :

- A slight decrease in the heating temperature leads to slower decrease of A_p which becomes less sensible to possible slight duration variations.
- In a similar way, if duration is above t3, the slow evolution of A_p value makes it less sensible to slight duration variations as well.

In our case, we chose to obtain a low value for A_p and worked at 550 °C.

During the 2nd treatment, braids are placed on supporting devices shaped to the final expected geometry. A cylinder is used for the head, while angle and diameter of the conical basis is obtained with a specific geometry (Figure III.25). Pictures III.26 and III.27 represent the final obtained braids for head and cone.

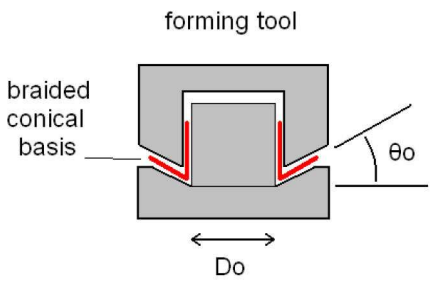

Fig III.25_ Schematic representation of the conical basis forming tool

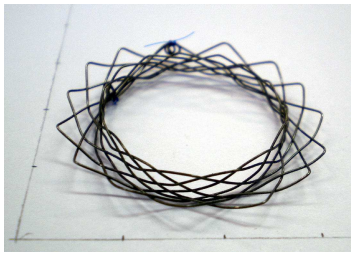

Fig III.26_ Braided conical stent basis

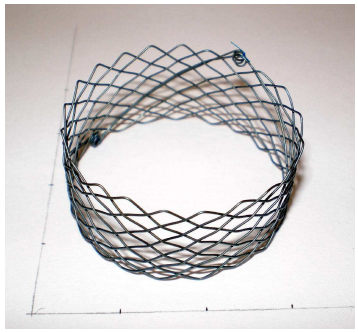

Fig III.27_ Braided cylindrical stent head

Shape setting of the posts

0.55 and 0.6 mm diameter nitinol wires are used to realize the posts and ensure minimum flexure. The loops located at each extremity must be of low size to prevent the posts from being too thick, especially in the sinuses. The stiffness and elasticity of the wire used doesn't make it possible to get them shaped in austenitic phase. The first treatment is therefore long (20min) and at low temperature (450°C), for the material to be in more malleable martensitic phase. Geometry is obtained through winding the wire around nails fixed on an aluminum plate. A second treatment at 550°C sets the post's final shape and decreases A_p (Fig III.28).

Fig III.28_ Posts

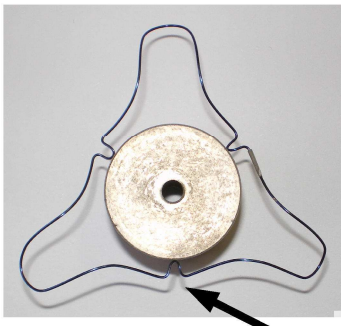

Fig III.29_ Top view of stent arms

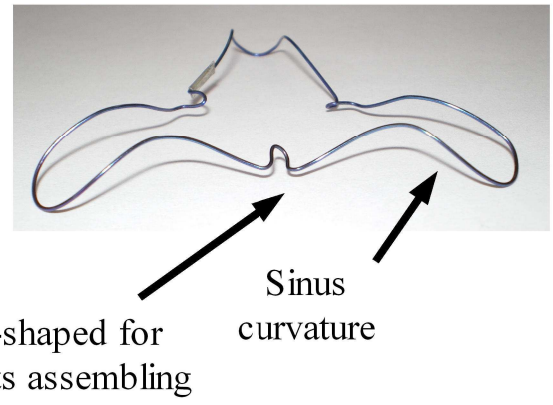

Fig III.30_ Front view of stent arms

Shape setting of the arms

Arms are shape set in only one step. A 550°C temperature is associated with a above t2 duration to minimize A_p value. The curvature geometry is forced thanks to a plate like for any other part of the stent, on which curved elements are fixed to give the sinus curvature to the wire. Pictures III.29 and III.30 represent the obtained arms.

Stent assembling

Figures III.31 and III.32 represent the stent after assembling. We note that the posts are covered with a textile sheath, on which valves and arms are sutured. The textile valve prosthesis does have a conical fabric rim, which is slightly sutured on the stent's conical surface (just enough to not prevent the stent compression). The rim will be positioned at the interface between stent cone and aortic ring tissues to prevent leakage.

Fig III.31_ Top view of the whole assembling stent

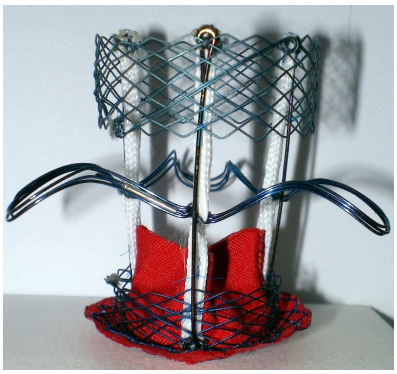

Fig III.32_ Side view of the whole assembling stent

Conclusion

The analysis and control of the nitinol properties through our experiments, allowed setting an adapted manufacturing procedure for each part of the stent. We show that the reproducibility depends on the heating temperature, duration and tooling fixture used. Our work made it possible to control and regulate the A_p temperature value, in order to be sure to obtain final stent parts in austenitic phase. The stent keeps thereof its elasticity and respects the compliance of the tissues.

Chapter IV TESTING BENCH

1 INTRODUCTION

Valves performances are generally characterized in two ways :

- static testing
- dynamic testing

Static testing is used to evaluate the leakage volume across the valve in closed position under static pressure. It provides information on valve behavior in diastole when valve is closed. Dynamic testing is done under pulsed flow and characterizes the dynamic valve leakage (closing time). The valve behavior during closing and opening phases is especially highlighted.

These tests are usually performed through mounting the valve on a rigid holder. Actually, our prosthesis is positioned only through shape matching : between cone and aortic annulus, arms and sinuses, head and aorta conduit. The positioning of the stent is dependent on the dimensions variations of the implantation environment. In the present work it is therefore essential to place the stented valve in an environment which reproduces the aortic root compliance for the ‘in vitro’ testing, for proper performances assessment. We present in this chapter the problems related to the testing bench we used, and the modifications we performed to encounter these problems.

2 THE MOCK AORTIC ROOT

Native aortic root is compliant. To characterize the stent's behavior in a compliant environment, we realized a root out of silicon material. The deformations undergone by this material under stress are close to the one of native tissues. Large elastic deformations can especially be obtained. Moreover, the material being transparent, it was possible to visualize the stent behavior in static and dynamic conditions under pulsed flow.

The silicon root is obtained through casting. The cast is composed of a core and an external hull. Cast dimensions are set according to :

- Native aortic root dimensions
- Aortic root dimensions changes over the cardiac cycle
- Cardiac pressure values range

The so molded mock aortic root is tested under pulsed flow to validate the dynamic compliance.

2.1 The native aortic root

The dimensions variations adopted to realize the mock root correspond to values given in literature [SWA.74]. For pressure variations between 80 mmHg and 130 mmHg variations are as follows :

- Aorta conduit : 30% enlargement
- Aortic ring : supposed to remain constant in diameter
- Sinus depth : variations around 20%

2.2 The mock silicon root

2.2.1 Description

The root was molded for a 21 mm diameter aortic ring. It is composed of 4 main parts : (1) the aorta, (2) the sinuses, (3) the aortic ring, (4) the bottom of the ring. (Fig.IV.1)

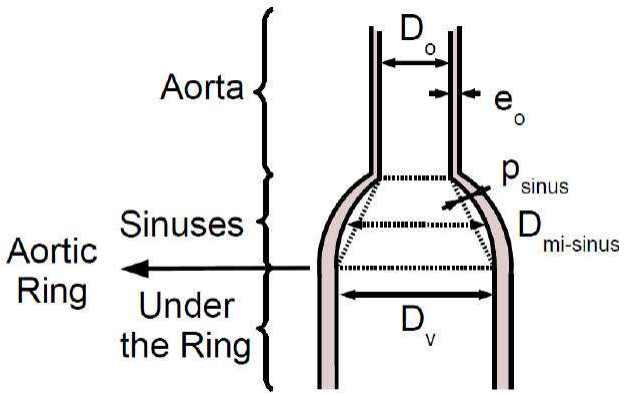

Fig.IV.1_ Schematic representation of the mock aortic root

Each part required distinct manufacturing features.

2.2.1.a The aorta

This part is cylindrically shaped with a D_{int} interior diameter and a thickness "e" when under pulsed flow. Dimensions at manufacturing state are e_0 and D_{int0} and can be calculated from different equations :

Systolic to diastolic enlargement

For D_1 = 21mm, → P_{dias} (D_1) = 80 mmHg (1.4)

For $D_2 = D_1.\Delta D_{dias/sys}$ → P_{sys} (D_2) = 130 mmHg (2.4)

Circumferential stress induced in the cylinder

$$\sigma = \frac{P\,D_{int.}}{2e} \qquad (3.4)$$

Wall thickness definition

We assume that when silicon deforms the thickness remains constant. This gives a relationship between the wall thickness value e and the other parameters (D_{int}, e_0, D_{int0}).

$$S = \frac{\pi}{4} e\left(e + 2D_{int.}\right) = \frac{\pi}{4} e_0\left(e_0 + 2D_{int.0}\right) \quad \rightarrow \quad e = \sqrt{D_{int.}^2 + \frac{4S}{\pi}} - D_{int.} \qquad (4.4)$$

Elastic modulus definition

The silicon elastic modulus is obtained from a traction testing done on a silicon sample. Stress and strain induced in the material are related with :

$$\sigma = E\frac{D_{int.} - D_{int.0}}{D_{int.0}} \qquad (5.4)$$

The combination of these equations leads to the relationship between the applied pressure P in the root and the corresponding deformation :

$$P = 2E\frac{D_{int.} - D_{int.0}}{D_{int.}D_{int.0}}\left(\sqrt{D_{int.}^2 + e_0\left(e_0 + 2D_{int.0}\right)} - D_{int.}\right) \qquad (6.4)$$

The values for e_0 and D_0 are calculated from equation (6.4) and the pressure conditions defined in equation (2.4).

The silicon used is of RTV 3428 (SiliconBlue). The root is manufactured with the obtained dimensions values : E = 280 kPa, e_0=2.2mm, D_0=17.3mm

2.2.1.b The sinuses

Sinuses must link the aorta conduit with D_0=17.3 mm to the aortic ring at 21 mm diameter. They are circular shaped is diastolic configuration. The silicon thickness should be so adapted along the sinus length to allow progressive dilatation. At mid-height of the sinus, mock thickness is about 3,1mm.

2.2.1.c The aortic ring

The aortic ring is realized at a 21 mm diameter. A rigid ring is molded in the silicon just below the aortic ring level to prevent the ring diameter from extending too much. This behavior respects the native ring behavior.

2.2.1.d The bottom of the ring

The rigid cylindrical ring goes from the aortic ring down to the extremity of the mock root, where the root is connected to rigid pipes of the bench. The ring prevents the root extension/collapsing below the aortic ring, which could interfere with the measure of the leakage volume.

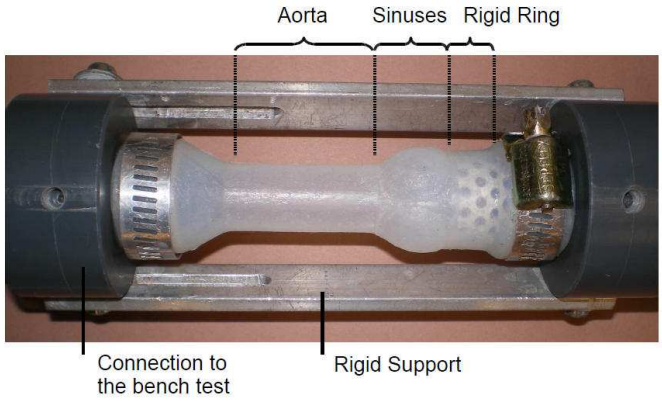

Fig.IV.2_ The mock silicon root connected to the testing bench

2.2.2 Aortic root characterization under pulsed flow

The mock aortic root is connected to the dynamic testing bench (described later in more details) for characterization. Axial root deformation is prevented to avoid biased measurements. Dimensions variations are recorded with video camera and compared with the instantaneous pressure signal. Results validate the silicon behavior, which respects the compliance value of the native root.

3 TESTING UNDER STATIC CONDITIONS

Static testing, already described before, should confirm that a valve prosthesis is flood tight enough in closed position. In our case, we will assess the efficiency of the stent anchoring in the aortic root under static pressure gradient.

3.1 The static testing bench

The bench consists in a water column under which the stented valve is placed in closed position. The leakage across the closed valve is measured as a function of the pressure generated by the water column (Figure IV.3 is an example of result obtained).

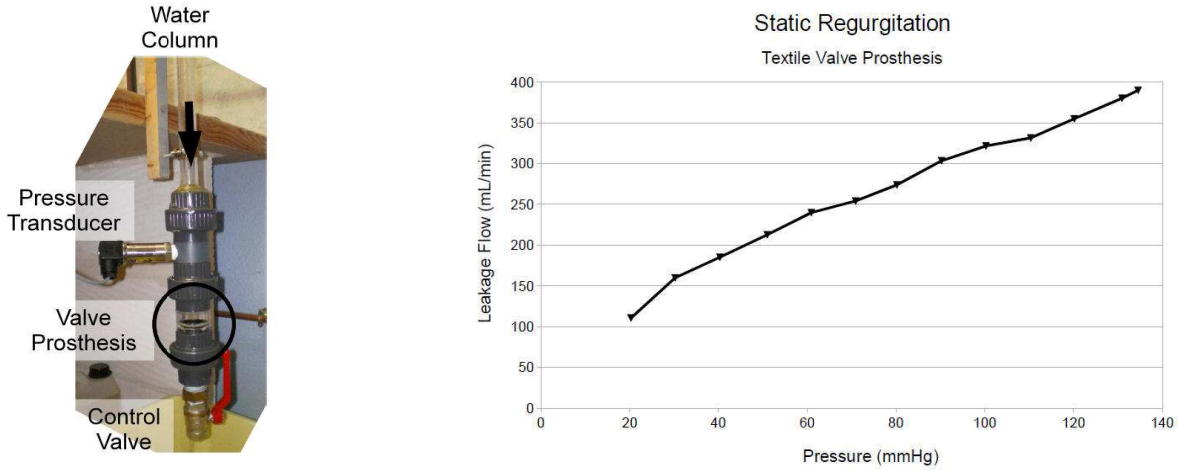

Fig.IV.3_ static regurgitation measurement (principle and typical result)

4 TESTING UNDER DYNAMIC CONDITIONS

In order to test the prototypes under dynamic conditions, we used a testing bench that had already been developed by Heim et al. The testing conditions respect the norm ISO/CD 5840 defined in September 2002 for heart valve prostheses testing.

4.1 The existing bench

The bench used is a cardiac simulator that was initially designed to test some textile heart valve prostheses mounted on rigid stents. The goal of the installation was to generate a pulsatile flow across a heart valve placed in aortic position at ventricle outflow track. However, for development time saving purpose, the bench is limited to one circulation. The model adopted to design the bench was the circulator from the Sheffield university [CHA.89]. It comprises a servo-system associated with a piston that generates a pulsed flow signal (70 beats/min, 70 ml/beat). The flow circulation goes first through the tested valve, than through a compliance volume placed behind the valve (to simulate the arteries elasticity) and finally goes back to the reservoir through a capillary resistance.

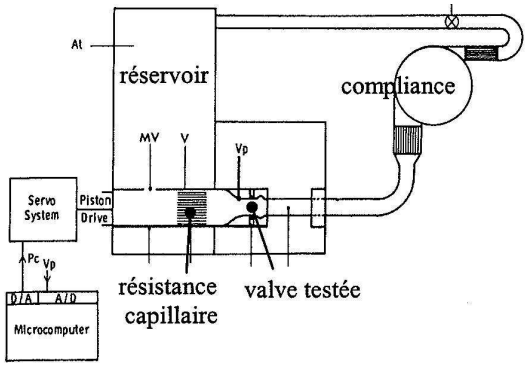

Fig.IV.4_ Shematic representation of the cardiac simulator

In that model, the arterial circulation is not separated from the flow generator through an artificial compliant ventricle, as can be seen with more technically advanced benches as the one of the BIOmeca lab in Marseille. Basically, if these benches are able to reproduce pressure and flow signals very close to physiological ones, they required long time of development and high money investment, what was lacking in the present project. This simplified device allowed, however, obtaining some interesting results about the behavior of a textile valve in comparison with other commercially available valves. The tests focused on

measurements of the closing time and the closing tightness of the valve. Figure IV.5 represents the pressure signal (before and after the valve) that could be obtained with the bench in its initial configuration.

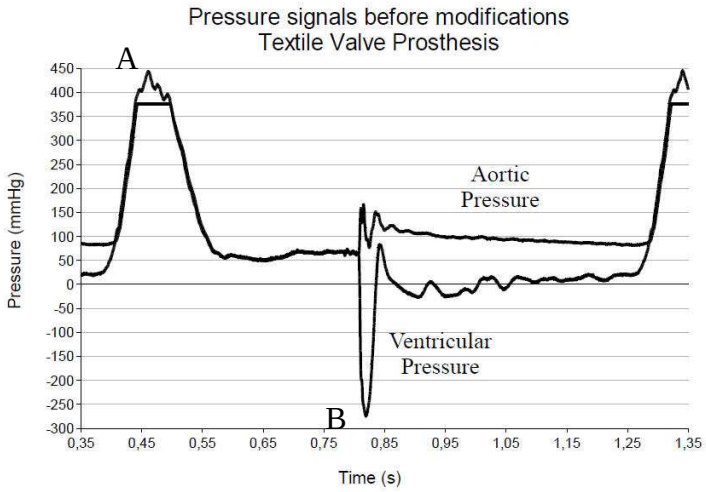

Fig.IV.5_ Pressure signals before bench modifications

The precision of the pressure signals obtained was sufficient to test a valve in a rigid environment, but did not completely satisfy the needs when testing the valved stent. The flexibility of the stent requires to take this time the compliance of the aortic root into consideration. Basically, the placement of the stent in the aortic root is dependent on the proper surface matching between the stent components and the root's contact surfaces. As already explained at the beginning of this report, the aortic root undergoes some geometrical dimensions variations under cyclic loading. The stent is required to follow these variations. It had therefore to be tested in an artificial compliant root, to validate its performances. The previously described pressure signal presented 2 major concerns related to these new tests. At the beginning of systole, the pressure head initially reached (point A on Fig IV.5) was much higher than the expected physiological 120mmHg. This pressure peak would tend to deform the compliant aortic root more than expected, and lead to biased dynamic behavior of the stent and measured performances. The second problem concerned the excessive low pressure value obtained on the ventricle side at valve closing (point B on IV.5). The exaggerated depression would also deform the compliant root more than expected, and lead to non exact measurements values. Hence, the bench was designed and modified again, in order to improve the pressure signals and correct the failing values.

4.2 Bench model

The existing bench was designed according to the Windkessel model (Fig IV.6). This model, proposed in 1899 by Otto Franck allows representing the behavior of the whole vascular system thanks to a combination of hydraulic components : (1) accumulators (reproduce the arterial elasticity or compliance and control the flow pressure), (2) diameter restrictions (reproduce the capillary resistance), (3) hydraulic valves (control the flow circulation).

Fig.IV.6_ Windkessel model

When the valve is open (systolic period), the ventricle flow goes through the capillary resistance for one part, while the other part accumulates in the compliance. In diastole (valve is closed), the flow volume accumulated in the compliance flows through the capillary resistance. From that model, applied to the physiological arterial blood flow conditions, the size of the bench components (resistance and compliance) could be calculated.

In reality, this model adopted for previous tests done on non stented valves presents some limits especially in systole. Actually, the model considers that systolic flow is constant, which is not the case. Native flow is pulsatile and sinus shaped versus time. The flow inertia needs first to be considered in order to get a pressure signal that respects the physiological signal in a better way. Second, the sinus flow pattern creates a pressure wave with a time period close to 0,957s (corresponds to the heart pace). This wave propagates over the whole circulation with a wave speed that depends on both the flow compressibility and the pipe mechanical characteristics. Every diameter restriction in the circulation loop, will then generate a reflection wave as soon as the main wave reaches it, and a water hammer will appear. The combination of these water hammers explains the pressure peaks reached with the existing bench at both systole (positive peak) and diastole (negative peak) begins.

In order to improve the pressure signal, we followed two strategies. First we used a new electrical model for the circulation loop, to calculate the compliance and resistance values necessary to approach the physiological pressure conditions. Second, we applied a theoretical water hammer model to our system to get an estimation of the water hammer effects. This model will help understand which part of the circuit had to be modified to reduce the water hammer effect and improve the pressure signal.

4.2.1 Electrical analogy

The following schema represents an electrical model of the circulation loop that takes the fluid inertia into account.

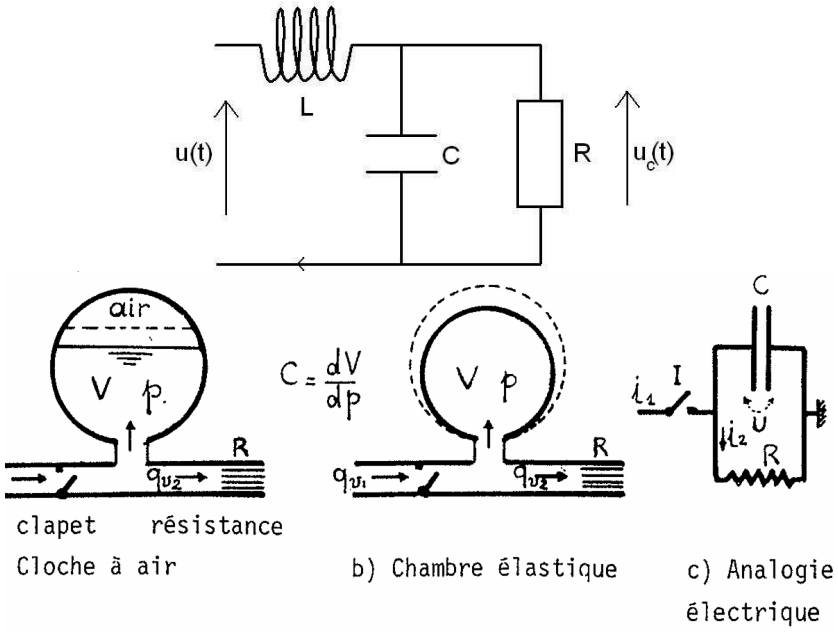

Fig.IV.7_ Windkessel model

With that approach the circulatory system can be modeled like an electrical circuit composed of a resistance R (simulates the capillary resistance), a capacity C (simulates the compliance volume), a self-inductance L (simulates the inertia of the fluid that is put in motion).
Finally the pressure in the system can be described with the following equation :

$$p = u(t) = L\frac{di}{dt} + u_c \qquad (9.4)$$

In which i(t) represents the flow signal that can be obtained from :

$$i(t) = \frac{u_c}{R} + C\frac{du_c}{dt} \qquad (10.4)$$

4.2.1.a The resistance R

In our bench, a ball valve is used to reproduce the capillary resistance. This choice makes it possible to regulate easily the resistance in practice. This kind of resistance induces a pressure drop, directly dependent on the flow value (maximal when flow velocity has reached its maximum). Hence, the value of R changes with instantaneous flow. We consider, however, in the model that R is constant. The theoretical calculation of R from the model will hence slightly change from the experimental value. But the order of magnitude of the average experimental value will however remain close to the theoretical one.

4.2.1.b The compliance C

The compliance present in the circulatory system can be defined with :

$$C = \frac{dV}{dP} = \frac{V}{\gamma P} \qquad (11.4)$$

P_0 and V_0, are respectively the initial air pressure and volume in the compliance related to the pressure P and volume V at any time with :

$$PV^{\gamma} = P_0 V_0^{\gamma} = constant\ value \qquad (12.4)$$

4.2.1.c The inertia L

The fluid column that needs to be put in motion represents the self inductance $L = \frac{\rho l}{S}$, (obtained for the fluid Euler equation).

In order to get an order of magnitude of these inertia effects we measured experimentally the pressure increase induced by the acceleration of a 1.5m long water column in a 21mm diameter conduit over a 0.15s period of time.

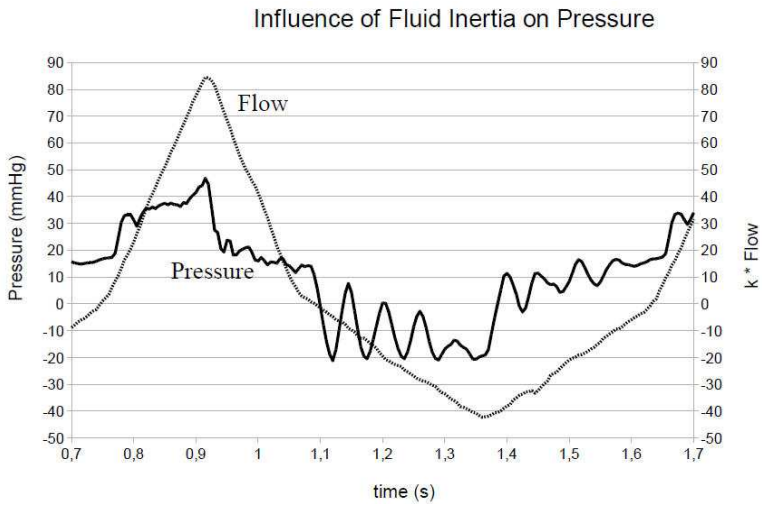

Fig.IV.8_ Influence of fluid inertia on pressure

We observe that a major pressure peak is reached even before flow motion starts, at begin of the flow signal when fluid begins to accelerate. This shows that fluid inertia cannot be neglected.

4.2.1.d The pressure signal

The physiological flow characteristics can be used to explain the value for i(t) in the electrical model. Indeed, the flow signal can be considered as sinusoidal with a maximum value I_0.

Systolic flow takes place over a t_s = 0.3s period of time, with a frequency corresponding to the heart pace of 70 beats/min. Diastolic phase duration is T_d = 0.5s.

$$i(t)=I_0\sin(\omega t) \qquad t\in[0;0{,}3\,s] \tag{13.4}$$

$$i(t)=0 \qquad t\in[0{,}3\,s;0{,}8\,s] \tag{14.4}$$

Expression of ω and Io can be obtained from (13.4) and boundary condition :

The systolic flow is null at the end of systole.

$$i(t_{sys})=I_0\sin(\omega t_{sys})=0 \quad \rightarrow \quad \omega=\pi/t_{sys} \quad (\omega=10.47 \text{ rad/s}) \tag{15.4}$$

The stroke volume V is about 70mL during systole.

$$V=\int i(t)=\int_0^{t_{sys}} I_0\sin(\omega t)dt \quad \rightarrow \quad I_0=\frac{V\omega}{2} \quad (I_0=366 \text{ ml/s}) \tag{16.4}$$

To solve equations (9.4) and (10.4), we study separately systolic and diastolic phase.

Diastole

In diastole, equations (9.4) and (10.4) could be rewritten as follow :

$$u(t)=u_c(t) \tag{17.4}$$

$$0=\frac{u_c}{R}+C\frac{du_c}{dt} \tag{18.4}$$

A solution of (18.4) can be easily obtained :

$$u(t)=K_{dias}e^{-t/\tau} \tag{19.4}$$

In which τ=RC represents the response time

The values of K_{dias} and τ can then be defined with equation (17.4) from boundary conditions related to pressure values at diastole start (P_1) and end (P_0) that must respect the physiological values :

$$\tau=RC=-t_d/\ln\left(\frac{P_0}{P_1}\right) \tag{20.4}$$

$$K_{dias}=P_1 \tag{21.4}$$

Systole

In order to easily solve equation (10.4), we are working with complex number. First we write the general solution of the homogeneous equation associated with (10.4), and then we find a particular solution of (10.4).

- General solution of the equation without second part (16.4)

The general solution of (18.4) is :

$$f(t) = K_1 e^{-t/\tau} \qquad (22.4)$$

- Particular solution of the equation (10.4)

We use the complex definition of (13.4).

$$i(t) = I_0 \sin(\omega t) = \Im(I_0 e^{j\omega t}) \qquad (23.4)$$

$$\text{and} \quad I(t) = I_0 e^{j\omega t} = \frac{U_c}{R} + C\frac{dU_c}{dt} \qquad (24.4)$$

A particular solution $U_c^p(t)$ can be so obtained from the complex definition of i(t) with (24.4) :

$$U_c^p(t) = K_2 e^{j\omega t} \qquad (25.4)$$

Equation (24.4) becomes in diastole, with complex definition :

$$I_0 e^{j\omega t} = \frac{1}{R} K_2 e^{j\omega t} + C\, j\omega e^{j\omega t} \qquad (26.4)$$

Which leads to

$$K_2 = \frac{R I_0}{1 + jRC\omega} = \frac{R I_0 (1 - jRC\omega)}{1 + (RC\omega)^2} \qquad (27.4)$$

We, however, take only the imaginary part of $U_c^p(t)$ into consideration to obtain $u_c^p(t)$:

$$u_c^p(t) = \frac{R I_0}{1 + (RC\omega)^2} \sin(\omega t) - \frac{R^2 C I_0 \omega}{1 + (RC\omega)^2} \cos(\omega t) \qquad (28.4)$$

- General solution of the equation (10.4)

Finally the global solution for $u_c(t)$ in systole can be written from equation (9.4) combined with the above obtained result.

$$u_c(t) = f(t) + u_c^p(t)$$

$$\rightarrow \qquad u_c(t) = K_1 e^{-t/\tau} + \frac{R I_0}{1 + (\tau\omega)^2} \sin(\omega t) - \frac{R^2 C I_0 \omega}{1 + (\tau\omega)^2} \cos(\omega t) \qquad (29.4)$$

From equation (10.4) we get the expression of the pressure signal p(t) = u(t)

$$u(t) = L\frac{di}{dt} + u_c(t) \qquad \rightarrow$$

$$u_{(t)} = L\,I_0\,\omega\cos(\omega t) + K_1 e^{-t/\tau} + \frac{R\,I_0}{1+(\tau\omega)^2}\sin(\omega t) - \frac{R^2 C\,I_0\,\omega}{1+(\tau\omega)^2}\cos(\omega t) \qquad (30.4)$$

The values of K_1 and R can then be defined with equation (30.4) and (20.4) from boundary conditions related to pressure values at systole start (P_1) and end (P_0) that must respect the physiological values :

$$R = \frac{1+(\tau\omega)^2}{I_0} \cdot \frac{P_1 - P_0 e^{-t_{sys}/\tau} + L\,I_0\,\omega\left(1+e^{-t_{sys}/\tau}\right)}{\tau\omega\left(1+e^{-t_{sys}/\tau}\right)}$$

$$K_1 = P_0 - L\,I_0\,\omega + \frac{R\,I_0\,\tau\,\omega}{1+(\tau\omega)^2}$$

With following values,

P_0=80 mmHg V = 70mL l = 1,5m

P_1=120 mmHg ρ = 100 Kg/m^3 d = 21mm

We obtain : τ= 1,37s R = 8,18.10^8 P_a.s/m^3 C =1,68.10^{-9} m^3/s

Figure IV.9 gives the theoretical pressure evolution with the bench characteristics

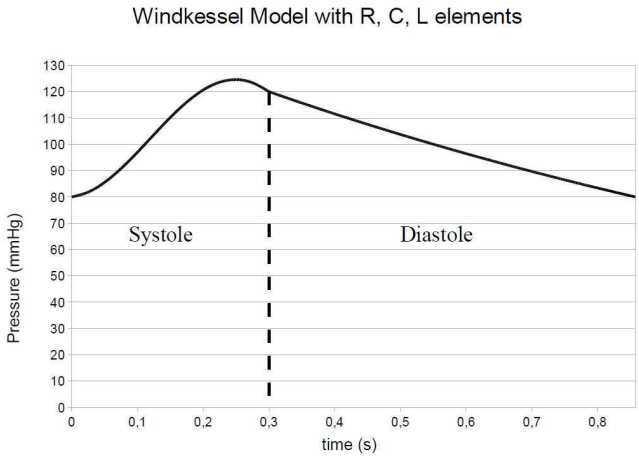

Fig.IV.9_ Bench pressure characteristics

However, the theoretical calculated values will need to be experimentally corrected in order to take the water hammer effect into consideration.

4.2.2 Water hammer model

Water hammer corresponds to a sudden pressure increase of a water column due to a sudden flow velocity variation (sudden stopping of a fluid in movement or sudden start of an initially static water column). It is characterized by the generation of a pressure wave, which partially propagates in the flow circuit, and partially reflects on any resistant surface present in the conduits. The reflections induce the sudden pressure peaks (assuming that the pipes do not undergo any deformation). The elasticity of arteries in vivo, indeed, prevents water hammer phenomenon from occurring on the heart valve.

4.2.2.a Role of inertia on water hammer

In order to first see experimentally which components are influent on water hammer in our circulation loop, we performed some tests with different pulsed signal shapes characterized with different “acceleration-deceleration” durations over a constant 0.3s period of time (100ms - 200ms; 150ms -150ms; 200ms -100ms).

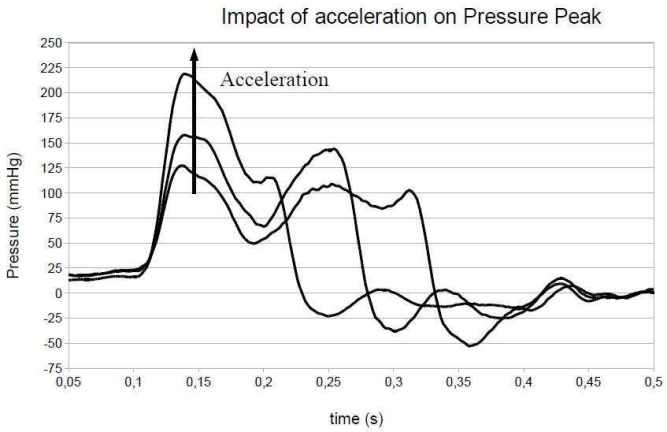

Fig.IV.10_ Acceleration value and pressure peak

We observe that the higher the acceleration, the higher the pressure peak due to inertia.

4.2.2.b Role of the pressure drop on water hammer

We tested the influence of the resistance value in the circuit on the first pressure peak. We observe that whatever the resistance, the first pressure peak keeps the same value.

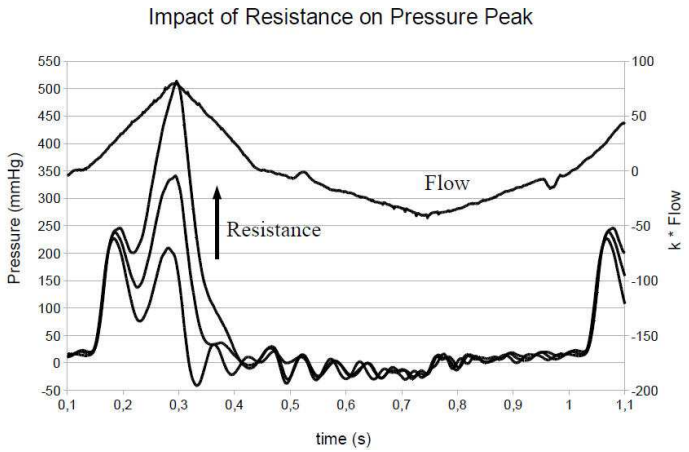

Fig.IV.11_ Resistance and pressure peak

4.2.2.c Theoretical water hammer model

The equations governing the water hammer are the continuity equation (mass equilibrium) and the momentum equation (2nd Newton law).

Continuity equation

The continuity equation is the differential equation that describes the conservative transport of the fluid mass defined with equation (31.4).

$\frac{dM}{dt}=0$ M being the mass (31.4)

Assuming that there's no pipe deformation, equation (31.4) can also be written in differential form as

$$\frac{\partial \rho}{\partial t}+div.(\rho U)=0 \qquad (32.4)$$

In which :

U = fluid velocity

ρ = density of the fluid

Considering the flow as unidirectional equation (32.4) becomes :

$$\frac{\partial \rho}{\partial t}+\frac{\partial(\rho U)}{\partial x}=0 \qquad (33.4)$$

$$\leftrightarrow \quad \frac{1}{\rho}\frac{\partial \rho}{\partial t}+\frac{\partial U}{\partial x}+\frac{U}{\rho}\frac{\partial \rho}{\partial x}=0 \qquad (34.4)$$

We replace $\frac{\partial \rho}{\partial t}$ with $\frac{\rho}{K}\frac{\partial p}{\partial t}$

In which :

K= water bulk modulus (Pa)

P = pressure (Pa)

Equation (34.4) becomes :

$$\left(\frac{\partial p}{\partial t}+\frac{\partial p}{\partial x}U\right)+K\frac{\partial U}{\partial x}=0 \qquad (35.4)$$

The term $\frac{\partial p}{\partial x}$ can be considered very small compared to $\frac{\partial p}{\partial t}$ and can be neglected while K can be written as a function of the wave velocity c with $K=\rho c^2$.

Equation (35.4) becomes :

$$\frac{\partial p}{\partial t}+\rho c^2\frac{\partial U}{\partial x}=0 \qquad (36.4)$$

Momentum equilibrium

Newton's second law can be written in a simplified form (viscous effect are neglected, flow is unidirectionnal).

$$\frac{\partial U}{\partial t}+\frac{1}{\rho}\frac{\partial p}{\partial x}=0 \qquad (37.4)$$

Water hammer is finally governed by equation (36.4) and (37.4).

Both equations can be combined after derivation with respect to x for equation (36.4) and t for equation (37.4) and obtain :

$$c^2\frac{\partial^2 F}{\partial x^2}-\frac{\partial^2 F}{\partial t^2}=0 \qquad (38.4)$$

In which F is a function that can be velocity U or pressure

The solution for such kind of equation is :

$$F=f\left(t-\frac{x}{c}\right)+g\left(t+\frac{x}{c}\right) \qquad (39.4)$$

In which f() represents a wave that propagates in positive direction, and g() represents a wave that propagates in negative direction.

Applying the general formulation to pressure, for instance, velocity can then be calculated from equation (36.4) and (37.4)

$$p = f\left(t-\frac{x}{c}\right)+g\left(t+\frac{x}{c}\right) \qquad (40.4)$$

$$q_v = \frac{S}{\rho c}\left[f\left(t-\frac{x}{c}\right)-g\left(t+\frac{x}{c}\right)\right] \qquad (41.4)$$

In every section of the circulation loop (located at a distance x from an origin) the wave generates a pressure increase p and a flow increase qv as function of the time respecting the above described equations. These increases are average values obtained for a mean flow stream, corresponding for the vascular blood circulation to 4,5l/min flow and 100mmHg. The impedance Z of any specific part of the conduit can then be defined as the ratio between flow and pressure.

$$Z = \frac{p}{q_v} = \frac{\rho c}{S}\cdot\frac{f\left(t-\frac{x}{c}\right)+g\left(t+\frac{x}{c}\right)}{f\left(t-\frac{x}{c}\right)-g\left(t+\frac{x}{c}\right)} \qquad (42.4)$$

4.2.2.d Assessing of Z for our bench configuration

The Z impedance value changes upon time t when x is considered fix, and changes upon x when time is considered fix. If the value f(t-l/c) obtained for the f wave at the location x=L along the pipe is known, the reflected wave g generated by any geometrical or mechanical singularity in the flow (defined with its impedance Z_l) can be written :

$$g\left(t+\frac{l}{c}\right) = f\left(t-\frac{l}{c}\right)\frac{Z_l\frac{S}{\rho c}-1}{Z_l\frac{S}{\rho c}+1} \qquad (43.4)$$

More generally, this equation is verified if g respects the general expression :

$$g\left(t+\frac{x}{c}\right) = f\left(t-\frac{2l-x}{c}\right)\frac{Z_l\frac{S}{\rho c}-1}{Z_l\frac{S}{\rho c}+1} \qquad (44.4)$$

This last equation allows to calculate at any location x the pressure increase induced by a positive wave reflecting on a Z_l impedance. We define therefore the corresponding impedance at any x location with :

$$Z=\frac{p}{q_v}=\frac{\rho c}{S}\cdot\frac{f\left(t-\frac{x}{c}\right)+f\left(t-\frac{2l-x}{c}\right)\frac{Z_l\frac{S}{\rho c}-1}{Z_l\frac{S}{\rho c}+1}}{f\left(t-\frac{x}{c}\right)-f\left(t-\frac{2l-x}{c}\right)\frac{Z_l\frac{S}{\rho c}-1}{Z_l\frac{S}{\rho c}+1}} \qquad (45.4)$$

In our case the wave signal can be considered as sinusoidal and can be written for calculation purpose as following :

$$f\left(t-\frac{x}{c}\right)=a\,e^{j\omega\left(t-\frac{x}{c}\right)} \qquad (46.4)$$

with a = real number

Hence we obtain for g :

$$g\left(t+\frac{x}{c}\right)=a\,e^{j\omega\left(t-\frac{2L-x}{c}\right)}\frac{Z_l\frac{S}{\rho c}-1}{Z_l\frac{S}{\rho c}+1} \qquad (47.4)$$

Finally, combining the complex numbers for f and g together Z can be written as :

$$Z=\frac{p}{q_v}=\frac{\rho c}{S}\cdot\frac{Z_l\frac{S}{\rho c}+j\ \tan\left(\omega\frac{l-x}{c}\right)}{1+j\frac{Z_l S}{\rho c}\tan\left(\omega\frac{l-x}{c}\right)} \qquad (48.4)$$

If we consider x=0 as the location at which we measure the pressure in the bench configuration, the final impedance will be :

$$Z=\frac{p}{q_v}=\frac{\rho c}{S}\cdot\frac{Z_l\frac{S}{\rho c}+j\ \tan\frac{\omega l}{c}}{1+j\frac{Z_l S}{\rho c}\tan\frac{\omega l}{c}} \qquad (49.4)$$

This general expression can describe some particular configurations:

1. If flow is constant (no wave) we have $\omega=0$ and $Z_0=Z_l$. Impedance correspond to the pressure drop across the different components present in the circulation loop (compliance volume, capillary resistance, valve, flow-meter)
2. If there's no component out of pipe present on the flow way (true along some parts of the loop) we have $Z_l=0$ and $Z_0=\rho c/S$ which corresponds to the own impedance of the pipe.

The bench circulation loop is characterized as following : wave is present, some parts of the conduit are characterized with pipe own impedance, and a few diameter restrictions generate wave reflection. A more precise analysis of the different parts of the circulation loop will help us to estimate the effective pressure head due to water hammer.

Pipe impedance

With no reflection g, the own impedance of pipes is given with :

$$Z_{pipe} = \frac{\rho c}{S} \qquad (50.4)$$

The wave velocity value depends on the pipe material, size and on the fluid compressibility

$$c = \sqrt{\frac{K'}{\rho}} \qquad (51.4)$$

$$K' = \frac{K}{1 + \frac{DK}{eE}} \qquad (52.4)$$

K = modulus of compressibility (5.10^{-10} Pa for water)

D = pipe diameter (30 mm on the average)

E = elastic modulus of the pipe material (3000 MPa)

e = pipe thickness (2 mm)

The calculation results in c = 488 m/s, and $Z_{pipe} = 9.94.10^{8}$ Pa.s/m

This value is to be considered if we have $\tan\left(\frac{\omega l}{c}\right)$ very small in equation (49.4), i.e.

$$\frac{\omega l}{c} < \pi \quad \Leftrightarrow \quad T < \frac{2l}{c} \qquad (53.4)$$

The period of the pressure wave should be thereof less than approximately 0.004 seconds. In reality, with a simulated 1 Hz heart pace on the bench the signal remains far over that value, and pipe impedance can hence be neglected.

Reflection on pipe diameter restrictions

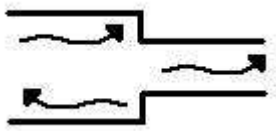

Fig.IV.12_ Reflection on pipe diameter restriction

Across a restriction, part of the initial wave reflects on the restriction, while part of it is transmitted and following equations are respected :

for the pressure signal

$$f(t)+g(t)=h(t) \tag{54.4}$$

for the flow signal (according to the impedance definition Z_0)

$$\frac{S_1}{\rho c_1}\left[f(t)-g(t)\right]=\frac{S_2}{\rho c_2}h(t) \tag{55.4}$$

This leads to :

$$\frac{h(t)}{f(t)}=\frac{2a_1}{a_1+a_2} \tag{56.4}$$

Where a_1 and a_2 represent the ratios $S_1/\rho c_1$ and $S_2/\rho c_2$ and $a_1>a_2$.

In our pipe system, 2 locations do generate some significant wave reflection: (1) at the junction between the pushing cylinder and the circulation pipes, (2) at the entry of the flow-meter device (of Coriolis type, with high diameter restriction). For both locations, we calculate the pressure increase due to water hammer and compare it with experimentally obtained values.

	Diameter changes	ΔPressure = h(t)/f(t) (calculated)	ΔPressure = h(t)/f(t) (measured)
Entry junction	40 - 25	1.6	1.77
Flow-meter	25 – (8 + 8)	2.0	2.35

Table IV.13_ experimental and theoretical values of pressure peak

We observe that there's good correlation between experiment and theory which tend to confirm the validity of the result. The next step consists in modifying the bench to limit these values. In order to overcome these non desired pressure increases, two main modifications were performed: (1) the flow meter was studied in more detail, (2) compliance was adapted to the signal.

4.3 Bench modifications

4.3.1 Flowmeter

The flow-meter used in the loop is of Coriolis type. It is located between the wave generator and the tested prosthesis. The way the flow-meter modifies the pressure signal can be observed in figure IV.14 in which pressure is plotted in a loop configuration with and without flow-meter.

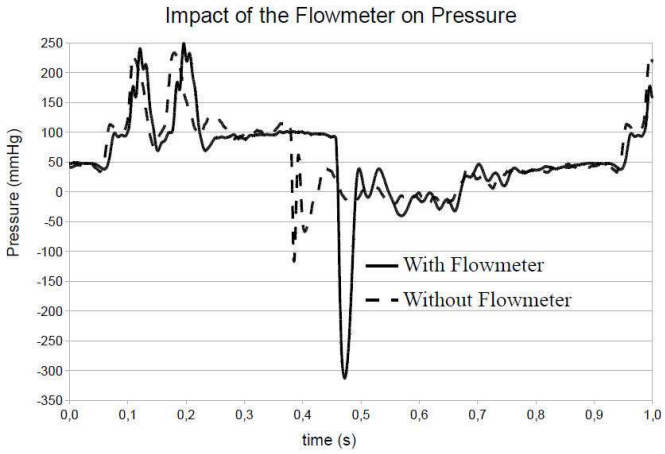

Fig.IV.14_ Influence of flow meter on pressure signal

Out of the pressure peaks induced at systole and diastole begin which were already talked about, one may note the delay induced by the device in the closing process (occurs at 0.45 s instead of 0.35 s). In order to define the exact role played by the flow-meter on pressure signal modification, we first tested if pressure drop across the device is of significance. Indeed, the device comprises a 8 mm diameter pipe, required by the Coriolis measurement process to reach the expected precision. High pressure drop is thereof induced at the input and the output of the device (the main circulation diameter is 21mm). Both experimental and theoretical obtained pressure drop values for the flow-meter are around $\Delta P=0.75\ Q^2$ with $\Delta P=$ pressure loss (mmHg), Q = circulation flow (l/min).

In a further step, we replaced in the circulation loop the flow-meter with a simple resistance that generates an equivalent pressure drop. We tested the device under pulsed flow conditions. The experimental pressure signal obtained with the flow-meter and with the resistance show that the first pressure peak is present with the flow meter and no present with the sole resistance.

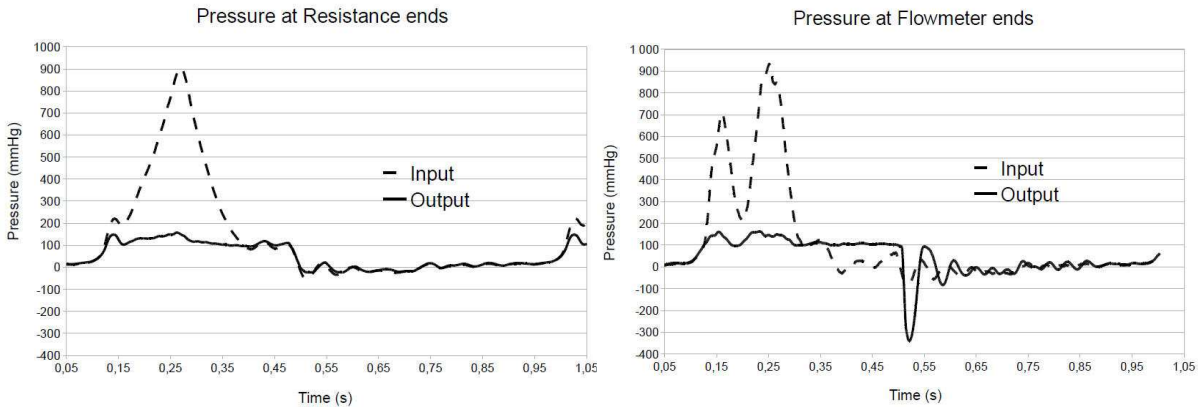

Fig.IV.15_ Pressure signal with flow-meter and with equivalent pressure drop resistance

It can be concluded from this result that the pressure drop is not the cause of the initial pressure peak. The 8 mm tube in the device is the main cause for the high water hammer at device entry. As to the depression observed at diastole begin, the water hammer occurs this time in the opposite direction during backflow. Valve closure is hence delayed. To prevent these non desired pressure peak phenomena from occurring, we decided to connect the flow-meter in a derivative way.

4.3.1.a Flow-meter modification

In order to reduce the flow that transits through the 8mm large pipe in the device, we connected a second pipe in parallel to the main stream. It was important to ensure with that procedure that the flow circulates same direction in both pipes. Once this condition was verified, we performed the calibration of the device, in order to get the relationship between the measured flow signal and the effective one.

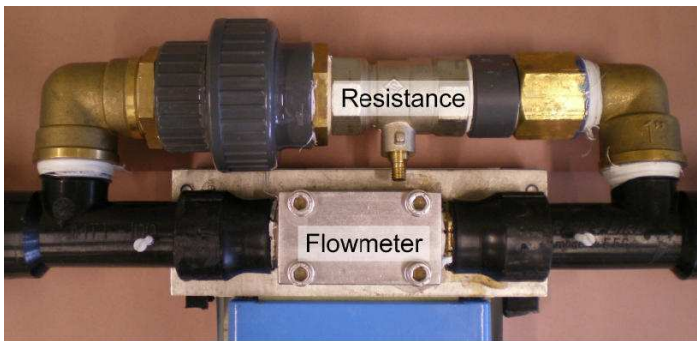

Fig.IV.16_ Derivated flowmeter

4.3.2.b Pressure drop in the derivation

In order to prevent recirculation in the derivation pipe, this needs to induce a pressure drop. That pressure drop is regulated experimentally to keep low but appropriate circulation in the

flow-meter. Basically, flow values in the 8mm tube must remain high enough to avoid precision loss in the measurements. On the other hand, the flow value must remain low enough to avoid pressure peaks. Figure IV.17 shows the improvement in the pressure signal with the derivated flow-meter.

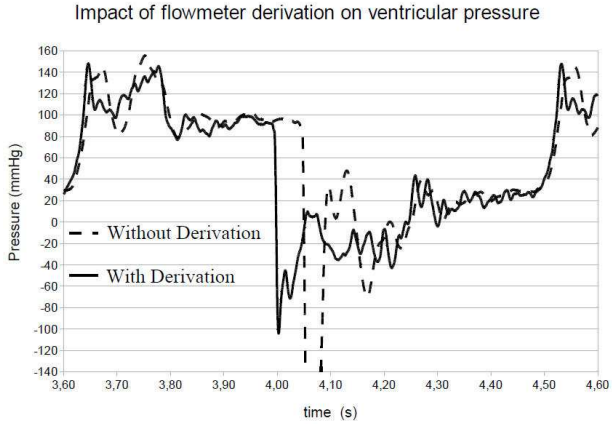

Fig.IV.17_ Pressure signal with and without derivation

Once the appropriate derivation setting is done, the flow-meter calibration can be realized. For that purpose the derivated flow-meter is placed under a water column. Pressure variation and instantaneous flow are recorded. A mechanical valve makes it possible to make the measurement for different flow values. Figure IV.18 represents the relationship between the effective measured flow values and the global flow in the circulation loop after calibration.

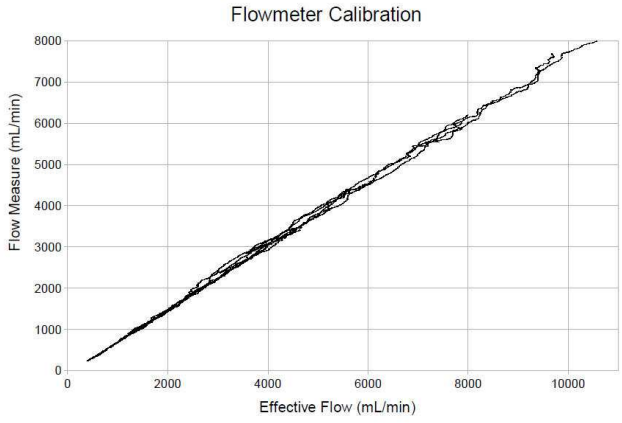

Fig.IV.18_ Calibration : measured flow versus effective flow

4.3.2 Compliance

The modifications in the compliance and resistance values, according to the new electrical model adopted, associated with the flow-meter modifications allowed reaching better pressure signals (Figure IV.17). To make the signal smoother, we inserted in addition a ventricular

compliance C_V between the signal generator and the flow-meter. The setting of the C_V value was done experimentally. In figure IV.19 we observe the influence C_V on the pressure signal for 3 different settings.

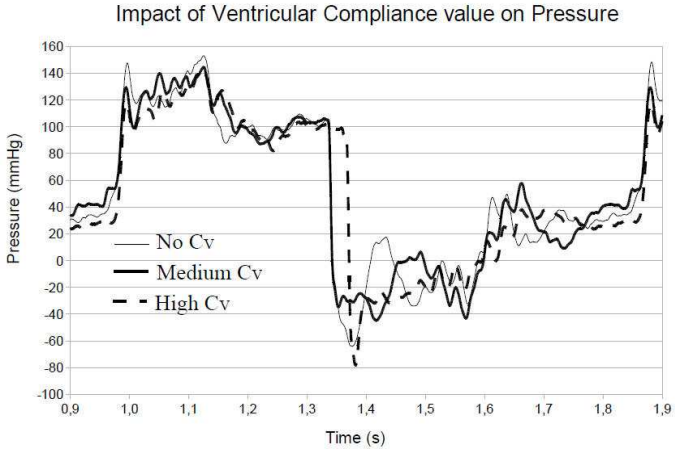

Fig.IV.19_ Influence of the ventricular compliance on the pressure signal

We observe that if the C_V value is too high, the valve closing is slightly delayed. Actually, the ventricular compliance tends to extend the ejection duration and hence delays the closing time. Its value is therefore reduced to the minimum. To realize further damping of the pressure signal, the compliance is associated in addition with a resistance. Indeed, some papers on the subject found in literature highlight the effect of resistance associated with compliance for pressure damping [PIC.66]. In our case the resistance is obtained with a flow restriction at the entry of the compliance. Figure IV.20 shows the influence of the restriction on the obtained signal.

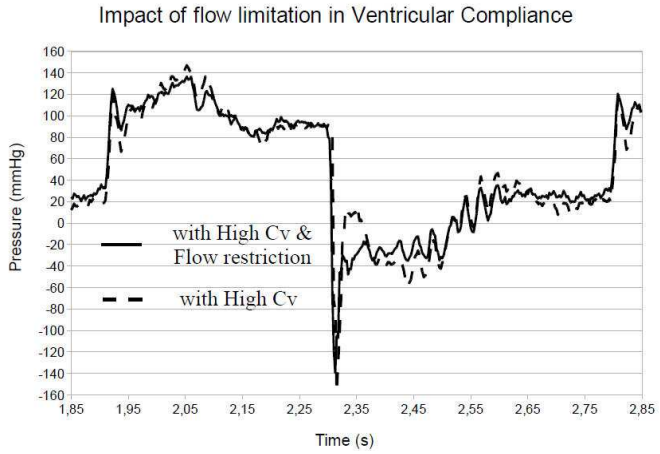

Fig.IV.20_ ventricular compliance with restriction

4.4 Conclusion

Figure IV.21 represents the testing bench with the main modifications : (1) flow-meter derivation, (2) addition of a ventricular compliance.

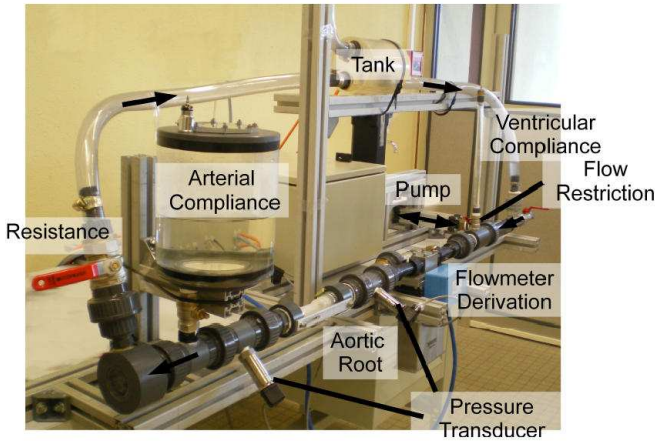

Fig.IV.21_ Final dynamic testing configuration

Figure IV.22 shows the final pressure signal obtained with that final configuration. The modifications damped the pressure peaks drastically and the signal is very close to the physiological one. As can be noted, the silicon root doesn't disturb the signal significantly.

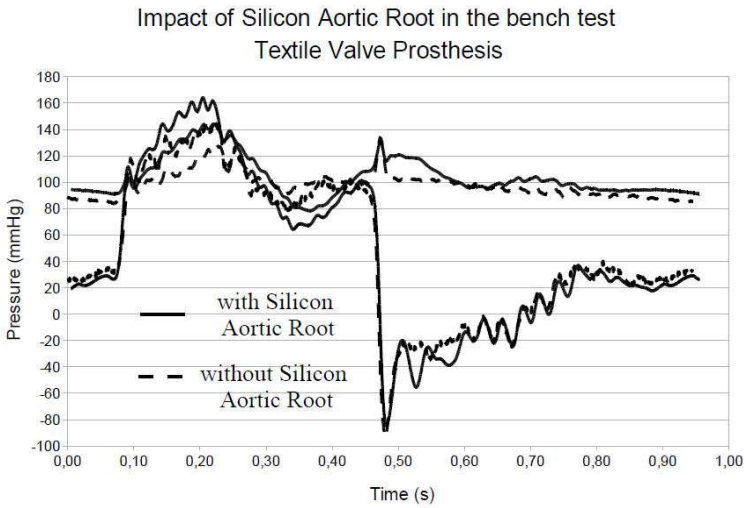

Fig.IV.22_ Pressure signal after modifications

Chapter V THE PROTOTYPE TESTING

1 INTRODUCTION

The goal of the work done in this chapter is to evaluate ‘in vitro’ the performances of the stented valve prototype. It is especially essential to assess if the prototype concept is valid, i.e. that the anchoring through surface matching is efficient. Different stent configurations have been tested, in order to assess the influence of geometrical parameters variations on the stent’s behavior. The parameters do have an influence either on the stent’s dimensions or on the stent’s rigidity. The rigidity influences the valve closing mechanism, while the dimensions influence the positioning of the stent in the root and affect leakage properties of the prosthesis. The way the stent affects the textile prosthesis is also studied, in comparing the stented valve performances with the performances of the non stented valve. Finally the prototype’s performances are compared with the performances of other commercially available valves.

2 OPERATING CONDITIONS

We present here how the tested valves are placed in the bench. The commercially available valves are mounted in a rigid root while the stented valve is mounted in compliant root.

2.1 Protheses placement

The ‘in vitro’ testing must assess the leakage properties of the tested prosthesis. Therefore the mounting in the testing root must be precisely defined, to prevent biased measurements due to placement differences.

2.1.1 The non stented prostheses

Valvular prostheses implanted with classic surgical procedure are used to be sutured to the aortic ring to prevent any paravalvular leakage. The in vitro testing of a prosthesis requires therefore to assemble the valve with the root in similar conditions.

The commercially available prostheses that we use in our testing procedure, to make some performances comparison, are the biological Mitroflow and the mechanical St Jude Bileaflet. The devices are originally mounted on a rigid polyester covered ring for surgical suture purpose. The ring is also used in vitro to test the prostheses in flood-tight configuration.

The textile prosthesis tested in vitro is developed in our lab. It is molded in a rubber silicon ring to get maintained in aortic position. A rigid PVC cuff helps to press the prosthesis on the aortic ring.

Figure V.1_ Textile prosthesis (left) and biological valve (right) positioning devices

2.1.2 The stented valve

The stented valve is placed in the compliant root manually at ambient pressure. The silicon dimensions are different between the rest state and under testing. At implantation time the positioning precision of the stent depends on the operator. Hence, for better relevance in the tests, it is essential to run some pulsed signal before any measurement is performed. The stent will position itself to its final position after a while.

2.2 Conditioning of the textile prostheses

To attest the stent's performances in vitro, we chose to associate it with a textile valve. The textile valve is obtained by shaping a polyester fabric. Picture V.2 represents a textile valve prosthesis, sutured to a conical basis.

If textile material makes it possible to vary easily valve's dimensions, it requires, however, specific treatment before testing.

Fig V.2_ Textile prosthesis positioning device

2.2.1 Textile structure and in vitro testing

Fabric permeability depends directly on yarn organization in the fabric structure. Textile used as heart valve is solicited in vitro under flexure and pressure stress, which largely modify the yarn reorganization. Figure V.3 shows the leakage evolution of a fabric valve over time. One may observe a continuous decrease in static leakage (on closed valve) over time.

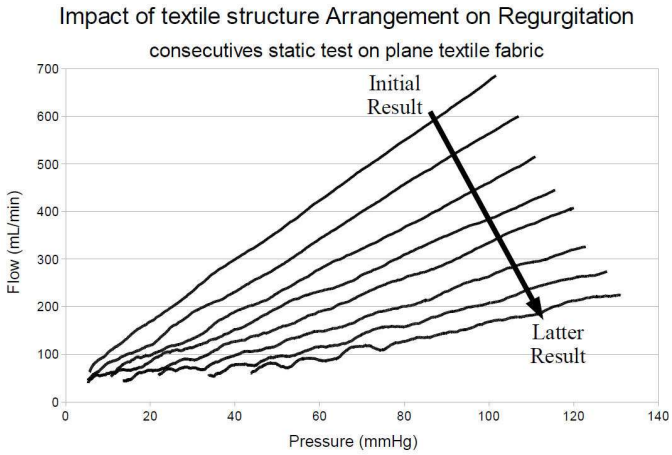

Figure V.3_ Fabric leakage versus time

2.2.2 Consequences on static regurgitation measurements

Because of this time related fabric rearrangement process, before any reliable regurgitation test can be performed two conditions must be respected:

- In order to get rid of the testing history of the material, the valvular prosthesis must be tested under physiological pulsed flow conditions, over a long enough period of time to stabilize the regurgitation values. Once stabilization is reached, fabric structure will not reorganize any more. The time required for that dynamic process being quite long, the valve is initially conditioned under static pressure (150mmHg) for 6 minutes

before dynamic conditioning. The following conditioning period lasts 20 minutes in our experiments.

- As to the static regurgitation assessment, successive measurements were not relevant. Indeed, static pressure from the water column acting on the material tends to reorganize the fabric structure at each test. Fabric must, therefore, be conditioned before measurements are performed.

Static and dynamic conditioning was performed before any regurgitation measurement.

2.3 Bench testing settings

The ISO/CD 5840 norm, which deals with heart-valve prostheses 'in vitro' testing, does not concern stented valves. We defined however a protocol for our experiments to be comparable.

2.3.1 Flow generator

All prostheses were tested under physiological conditions, at 70 beats/min with a 70 mL ejection volume. Systole and diastole durations are respectively 300ms and 557ms.

2.3.2 Compliance

For all tests aortic and ventricular compliances were set at :

- C_a = 1.84 mL/mmHg
- C_v = 0.02 mL/mmHg

The compliance of the mock aortic root is considered, even when tests are performed on textile, biological or mechanical valve (mounted in rigid root as previously described). The compliant root is therefore placed in addition to the rigid one.

2.3.3 Resistance

Resistance value is set so as to obtain a 100mmHg pressure gradient over the valve in diastole. Systolic peak pressure is then 160mmHg.

2.3.4 Fluid

The ideal fluid for 'in vitro' testing should be blood analog, with controlled density and viscosity. We chose to work with water to make the testing easier. Basically, the goal of the

testing process was to assess the influence of the stent on the global prosthesis behavior, and to compare the performances with the ones of other devices. The flow characteristics do not play a big role in that approach.

3 STENTED VALVE PERFORMANCES VERSUS FEATURES DEFINITION

Dimensions as well as rigidity of the stent's elements, influence the performances of the endoprosthesis. As already cited in the previous chapters, the stent can be characterized with following features :

- Head height (H)
- Cone angle (θ)
- Cone width (l)
- Arms stiffness
- Posts stiffness

To find the best dimension and structure combination for the stent, we varied these features, and compared the prototypes performances. The features were separated in two classes.

- Features related to dimensions, which characterize the positioning of the stent in its environment.
- Features related to the stent's rigidity, which characterize the stress induced by the stent on the surrounding tissues.

The testing of different combinations of these features will help find the stent that ensures optimum anchoring and leakage properties.

3.1 Dimension features

The dimension features are described here in more detail, to assess their possible influence on 'in vitro' behavior.

3.1.1 Head Height

The head of the stent is supposed to center and orient the device axially. To make the implantation process easier, it is interesting to minimize the length of the stent. However, if the head of the stent is not long enough, the device may tilt. The influence of the length was therefore assessed. Two heights were tested in respect to the following criteria :

- The posts height was adjusted.
- The nitinol wire diameter is adjusted to keep the same pressure applied on the aortic wall.

3.1.2 Cone angle

The cone angle plays an essential role in the anchorage of the stent. The lower the angle value, the lower the prosthesis migration risk. However, with to low angle values, the cone may interfere with the sinuses. Two angle values were compared : low and average.

3.1.3 Cone width

The cone width influences the sealing of the prosthesis on the aortic root. One may assume that the higher the width, the better the sealing, but the bigger the risk of interference with the back of the sinuses. A cone with average width value was compared with a cone with larger value.

3.1.4 Arms length/shape

To prevent flow disturbances in the sinuses, it would be of interest to minimize the length of the arms in the sinuses. Two stents were compared : one with longer arms, the other with short arms.

3.2 Structure features

One of the main goal of the in vitro testing, is to validate the assumption that the stented valve can remain in position under pulsed flow, with only low expansion force. Measurements performed with varying the stiffness of both arms and posts, will make it possible to assess the minimum required stiffness of the elements.

3.2.1 Arms flexibility

Arms are essential parts of the stent, which prevent the device from axial translation. They press on the upper part of the sinuses, and guarantee that contact between cone and aortic ring always occurs. As already presented in Chapter II, the effort applied in the sinuses should be as limited as possible, to prevent tissue degradation and traumatism. To validate the theoretical model presented, we tested three prototypes with three different arm rigidities : high, medium, low. The highest rigidity corresponds nearly to a configuration, in which compliance is completely impeached over the cardiac cycle.

3.2.2 Post rigidity

The stent's posts play different roles :

- They link the different stent parts and bring cohesion to the device
- They hold the valve leaflets

Enough rigidity is required to fulfill these duties. Percutaneous implantation requires however flexibility. Compromise needs to be found. The experiments will be realized with two rigidity values for the posts.

3.3 Finally adopted geometry parameters

Table V.4 lists the values adopted for the realization of the different stents elements.

		Sample 1	Sample 2	Sample 3	Sample 4	Sample 5
Head	braided parameters	i=7 j=5	**3 * (i=7 j=3)**	i=7 j=5	i=7 j=5	i=7 j=5
	NiTi wire diameter (mm)	0.26	**0.26**	0.26	0.26	0.26
Conical basis	Angle (°)	40	40	**20**	40	40
	Width (mm)	6	6	6	**8**	6
Posts	NiTi wire diameter (mm)	0.55	0.55	0.55	0.55	**0.6**
Arms	Nb of wires	3	3	3	3	3
	Length	long	long	long	long	long

		Sample 5	Sample 6	Sample 7
Head	braided parameters	i=7 j=5	i=7 j=5	i=7 j=5
	NiTi wire diameter	0.26	0.26	0.26
Conical basis	Angle	40	40	40
	width	6	6	6
Post	Nitinol wire diameter	0.6	0.6	0.6
arms	nb of wires	3	**2**	**1**
	length	long	long	long

		Sample 6	Sample 8
Head	braided parameters	i=7 j=5	i=7 j=5
	NiTi wire diameter	0.26	0.26
Conical basis	Angle	40	40
	width	6	6
Post	Nitinol wire diameter	0.6	0.6
arms	nb of wires	2	2
	length	long	**short**

Sample 7	Sample 9
i=7 j=5	**i=7 j=3**
0.26	**0.203**
40	40
6	6
0.6	0.6
1	1
long	long

Table V.4_ values adopted for the realization of the different stents elements.

4 THE TESTING

Three different kinds of tests have been performed. First we tested the influence of the previously listed features on the prosthesis behavior under defined testing conditions. Second, we compare the performances of the textile stented valve with the ones of the non stented textile valve, to assess the influence of the stent on the behavior. Finally we compare the stented valve with other commercially available prostheses : a biological (Mitroflow) and a mechanical (St Jude bileaflet).

4.1 Performances of the stented valve

The performances of the stented valve depend first on the performances of the stent, and second on the performances of the valve. The stent's features may influence both. We study hence simultaneously the behavior of the stent in the compliant aortic root, and the static and dynamic leakage of the device. The measured regurgitation is influenced by the stent in two ways :

- The bad positioning of the stent in the root will lead to leakage.
- The valve is connected to the stent, and its closing behavior will depend on the stent's rigidity.

Regurgitation measurements are represented in 3 different ways :

- Tests under static pressure are performed and leakage flow across the valve in closed position is plotted versus pressure applied.
- Diastolic closing flow is at last plotted versus time. This gives information on the volume flowing through the valve while closing. Closing duration can then be assessed.
- Under pulsed flow, we measured the global back-flow as a percentage of stroke volume.

All the prototypes are positioned in the compliant aortic root for static and dynamic testing.

4.1.1 Placement in the aortic root

If the stent is badly positioned in the aortic root, leakage volume across the closed valve occurs. Basically, if the stent is badly oriented in the implantation environment, the contact zone between the cone and the aortic ring is badly realized : para-valvular leakage increases. This phenomenon can be particularly noted under static testing conditions. The design parameters that influence the positioning of the stent are listed below.

4.1.1.a Cone width

Two prototypes are compared. The first is characterized with a standard cone width (described as reference cone), while the cone width of the second was extended. Figure V.5 shows the measured regurgitation values obtained.

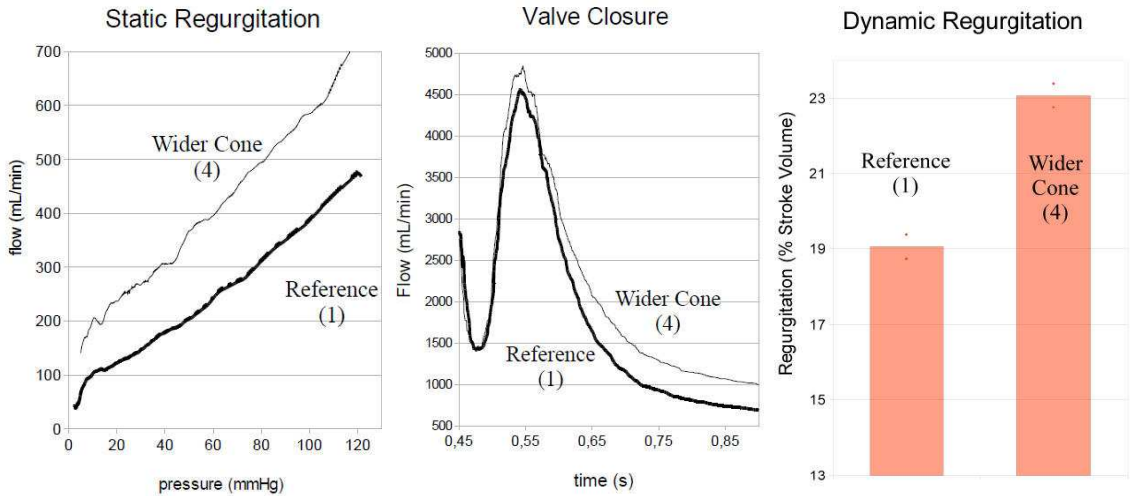

Fig.V.5_ cone width variation

We note that static as well as dynamic regurgitation increases for larger cone width value. This can be explained by the fact that the conical basis becomes too large to push on the aortic ring. The cone tends to push on the bottom of the sinuses, which leads to bad sealing and leakage. As to the valve closing time, it is only slightly modified. Actually the closing process is mainly conditioned by the flow vortex generated in the sinuses. To increase the cone width doesn't modify the leaflet facing the sinuses. Flow circulation in the sinuses is therefore not modified, and closing duration keeps the same.

A wider cone doesn't only increase static regurgitation, but also may lead to worse tissue degradation. Actually, when stent pushes on the sinus tissues rather than on the aortic ring, the stress transfer generates sinus tissues degradation. The cone width must be therefore limited.

However, if the cone is not wide enough two more problems may appear :

- Cone positioning may be disturbed for large ring diameter variations over the cardiac cycle
- The stent must be axially well oriented for precise cone-ring matching. The cylindrical head of the stent plays a large role in that matter as we show in further results.

4.1.1.b Cone angle

Two prototypes are compared. The first is characterized with a standard cone angle (described as reference cone), while the cone angle of the second was reduced. The reference angle value corresponds to the native angle between the bottom of the sinuses and a vertical cut plan of the root. Figure V.6 shows the measured regurgitation values obtained.

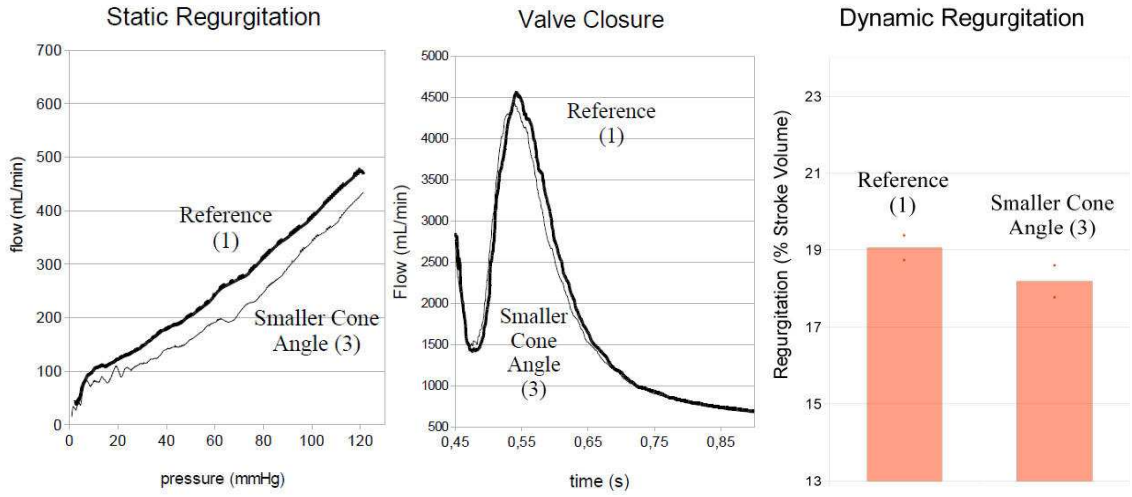

Fig.V.6_ cone angle variation

A slight decrease in both static and dynamic regurgitation values is observed. Basically, reducing the angle leads to better matching with increased contact surface between aortic ring and cone. Sealing is hence better ensured and shows reduced static leakage. As to dynamic regurgitation, lower angle leads to more secure axial positioning. Actually, the higher the angle the better the device is centered in the aortic ring. With lower angle value, the risk of stent tilting is increased in spite of the role played by the head in that way.

An ideal configuration will be a conical basis with minimum angle value, which provides enough sealing over the whole cardiac cycle and axial positioning of the device.

4.1.1.c Length of the arms

Two prototypes are compared. The first is characterized with arms long enough to cover nearly the whole sinus surface (described as reference), while the second is characterized with much shorter arms, which push only in the upper part of the sinuses. It is first important to note that with short arms, it's not possible to respect the geometry of the sinuses. Figure V.7 shows the sinus deformation at end of diastole. High local deformation is a characteristic of that configuration. The effort from the arm on the sinus is actually not spread on the whole sinus tissue, and with shorter arms, the effort value is increased as well. Results are presented in Figure V.8

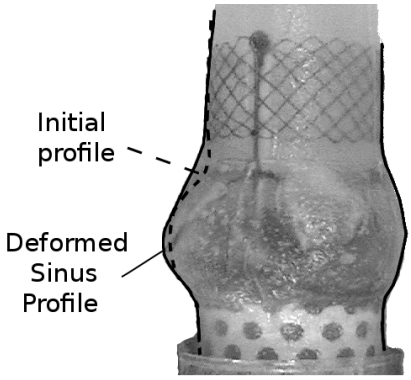

Fig.V.7_ sinus deformation induced by short stent arms compared to long stent arms.

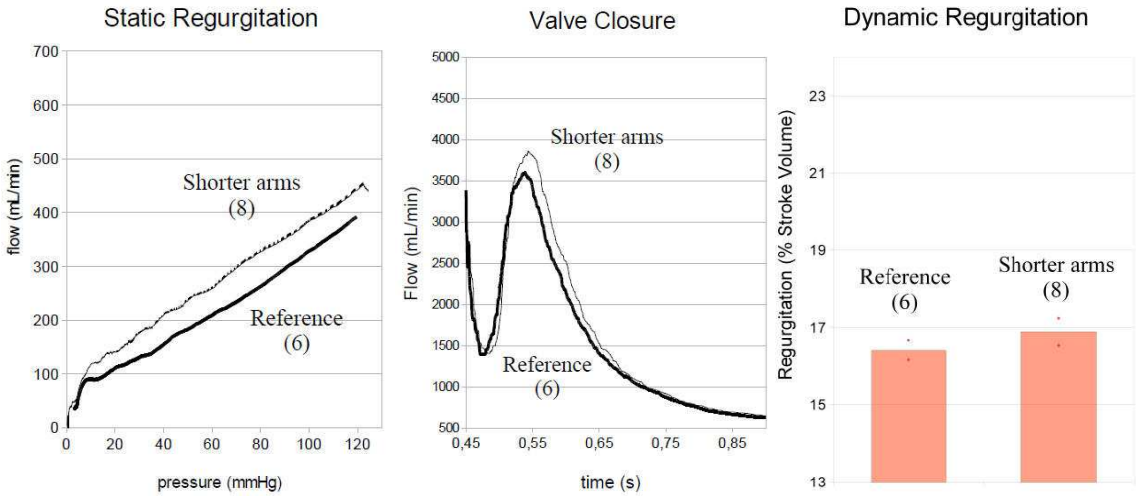

Fig.V.8_ arms length and regurgitation

Static as well as dynamic regurgitation values are increased with shorter arms. While systolic anchoring is provided, the local deformation induced in the sinuses lead to tissue axial extension. The resulting effort applied by the cone on the aortic ring is hence reduced. Para-valvular leakage is increased. As to the influence of the rigidity increase due to arms shortening on the global dynamic prosthesis behavior, it will be studied further in this work.

Ideal stent design should be characterized with arms long enough to apply pressure on sufficient sinus surface. Static regurgitation would be limited and tissue degradation as well.

4.1.1.d Cylindrical head

Braid cohesion

Two prototypes with different head heights are compared. One is considered as the reference, while the other one is characterized with a smaller head. The braiding parameter j, that defines the number of meshing cells over the head's height, is different between the two prototypes. Following consequences can be noted :

- A shorter head leads to fewer crossing points in the braided structure.
- To keep the same theoretical mechanical behavior for both heads, the wire used for the smaller one is chosen of lower diameter. Actually, with less long wire parts in the shortest braided structure, the wire stiffness is increased. Wire diameter reduction compensates this.

Results are presented in figure V.9.

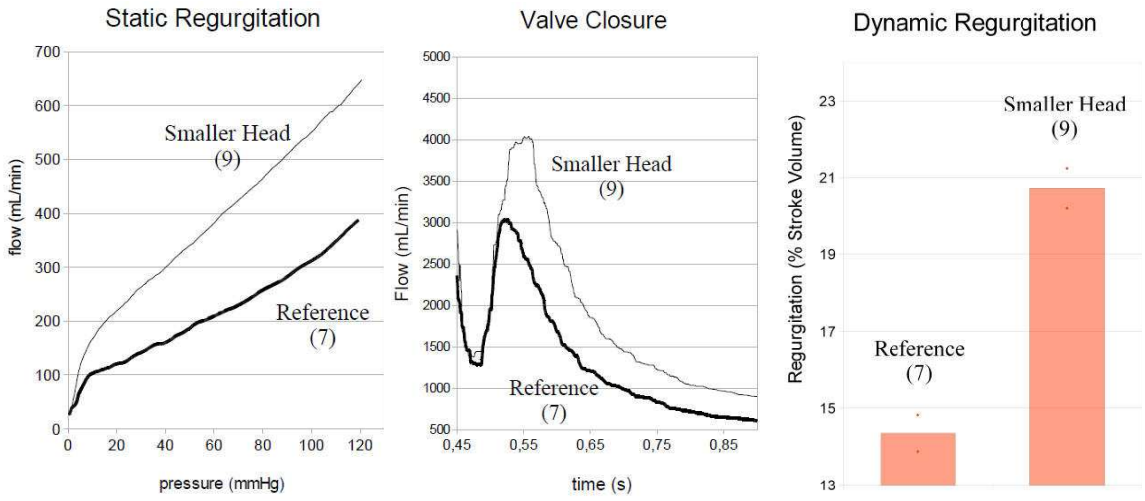

Fig.V.9_ regurgitation and head's height

Apart from the theoretical mechanical characteristics of the shorter head, we note that the cohesion of the braid is drastically reduced with dramatic consequences on regurgitation performances. The shorter head, with not enough cohesion, deforms more than expected and axial positioning is not ensured anymore. Positioning of the prosthesis on the aortic ring becomes very hazardous. Stent tilting is not completely impeached. Static leakage is hence increased.

Moreover, the stent slight tilting that occurs under pulsed testing conditions, has also consequence on the valve closing process, with higher closing volume. When the stent tilts, the leaflets change slightly their position from the sinuses, and prevent the sinus vortex to occur in a correct way. Valve closing becomes very dependent from just the pressure gradient across the valve at diastole begin. Valve closure is delayed, while closing volume increases.
It can be concluded that with poor cohesion in the braid, and exaggerated deformation of the head, the stent axial positioning cannot be realized. The regurgitation of the prototype is indeed very dependent on correct positioning of the cone on the aortic ring. Braiding parameters need to be changed for shorter head manufacturing.

Height of the braided head

Two prototypes with different height value are compared, but wire diameter is this time increased for the shorter head to ensure braid's cohesion. The radial stiffness of the shorter head is thereof slightly increased, which leads to lower radial compliance of the implanted device. Results are presented in Figure V.10.

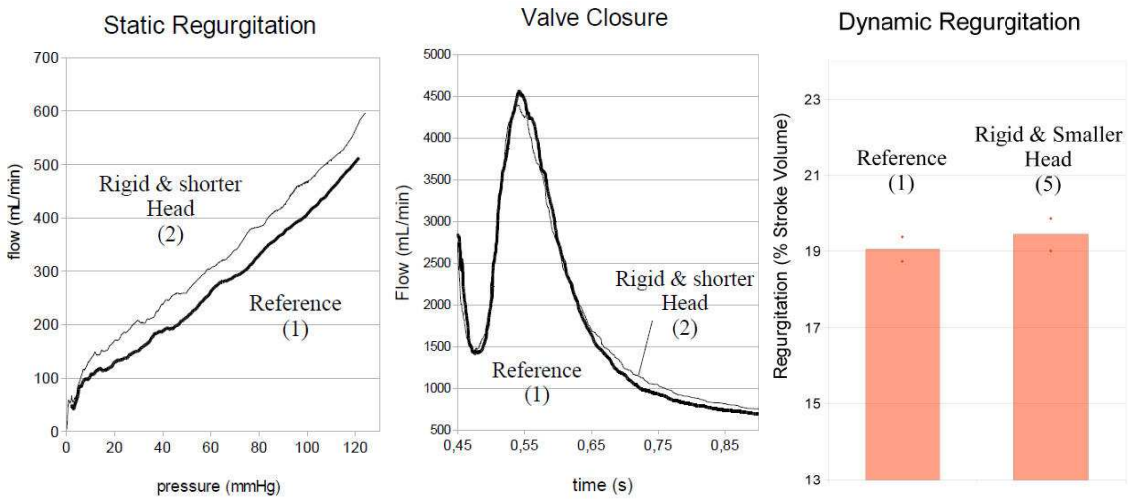

Fig.V.10_ regurgitation and head's height

We note that under dynamic working conditions the closing volume is nearly the same for both prototypes. Static regurgitation is however higher for the shorter head, and this in spite of higher rigidity. These results show that reduced height is not sufficient for the head to position axially the stent in the aortic root.

The optimal head must be developed in taking two aspects into consideration : (1) the height, (2) the radial stiffness. Braid's cohesion must be sufficient, but limit radial pressure acting on surrounding tissues. Braiding with numerous low diameter wires could be a solution. As to the height, it must be high enough to ensure efficient positioning, but short enough to make percutaneous implantation easier. For further testing, we adopt a long head with fine braiding to prevent leakage due to bad axial positioning

4.1.2 Valve closing time

Para-valvular leakage due to biased stent placement in the aortic root is important as we analyzed above. But the influence of the stent on the dynamic behavior of the valve itself is also a main concern. The measurement of a closing time modification associated with no increase in static leakage highlights this influence. The valve behavior modifications are in particular related to the stent's stiffness. We study below the influence of the rigidity of the different stent's parts on the valve dynamic performances

4.1.2.a Rigidity of the arms

To assess the arms influence on the valve performances, we compare prototypes realized with arms characterized with different stiffness. The arms are identically shaped, but realized with 1, 2 or 3 Nitinol wires. The 3 wires configuration prevents nearly any compliance movement for the sinuses, while in the other cases, compliance is respected. Results are presented in Figure V.11.

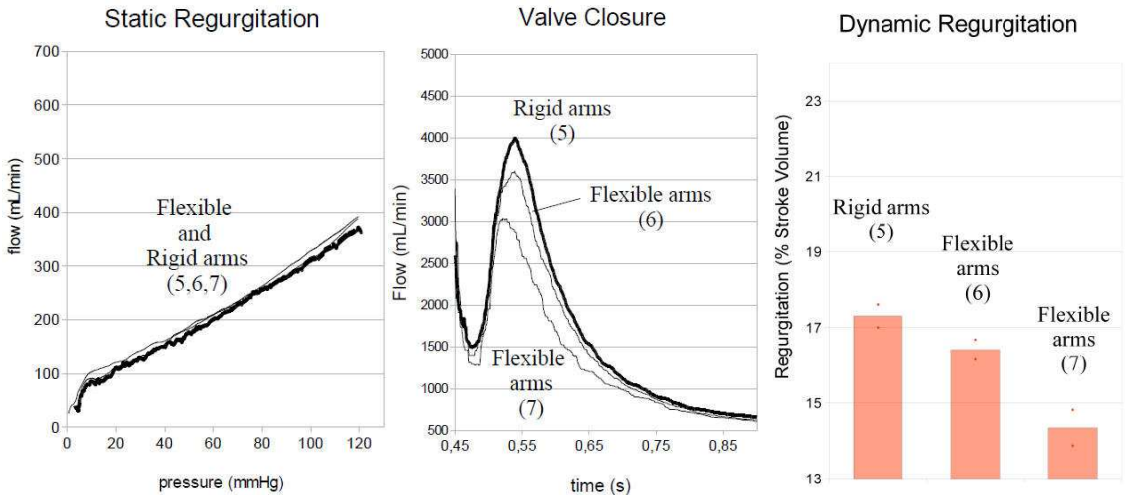

Fig.V.11_ regurgitation and arms's flexibility

The experiments lead to different conclusions. First, from a qualitative point of view, we observe that the use of flexible arms is sufficient to ensure precise stent anchoring in the compliant aortic root. Second, we note that static leakage is not influenced by the arms rigidity, which means that the positioning of the stent in the aortic root is not affected by changes in the arms rigidity. On the contrary, arms rigidity has influence on dynamic regurgitation results. With arms characterized with low rigidity, the closing volume is reduced. Basically, arms are linked to the stent's posts. The more rigid they are, the more they tend to flex the posts. The posts flexure can be observed dynamically on the bench when stent is under pulsed flow.

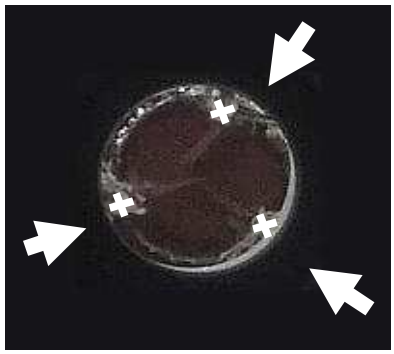

Fig.V.12_ top view of the stented valve in diastole. 3 arrows note the posts location

The closing delay induced by the deformation of the posts can be explained qualitatively as follows : rigid arms tends to flex the posts which consequently put valve commissures closer. Valve leaflets are then solicited on a minimize area. Valve opening and closing require thus increased bending energy, there are more folds on each leaflet.

The results highlight the relationship between the arms, the posts and the valve itself and how the dynamic regurgitation of the prosthesis is conditioned by the different stent elements. Arms with low rigidity seem to be better adapted to stent's requirements. They allow anchoring the stent in the aortic environment while respecting tissue compliance. Moreover, low rigidity of the arms leads to lower valve closing volume and shorter closing duration.

4.1.2.b Rigidity of the posts

The results presented above, show that the posts deformation influences the valve closing dynamic. We compare in that section two prototypes realized with two different post rigidities. The reference is considered to be the prototype assembled with the less rigid posts. In figure Fig.V.13 are represented the obtained results.

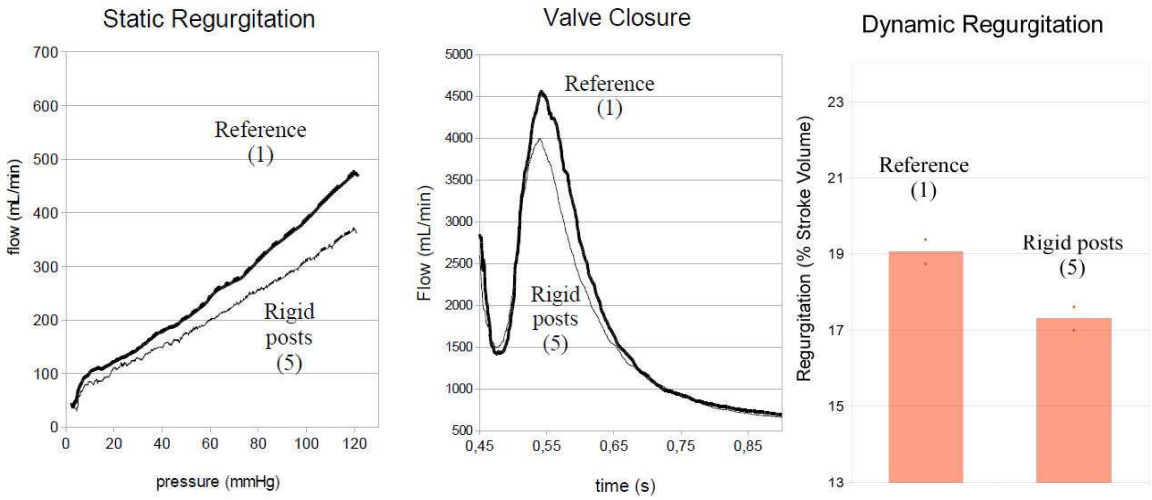

Fig.V.13_ Regurgitation and posts rigidity

The more rigid the posts are, the less dynamic regurgitation is observed. With less rigid posts, which tend to flex, the valve closure is delayed. The obtained results, validate the mechanism already described previously. Moreover, the use of more rigid posts leads to less static leakage for the valve, which is independent from the closing mechanism. This can be explained with the fact that the posts provide rigidity to the whole device. Their deformation leads to global deformation of the stent. Axial positioning of the conical basis on the aortic ring thanks to the cylindrical head is hence disturbed. Head guaranties axial positioning, only with non deformable posts. Only then, leakage is prevented.

We can conclude that optimum behavior for the stent is obtained with high rigid posts. Stent axial positioning is then ensured and regurgitation is limited.

4.1.3 Conclusion

The tests performed have highlighted which influence the different stent features had on the dynamic behavior of the stented valve. The device performances can be optimized on the basis of these results. However, we note that the high posts rigidity that is required to reach expected regurgitation performances, is not compatible with percutaneous implantation. Further work need to be done on the stent's design to separate arms and posts behavior. A new way of assembling the stent parts together need to be developed in that way.

4.2 Stented valve and other protheses

4.2.1 Stented and non-stented textile valve

We focus in this section on the influence of the stent on the textile valve behavior. We compare the performances of the stented valve (reference 7) with the ones obtained with a non stented textile valve mounted on a rigid support. Figure V.14 represents the regurgitation performances of the two valves.

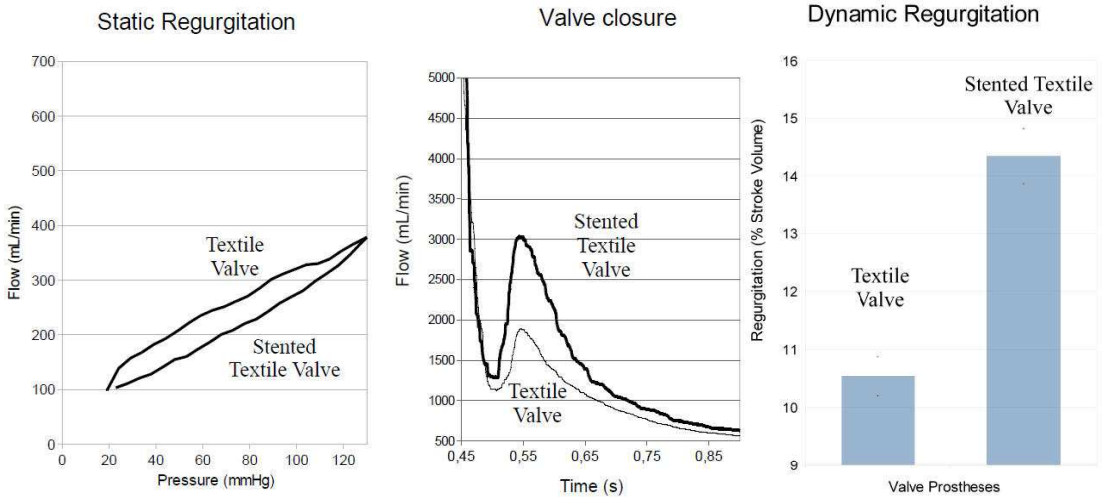

Fig.V.14_ stented and non stented textile valve

In terms of static regurgitation, the stented valve is more efficient than the non stented valve. First, the stent's specific conical geometry makes it possible to ensure tight sealing at the cone-ring interface, with limited para-valvular leakage. Moreover, the deformation of the posts under static pressure, leads to radial movement of the valve commissures towards the aortic root axis. Good coaptation between the leaflets is realized. On the contrary, when valve is mounted on a rigid support, this deformation and the commissure movement doesn't occur. The commissure's position is, in that case, largely dependent on the way the valve is mounted on the rigid support. Irregular positioning may hence lead to increased static leakage for the valve. As to the dynamic regurgitation, results are better for the non stented textile valve. Dynamic leakage is around 38 % higher but remains globally in low range. Closing volume is higher and closing time is delayed. This can be explained, as already described above, through the flexing of the posts, which tend to deform the whole device and modify the sealing under dynamic conditions. The leaflets are linked to the posts, and excessive posts deformation modifies the coaptation conditions. The required leaflet bending energy increase , valve closing is hence delayed.

Performances of the stented valve are good under static conditions, but are not completely satisfying under pulsed conditions. Assembling of the stent's parts must be optimized in further developments to improve the dynamic performances.

4.2.2 Stented valve and other commercially available prostheses

The stented valve (reference 7) is compared to other commercially available prostheses: a mechanical and a biological. Figure V.15 presents the obtained results.

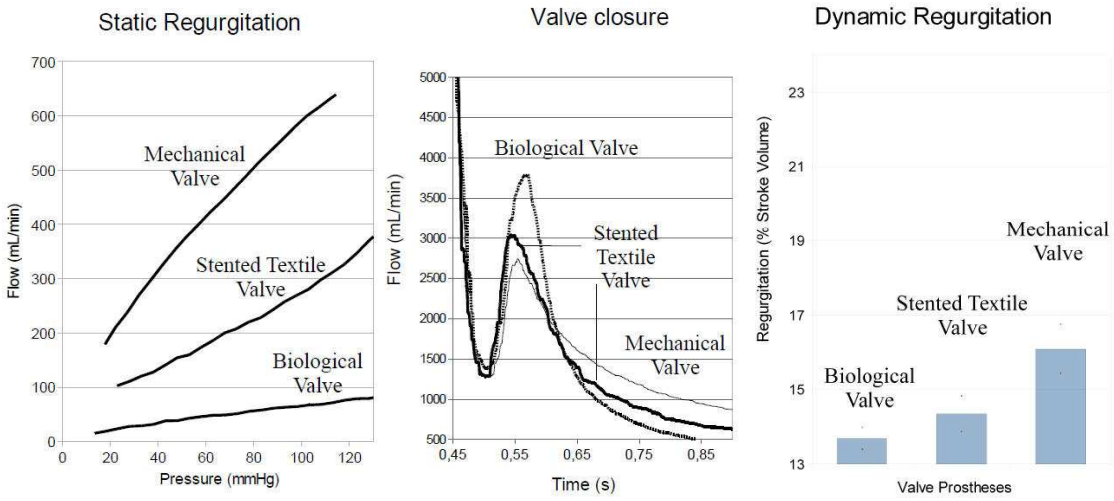

Fig.V.15_ stented valve, mechanical valve and bioprosthesis

When compared to biological valve, the static regurgitation of the stented textile valve is much higher. Basically, textile material is porous and less flood tight than biological tissue. Static leakage will always exist for such kind of material. When compared with the mechanical valve, the stented valve presents better results. Mechanical valve is indeed characterized with running clearance. Our prototype shows encouraging performances from that point of view.

As to the dynamic regurgitation properties, the stented valve is in the range of other standard valves and this, in spite of delayed closing due to flexible posts. Moreover, significant improvements through design optimization of the stented valve are still possible.

In vitro results show that the endoprosthesis is already characterized with acceptable static as well as dynamic performances in comparison to what is expected in the field. Moreover, the improvement margin is large.

5 CONCLUSION

The in vitro testing results presented in this chapter, have highlighted that the in vitro behavior of the stented valve is close to what is expected for such device. The stent ensures good anchoring in the mock aortic root, under physiological testing conditions without excessive radial expansion force. Static and dynamic regurgitation performances are in the range of the ones for other available prostheses. The results highlight the role played by the stent's features on the stented valve performances. These features are to be optimized in further design and assembling developments, in order to improve the stent's global behavior.

CONCLUSION AND FUTURE WORK

With the present work we tested the feasibility of realizing a stented valve, which positioning in the aortic root is guaranteed though surface matching rather than through high expanding force. The bibliographic work highlights the interest of developing non-invasive technical valve replacement with specific design, to meet the specific requirements of heart valve. Basically, the use of classic cylindrical stents associated with biological valves in the already performed clinical trials proved the feasibility of percutaneous valve implantation. However, migration problems as well as surrounding tissues degradation were reported by the pioneers. Many stent prototypes are today under development, but only few are not based on high expansion force. The market is there, and the medical community shows big interest in the development of specific solutions, which could overcome the drawbacks of classic cylindrically shaped stents.

The design we have presented tends to respect the geometry of the native aortic root. The stent is maintained through geometrical positioning. A conical basis is placed on the aortic ring and transmits the whole diastolic pressure force to it. The role of the ring is thus respected. The positioning of three arms in the upper part of the sinuses prevents the stent from translating under dynamic flow pressure in systole. The mechanical behavior model we have proposed for the arms, shows that the compliance of the sinuses can be respected if the arms are dimensioned in respect to the compliance requirements. As to the braided parts, we showed that with appropriate wire diameter, it is possible to obtain head and cone structures with enough rigidity to withstand diastolic pressure without braid collapsing. The assembling of all the parts can be done with respect to the sliding freedom of head and cone along the posts. The stent's global length can thus be kept constant between compressed and deployed states. The implantation with limited length through tortuous arteries is hence easier.

The detailed study of the braiding conditions presented in the third chapter, allowed us realizing braided structures made from a unique continuous wire. This specific configuration prevents the stent from being characterized with too many discontinuities, which could

disturb blood flow and generate blood clots. Another advantage of the continuous wire configuration is that the tissue-stent interaction is less degrading for the tissues. With fewer wire extremities, risk of injury is limited.

In order to test the performances of the stent prototype in physiological conditions, it was necessary to implant the stent in a mock compliant aortic root. Indeed, the elasticity of the implantation environment has much influence on the stent's behavior. However, the deformation undergone by the root is highly pressure dependant. The already existing testing bench was characterized with non desired pressure peaks that would exaggerate the root's deformation. The fluid mechanics study conducted in chapter four made it possible to control more precisely the pressure conditions of the bench, and do the necessary modifications in order to obtain the expected pressure values over the cardiac cycle. The final signal reached after modification respected precisely the native signal.

On the basis of physiological testing conditions, it was possible to test the performances of the prototypes in terms of static and dynamic regurgitation. The results are particularly encouraging because they show that the stent associated with a textile valve is flood tight enough. Under static conditions, even at higher pressure, the contact between the conical basis of the stent and the aortic ring is maintained. Moreover, the braided head of the stent deforms with the aorta expansion and the contact between head and aorta conduit is maintained as well over the whole cardiac cycle. The head prevents the stent from tilting even at high pressure. Its function is hence validated. As to the results obtained under dynamic conditions, they validate the role played by the stent's arms. Under pulsed flow, the stent keeps the position and doesn't translate upwards. However, the arms flex slightly over the cardiac cycle and make it possible to keep the compliance for the sinuses. We proved, hence, that the stent respects the dynamic behavior of the aortic root. Tissue degeneration due to exaggerated stress should be limited in vivo.

When compared to other commercially available prostheses, one can observe that the performances of the stented valve are very close from what can be expected for such kind of device. The prototypes seem to satisfy the physiological needs.

At last, we performed some tests varying different design parameters. The results highlight how influent design criteria are on the dynamic behavior of the prototypes. We note especially that head, arms and cone play each an essential and equivalent role in the stent's performances. First, a long enough cylindrical head prevents stent from tilting and ensures precise positioning on the aortic ring. Second, a too low cone angle leads to interaction between cone and sinus depth. On the other hand, if the cone angle is too big, the stent

doesn't push enough on the ring and positioning is not ensured enough precisely, which leads to valve leakage. As to the arms, they need to be long enough to spread the effort in the sinuses and their rigidity must be low enough to keep the compliance of the sinuses. At last, the tests highlighted the role played by the posts in the valve dynamic behavior. If the posts are not rigid enough, the energy required to close the valve through leaflet flexure is higher. The valve closing is hence delayed, and the dynamic leakage is increased.

The work done up to now and the results obtained in vitro validate the principle of the stent. We proved that it is possible to realize a stent that is positioned through surface matching rather than exaggerated expansion force. The performances of the stented valve are in the range of the expectations for heart valve replacement prostheses. Qualitative tests proved that after compressing the stent by hand to low diameter, it recoils when compression force is removed.

However, some questions remain and need to be answered in further work, with focus on three points. First, no trials have been performed yet to insert the stent in a catheter. This is a major issue for that kind of device. It is particularly essential to assess how the catheter must be designed to ensure precise expansion of the different stent's parts. Future work must be done on the development of the catheter. Moreover, to assess the way the stent may position itself in the aortic root, some tests must be performed first in explanted aortic roots using some radiographic and fluoroscopic imaging techniques. The imaging technique must make it possible to see if each of the stent's arms is properly positioned in the each sinus. The stent's axial positioning must be controlled as well to ensure that the cone deploys at the right level in the aortic root. A second issue that is essential to deal with is the durability of the implantation. We tested the device only on short periods of time. Longer lasting fatigue testings should confirm that the positioning of the device is guaranteed on the long term, and that the stented valve doesn't move over successive cardiac cycles. At last, some implantations must be performed in animal in order to test the thrombogenicity of the device. Indeed, the arms are positioned in the upper part of the sinuses and over the coronary ostia. It is therefore essential to assess if there's a risk of obstructing the coronary arteries with the geometry adopted for the arms. More generally, optimization must be performed at two main levels. First the interaction of blood with all the stent's parts must be analyzed. The results will help to optimize the geometry in order to obtain a prototype that disturbs blood flow as little as possible. Second, performances must be improved through design optimization. The tested prototypes, for example, were realized with flexible posts. In practice, one of the main

functions of the post is to link the head and the cone. Too much flexibility in the posts, lead to exaggerated flexure which induces global stent deformation. Leakage may thereof be increased. Basically a compromise must be found between low rigidity for easy implantation, and higher rigidity to keep enough rigidity for the stent. These aspects can be studied more in detail only after animal implantation has been performed. Moreover, the way the stent was assembled up to now may lead to suture ruptures. Optimization must hence also concern the assembling process. The final goal is to be able to realize the stent's geometry in one way rather than through assembling separate parts, for more reliability in work after implantation.

LITERATURE CITED

[ALL.04] DE.Allie, CJ.Hebert, CM.Walker, Nitinol stent fractures in the SFA, Endovascular Today, 2004, 22-34.

[AND.00] RH.Anderson, Anatomy : clinical anatomy of the aortic root, Heart, 2000, 84, 670-673.

[AND.92] HR.Andersen, LL.Knudsen, JM.Hsenkam, Transluminal implantation of artificial heart valves. Description of a new expandable aortic valve and inital results with implantation by cathter technique in closed chest pigs, Eur Heart J, 1992, 13(5), 704-8.

[ARO.89] KV.Arom, DM.Nicoloff, TE.Kersten, Ten years' experience with the St. Jude Medical valve prosthesis, Ann Thorac Surg, 1989, 47, 831-837.

[BAB.03] E.Babalik, M.Gülbaran, T.Gürmen, S.Öztürk, Fracture of popliteal artery stents, Circ J, 2003, 67, 643-645.

[BAL.97] PD.Ballyk, C.Walsh, J.Butany, and M.Ojha, Compliance mismatch may promote graft-artery intimal hyperplasia by altering suture-line stresses, J Biomech, 1997, 31, 229–237.

[BAU.04] F.Bauer, H.Eltchaninoff, C.Tron. et al, Acute improvement in global and regional left ventricular systolic function after percutaneous heart valve implantation in patients with symptomatic aortic stenosis, Circulation, 2004, 110, 1473–1476.

[BED.06] Bedoya J, Meyer CA, Timmins LH, Moreno MR, Moore JE, Effects of stent design parameters on normal artery wall mechanics, J Biomech Eng, 2006, 128(5), 757–765.

[BEL.08] C.J.Beller et al, Gender-specific differences in aortic sinus curvature during aging: an anatomical and computational study. Cardiovascular Pathology (2008), Article in press, doi:10.1016/j.physletb.2003.10.071

[BER.00] JL.Berry, A.Santamarina, JE.Moore Jr, S.Roychowdhury, and WD.Routh, Experimental and computational flow evaluation of coronary stents, Ann Biomed Eng, 2000, 28, 386–398.

[BER.02] JL.Berry, E.Manoach, C.Mekkaoui, PH. Rolland, JE.Moore Jr, and A.Rachev, Hemodynamics and wall mechanics of a compliance matching stent: In vitro and in vivo analysis, J. Vasc. Intervent Radiol, 2002, 13, 97–105.

[BER.97] JL.Berry, JE.Moore Jr, VS.Newman, and WD.Routh, In vitro flow visualization in stented arterial segments, J Vasc Invest, 1997, 3, 63–68.

[BON.00a] P.Bonhoeffer, Y.Boudjemline, Z.Saliba, et al, Percutaneous replacement of pulmonary valve in a right-ventricle to pulmonary-artery prosthetic conduit with valve dysfunction, Lancet, 2000, 356, 1403-5.

[BON.00b] P.Bonhoeffer, Y.Boudjemline, Z.Saliba, et al, Transcatheter implantation of a bovine valve in pulmonary position, Circulation, 2000, 102, 813-6.

[BOS.06] M.Bosiers, K.Deloose, J.Verbist, P.Peeters, Will absorbable metal stent technology change our practice?, J Cardiovasc Surg, 2006, 47, 393-397.

[BOU.02a] Y. Boudjemline, P.Bonhoeffer, Percutaneous implantation of a valve in the descending aorta in lambs, European Heart Journal, 2002, 23, 1045-1049.

[BOU.02b] Y.Boudjemline and P.Bonhoeffer, Steps toward percutaneous aortic valve replacement, Circulation 2002, 105, 775–778.

[BUR.06] HM.Burt, WL.Hunter, Drug-eluting stents: A multidisciplinary success story, Adv Drug Deliv, 2006, 58, 350-357.

[CHA.89] J.Chambers, T.Cochrane, The Gorlin formula validated against directly observed orifice area in porcine mitral bioprostheses, J Am Coll Cardiol, 1989, 13, 348-353.

[CHO.06] JS.Cho, S.Haider and MS.Makaroun, US multicenter trials of endoprostheses for the endovascular treatment of descending thoracic aneurysms, Journal of Vascular Surgery, 2006, 43(2), A12-A19.

[CHR.92] GW.Christie, Computer modelling of bioprosthetic heart valves, European Journal of cardiothoracic surgery, 1992, 6, S995-S101.

[CHU.96] CL.Chu, SK.Wu, YC.Yen. Oxidation behavior of equiatomic TiNi alloy in high temperature air environment, Materials Science and Engineering,1996, A216,193-200.

[CRA.83] A.Cragg, G.Lund, J.Rysavy, F.Castaneda, WR.Castaneda-Zuniga, K.Amplatz, Nonsurgical placement of arterial endoprostheses: a new technique using nitinol wire, Radiology, 1983, 147, 261– 263.

[CRI.02] A.Cribier, H.Eltchaninoff, A.Bash, et al, Percutaneous transcatheter implantation of an aortic valve prosthesis for calcific aortic stenosis : first human description, Circulation, 2002, 106, 3006-8.

[CRI.04] A.Cribier, H.Eltchaninoff, C.Tron, F.Bauer, C.Agatiello, L.Sebagh, A.Bash, D.Nusimovici, PY.Litzler, JP.Bessou, MB.Leon, Early experience with percutaneous transcatheter implantation of heart valve prosthesis for the treatment of end-stage inoperable patients with calcific aortic stenosis, J Am Coll Cardiol, 2004, 43, 698–703.

[CRI.06] A.Cribier, H.Eltchaninoff, C.Tron et al., Treatment of calcific aortic stenosis with the percutaneous heart valve: mid-term follow-up from the initial feasibiblity studies: the French experience, J Am Coll Cardiol, 2006, 47, 1214–1223.

[CRI.86] A.Cribier, T.Savin, N.Saoudi, P.Rocha, J.Berland, B.Letac, Percutaneous transluminal valvuloplasty of acquired aortic stenosis in elderly patients : an alternative to valve replacement, Lancet, 1986, 1, 63-7.

[DAT.02] JB.Dattilo, DC.Brewster, CM.Fan, et al, Clinical failures of endovascular abdominal aortic aneurysm repair: incidence, causes, and management, J Vasc Surg, 2002, 35, 1137–1144.

[DAV.06] MJ.Davidson, JK.White, DS.Baim, Percutaneous therapies for valvular heart disease, Cardiovascular Pathology, 2006, 15, 123– 129.

[DEL.97] A.Delfino, N.Stergiopulos, JE.Moore Jr., and JJ.Meister, Residual strain effects on the stress field in a thick wall finite element model of the human carotid bifurcation, J Biomech, 1997, 30, 777–786.

[DEP.92] N.DePaola, MA.Gimbrone, PF.Davies, and CF.Dewey, Vascular endothelium responds to fluid shear stress gradients, Arterioscler Thromb, 1992, 12:1254–1257.

[DOT.83] CT.Dotter, RW.Bushmann, MK.McKinney, J.Rösch, Transluminal expandable nitinol coil stent grafting: preliminary report, Radiology, 1983, 147, 259– 260.

[DUD.02] SH.Duda, B.Pusich, G.Richter, et al, Sirolimus-eluting stents for the treatment of obstructive superficial femoral artery disease: six-month results, Circulation, 2002, 106, 1505-1509.

[DUE.00] TW.Duerig, DE.Tolomeo, M.Wholey, An overview of superelastic stent design, Min Invas Ther & Allied technol, 2000, 9, 235-246.

[DYE.00] JF.Dyet, WG.Watts, DF.Ettles, AA.Nicholson, Mechanical Properties of metallic stents : How do these properties influence the choice of the stent for specific lesions ? CardioVasc and Interv Radiol, 2000, 23, 47-54.

[EDE.98] ER.Edelman, C.Rogers, Pathobiologic responses to stenting, Am. J. Cardiol, 1998, 81, 4E–6E.

[EUR] Euroflex, Nitinol SE508 Wire Material Data, disponible sur : http://www.nitinol-europe.com/pdfs/EUROFLEX_datasheet03.pdf (consultée le 24/03/2009).

[FAT.03] R.Fattori, T.Piva, Drug-eluting stents in vascular intervention, Lancet 2003, 361, 247-249.

[FAV.06] D.Favier et al, Influence of thermomechanical processing on the superelastic properties of a Ni-rich Nitinol shape memory alloy, Material Science and engineering, 2006, A429, 130-136.

[FER.04] M.Ferrari, et al, Transarterial aortic valve replacement with a self expanding stent in pigs, Heart, 2004, 90, 1326-1331.

[FER.99] C. Ferraresi, AM.Bertetto, L.Mazza, D.Maffiodo, W.Franco, One dimensional experimental mechanical characterisation of porcine aortic root wall, Med Biol Eng Comput 1999, 37, 202-207

[FIS.04] RD.Fish, Percutaneous heart valve replacement enthusiasm tempered, Circulation, 2004, 110, 1876-8.

[FOK.04] AA.Fokin, F.Robicsek, JW.Cook, MJ.Thubrikar, J.Schaper, Morphological changes of the aortic valve leaflets in non-compliant aortic roots : in vivo experiments, J Heart Valve Dis, 2004, 13, 444-451.

[FOR.01] L.Formaggia, F.Nobile, and A.Quarteroni, A one dimensional model for blood flow: Application to vascular prosthesis, In: MSCOM2000, edited by T. Miyoshi. Berlin: Springer, 2001.

[GAR.00] J.M Garasic et al, Stent and Artery Geometry Determine Intimal Thickening Independent of Arterial Injury, Circulation, 2000, 101, 812-818.

[GRU.06] E.Grube, et al, Percutaneous Implantation of the CoreValve Self-Expanding Valve Prosthesis in High-Risk Patients With Aortic Valve Disease, The Siegburg First-in-Man Study, Circulation, 2006, 114, 1616-1624.

[GRU.77] AR.Gruentzig, RK.Myler, ES.Hanna, MI.Turina, Coronary transluminal angioplasty [abstract], Circulation, 1977, 84, 55-6.

[HAN.05] GS.Hanzel, PJ.Harrity, TL.Schreiber, WW.O'Neill, Retrograde percutaneous aortic valve implantation for critical aortic stenosis, Catheter Cardiovasc Interv, 2005, 64, 322-6.

[HEI.04] F.Heim, Développement d'une prothèse de valve cardiaque en matériau textile, Thèse de doctorat en Science de l'Ingénieur, Mulhouse, Université de Haute Alsace, 2004

[HER.02] NR.Hertzer, EJ.Mascha, MT.Karafa, et al, Open infrarenal abdominal aortic aneurysm repair: the Cleveland Clinic experience from 1989 to 1998, J Vasc Surg, 2002, 35, 1145–1154.

[HOF.96] R.Hoffman, GS.Mintz, GR.Dussaillant, JJ.Popma, AD.Pichard, LF.Satler, KM.Kent, J.Griffin, and MB.Leon, Patterns and mechanisms of in-stent restenosis, A serial intravascular ultrasound study, Circulation 1996, 94, 1247–1254.

[HOF.97] R.Hoffmann, GS.Mintz, K.Kent, L.Satler, A.Pichard, J.Popma, and M. Leon, Serial intravascular ultrasound predictors of restenosis at the margins of Palmaz–Schatz stents, Am. J. Cardiol, 1997, 79, 951–953.

[HOH.99] M.Höher, J.Wöhrle, OC.Grebe, et al, A randomized trial of elective stenting after balloon recanalization of chronic total occlusions, J Am Coll Cardiol 1999, 34, 722-729.

[HOW.01] MH.Howell, N.Strickman, A.Mortazavi, et al, Preliminary results of endovascular abdominal aortic aneurysm exclusion with the AneuRx stent-graft, J Am Coll Cardiol, 2001, 38, 1040–1046.

[HUB.04] CH.Huber, P.Tozzi and AF.Corno et al., Do valved stents compromise coronary flow ?, Eur J Cardiothorac Surg, 2004,25, 754–759.

[HUB.05] CH.Huber, LH.Cohn and LK.von Segesser, Direct-access valve replacement: a novel approach for off-pump valve implantation using valved stents, J Am Coll Cardiol, 2005, 46, 366–370.

[HUM.02] J.Humphrey, and S.Na. Elastodynamics and arterial wall stress. Ann. Biomed. Eng, 2002, 30, 509-23.

[IND.03] C.Indolfi, A.Mongiardo, A.Curcio and D.Torella, Molecular Mechanisms of In-Stent Restenosis and Approach to Therapy with Eluting Stents, Trends in Cardiovascular Medicine, 2003, Volume 13, Issue 4, Pages 142-148.

[IUN.03] B.Iung, G.Baron, EG.Butchart, et al, A prospective survey of patients with valvular heart disease in Europe : The Euro Heart Survey on Valvular Heart Disease, Eur Heart J, 2003, 24, 1231-43.

[JMM] Johnson Matthey Medical, Measuring Transformation Temperatures in Nitinol Alloys, disponible sur : http://jmmedical.com/resources/211/Measuring-Transformation-Temperatures-in-Nitinol-Alloys.html (consultée le 24/03/2009).

[KAN.82] S.Kan, RI.White, SE.Mitchell, TJ.Gardner, Percutaneous balloon valvuloplasty: a new method for treating congenital pulmonary-valve stenosis, N Engl J Med, 1982, 307, 540-2.

[KAS.01] A.Kastrati, J.Mehilli, J.Dirschinger, et al, Intracoronary stenting and angiographic results: strut thickness effect on restenosis outcome (ISARSTEREO) trial, Circulation, 2001, 103, 2816–2821.

[KOR.98] R.Kornowski, MK.Hong, FO.Tio, O.Bramwell, H.Wu, MB.Leon, In-stent restenosis : contributions of inflammatory responses and arterial injury to neointimal hyperplasia, J Am Coll Cardiol, 1998, 31, 224-230.

[KRO.04] K.Kroger, F.Santosa, M.Goyen, Biomechanic-al incompatibility of popliteal stent placement, J Endovasc Ther, 2004, 11, 686-694.

[KUE.03] T.Kuehne, M.Saeed, CM.Higgins, K.Gleason, GA.Krombach, OM.Weber, et al, Endovascular stents in pulmonary valve and artery in swine: Feasibility study of MR imaging-guided deployment and postinterventional assessment, Radiology, 2003, 226, 475-81.

[LIF.02] Lifeline Registry of Endovascular Aneurysm Repair Steering Committee. Lifeline Registry of Endovascular Aneurysm Repair: registry data report, J Vasc Surg, 2002, 35, 616–620.

[LIU.97] Y.Liu, X.Chen, PG Mc Cormick, Effect of low temperature ageing on the transformation behaviour of near equiatomic NiTi, Journal of Materials Science, 1997, 32, 5979-5984.

[LUT.02] G.Lutter, D.Kuklinski, G.Berg, P.von Samson, J.Martin, M.Handke, P.Uhrmeister, F.Beyersdorf, Percutaneous aortic valve replacement: an experimental study. I. Studies on implantation, J Thorac Cardiovasc Surg, 2002, 123, 768–76.

[LUT.04] G.Lutter, R.Ardehali, J.Cremer, P.Bonhoeffer, Percutaneous valve replacement: current state and future prospects, Ann Thorac Surg, 2004, 78, 2199–2206.

[MED.05] MedTech Insight 2005

[MIL] Millenium Inorganic Chemicals, TiO2 Fundamentals, disponible sur : http://www.millenniumchem.com/, (consultée le 24/03/2009).

[MOH.00] Z.Mohammed, JE.Moore Jr, A.Rachev, JL.Berry, and E.Manoach, Stress concentration reduction in stented arteries using compliance transitioning, Int J Cardiovasc Med Sci 2000, 3, 137–147.

[MOO.02] J E.Moore Jr, JL.Berry. Fluid and Solid Mechanical Implications of Vascular Stenting, Annals of Biomedical Engineering, 2002, Vol. 30, pp. 498–508.

[MOR.03] N.Morgan, M.Broadley, Taking the art out of smart! - Forming processes and durability issues for the application of NiTi shape memory alloys in medical devices. Proceedings from the Materials & Processes for Medical Devices Conference. 8-10 Sept 2003, Anaheim, California.

[MYE.00] Myers KA, How will endoluminal grafting for aneurysms be judged, J Endovasc Ther, 2000, 7, 101-104.

[MYK.95] P.S.U.Myken et al., Mechanical versus biological valve prosthesis : a ten year comparison regarding function and quality of life, Ann Thorac, Surg, 1995, 60, S447-452.

[NDC] Nitinol Device Components, Nitinol Facts, disponible sur : http://www.nitinol.info/pdf_files/nitinol_facts.pdf (consultée le 24/03/2009)

[OXE.03] H.Oxenham, et al., A twenty-year comparison of a Bjork-Shiley mechanical heart valve with porcine bioprosthesis, Heart, 2003, 89, 715-721.

[PAL.87] JC.Palmaz, DJ.Kopp, H.Hayashi, et al, Normal and stenotic renal arteries: experimental balloon-expandable intraluminal stenting, Radiology, 1987, 164, 705–708.

[PAR.95] JC.Parodi et al, Transfemoral endovascular stented graft repair of an abdominal aortic aneurysm, Ach Surg, 1995, 130, 549-552.

[PEL.00] A.R.Pelton, J.DiCello, S.Miyazaki, Optimisation of processing and properties of medical grade Nitinol wire, Min Ivas Ther & Allied Technol, 2000, 9(1), 107-118.

[PIC.66] G.Picollier. Etude de la stabilité des chambres d'équilibre, 2nd Thèse de doctorat en Science de l'Ingénieur, Grenoble, 1966. disponible sur : http://tel.archives-ouvertes.fr/docs/00/28/03/89/PDF/ 2eme_These_Piccolier.Gerard_1966.pdf

[QUA.05] R.Quaden, T.Attmann, A.Boening, J. Cremer and G.Lutter et al, Percutaneous aortic valve replacement: resection before implantation, European Journal of Cardio-thoracic Surgery, 2005, 27, 836–840.

[RAC.00] A.Rachev, E.Manoach, JL.Berry, and JE.Moore Jr, A model of stress induced geometrical remodeling of vessel segments adjacent to stents and artery/graft anastomoses, J Theor Biol, 2000, 206, 429–443.

[RAV.04] K.Ravi-Chandar, R.Wang, Mechanical response of a metallic aortic stent: Part I: Pressure-diameter relationship, Journal of applied mechanics, 2004, 5, 697-705.

[REI.71] RL.Reis, WD.Hancock, JW.Yarborough, DL.Glancy, AG.Morrow, The flexible stent. A new concept in the fabrication of tissue heart valve prostheses, J Thorac Cardiovasc Surg, 1971, 42, 683-693.

[ROC.98] D.Rockwell, Vortex-body interactions, Annu Rev Fluid Mech, 1998, 30, 199–229.

[ROG.99] C.Rogers, DY.Tseng, JC.Squire, and ER.Edelman, Balloon-artery interactions during stent placement, Circ Res, 1999, 84, 378–383.

[ROU.83] EP.Rousseau, AAH.Sauren, MC.van Hout, Elastic and viscoelastic material behaviour of fresh and glutaraldehyde-treated porcine aortic valve tissue, J Biomech, 1983, 16, 339-348.

[ROU.87] Rousseau H, Puel J, Joffre F, et al. Self-expanding endovascular prosthesis: an experimental study. Radiology 1987; 164:709 –714.

[SAC.96] BA.Sacks, A.Miller, M.Gottlieb, Fracture of an iliac artery Palmaz stent, J Vasc Intervent Radiol, 1996; 7, 53-55.

[SAN.69] MP.Sands, EA.Rittenhouse, H.Mohri, KA.Merendino, An anatomical comparison of human, pig, calf and sheep aortic valves, Ann Thorac Surg, 1969, 8, 407-14.

[SAV.07] MP. Savage et al, The dark side of High Pressure stent deployment, J Am Coll Cardiol, 2007, 29, p368.

[SER.02] PW.Serruys, BJ.Rensing editors, Handbook of coronary stents. 4th edn. London : Martin Dunitz, 2002.

[SER.94] PW.Serruys, P.de Jaegere, F.Kiemeneij, et al, A comparison of balloon-expandable -stent implantation with balloon angioplasty in patients with coronary artery disease, Benestent Study Group, N Engl J Med, 1994; 331, 489-495.

[SIG.87] V.Sigwart, J.Puel, V.Mirkovitch, F.Joffre, L.Kappenberger, Intravascular stents to prevent occlusion and restenosis after transluminal angioplasty, N Engl J Med, 1987, 316, 701–706.

[SIL.85] MA.Silver, WC.Roberts, Detailed anatomy of the normally functioning aortic valve in hearts of normal and increased weight, Am J Cardiol, 1985, 55, 454.

[SIM.00] C.Simon, JC.Palmaz, and EA.Sprague, Influence of topography on endothelization of stents: Clues for new designs, J. Long-Term Effects Med. Implants, 2000, 10, 143–151.

[SPR.97] EA.Sprague, J.Luo, and JC.Palmaz, Human aortic endothelial cell migration onto stent surfaces under static and flow conditions, J Vasc Interv Radiol, 1997, 8, 83–92.

[STA.06] C.Stacchino, G.Burriesci, G.Righini, Cardiac Valve Prosthesis, WO 2006/085225 A1, 10 Feb 2006.

[STA.96] B.Stanek, D.Liepsch, and G.Pflugbeil, Flow studies of stents in models of the carotid artery, Third World Congress of Biomechanics, 1998, p. 206a.

[STE.81] AA.van Steenhoven, C.Verlaan, In vivo cinematographic analysis of behavior of the aortic valve. Am J Physiol, 240, H286, 1981;

[STO.04] D.Stoeckel, A.Pelton, T.Duerig, Self expanding nitinol stents, material and design considerations, Eur Radiol (2004) 14:292–301

[SUL.02] T.M.Sullivan et al. Effect of endovascular stent strut geometry on vascular injury, myointimal hyperplasia, and restenosis, J Vasc Surg, 2002, 36, 143-149.

[SUT.95] JP.Sutton, S.Yen Ho, RH.Anderson, The forgotten interleaflet triangles: a review of the surgical anatomy of the aortic valve, Ann Thorac Surg, 1995, 59, 419-427.

[SWA.74] W.Swanson, R.Clark, Dimensions and geometric relationships of the human aortic value as a function of pressure, Circ Res, 1974, 35, 871-882.

[THO.06] T.Thom, N.Haase, W.Rosamond, et al, Heart disease and stroke statistics – 2006 update, A report from the American Heart Association Statistics Committee and Stroke Statistics Subcommittee, Circulation, 2006, 113, 85-151.

[THU.77] M.Thubrikar, R.Harry, Normal aortic valve function in dogs, Am J Cardiol, 1977, 40, 563-8.

[THU.81] M.Thubrikar, WC.Piepgrass, TW.Shaner, SP.Nolan, The design of the normal aortic valve, Am J Physiol, 1981; 241, H795-801.

[THU.86] MJ.Thubrikar, SP.Nolan, J.Aouad and JD.Deck, Stress sharing between the sinus and leaflets of canine aortic valve, The annals of thoracic surgery, 1986, 42, 434-440.

[THU.90] M.Thubrikar, The aortic valve, Boca Raton, Florida : CRC Press, Inc., 1990.

[TOM.92] R.Tominaga, HE.Kambic, H.Emoto, H.Harasaki, C.Sutton, and J.Hollman, Effects of design geometry of intravascular endoprostheses on stenosis rate in normal rabbits, Am Heart J, 1992, 123:21–28.

[TRU.95] GA.Truskey, KM.Barber, TC.Robey, LA.Olivier, and MP.Combs, Characterization of a sudden expansion flow chamber to study the response of endothelium to flow recirculation, J Biomech Eng, 1995, 117, 203–210.

[VAH.04] A.Vahanian, IF.Palacios, Percutaneous Approaches to Valvular Disease, Circulation, 2004, 109, 1572-1579.

[VER.00] H.Vernhet, JM.Juan, R.Demaria, MC.Lauraire, JP.Senac, M.Dauzat, Acute changes in aortic wall mechanical properties after stent placement in rabbits, J Vasc Interv Radiol, 2000, 11, 634-638.

[VER.03a] H.Vernhet, B.Jean, S.Lust, et al, Wall mechanics of the stented extra-cranial carotid artery, Stroke, 2003, 34, 222-224.

[VER.03b] H.Vernhet, R.Demaria, JM.Juan, et al, Wall mechanics of the stented rabbit aorta : Long-term study and correlation with histological findings, J Endovasc Ther, 2003, 42, 389-394.

[VES.89] I.Vesely, D.Boughner, Analysis of the bending behaviour of porcine Xenograft leaflet and of natural aortic valve material : bendinf stiffness, neutral axis and shear measurements, J Biomech, 1989, 22, 655-659.

[WAL.00] PW.Walsh, F.Berkani, and JE.Moore Jr, Stented flow chamber for endothelial cell migration studies, In: Prendergast PJ, Lee TC, Carr AJ, eds. Proceedings of the European Society of Biomechanics Conference, Dublin. Dublin: Royal Academy of Medicine in Ireland, 2000, p. 301.

[WAL.91] Wallsten et al, Self expanding prosthesis, US Patent 5061275, 1991, Oct 29.

[WAN.07] J.Wang, R.Milner, Review of Current Thoracic Endografts with or Pending FDA Approval, Vasc Dis Manage, 2007, 4,142-147.

[WEB.06] JG.Webb, and al, Percutaneous aortic valve implantation retrograde from the femoral artery, Circulation, 2006, 113, 842-850.

[WEL.02] FGP.Welt; R.Campbell, Inflammation and Restenosis in the Stent Era, Arteriosclerosis Thrombosis and Vascular Biology, 2002, 22, 1769.

[YAZ.04] S.Yazdani, J.Moore, J.Berry, P.Vlachos, DPIV Measurements of flow disturbances in stented artery models : adverse affects of compliance mismatch, J of Biomech Eng, 2004, 126, 559-566.

[YEU.04] KWK.Yeung, KMC.Cheung, WW.Lu, CY.Chung. Optimization of thermal parameters to alter austenitic phase transition temperature of Niti alloy for medical implant. Materials science and engineering, 2004, A383, 213-218.